Carbon Rich Organometallics: From Mixed Valency To Redox Active Ligands

MAN, WING,YANG

Carbon Rich Organometallics:

From Mixed Valency To Redox Active Ligands

Wing Yang Man MChem (Hons)

Department of Chemistry

A Thesis submitted in part fulfilment of the requirements for the degree of Doctor of Philosophy at Durham University

Statement of Copyright

Declaration

The work described in this thesis was carried out at the University of Durham, Department of Chemistry, between October 2009 and September 2012. All the work is that of the author unless stated otherwise, and it has not been submitted for a degree at this or any other university.

Memorandum

Part of this work has been the subject of the following published articles:

7. **Synthesis, structure and redox properties of tris(pyrazolyl)borate-capped ruthenium vinyl complexes.**

   J.D. Farmer, W.Y. Man, M.A. Fox, D.S. Yufit, J.A.K. Howard, A.F. Hill, P.J. Low, *J. Organomet. Chem.*, 2012, **721**, 173.

6. **Synthesis and characterisation of dithia[3.3]paracyclophane-bridged binuclear ruthenium vinyl and alkynyl complexes.**

   J.-L. Xia, W.Y. Man, X. Zhu, C. Zhang, G.-J. Jin, P.A. Schauer, M.A. Fox, J. Yin, G.-A. Yu, P.J. Low, S.H. Liu, *Organometallics*, 2012, **31**, 5321.

5. **Synthesis, structure and electrochemical properties of triarylamine bridged dicobaltdicarbon tetrahedrane clusters.**

   W.Y. Man, K.B. Vincent, H.J. Spencer, D.S. Yufit, J.A.K. Howard, P.J. Low, *J. Cluster Sci.*, 2012, **23**, 853.

4. **The synthesis, molecular and electronic structure of cyanovinylidenes.**

   E.M. Long, N.J. Brown, W.Y. Man, M.A. Fox, D.S. Yufit, J.A.K. Howard, P.J. Low, *Inorg. Chim. Acta*, 2012, **380**, 358.

3. **Cross-coupling reactions of gold(I) alkynyl and polyyndiyl complexes.**

   W.Y. Man, S. Bock, N.N. Zaitseva, M.I. Bruce, P.J. Low, *J. Organomet. Chem.*, 2011, **696**, 2172.

2. **Spectroscopic and computational studies of the ligand redox non-innocence in mono- and binuclear ruthenium vinyl complexes.**

   W.Y. Man, J.-L. Xia, N.J. Brown, J.D. Farmer, D.S. Yufit, J.A.K. Howard, S.H. Liu, P.J. Low, *Organometallics*, 2011, **30**, 1852.

1. **Self-assembled molecular wires from organoiron metalloligand and ruthenium tetramesitylporphyrin.**

   F. Malvolti, P. Le Maux, L. Toupet, M. E. Smith, W. Y. Man, P. J. Low, E. Galardon, G. Simonneaux, F. Paul, *Inorg. Chem.*, 2010, **49**, 9101.

Part of this work has been subject of the following presentations:

5. **XXV International Conference on Organometallic Chemistry**

   Lisbon, Portugal, September 2012

   Poster entitled: Triarylamine bridged dicobaltdicarbon tetrahedrane clusters

4. **Dalton Conference**

   Warwick, England, April 2012

   Talk entitled: Redox chemistry of Tp and PMe_3 coordinated ruthenium vinyl complexes

3. **Electrochemical Horizons**

   Bath, England, September 2011

   Talk entitled: Redox non-innocence of ruthenium vinyl complexes

2. **Durham University Postgraduate Symposium**

   Durham, England, June 2011

   Poster entitled: Electronic interactions in polymetallic complexes

1. **Universities of Scotland Inorganic Chemistry Conference**

   Durham, England, July 2010

   Poster entitled: Redox non-innocence of ruthenium vinyl complexes

Abstract

This thesis sets out to explore the electronic structures and redox properties of organometallic complexes. The mixed valence states of these complexes have been investigated and classified. Chapter 1 introduces the general area and provides a brief summary of the theory to electron transfer. The concepts discussed in Chapter 1 are developed further in subsequent Chapters.

A trimetallic molecular assembly featuring two redox-active organoiron fragments connected *via* a central ruthenium tetramesitylporphyrin socket through pendant pyridyl moieties was investigated using electrochemical and UV-vis-NIR/IR spectroelectrochemical studies. Electrochemical studies reveal three reversible oxidation waves, the first two of which can be attributed to the stepwise oxidation of the iron centres. The redox separation between these iron redox waves was found to be constant regardless of electrolyte composition, suggesting a "through bond" mechanism for electronic interactions between the iron centres. An analysis of the near-IR band in the mixed valence state suggests the assignment of $[\{Cp^*(dppe)(Py\text{-}4\text{-}C{\equiv}C)Fe\}_2(\mu\text{-}Ru(TMP))]^+$ as a strongly coupled, Class II mixed valence complex in which the NIR band arises from genuine metal to metal charge transfer (IVCT) processes.

Iron alkynyl complexes Fe(C≡CR)(PP)(Cp') are well known to exhibit metal localised redox properties, whilst the alkynyl ligand in analogous alkynyl ruthenium complexes is redox-active. In order to tune the metal coordination sphere, to explore further the redox activity of carbon rich ligands bound to ruthenium, a series of complexes of the general form $Ru(CH=CHC_6H_4R\text{-}4)(CO)(PPh_3)Tp$ where R = $N(C_6H_4Me)_2$, OMe, CH_3, CO_2Me, NO_2 were synthesised, crystallographically characterised and investigated using electrochemical, UV-vis-NIR/IR spectroelectrochemical studies and DFT computational methods. IR spectroelectrochemical studies and DFT computations are consistent, with descriptions of the vinyl ligand as being redox-active, as developed by Winter and co-workers for some related mono- and bimetallic ruthenium vinyl complexes. Studies of $Ru(CH=CHC_6H_4R\text{-}4)(CO)(PPh_3)Tp$, $Ru(CH=CHC_6H_4Me\text{-}4)Cl(CO)Cl(PMe_3)_3$ and $[\{(PMe_3)_3(CO)ClRu\}_2(\mu\text{-}CH=CHC_6H_4CH=CH)]$ reveal that the bridging ligand is also heavily involved in the oxidation process. A three state model in which the bridge is appreciably involved in the stabilisation of charge is required to rationalise experimental data including electronic spectra, consistent with theoretical findings. In seeking to fine tune the electronic character of ruthenium based $[\{L_nRu\}_2(\mu\text{-bridge})]^{n+}$, vinyl and alkynyl complexes featuring a dithia[3.3]cyclophane moiety were investigated. In both cases, the bridging moiety was found to be heavily involved in the oxidation processes.

The triarylamine ligand moiety has attracted attention due to its potential to promote electronic interactions between three metal sites, through a central nitrogen atom. The synthesis, crystallographic characterisation, electrochemical and spectroelectrochemical response of one, two and three cluster centres on a triarylamine core have been examined. Experimental results point towards a localised structure, with no electronic interaction between the cluster moieties, which are examples of Class I Robin and Day mixed valence complexes.

Pre-formed gold alkynyl and diyndiyl complexes can be cross-coupled with aryl halides in the presence of both Pd(II) and Cu(I) catalysts under mild conditions in ether based solvents at room temperature, without the need for an additional base. These gold-mediated Sonogashira reactions likely proceed *via* the transmetallation of the alkynyl fragment from Au(I) to Cu(I), prior to entry to a conventional Sonogashira reaction. These reactions present alternative methods to prepare differentially substituted diynes, without the need to expose the C-H functionality of longer chain polyynes, which can be inherently unstable.

Acknowledgements

Firstly, I would like to thank Prof. Paul J. Low for giving me the opportunity to carry out a PhD under his supervision, and for his continued help and guidance during the course of my studies at Durham University. My thanks are extended to Dr. Mark A. Fox for his invaluable synthetic discussions and for his computational expertise. I am also grateful to Durham Doctoral Training Account for funding.

I would like to thank all former and current members of the PJL research group. In particular, Dr. Neil J. Brown, Dr. Julian D. Farmer and Mr Sören Bock for the parts that they have played in my development as a chemist, for being an absolute pleasure to work with, and for their friendship. Thanks also go to the Analytical Services team at Durham University; especially Mr Ian McKeag from NMR and Dr. Dmitry S. Yufit from X-ray crystallography.

Finally, I would like to thank my family and friends for their love and patience; my mum and dad, without whom this would not have been possible; Dave and Kin for always being there; Mrs Elizabeth Snyder for believing in me and Nick, for making things that little bit easier. This thesis is dedicated to my gran; she is a beautiful person, whom I love very much.

Abbreviations

°	degree
°C	degree Celsius
δ	chemical shift (ppm)
Δ	difference
$\Delta E_{1/2}$	difference in half wave potential (mV, V)
ΔE_p	peak potential difference (mV, V)
ε	molar extinction coefficient ($M^{-1}cm^{-1}$)
θ	dihedral angle, torsion angle (°)
Å	Ångstrom
ASAP	Atmospheric Solids Analysis Probe
bpy	bipyridine
$[BAr^F{}_4]^-$	$[B(C_6F_5)_4]^-$ anion
B3LYP	Becke 3-Parameter Lee-Yang-Parr
ca.	circa
C	Coulomb
cm^{-1}	wavenumber (reciprocal centimetres)
Cp	cyclopentadienyl
Cp*	1,2,3,4,5-pentamethylcyclopentadienyl
CV	cyclic voltammetry
d	doublet
ddt	doublet of doublet of triplets
dmpe	1,2-bis(dimethylphosphino)ethane
dppe	1,2-bis(diphenylphosphino)ethane
dppm	1,2-bis(diphenylphosphino)methane
dppf	1,1'-bis(diphenylphosphino)ferrocene
dt	doublet of triplets
DCE	dichloroethene

DCTB	*trans*-2-[3-(tert-butylphenyl)-2-methyl-2-propenylidene]malonitrile
DFT	density functional theory
eq	equivalent
$E_{1/2}$	half wave potential (V)
E_{pa}	peak anodic potential (V)
E_{pc}	peak cathodic potential (V)
EPR	electron paramagnetic resonance
ES	electrospray
ESR	electron spin resonance
F	Faraday constant (96485 C)
$[Fc]PF_6$	ferricenium hexafluorophosphate
$FcH^*/[FcH^*]^+$	decamethylferrocene/decamethylferricenium couple
$FcH/[FcH]^+$	ferrocene/ferricenium couple
GC	gas chromatography
GC-MS	gas chromatography mass spectrometry
h	hour(s)
HOMO	highest occupied molecular orbital
HOSO	highest occupied spin orbital
Hz	hertz
i_{pa}	peak anodic current (A)
i_{pc}	peak cathodic current (A)
IC	interconfigoration
IR	infra-red
IVCT	intervalence charge transfer
K	Kelvin
K_c	comproportionation constant
LMCT	ligand to metal charge transfer
MLCT	metal to ligand charge transfer
LANL2DZ	Los Alamos National Laboratory double-ζ
LLCT	ligand to ligand charge transfer
LUMO	lowest unoccupied molecular orbital
LUSO	lowest unoccupied spin orbital

m	medium
mg	milligrams
mmol	millimole
mV	millivolt
MALDI	matrix assisted laser desorption ionisation
MO	molecular orbital
ML-LCT	metal ligand to ligand charge transfer
MV	mixed valence
m/z	mass per unit charge
NBu_4PF_6	tetrabutylammonium hexafluorophosphate
NIR	near-infrared
NMR	nuclear magnetic resonance
obsd	observed
OTTLE	optically transparent thin layer electrode
Ph	phenyl
PMe_3	trimethylphosphine
PPh_3	triphenylphosphine
Pyr	pyrenyl
ppm	parts per million
prep TLC	preparative thin layer chromatography
py	pyridyl
PSEPT	polyhedral skeletal electron pair theory
rt	room temperature
R	general organic group
ROP	ring opening polymerisation
s	singlet (NMR)
s	strong (IR)
s^{-1}	reciprocal seconds
SCE	saturated calomel electrode
SEP	skeletal electron pairs
t	triplet
td	triplet of doublets
tol	tolyl

TD-DFT	time dependent-density functional theory
THF	tetrahydrofuran
TLC	thin layer chromatography
TMEDA	tetramethylethylenediammine
TMP	tetramesitylporphyrin
TMS	trimethylsilyl group
TMSA	trimethylsilylacetylene
Tp^{-}	tris(pyrazolyl)borate anion
vs	very sharp
vw	very weak
V	volt
w	weak

Table of Contents

Chapter 5. Triarylamine Bridged Dicobaltdicarbon Tetrahedrane Clusters

Chapter 1. Introduction

In 1977, Macdiarmid and co-workers found that upon doping poly(acetylene) with a halide the material becomes electrically conducting.[1] In this process, a halogen, for example I_2 oxidises the conjugated polymer and creates a radical cation. This can be regarded as the removal of an electron from the valence band, providing a pathway for hole conduction (*p*-doping), Figure 1.1. Alternatively, reduction by an alkali metal such as Na reduces the polymer to create a radical anion, whereby conduction proceeds *via* electron transport (*n*-doping), Figure 1.1. Since then, organic conducting polymers such as poly(phenylenevinylene), poly(thiopene) and poly(fluorene) derivatives, Figure 1.2, have been explored for their potential use in light emitting diodes, photodiodes and in lasers.[2,3]

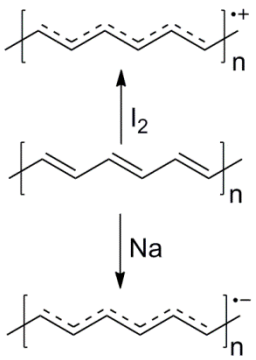

Figure 1.1. Schematic representation of *p*- and *n*-doping of poly(acetylene) with I_2 and Na as an oxidant and reductant respectively.

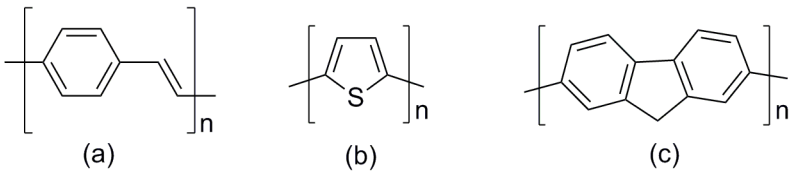

Figure 1.2. Conjugated polymers (a) poly(phenylenevinylene), (b) poly(thiopene) and (c) poly(fluorene).

The introduction of a metal into a polymer backbone presents several advantages over their conventional organic π-conjugated polymers. For example, by varying the ligands attached to the metal centre the solubility of the polymer, and hence its processing characteristics, can be tuned without altering the electronic properties of the metallopolymer (a metal-containing polymer).[4] The electronic characteristics of metallopolymers can be modified by varying the nature of the included metal, ancillary ligands or spacer groups. This synthetic and electronic flexibility has been critical to the emergence of metallopolymers as functional materials, for example as sensors, memory elements or light emitting devices.[5-7]

In 1955, the first metallopolymer poly(vinylferrocene), Figure 1.3, was reported.[8] The field has expanded dramatically, and metallopolymers containing main group (p-block), transition metals (d-block) or lanthanide and actinide (f-block) elements are now well established.[9-11] These polymers can be classified according to a number of structural types, defined by the location of the metal centres and the nature of the linkages between them. For example, the metal can reside in the main chain, or side group structure and the metallopolymer can be linear, or dendritic, Figure 1.4.[12] The synthetic approaches to this class of molecule are dictated by the nature of the metal and the

organic components which link them. For example, Manners has established a ring opening protocol based on ferrocenophanes which has been met with outstanding success in the preparation of a vast array of ferrocenyl polymers, *vide infra*. [13-16]

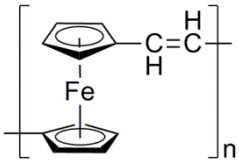

Figure 1.3. Poly(vinylferrocene).

Metallopolymers based on alkynyl functional groups can typically be prepared using three general approaches; dehydrohalogenation, oxidative coupling and alkynyl ligand exchange, Scheme 1.1. In dehydrohalogenation based approaches, a metal bis(halide) L_nMX_2, and a (bis)terminal alkyne, HC≡C-R-C≡CH, are reacted with a source of cuprous halide in an amine solvent often under reflux conditions, Scheme 1.1a. The reaction proceeds in the same manner as the initial steps of the Sonogashira cross-coupling reaction, with formation of an intermediate copper species and the metal halide to regenerate a copper halide and the new metal-alkynyl complex. In oxidative coupling based approaches trans (bis)acetylide monomers can be converted to polymeric materials, for example using typical Hay conditions ($[Cu(tmeda)]^+$ / O_2], Scheme 1.1b. However, the inherent instability of dihalo nickel complexes in amine solvents and bis(alkynyl) complexes in oxidising media have deemed these methods not suitable for the preparation of nickel metallopolymers. The group of Hagihara have demonstrated that nickel acetylide polymers can be prepared *via* milder alkynyl ligand exchange reactions (Scheme 1.1c) catalysed by CuI in amine solvents, as described above.[17]

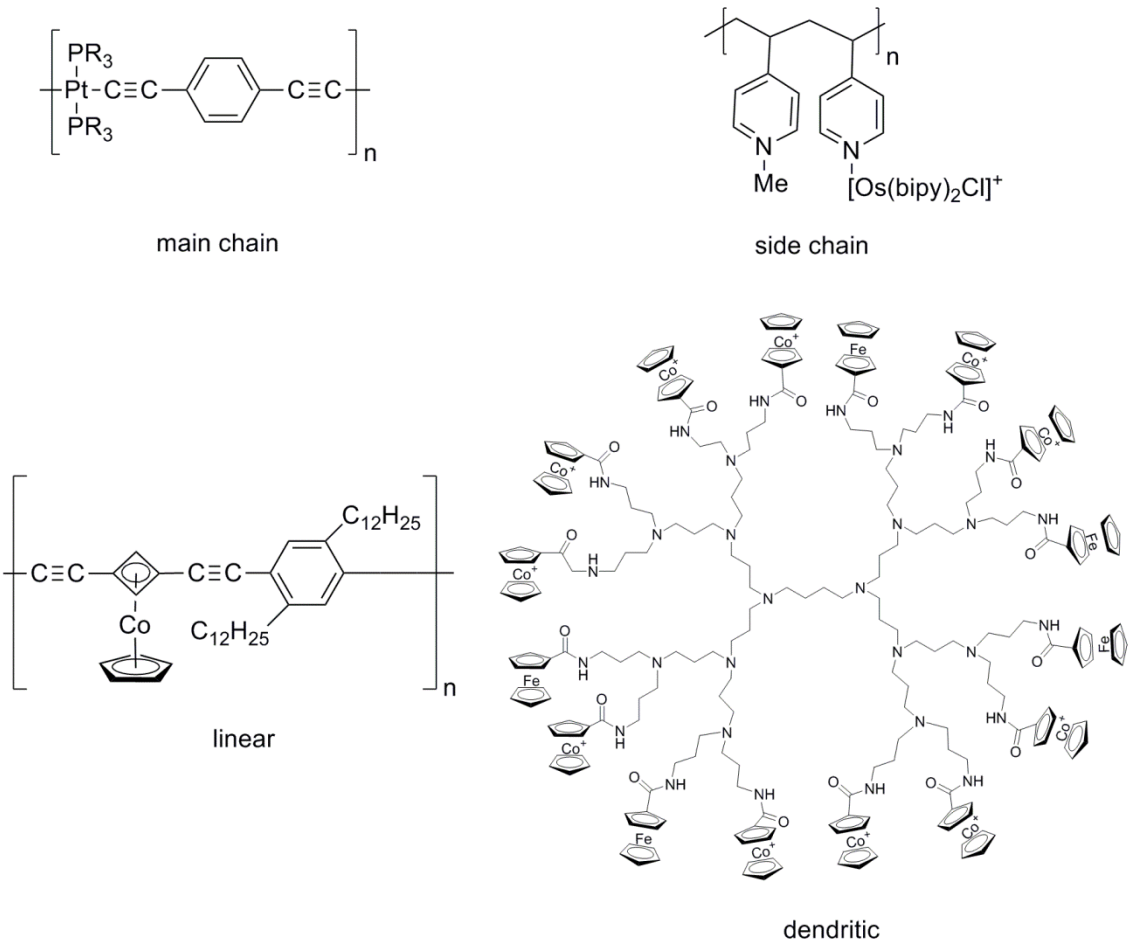

Figure 1.4. Structures of metallopolymers.

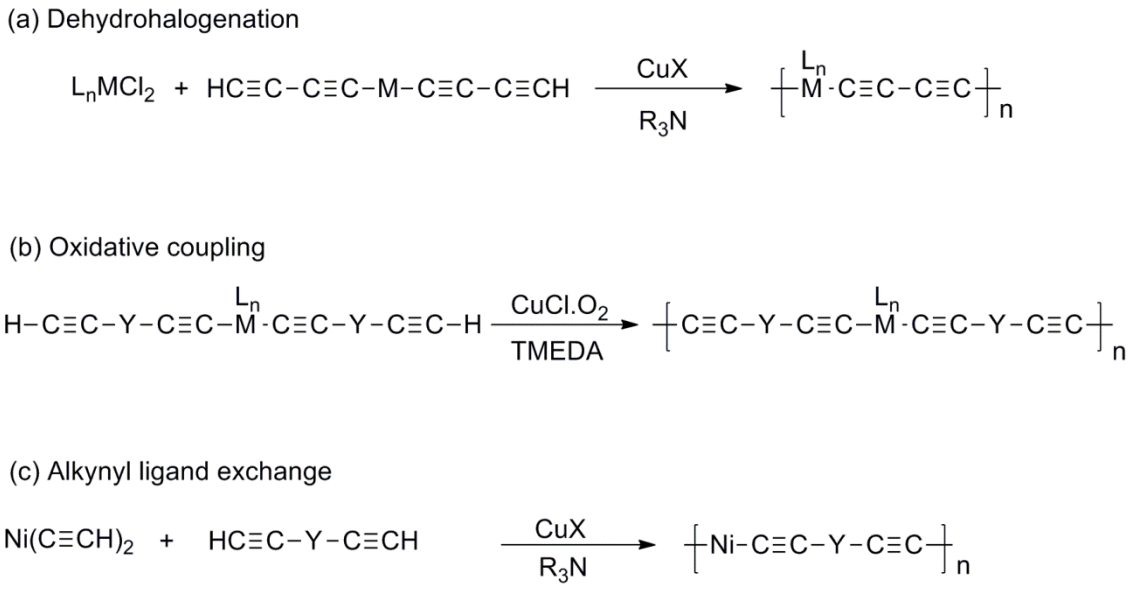

Scheme 1.1. General synthetic routes to metallopolymers, where M = *trans*-Pt$(PR_3)_2$, *trans*-Pd$(PR_3)_2$ and Y = an aromatic spacer.

In the metallopolymer field, advances have often been hampered by synthetic and solubility issues, which have made the characterisation of metallopolymers difficult. However, in the last two decades, new synthetic methods have been developed which are compatible with the presence of metal centres and have subsequently led to a range of well defined and well characterised molecular weight polymers. For example Lewis, Johnson and co-workers have synthesised metallopolymers through the reaction of a transition metal halide of the general form *trans*-$[M(PBu_3)_2Cl_2]$ where M = Ni, Pd, Pt with a bis(trimethylstannyl)acetylide species, $Me_3SnC{\equiv}CC_6H_4C{\equiv}CSnMe_3$ to generate the polymeric *trans*-$[M(PBu_3)_2C{\equiv}CC_6H_4C{\equiv}C]_n$ species in toluene at 50 °C with a catalytic amount of CuI, Scheme 1.2a. [18-20]

Manners and co-workers have also investigated thermal ring opening polymerisations (ROP) of ferrocenophanes, which are highly strained molecules, and undergo ROP to yield high molecular weight poly(ferrocenylsilanes), Scheme 1.2b.[21] In the presence of small quantities of an anionic initiator, living polymerisation sequences which are free of chain transfer and termination reactions can also be induced, leading to a range of metallopolymers with narrow polydispersities, Scheme 1.2c.[13-16] Recently, Humphrey and co-workers have used 'steric control' as a way of affording higher generation ruthenium alkynyl based dendrimers, Figure 1.5,[22-24] and some mixed ruthenium platinum dendrimers in an efficient manner, making use of metallation, palladium catalysed cross-coupling and desilylation protocols.[25]

With the synthetic routes to metallopolymers firmly established, there has been a recent extension of ideas based on linear and dendritic metallopolymeric systems to two and three dimensional networks and lattices. For example, Bunz and co-workers have explored the coordination of organic ligands with transition metal anions by self-assembly to create networks of various sizes, shapes of channels and cavities in square rod, ladder and lattice networks.[26-29]

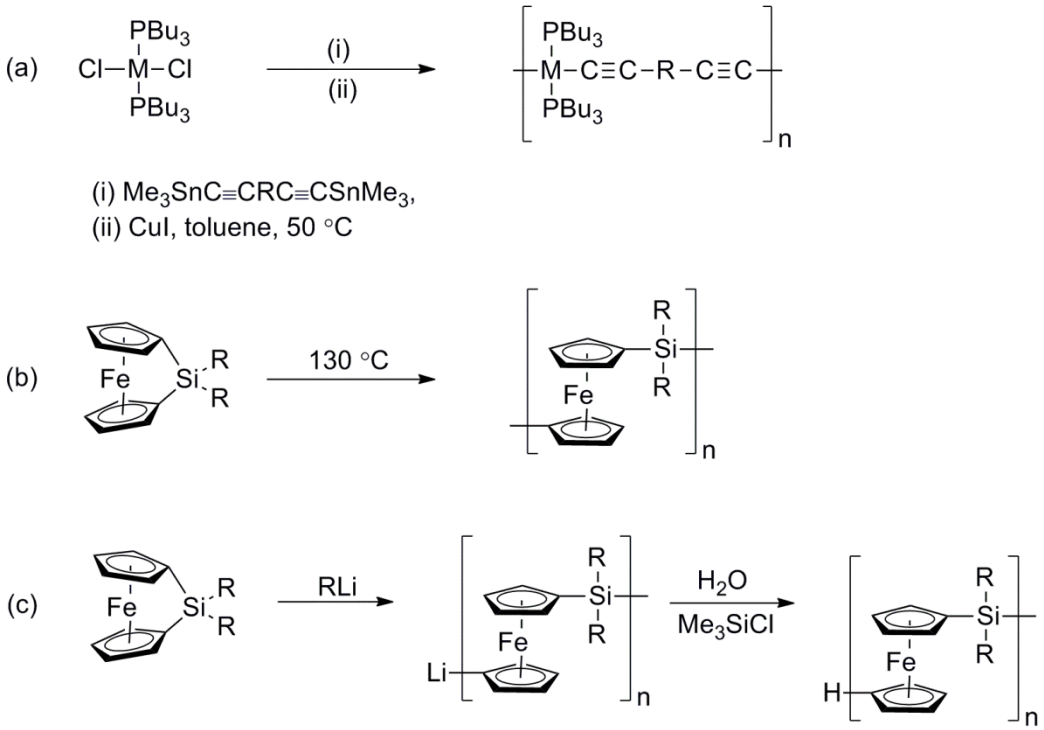

Scheme 1.2. Synthetic methods to metallopolymers.

The ability to control electronic structure as a function of the metal and organic fragment promises a great deal in terms of the preparation of optoelectronic materials with designed properties. For example, Humphrey and co-workers have also explored the synthesis of ruthenium alkynyl dendrimers *via* an iterative convergent approach, with a view to exploiting these molecules for their non-linear optical responses.[22,24,30,31] Metallopolymers have also been at the forefront in many of the original ideas in the

preparation of molecular wires and conducting polymers.[9,32] However, studies of mechanisms of intramolecular charge transport are complicated by polydispersity, solubility and structural distortion,[33] and different charge transfer mechanisms that evolve as a function of distance (i.e. superexchange *vs.* hopping).[34-37] Whilst metallopolymers remain a source of considerable interest, historically, questions concerning intramolecular charge transfer between metal centres linked by conjugated bridging elements have been investigated using smaller, bimetallic model systems. These smaller systems, and the methods for assessing 'intramolecular electronic interactions', are addressed in more detail in the following section.

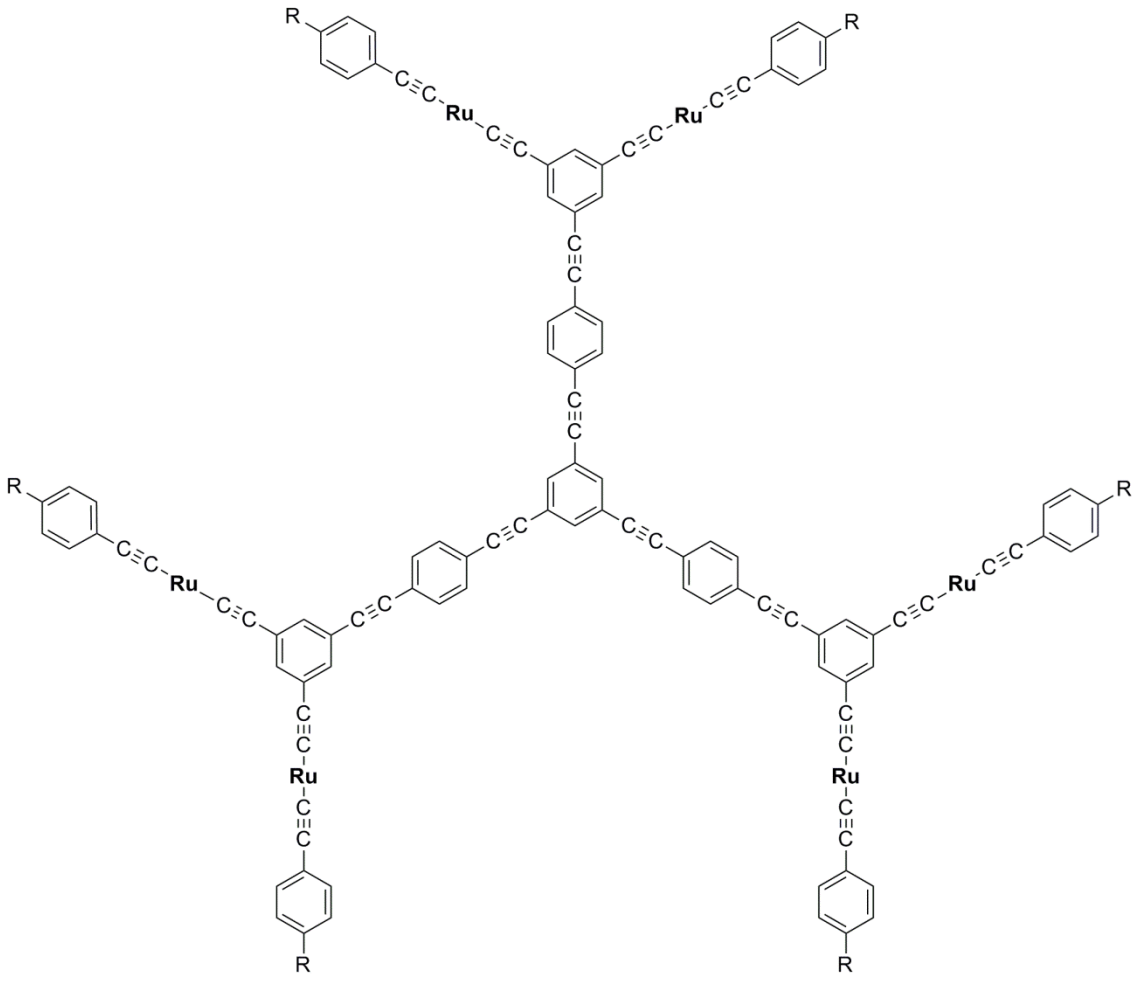

Figure 1.5. Ruthenium alkynyl dendrimer system, where Ru = Ru(dppe)$_2$.

1.1. Mixed Valence Complexes

Bimetallic complexes where two metal centres are connected *via* a conjugated bridge are ideal molecular systems by which we can explore and understand the intramolecular electron transfer reaction. Consider for example two identical metal centres, M, linked by a bridging ligand. On oxidation of the complex **M-M**, an electron is removed. This leads to the generation of a mixed valence (MV) complex, where an element exists in more than one oxidation state. The sequential removal of one and two electrons, at a potential E_1 and E_2 leads to the formation of the mono- and dicationic species respectively, which exist in a series of one-electron transfer equilibria. Providing that the nature of the oxidation waves are reversible, the redox potential difference, ΔE can be calculated.

$$\text{M-M} \underset{}{\overset{E_1}{\rightleftharpoons}} [\text{M-M}]^{+} \overset{E_2}{\rightleftharpoons} [\text{M-M}]^{2+}$$

$$\Delta E = E_2 - E_1$$

From electrochemical data, the comproportionation constant, K_c which reflects the thermodynamic stability of the MV state, that is, the stability of the complex [**M-M**]$^{+}$ relative to **M-M** and the dicationic [**M-M**]$^{2+}$ can be determined.

$$2[\text{M-M}]^{+} \overset{K_c}{\rightleftharpoons} \text{M-M} + [\text{M-M}]^{2+}$$

$$K_c = \frac{2[\boldsymbol{M-M}]^{+}}{[\boldsymbol{M-M}][\boldsymbol{M-M}]^{2+}}$$

K_c can be derived from the Nernst equation

$$\Delta E = \Delta E^0 - \frac{RT}{nF} lnK_c$$

$$K_C = exp\left(\frac{\Delta EF}{RT}\right)$$

where ΔE is the redox potential difference in Volts, F is the Faraday constant (96485 C), R is the gas constant (8.314 J mol^{-1} K^{-1}) and T is the temperature (K).

For bimetallic complexes, ΔE is sensitive to a number of contributing factors which include electrostatic and solvation factors, ion-pairing interactions, structural changes to metal sites and, or the bridge, the π-donor acceptor character of supporting and bridging ligands in addition to the "resonance" stabilisation factor. Of these terms, only the latter constitutes a contribution from a metal-metal interaction, whilst the total value of ΔE, and hence the overall free energy of comproportionation, ΔG_c is dependent on all these terms.[38]

$$\Delta G_c^\circ = -RTInK_c = -nF(\Delta E)$$

In seeking to assess bridge mediated electronic interactions between M and M^+, it is imperative to ensure that steps are taken to ensure that redox events can be wholly attributed to the metal redox sites. In addition, even when there are no "through bond" contributors to the electronic interactions between redox states, electrostatic effects can

still give rise to a rich electrochemical response. In weakly interacting systems, through space interactions i.e. those propagated by Coulombic effects through the surrounding medium can be distinguished from genuine through bond effects, i.e. those mediated by the bridge, by following the apparent coupling as a function of bridge length or degree of π-conjugation, and for bridges of fixed length, by changes in the degree of bridge geometry or degree of π-conjugation.

Geiger and co-workers[39-41] have recently carried out a series of studies to differentiate between through bond and through space effects in an analyte containing two (or more) redox-active metal centres by comparing the electrochemical response in an electrolyte containing a more traditional $[BF_4]^-$ or $[PF_6]^-$ anion to results from electrolytes containing a weakly coordinating $[B(C_6F_5)_4]^-$ or $[B(C_6H_3(3,5\text{-}CF_3)_2)_4]^-$ anion. Since the ion-pairing strength of the more strongly coordinating traditional anions impart a significant lowering of the $\Delta E_{1/2}$ potentials for the two redox processes, it can lead to a situation where a single unresolved oxidation wave is observed. However, by employing a weakly coordinating anion, there is a magnification in the separation of the $\Delta E_{1/2}$ potentials. This pattern of behaviour is indicative of a substantial through space contribution to the electrochemical response. On the other hand, a more limited change in $\Delta E_{1/2}$ between the first and second redox potentials with variation of electrolyte is representative of a significant through bond interaction between the electrophores.[40-42] Whilst all due care can be taken to ensure that the variations in $\Delta E_{1/2}$ truly reflects the resonance stabilisation through bond contribution, the limitations of electrochemistry mean that $\Delta E_{1/2}$ is not the best measure of electronic interactions between two redox-active sites across a bridge. Over the years, the classification of MV complexes has been addressed using alternate methods of spectral analysis.

In the late 1960's, Robin and Day proposed a classification scheme for MV complexes based on the electronic interactions between the redox termini M and M^+ within a bimetallic complex, in the two states M^+-M (**X**) and M-M^+ (**Y**).[43] In Class I MV complexes, the interactions between M and M^+ are so weak, that the distinct properties of each site are observed, Figure 1.6. The oxidation event is thus localised on a single metal centre and there is no or minimal interaction between the two sites. In this instance, the difference between the first and second oxidation redox events is limited to a small statistical factor of 35.6 mV.

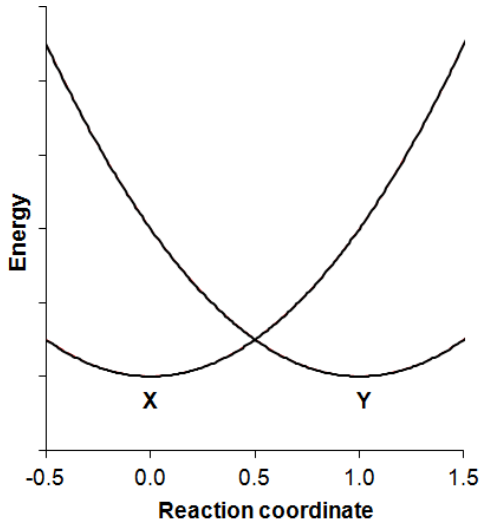

Figure 1.6. Potential energy surfaces in a ligand bridged bimetallic complex with negligible coupling.

On the opposite side of the extreme in Class III MV complexes, the interaction between M and M^+ is so strong that the individual character of each site is lost and the complex behaves as a single entity which undergoes two sequential one electron redox processes. In this case, the potential energy curves are so strongly coupled that they form a single

minimum ground state (**XY)**, and give rise to an excited adiabatic state (**Z**), Figure 1.7. Using a simple electrostatic argument, the second oxidation potential E_2 is expected to be shifted anodically to the first oxidation potential, E_1 because it is more thermodynamically unfavourable to remove an electron from a positively charged $[M\text{-}M]^+$ than a parent neutral [M-M] complex. However, subtle situations can also arise where solvent induced stabilisation of the charged states is sufficient to invert the first and second oxidation potentials. For example, whilst the monocationic species may be sufficiently delocalised that it serves to decrease the net charge density and reduce solvation effects, in the dicationic species, charge localisation at the ends of the molecule may become more pronounced. As a result, there is a decrease in electrostatic interactions and an increase in stabilisation induced by solvation effects. This can decrease the value of the redox potential difference and ultimately give rise to a single apparent two electron process. Thus, assessing electronic structure based on the separation of the two redox waves, whilst a commonly employed argument in the literature, is fundamentally unsound.

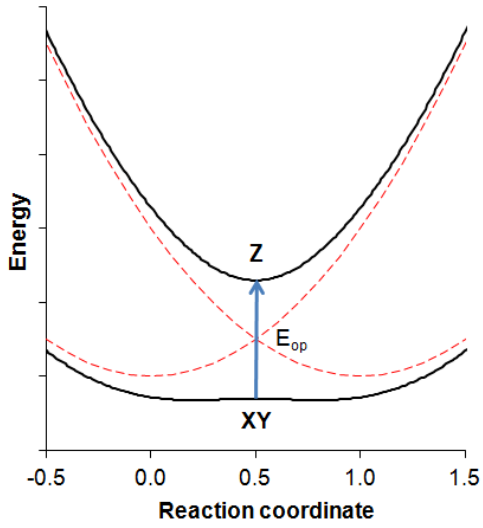

Figure 1.7. Potential energy curve in a ligand bridged bimetallic complex with strong electronic coupling. The dotted and solid curves represent the diabatic and adiabatic surfaces respectively.

In between these extremes lie Class II MV complexes, in which the potential energy surfaces for the two localised descriptions are only subtly mixed giving rise to a double minimum in the ground state curve (**XY**) and an excited adiabatic state (**Z**), Figure 1.8. Thus in addition to the properties associated with the distinct sites, new properties related to the thermal and photochemical intramolecular electron transfer reaction are also observed.[44] With regards to the thermal pathway, according to the Franck Condon Principle, electron motion (10^{-15} s) occurs at a rate much faster than nuclear motion (10^{-13} s). Instantaneous electron transfer from the M^+-M to M-M^+ state would lead to a vibrationally excited state, in which a species with charge M^+ is formed in the equilibrium geometry of M, and vice versa, which is forbidden on the grounds of energy conservation. The nuclear configurations at each site must therefore reorganise and reach an intermediate geometry prior to electron transfer, hence giving rise to a thermal activation barrier to the electron transfer process (E^*_{th}), Scheme 1.3 upper path.

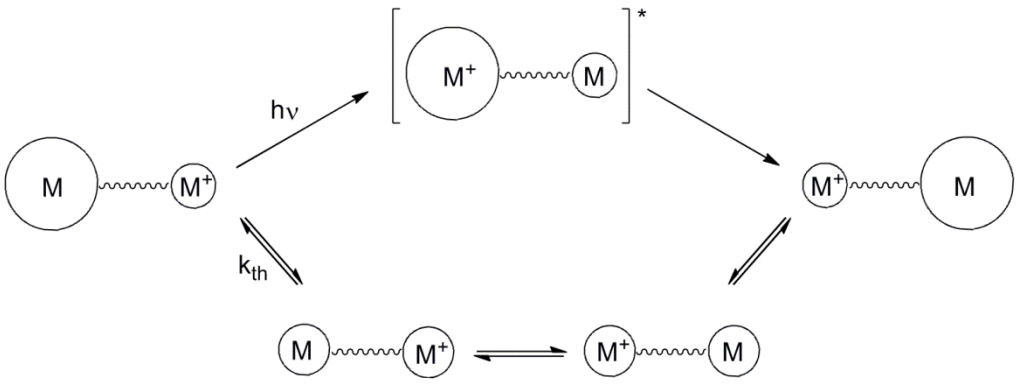

Scheme 1.3. Thermal and optical electron transfer processes in a MV complex.

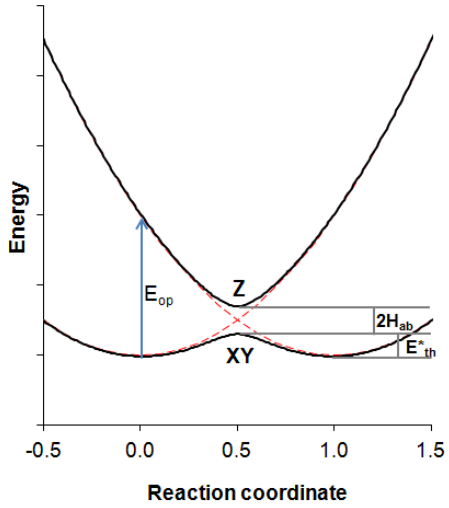

Figure 1.8. Potential energy curve in a ligand bridged bimetallic with weak coupling. The solid and dotted curves represent the diabatic and adiabatic surfaces respectively.

In a Class II MV complex, electron transfer from M^{+}-M to M-M^{+} can also take place *via* an optically induced electron transfer. This leads to the development of a characteristic broad solvent dependent absorbance band in the near infrared (NIR) region, which is often referred to as an intervalence charge transfer (IVCT) transition. Hush has provided a theoretical model linking the parameters of IVCT bands to barriers for electron transfer, as derived from Marcus theory.[45,46]

$$\nu_{max} = h\nu = \lambda_i + \lambda_o + \Delta E_0 + \Delta E'$$

where the Franck-Condon factors λ_i and λ_o correspond to the reorganisation energies within the inner- and outer-sphere respectively, ΔE_0 is the energy difference between the vibrationally relaxed initial and final states in the absence of electronic coupling and $\Delta E'$ reflects the additional energy contributions due to spin orbit coupling and ligand field asymmetry.[47]

The frequency of the optical transition, E_{op} can be related to the activation energy of thermal electron transfer, E^*_{th}.

$$E_{op} = 4E^*_{th}$$

From this relationship, Hush predicted that for an optical absorption band of a weakly coupled symmetric species, the bandwidth at half height intensity $\Delta\nu_{1/2}$ is a function of the band maximum ν_{max} and the coupling parameter H_{ab}.

$$\Delta\nu_{1/2} = \sqrt{2310\nu_{max}}$$

$$H_{ab} = \frac{2.06 \times 10^{-2}}{r_{ab}} \sqrt{\nu_{max}\varepsilon_{max}\nu_{1/2}}$$

where ν_{max} is the energy ε_{max} is the intensity of the band, and r_{ab} the effective electron transfer distance.

For a Class II MV complex, the bandwidth at half height of the IVCT transition can be larger than or close to the theoretical value derived from the Hush analysis. However, in a Class III MV complex, a photoinduced electron transfer leads to an electronic transition between two delocalised molecular orbitals. This gives rise to an electronic absorption band which is solvent independent (solvent sphere reorganisation is not necessary) and usually narrower than that derived from the Hush relationships. In Class III MV systems, the coupling constant is given by

$$2H_{ab} = \lambda$$

In reality, the transition between the localised to delocalised limit is not abrupt, but rather, there is a gradual change in behaviour. This has led to the addition of several new sub-classes in the original Robin and Day system. For example Class II-III MV complexes, which exhibit intermediate behaviour between that of Class II and Class III MV complexes, are those in which electron transfer is faster than solvent reorganisation. Following an ongoing debate which has been alive since the 1960's, there is now a general consensus that the Cruetz-Taube ion (Figure 1.9) is delocalised, though there is evidence for localisation, and thus it is a typical example of a Class II-III MV complex.[48] The parameters which define the localisation and delocalisation limit centre upon the relative magnitude of the coupling parameter and the reorganisation energy. When describing MV complexes, it is important to define localisation, averaging and delocalisation with care, for example in Class II and Class III MV complexes, the solvent and exchanging electron is localised and delocalised respectively, whereas in Class II-III MV complexes, the solvent is averaged whilst the exchanging electron is localised. The solvent averaging in Class III MV complexes ultimately leads to narrow bandwidths, and the absence of a solvent independent IVCT transition is evidence that the solvent is no longer strongly coupled to the electron transfer.[48]

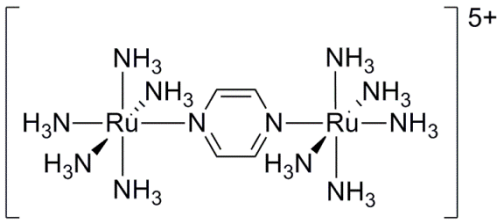

Figure 1.9. The Cruetz Taube ion.

The shift between the localised to delocalised regimes is driven by the increase in the coupling parameter H_{ab}. This can have an effect on the IVCT band shape for a symmetrical dinuclear MV complex.[47] For example, when $2H_{ab} << \lambda$, then this produces a Gaussian shaped contour that is symmetrical, Figure 1.10a and b. However, as H_{ab} increases, the band becomes truncated on the low energy side, which is characteristic of IVCT bands which are Gaussian on the high energy side, and progressively "cut off" on the low energy side. At the transition between Class II and Class III MV complexes where $2H_{ab} = \lambda$, the band retains intensity at higher energy, Figure 1.10c. When $2H_{ab} > \nu_{max}$, the asymmetrically shaped band shifts to even higher energy, increases in intensity and becomes narrower, Figure 1.10d.

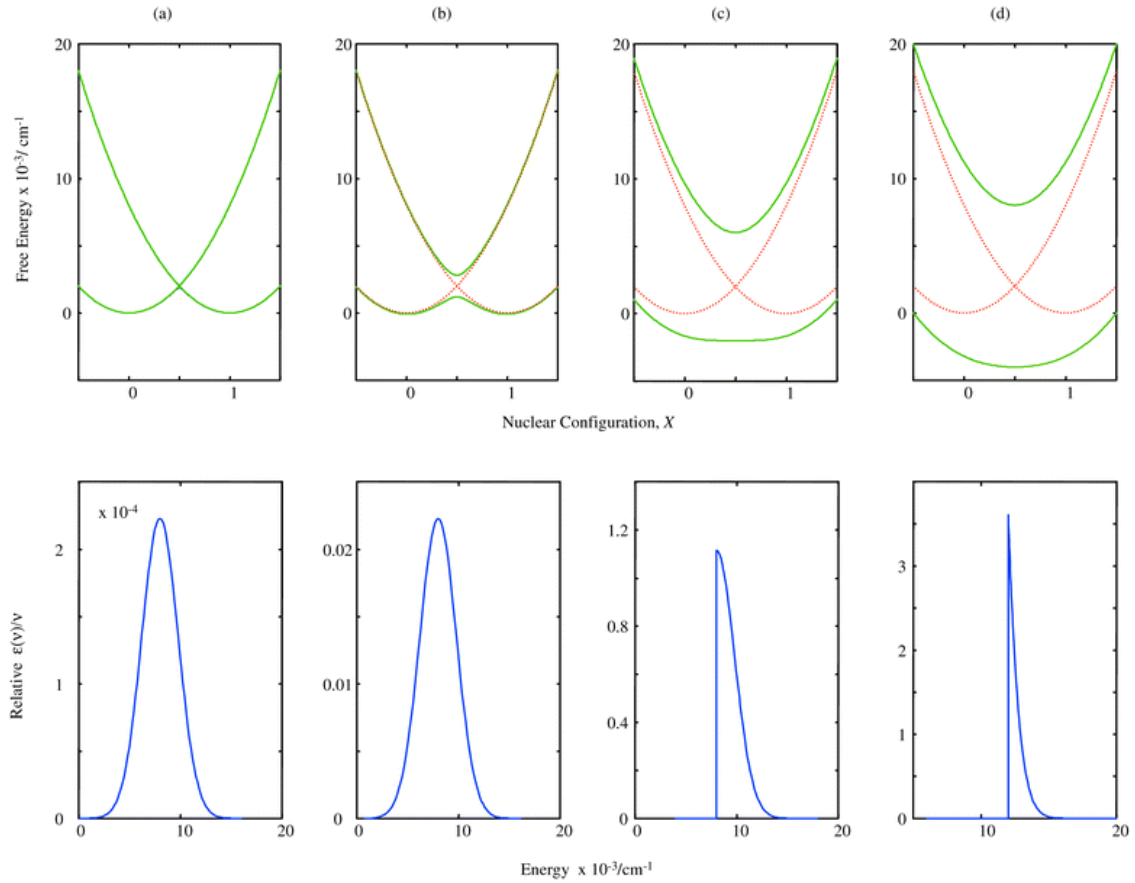

Figure 1.10. The two state classical model: potential energy surfaces and band shape predictions for a symmetrical MV system as the coupling becomes stronger and stronger.

The analysis of IVCT bands can however, also be complicated by the presence of multiple underlying IVCT transitions which arise from the effects of ligand field asymmetry and spin-orbit coupling effects.[49] Ligand bridged bimetallic d^6 – d^5 complexes can exhibit up to five low energy transitions, three of IVCT and two of interconfigorational (IC) origin, Figure 1.11. If the spacing between the spin orbit states is sufficiently large, then three distinguishable IVCT transitions can be observed, although they can be closely spaced. The IC (d-d) bands can be found in the near-IR region and overlap with genuine IVCT bands, as can transitions to higher bridge states. The IC bands are generally low in intensity because they are Laporte forbidden, but can also gain intensity through intensity borrowing through spin-orbit mixing and metal-ligand mixing.[48]

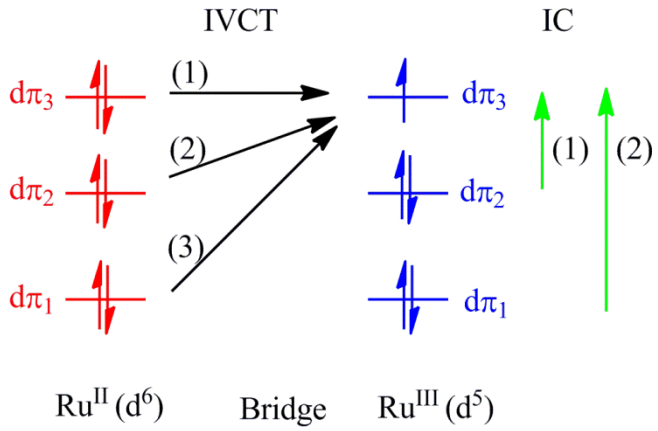

Figure 1.11. Intervalence (IT) and interconfigorational (IC) transitions in d^6-d^5 MV systems.[49]

Moving beyond the initial Hush (two state) model, the three state model,[50] proposed by Brunschwig, Cruetz and Sutin, provides an extension to the classical two state model by incorporating a third electronic state which accounts for the role of the bridging ligand (**W**) in mediating electronic coupling between the metal based sites. In these systems, the direct coupling between the metal centres is essentially zero, with electron transfer mediated by charge transfer to or from a bridging group (**W**) that is sufficiently low in energy, thus giving rise to the three state model, Figure 1.12. The major difference between the two and three state model is the allowance of the latter for a second absorption, of either MLCT or LMCT character, at higher energy than IVCT. In the three state model, as the coupling increases within the Class II regime, the intensity of both MLCT / LMCT and MMCT transition also increases, Figure 1.13a and 1.13b. At the Class II-III transition, the MLCT / LMCT intensity vanishes and the MMCT transition becomes narrow and intense, Figure 1.13c. The inclusion of a fourth electronic state is sometimes required to qualitatively reproduce the experimental observation of multiple MLCT transitions for strongly coupled systems.

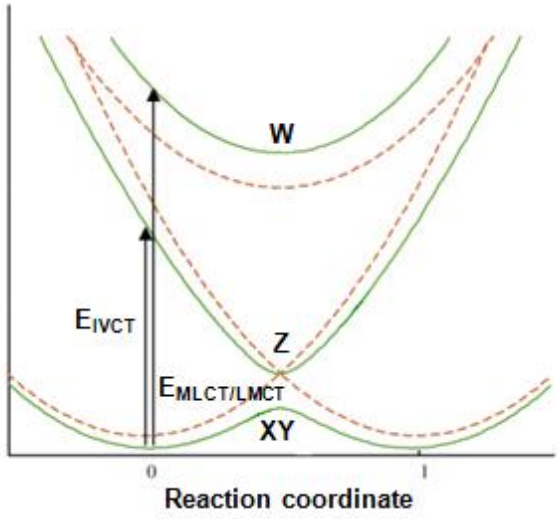

Figure 1.12. Three state model with a low lying bridge state (W).

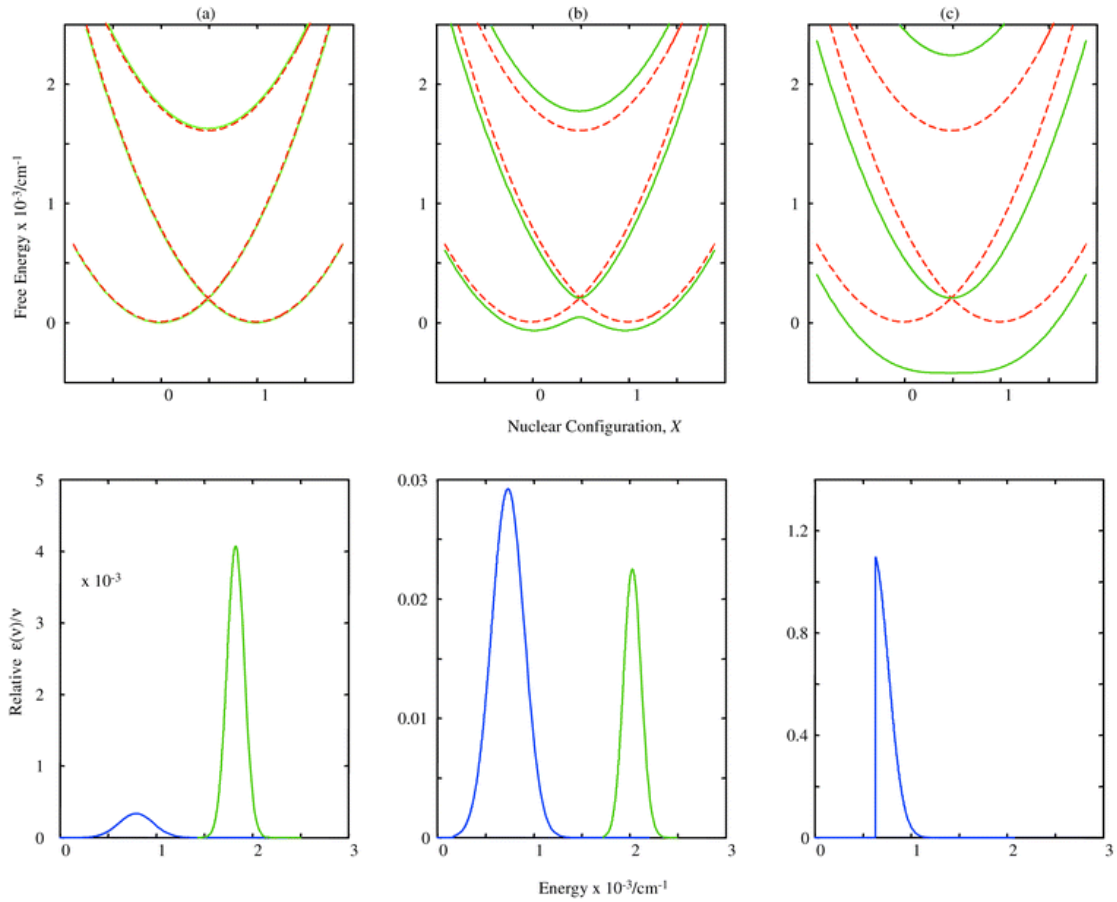

Figure 1.13. The three state model: potential energy surfaces and band shape predictions for a symmetrical MV system which incorporate a low lying bridge state. In the simulations, the blue band is the IVCT transition, whilst the green band is the MLCT / LMCT transition.

The assessment of the electronic nature of MV complexes is not restricted to electronic spectroscopic data. In a series of ligand bridged bis(ruthenium) cluster complexes, Kubiak and co-workers have used the ν(C≡O) band to monitor the rate of electron exchange as a function of the bridge structure[51-54] and solvation environment,[55] with it being possible to fine tune the electronic coupling between the cluster units, Figure 1.14, by alternating the nature of the ancillary ligands attached to the pyrazine ring. These reduced bis(cluster) ruthenium complexes have been considered in terms of a three state model, with the additional unpaired electron exchanging between any of the two cluster band states and a bridge based electronic state.[53] When this three state model is extended into a five state model, Figure 1.15, the energies and molecular

orbitals of the ancillary pyridyl ligands are considered, as the ligands attached can also affect the electronic interactions between the two redox sites. Whilst the electronic behaviour of the MV transition is not remarkably different from the three state model, involving two symmetry allowed transitions of the single electron from the bridge to two individual nitrogen atoms.[51]

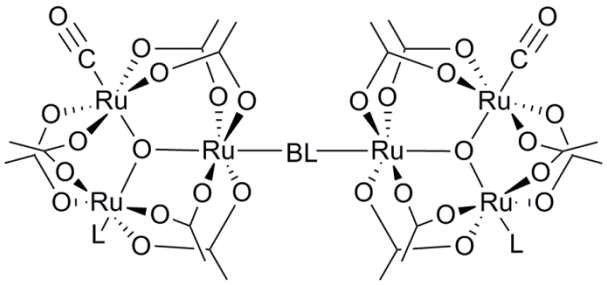

Figure 1.14. Ligand bridged bis(ruthenium) cluster complexes.

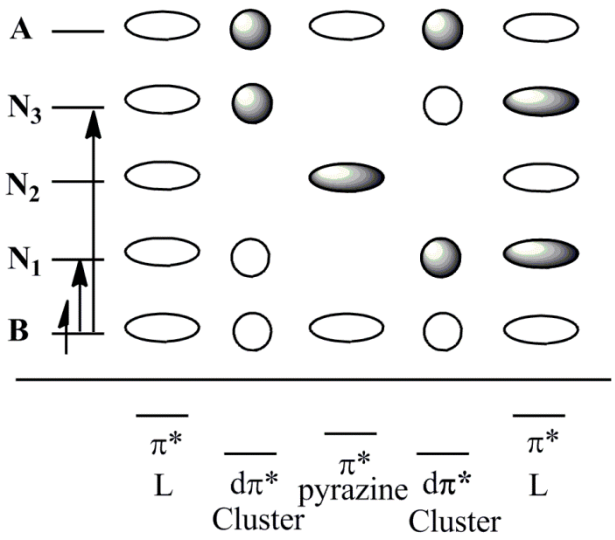

Figure 1.15. Molecular orbitals in a five state model, with electron occupation in the reduced ligand bridged bis(ruthenium) cluster complexes. The two symmetry allowed transitions are shown on the left of the diagram.

Recently, Chisholm and co-workers[56] have prepared and studied a series of oxalate bridged complexes of the general form $[\{(^tBuCO_2)_3MM\}_2\text{-}(\mu_2\text{-}O_2CCO_2)]$ where MM = Mo_2, MoW and W_2 as test beds for MV theory, as a function of temperature and solvent. Whilst in the oxidised states, the presence of an IVCT transition which is solvent independent is consistent with a Class III MV complex according to the Robin and Day classification scheme, the existence of both a solvent independent IVCT and MLCT transition in the neutral and oxidised states has led to the proposal of a new class of MV complexes, Class IV.

Over the years, the vast majority of work has focused on the characterisation of MV systems where two metal centres are connected *via* a conjugated bridge. Organic MV systems, for example compounds based on triarylamine groups, are gaining increasing attention as models by which the electron transfer can be modelled.[57-60] New developments are also emerging, with reports of MV complexes with an inverse architecture incorporating two organic redox centres, connected through a central organometallic based bridge appearing in the literature.[61,62] For example, Parise and co-workers have investigated some bis(ditolyl-3-pyridylamine) ruthenium bridged bipyridine complexes[63] and S.R. Marder and co-workers a bis(alkynyl triarylamine) platinum complex,[64] with experimental studies suggesting the oxidised form of this complex to be an example of a weakly coupled Class II MV complex.

1.1.1 Thesis Outline

The removal of an electron from a bimetallic complex where two metal centres are connected *via* a conjugated bridge leads to the generation of a MV complex. In a Class II MV complex, the presence of a low energy transition in the near-IR region is characteristic of a metal-metal charge transfer transition. However, this metal-metal charge transfer transition may not be genuine, and is dependent on the involvement of the bridge (or how low lying it is), which can lead to a situation where the unpaired electron or hole is heavily localised on the bridging ligand.

This thesis will explore and address the challenges in rationalising the electron transfer reaction in some linear and Y-shaped carbon rich organometallic complexes, where two and three metal centres are connected by an organic bridging ligand, respectively. These complexes will first be synthesised and then investigated using a number of techniques such as cyclic voltammetry, spectroscopy, together with supporting computational studies to allow for the rationalisation of their electronic structures. At the heart of this thesis is the concept of genuine MV complexes (Chapter 2), to complexes which feature redox non-innocent bridging ligands (Chapter 3 and 4), to those redox centres where there exists no interaction (Chapter 5). In addition to this, we shall also explore some gold mediated Sonogashira reactions (Chapter 6). Each Chapter carries an introduction that more precisely defines the background to the particular area of study described.

1.1.2 References

(1) Shirakawa, H.; Louis, E. J.; MacDiarmid, A. G.; Chiang, C. K.; Heeger, A. J. *J. Chem. Soc., Chem. Commun.* **1977**, 578.
(2) Burroughes, J. H.; Bradley, D. D. C.; Brown, A. R.; Marks, R. N.; Mackay, K.; Friend, R. H.; Burns, P. L.; Holmes, A. B. *Nature* **1990**, *347*, 539.
(3) Granström, M. *Polym. Adv. Technol.* **1997**, *8*, 424.
(4) Frapper, G.; Kertesz, M. *Inorg. Chem.* **1993**, *32*, 732.
(5) Holliday, B. J.; Stanford, T. B.; Swager, T. M. *Chem. Mater.* **2006**, *18*, 5649.
(6) Choi, T.-L.; Lee, K.-H.; Joo, W.-J.; Lee, S.; Lee, T.-W.; Chae, M. Y. *J. Am. Chem. Soc.* **2007**, *129*, 9842.
(7) Knapton, D.; Rowan, S. J.; Weder, C. *Macromolecules* **2005**, *39*, 651.
(8) Arimoto, F. S.; Haven, A. C. *J. Am. Chem. Soc.* **1955**, *77*, 6295.
(9) *Metal-Containing and Metallosupramolecular Polymers and Materials*; Schubert, U. S.; Newkome, G. R.; Manners, I., Eds.; American Chemical Society, Washington, DC, 2006.
(10) *Metal-Containing Polymeric Materials*; C.U. Pittman, J.; C.E. Carraher, J.; Zeldin, M.; Sheats, J. E.; Culbertson, B. M., Eds.; Plenum Press, 1996.
(11) Stanley, J. M.; Holliday, B. J. *Coord. Chem. Rev.* **2012**, *256*, 1520.
(12) Whittell, G. R.; Manners, I. *Adv. Mater.* **2007**, *19*, 3439.
(13) Ni, Y. Z.; Rulkens, R.; Manners, I. *J. Am. Chem. Soc.* **1996**, *118*, 4102.
(14) Rulkens, R.; Gates, D. P.; Balaishis, D.; Pudelski, J. K.; McIntosh, D. F.; Lough, A. J.; Manners, I. *J. Am. Chem. Soc.* **1997**, *119*, 10976.
(15) Jäkle, F.; Rulkens, R.; Zech, G.; Foucher, D. A.; Lough, A. J.; Manners, I, *Chem. Eur. J.*, **1998**, *4*, 2117.
(16) Gomez-Elipe, P.; Resendes, R.; Macdonald, P. M.; Manners, I. *J. Am. Chem. Soc.* **1998**, *120*, 8348.
(17) Sonogashira, K.; Ohga, K.; Takahashi, S.; Hagihara, N. *J. Organomet. Chem.* **1980**, *188*, 237.
(18) Davies, S. J.; Johnson, B. F. G.; Khan, M. S.; Lewis, J. *J. Chem. Soc., Chem. Commun.* **1991**, 187.
(19) Khan, M. S.; Davies, S. J.; Kakkar, A. K.; Schwartz, D.; Lin, B.; Johnson, B. F. G.; Lewis, J. *J. Organomet. Chem.* **1992**, *424*, 87.
(20) Khan, M. S.; Kakkar, A. K.; Ingham, S. L.; Raithby, P. R.; Lewis, J.; Spencer, B.; Wittmann, F.; Friend, R. H. *J. Organomet. Chem.* **1994**, *472*, 247.
(21) Foucher, D. A.; Tang, B. Z.; Manners, I. *J. Am. Chem. Soc.* **1992**, *114*, 6246.
(22) Hurst, S. K.; Cifuentes, M. P.; Humphrey, M. G. *Organometallics* **2002**, *21*, 2353.
(23) Powell, C. E.; Hurst, S. K.; Morrall, J. P.; Cifuentes, M. P.; Roberts, R. L.; Samoc, M.; Humphrey, M. G. *Organometallics* **2007**, *26*, 4456.
(24) Green, K. A.; Cifuentes, M. P.; Samoc, M.; Humphrey, M. G. *Coord. Chem. Rev.* **2011**, *255*, 2025.
(25) Powell, C. E.; Cifuentes, M. P.; Humphrey, M. G.; Willis, A. C.; Morrall, J. P.; Samoc, M. *Polyhedron*, **2007**, *26*, 284.
(26) Dong, Y. B.; Layland, R. C.; Smith, M. D.; Pschirer, N. G.; Bunz, U. H. F.; zur Loye, H. C. *Inorg. Chem.* **1999**, *38*, 3056.
(27) Dong, Y. B.; Layland, R. C.; Pschirer, N. G.; Smith, M. D.; Bunz, U. H. F.; zur Loye, H. C. *Chem. Mater.* **1999**, *11*, 1413.

(28) Pschirer, N. G.; Ciurtin, D. M.; Smith, M. D.; Bunz, U. H. F.; zur Loye, H. C. *Angew. Chem. Int. Ed.*, **2002**, *41*, 583.
(29) Bunz, U. H. F. *Chem. Rev.* **2000**, *100*, 1605.
(30) McDonagh, A. M.; Humphrey, M. G.; Samoc, M.; Luther-Davies, B. *Organometallics* **1999**, *18*, 5195.
(31) Cifuentes, M. P.; Powell, C. E.; Morrall, J. P.; McDonagh, A. M.; Lucas, N. T.; Humphrey, M. G.; Samoc, M.; Houbrechts, S.; Asselberghs, I.; Clays, K.; Persoons, A.; Isoshima, T. *J. Am. Chem. Soc.* **2006**, *128*, 10819.
(32) Whittell, G. R.; Hager, M. D.; Schubert, U. S.; Manners, I. *Nat. Mater.* **2011**, *10*, 176.
(33) Holliday, B. J.; Swager, T. M. *Chem. Commun.* **2005**, 23.
(34) Naleway, C. A.; Curtiss, L. A.; Miller, J. R. *J. Phys. Chem B*, **1991**, *95*, 8434.
(35) Winters, M. U.; Pettersson, K.; Mårtensson, J.; Albinsson, B. *Chem. Eur. J*, **2005**, *11*, 562.
(36) Pourtois, G.; Beljonne, D.; Cornil, J.; Ratner, M. A.; Bredas, J. L. *J. Am. Chem. Soc.* **2002**, *124*, 4436.
(37) Wenger, O. S. *Acc. Chem. Res.* **2010**, *44*, 25.
(38) Low, P. J.; Brown, N. J. *J. Cluster Sci.* **2010**, *21*, 235.
(39) Barrière, F.; Camire, N.; Geiger, W. E.; Mueller-Westerhoff, U. T.; Sanders, R. *J. Am. Chem. Soc.* **2002**, *124*, 7262.
(40) Barriere, F.; Geiger, W. E. *J. Am. Chem. Soc.* **2006**, *128*, 3980.
(41) Geiger, W. E.; Barriere, F. *Acc. Chem. Res.* **2010**, *43*, 1030.
(42) Diallo, A. K.; Daran, J.-C.; Varret, F.; Ruiz, J.; Astruc, D. *Angew. Chem. Int. Ed.* **2009**, *48*, 3141.
(43) Robin, M. B.; Day, P. *Adv. Inorg. Chem. Radiochem.* 1968, **10**, 247-422.
(44) Creutz, C. *Prog. Inorg. Chem.* **1983**, *30*, 1.
(45) Allen, G. C.; Hush, N. S. *Prog. Inorg. Chem.* **1967**, *8*, 357.
(46) Hush, N. S. *Prog. Inorg. Chem.* **1967**, *8*, 391.
(47) D'Alessandro, D. M.; Keene, F. R. *Chem. Soc. Rev.* **2006**, *35*, 424.
(48) Demadis, K. D.; Hartshorn, C. M.; Meyer, T. J. *Chem. Rev.* **2001**, *101*, 2655.
(49) Rocha, R. C.; Rein, F. N.; Jude, H.; Shreve, A. P.; Concepcion, J. J.; Meyer, T. J. *Angew. Chem.* **2008**, *120*, 513.
(50) Brunschwig, B. S.; Creutz, C.; Sutin, N. *Chem. Soc. Rev.* **2002**, *31*, 168.
(51) Salsman, J. C.; Ronco, S.; Londergan, C. H.; Kubiak, C. P. *Inorg. Chem.* **2005**, *45*, 547.
(52) Ito, T.; Hamaguchi, T.; Nagino, H.; Yamaguchi, T.; Kido, H.; Zavarine, I. S.; Richmond, T.; Washington, J.; Kubiak, C. P. *J. Am. Chem. Soc.* **1999**, *121*, 4625.
(53) Londergan, C. H.; Kubiak, C. P. *J. Phys. Chem. A*, **2003**, *107*, 9301.
(54) Glover, S. D.; Goeltz, J. C.; Lear, B. J.; Kubiak, C. P. *Coord. Chem. Rev.* **2010**, *254*, 331.
(55) Londergan, C. H.; Salsman, J. C.; Ronco, S.; Dolkas, L. M.; Kubiak, C. P. *J. Am. Chem. Soc.* **2002**, *124*, 6236.
(56) Lear, B. J.; Chisholm, M. H. *Inorg. Chem.* **2009**, *48*, 10954.
(57) Lambert, C.; Nöll, G. *J. Am. Chem. Soc.* **1999**, *121*, 8434.
(58) Lambert, C.; Noll, G.; Schelter, J. *Nat. Mat.*, **2002**, *1*, 69.
(59) Lambert, C.; Amthor, S.; Schelter, J. *J. Phys. Chem. A* **2004**, *108*, 6474.
(60) Heckmann, A.; Lambert, C. *Angew. Chem. Int. Ed.*, **2012**, *51*, 326.
(61) Adams, D. M.; Hendrickson, D. N. *J. Am. Chem. Soc.* **1996**, *118*, 11515.
(62) Chang, H.-C.; Miyasaka, H.; Kitagawa, S. *Inorg. Chem.* **2000**, *40*, 146.

(63) Ramírez, C. L.; Pegoraro, C. N.; Filevich, O.; Bruttomeso, A.; Etchenique, R.; Parise, A. R. *Inorg. Chem.* **2012**, *51*, 1261.
(64) Jones, S. C.; Coropceanu, V.; Barlow, S.; Kinnibrugh, T.; Timofeeva, T.; Bredas, J. L.; Marder, S. R. *J. Am. Chem. Soc.* **2004**, *126*, 11782.

Chapter 2. Self-Assembled Molecular Wires

2.1 Introduction

Ligand bridged bimetallics featuring two metal centres connected *via* a conjugated bridge and MV species derived from them are ideal systems by which we can study the intramolecular electron transfer reaction. In this regard, alkyne-based bridging ligands offer many special advantages, being highly conjugated and possessing cylindrical or pseudo-cylindrical symmetry. However, the synthetic access to such molecular-based bimetallic systems heavily depends on the availability of a suitable bis(alkyne) precursor of a carbon spacer and by the existence of suitable metallation, purification and oxidation protocols.[1] To date, a number of iron based molecular systems have been synthesised, for example [{Cp*(dppe)Fe}$_2$(μ-C≡C-C≡C)] (**1**), [{Cp*(dppe)Fe}$_2$(μ-C≡C-C_6H_4-C≡C)] (**2**) and [{Cp*(dppe)Fe}$_2$(μ-C≡C-(C_6H_4)$_2$-C≡C)] (**3**) to name but a few, Figure 2.1.

In MV complexes, the polyyne bridge, -(C≡C)$_n$-, has been demonstrated to be effective at mediating electron transfer between iron centres. For example, complex **1** exhibits two reversible oxidation waves in 0.1 M NBu_4PF_6 / CH_2Cl_2 vs. SCE ($E_{1/2}$ = –0.67, 0.05 V; $\Delta E_{1/2}$ = 720 mV), and spectroscopic characteristics indicative of strong coupling in [**1**]PF_6.[2] However, as the length of the carbon chain increases i.e. beyond eight,[3] there is notable decrease in the stability of MV complexes, and in the magnitude of the electronic interactions compared to shorter length carbon chains.[4]

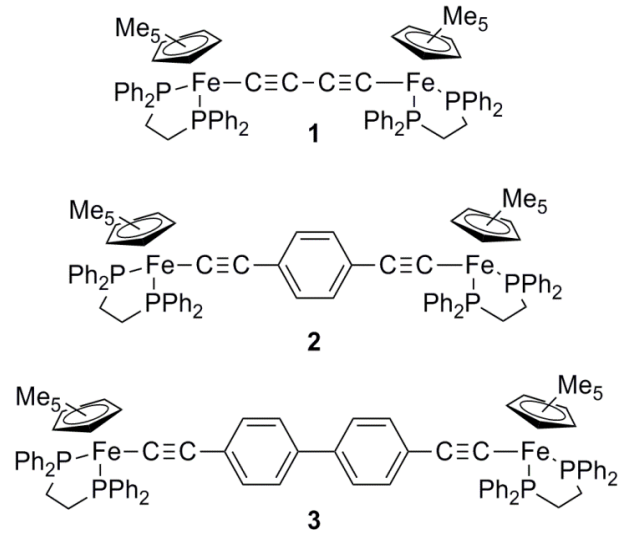

Figure 2.1. Complexes 1 – 3.

In order to improve the stability of these complexes, Lapinte and co-workers have modified the bridge through the insertion of a 1,4-phenylene moiety into the butadiyndiyl bridge. Complex **2** exhibited two reversible oxidation waves in 0.1 M NBu_4PF_6 / CH_2Cl_2 vs. SCE ($E_{1/2}$ = –0.27, 0.01 V; $\Delta E_{1/2}$ = 280 mV), with a significant decrease in the electronic interactions from that of **1**.[5] The conceptual insertion of a further 1,4-phenylene unit into **2** leads to the formation of **3**, which exhibits a single, two electron reversible wave and which represents a further decrease in the magnitude of electronic interaction between the two iron centres.[6] In **3**, the $E_{1/2}$ of the first and second redox waves were derived from the midpoint between the anodic and cathodic peaks and the distance between them, with $E_{1/2}$ falling at –0.17 and –0.11 V in 0.1 M NBu_4PF_6 / CH_2Cl_2 vs. SCE. This was possible because there were negligible variations in ΔE_p as a function of the scan rate and hence the kinetics of the electron transfer does not affect the cyclic voltammetric response.

The large redox potential differences in **1** and **2** led to significant K_c values of 1.6 x 10^{12} and 2.6 x 10^4 respectively, suggesting that the MV states are stable enough to be generated, and to exist free of the neutral and dicationic forms of the complexes. Subsequent reaction of **1** and **2** with one and two equivalents of Fc[PF_6] by chemical oxidation led to the generation of [**1**]PF_6, [**1**][PF_6]$_2$, [**2**]PF_6 and [**2**][PF_6]$_2$, which were isolated as solids. The IR spectrum of [**1**]PF_6 revealed two bands corresponding to the symmetric and asymmetric ν(C≡C) stretches at 1880 and 1973 cm^{-1} which occurs at a frequency intermediate between **1** (ν(C≡C) 1880, 1955 cm^{-1}) and [**1**][PF_6]$_2$ (ν(C≡C) 1950, 2160 cm^{-1}).[2] This reveals the delocalised nature of [**1**]PF_6 and implies that the rate of electron transfer is faster than 10^{12} s^{-1}. In [**1**]PF_6 a unique low energy absorption in the NIR region was assigned to an IVCT transition. The fact that the position of this IVCT band was independent of solvent and that the bandwidth at half height ($\Delta\nu_{1/2}$) was significantly narrower than that derived from Hush's relationship[7] is consistent with the assignment of [**1**]PF_6 as a Class III MV complex.[8]

On the other hand, [**2**]PF_6 was found to exhibit characteristics of both a localised and delocalised MV complex. For example, in ^{57}Fe Mössbauer spectroscopy, which is often used to differentiate the oxidation states of iron atoms, [**2**]PF_6 revealed the presence of Fe(II), Fe(III) and an intermediate valence state.[5] The valence trapped and detrapped signal ratios were also found to depend on the solid sample, with multiple recrystallisations also leading to a variation in the percentage of valence detrapped form (44 – 77 % at 77 K). Likewise, IR spectroscopy did not afford an unambiguous conclusion that [**2**]PF_6 was valence trapped or detrapped. Taken together, these results indicate that [**2**]PF_6 exhibits characteristics of both a localised and delocalised MV complex.[9] More recent studies with analogous ruthenium species suggest that the

relative conformation of the aryl ring in the bridge relative to the Fe(dppe)Cp* fragments may play a significant role in governing the electronic structure.[10]

The small potential difference in **3** of ca. 60 mV between the calculated redox potentials leads to a K_c of ca. 10; this value is small and very close to the statistical limit of 4.[6] Chemical oxidation of **3** with two equivalents of $Fc[PF_6]$ led to the formation of $[\mathbf{3}][PF_6]_2$. The MV complex $[\mathbf{3}]PF_6$ was generated through mixing equimolar amounts of **3** and $[\mathbf{3}][PF_6]_2$, though it is unlikely to exist free of the latter forms. Nevertheless, a new unique transition developed in the NIR region, which was not present in solution of pure **3** or $[\mathbf{3}][PF_6]_2$ and which exhibited solvatochromic behaviour. The experimental bandwidth at half height is in excellent agreement with the theoretical value, revealing $[\mathbf{3}]PF_6$ as an example of a weakly coupled Class II MV complex according to the Robin and Day classification scheme.

2.1.1 Pyridine as a Coordinating Unit

In order to access less synthetically demanding routes towards organoiron wire-like molecules, the coordination reactions of some mononuclear compounds in which a redox active organoiron fragment is appended to a coordinating pyridine unit[11-13] has attracted interest. For example, from the Sonogashira coupling of [Fe(C≡CH)(dppe)Cp*] and 4-bromopyridine, Lapinte and co-workers have synthesised the complex [Fe(C≡C-4-Py)(dppe)Cp*] (where Py = pyridine), which following reaction with half an equivalent of $[PdCl_2(PhCN)_2]$ yielded the trimetallic assembly, $[\{Cp^*(dppe)(Py\text{-}4\text{-}C{\equiv}CFe\}_2(\mu\text{-}PdCl_2)]$, Figure 2.2. However, electrochemical studies

reveals a single wave for the two Fe(II)/Fe(III) redox processes, whilst the NIR spectra does not exhibit a low energy band indicative of IVCT. Thus, there is negligible coupling between the iron centres through the platinum atom, showing that adiabatic electron transfer is weak or non-existent, and so is a Class I MV complex.[14]

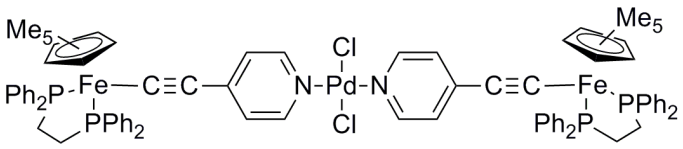

Figure 2.2. The trimetallic assembly [{Cp*(dppe)(Py-4-C≡C)Fe}$_2$(μ-PdCl$_2$)].

Since this initial report, research in this field has expanded to incorporate a variety of redox active metals attached to a central connector. For example, Che and co-workers have reported the synthesis of molecular rods based on a ruthenium(II) macrocyclic bis(acetylide) building block, with rhenium end groups.[15] This occurs *via* the reaction of [RuCl$_2$(16-TMC)]Cl where TMC = 1,5,9,12-tetramethyl-1,5,9,13-tetraazacyclohexadecane) with zinc amalgam, NaOMe and 4-ethynylpyridine to generate [Ru(C≡C-4-Py)$_2$(16-TMC)], which when reacted with two equivalents of [Re(bpy)(CO)$_3$(MeCN)]OTf (bpy = bipyridine) leads to the formation of [{Re(bpy)(CO)$_3$}{μ-Ru(C≡C-4-Py)(16-TMC)}](OTf)$_2$, Figure 2.3.

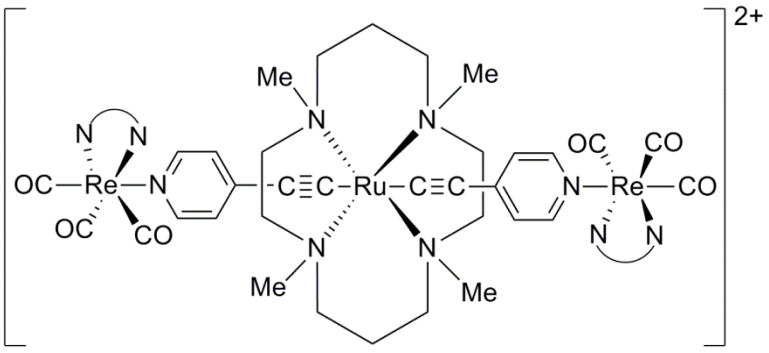

Figure 2.3. The trimetallic assembly [{Re(bpy)(CO)$_3$}$_2${μ-Ru-(C≡C-4-Py)$_2$(16-TMC)}](OTf)$_2$.

Kühn[16] and Hor and co-workers[17] have also explored the reactions of *cis*-$[RuCl_2(dppm)_2]$ and *trans*-$[RuCl_2(dmpe)_2]$ (dppm = bis(diphenylphosphino)methane and dmpe = 1,2-bis(dimethylphosphino)ethane) in a stepwise manner, generating trimetallic assemblies of interest. For example, the reaction of *cis*-$[RuCl_2(dppm)_2]$ with HC≡CPy-4.HCl and $NaPF_6$ gives rise to a mononuclear Ru(II) complex with a pendant pyridyl moiety, which when reacted with $[MCl_2(CH_3CN)_2]$ in CH_2Cl_2 at room temperature gives $[(dppm)_2(Py\text{-}4\text{-}C{\equiv}C)Ru\}_2(\mu\text{-}PdCl_2)]$, Figure 2.4. Similarly, the reaction of a bis(pyridylacetylide) ruthenium complex with two equivalents of $[\{Re(bpy)(CO)_3\}(MeCN)](OTf)]$ in THF under reflux gave $[\{Re(bpy)(CO)_3\}_2(\mu\text{-}Re(C{\equiv}C\text{-}4\text{-}Py)_2(dppe)_2\}](OTf)_2$, Figure 2.4. Key to the syntheses of these complexes is the control of metal alignment through the use of geometrically defined spacers as the bidentate dppm and dmpe ligands are located *trans* about the ruthenium, giving way for the coordination of one or two acetylide pyridine moieties. However, while trimetallic molecular based systems have been successfully synthesised through the coordination reactions of the pyridine unit, the redox responses of these systems have either been little explored in the context of MV complexes, or give rise to valence states where metal centres are localised and non-interacting.[14]

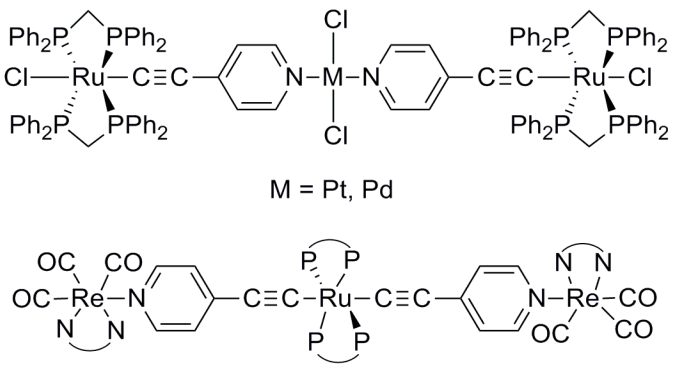

Figure 2.4. Examples of complexes synthesised by Kühn, Hor and co-workers.

2.1.2 Towards a Metal-based Bridge

Porphyrins are chemically and thermally stable molecules, with the ability to complex to both main group and transition metal ions.[18] Since the seminal work of Taube and co-workers, it has been widely established that the MV dimers of ruthenium(II) and osmium(II) possess electrons that are easily delocalised through π-acid ligands.[19-21] The potential of metalloporphyrins incorporating Ru(II) and Os(II) as conducting polymers has also been noted. For example, Collman and co-workers have synthesised octaethylporphyrin coordination polymers featuring pyrazine and 4,4'-bipyridine ligands, Scheme 2.1, which when oxidised with a non-stoichiometric amount of oxidant, typically I_2, $[Fc]PF_6$ or molecular O_2 form highly conductive polymers.[18] Electrochemical studies reveal the presence of metal centred anodic waves which reside at a significantly lower potential than the first ring oxidation of the porphyrin ring, implying that the metal centres are involved in the conduction. In addition, optical studies reveal the presence of a unique low energy transition in the NIR region on doping. Launay and workers also reported similar observations in some ruthenium porphyrin oligomers bridged by pyrazine and 4,4-azopyridine ligands (Scheme 2.1) i.e. a reversible oxidation wave for the Ru(II/III) redox couple was observed, and an IVCT band which was unique to the MV state.[22]

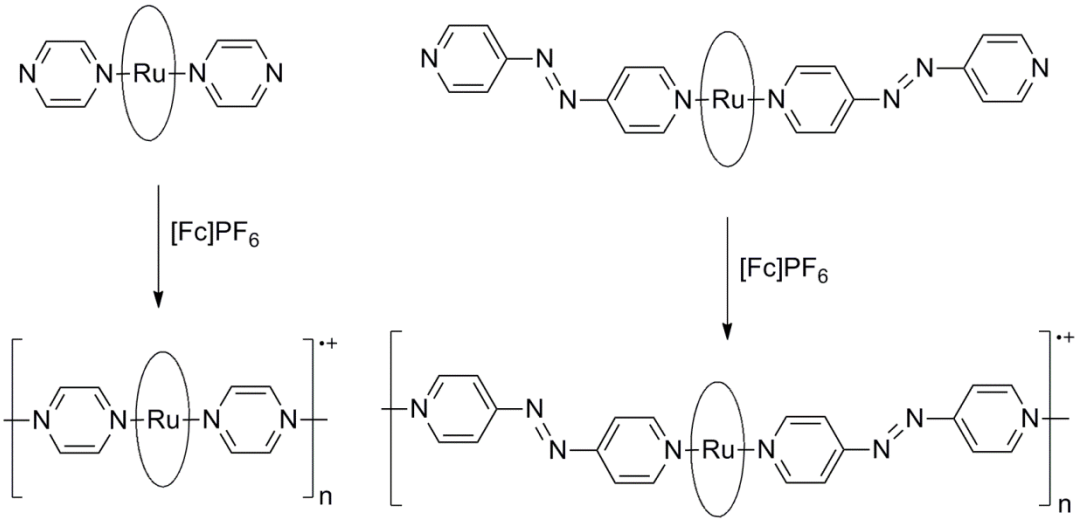

Scheme 2.1. Ruthenium octaethylporphyrin polymers featuring pyrazine and 4,4'-bipyridine ligands. The octaethylporphyrin motif is shown schematically as a ring.

In this Chapter, a simple synthetic route to a trimetallic molecular assembly featuring two redox-active organoiron fragments connected through a pendant 4-pyridyl moiety to a central ruthenium tetramesitylporphyrin 'socket' is described. The redox properties of this self-assembled molecular wire will be examined by electrochemical techniques, and the MV state examined by IR and NIR spectroscopy. The potential of these assemblies to behave as a molecular wire will be assessed through the classification of the MV state using the Robin and Day system.

2.2 Synthesis

The synthesis, characterisation and initial electrochemistry studies were carried out by colleagues at the University of Rennes 1, France. The reaction of two equivalents of the metallo-ligand [Fe(C≡C-4-Py)(dppe)Cp*][14] (**4**) with [(TMP)Ru($CH_3CN)_2$] (**5**) (which contains two labile acetonitrile ligands)[23] proceeded smoothly by self-assembly to give the trimetallic molecular wire **6**, Scheme 2.2, with the steric effects of the mesityl groups at the meso positions of the porphyrin ring not detrimental to the coordination chemistry of **4**.

2.2.1 Spectroscopic Investigations

The identity of **6** was confirmed by the usual spectroscopic methods including single crystal X-ray diffraction by the Rennes team, and presented here for completeness. The complexation of the metallo-ligand **4** to the Ru(II) centre of tetramesitylporphyrin (TMP) (**5**) was indicated by the characteristic shift of the pyridyl protons in ^{1}H NMR to high field due to the proximity to the porphyrin ring and associated currents,[24-27] with the pyridyl protons observed as doublets 4.96 and 3.31 ppm ($^3J_{HH}$ = 7 Hz) in benzene-d_6. A small shift in the IR spectrum of **6** was also observed in Δν(C≡C) relative to **4** by 15 cm^{-1} to lower wavenumbers.

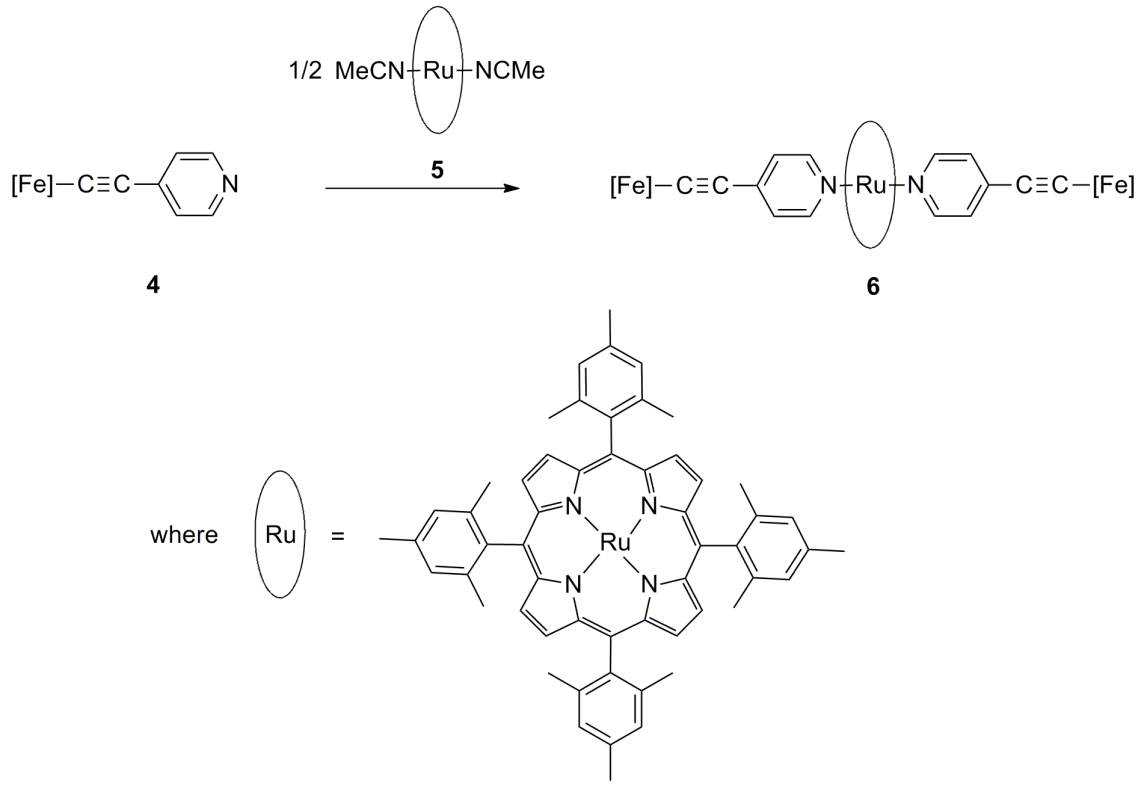

Scheme 2.2. Synthesis of the trimetallic molecular wire 6 where [Fe] = Fe(dppe)Cp*.

2.3 Molecular Structures

In complex **6**, the ruthenium atom resides in a distorted octahedral geometry. The potential of **6** to act as a multimetallic rod lies in its linear molecular axis, with a significant separation of ca. 19 Å between the two iron atoms. The geometry of the porphyrin moiety about the ruthenium metal centre is fixed, such that the coordination of two equivalents of the metallo-ligand **4** occurs in the vacant sites, that are *trans* disposed with the pyridine atoms lying in the same plane. The C37-C38 bond distances in **6** fall within the expected range, and are similar to those reported in iron acetylide complexes.[28-31] The Ru-N5 bond length of 2.073(5) is similar to a literature compound.[32] There is a distortion in the N2-Ru1-N1 bond angle (86.38(19) °) from octahedral geometry, presumably due to the steric congestion about the ruthenium atom.

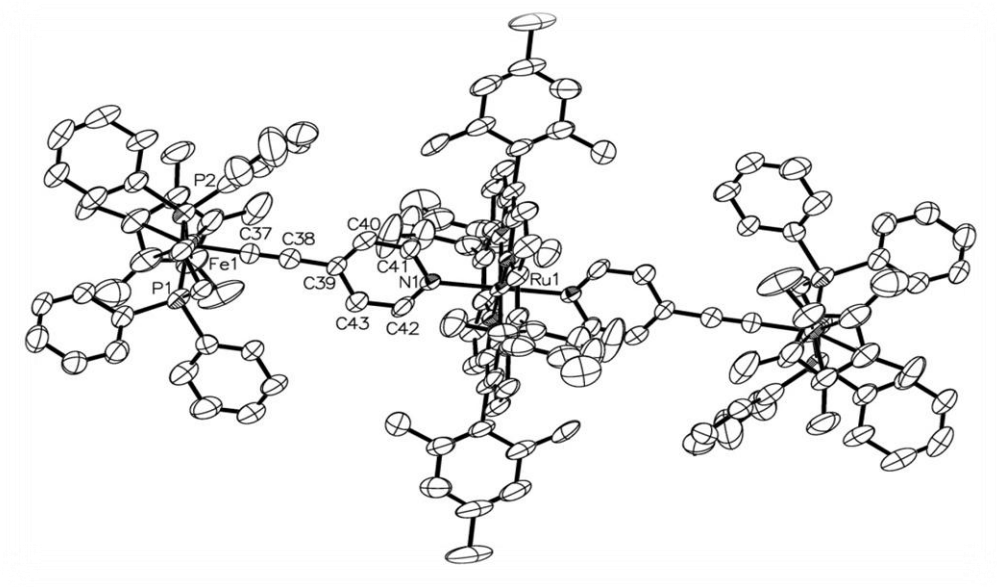

Figure 2.7. Molecular structure of 6. Thermal ellipsoids are plotted at the 50 % probability level.

Selected bond lengths (Å): Fe1-$(Cp^*)_{centroid}$ 1.726; Fe1-P1 2.161(2); Fe1-P2 2.186(2); Fe1-C37 1.879(7); C37-C38 1.205(9); C38-C39 1.420(9); C39-C40 1.362(9); C40-C41 1.371(9); C41-N5 1.334(7); N5-Ru1 2.073(5). Selected bond angles (°): P1-Fe1-P2 86.47(8); Fe1-C37-C38 1.77.7(7); C37-C38-C39 178.1(8); N2-Ru1-N1 86.38(19); $(Cp^*)_{centroid}$-Fe1-C39-C40 -14.2.

2.4 Cyclic Voltammetry

The compounds **4**, **5** and **6** were supplied by the Rennes team for further assessment using electrochemical and spectroelectrochemical methods in Durham. The oxidation of an iron centre in **4** occurs at a much lower potential than a ruthenium centre in **5**, according to expectations ($E_{1/2}$ = –0.03 V **4**; 0.79 V **5**). The trimetallic complex **6** exhibits three reversible oxidation waves at $E_{1/2}$ = –0.11, 0.02 and 0.27 V vs SCE in 0.1 M NBu_4PF_6 / CH_2Cl_2, Table 2.1. The first two waves can be assigned to the stepwise oxidation of the two iron moieties, and the latter wave can be attributed to the oxidation of the ruthenium centre of the porphyrin ring.[33] The ruthenium based oxidation in **6** is noted to occur at a much lower oxidation potential than **5** consistent with the substitution of acetonitrile ligands by the much more electron donating pyridyl moiety.

Table 2.1. The electrochemical response of compounds 4 – 6 in 0.1 M NBu_4PF_6 / CH_2Cl_2 with a Pt electrode, v = 100 mV s^{-1}. Values referenced to SCE = 0 V.

Complex	$E_{1/2}$ (1)/ V	$E_{1/2}$ (2) / V	$E_{1/2}$ (3) / V
4	–0.03	-	-
5	0.79	-	-
6	–0.11	0.02	0.27

However as discussed in Chapter 1, the separation of the first two redox potentials is determined by a number of factors including electrostatic and solvation factors, ion-pairing interactions and resonance stabilisation factors, amongst others.[34] In order to differentiate between through bond and through space interactions, the electrochemical response of **6** was also examined in 0.1 M $NBu_4[BAr^F{}_4]$ / CH_2Cl_2 where $[BAr^F{}_4]^-$ = $[B(C_6F_5)_4]^-$. As noted in Chapter 1, the low coordinating properties of the $[BAr^F{}_4]^-$ anion serve to limit stabilisation arising from ion-pairing effects, and maximise contributions arising from 'through space' or electrostatic terms.[35-37] The iron redox

waves in **6** were found to exhibit the same separation as in 0.1 M NBu_4PF_6 / CH_2Cl_2 ($\Delta E_{1/2}$ = 0.13 V), thus suggesting that the separation of the iron redox waves is more closely associated with electronic (through bond) effects between the metals as opposed to electrostatic, solvation, ion-pairing or other 'through space' factors. In addition, the significant separation in **6** of the two iron centres ($d_{Fe\text{-}Fe}$ ~ 19 Å) also argues against significant Coulombic interactions between the redox sites. The separation of the first and the second iron-based redox processes ($E_{1/2}$ = –0.11 V, 0.02 V; $\Delta E_{1/2}$ = 0.13 V) leads to the calculation of a comproportionation constant (K_c) of ca. 160,[38] a value which suggests that the Fe^{III}/Fe^{II} mixed-valent complex $[\mathbf{6}]^+$ has sufficient thermodynamic stability to be generated in solution.

2.5 IR and NIR Spectroscopy

In seeking to further establish the nature of the redox processes in **6**, IR spectroelectrochemistry studies can be performed, using a vibrational probe, for example an acetylide ligand, the stretching frequency of which can act as an indicator of metal oxidation state. Thin layer spectroelectrochemistry has long been used in conjunction with additional techniques for example DFT studies to aid in the elucidation of the electronic structure of many organometallic molecular wire-type systems. Importantly, IR spectroelectrochemistry provides an alternative technique by which we can generate oxidised species in solution through the application of a potential, without the need for the use of chemical oxidation protocols which can sometimes lead to the isolation of stable (or unstable) oxidised complexes, as a salt.

When the frontier orbitals of a complex arise from the extensive mixing of the metal d orbitals and the cylindrical π-orbital system, the ν(C≡C) bond will be strongly affected by the removal of an electron from the complex. This is a case that is commonly encountered in ruthenium acetylide complexes such as Ru(C≡CAr)dppe)Cp*, whereby the removal of an electron can cause changes in $\Delta\nu$(C≡C) of up to 145 cm^{-1}. This large shift in $\Delta\nu$(C≡C) is a result of an oxidation process on a frontier orbital which is heavily localised on the acetylide ligand.[39,40] On the other hand, when smaller changes are observed in $\Delta\nu$(C≡C) between the neutral and oxidised complexes as is evident in molybdenum acetylide complexes such as Mo(C≡CR)(dppe)(C_7H_7), then this suggests that there is little mixing between the metal d orbitals and the acetylide π-orbitals in the HOMO, indicative of a metal centred oxidation.[41, 42]

Since complex **6** contains an acetylide ligand, IR spectroelectrochemical techniques were employed to confirm the Fe-localised nature of the first oxidation process and to explore the nature of the MV complex $[\mathbf{6}]^+$. On oxidation of **6** in 0.1 M NBu_4PF_6 / CH_2Cl_2, the split ν(C≡C) bands at 2035(m) and 2018(m) evolved into two bands in $[\mathbf{6}]^+$ at 2016(w) and 1947(m) cm^{-1}, Figure 2.5. The complex $[\mathbf{6}]^+$ is remarkably similar to the IR profile of $[\mathbf{2}]^+$, which features two bands at 2016 and 1934 cm^{-1}.[6] The presence of multiple ν(C≡C) bands in iron alkynyl complexes is common, and often attributed to Fermi coupling.[43] We have not sought to address this long standing issue, but rather have used the ν(C≡C) band pattern as a qualitative measure.

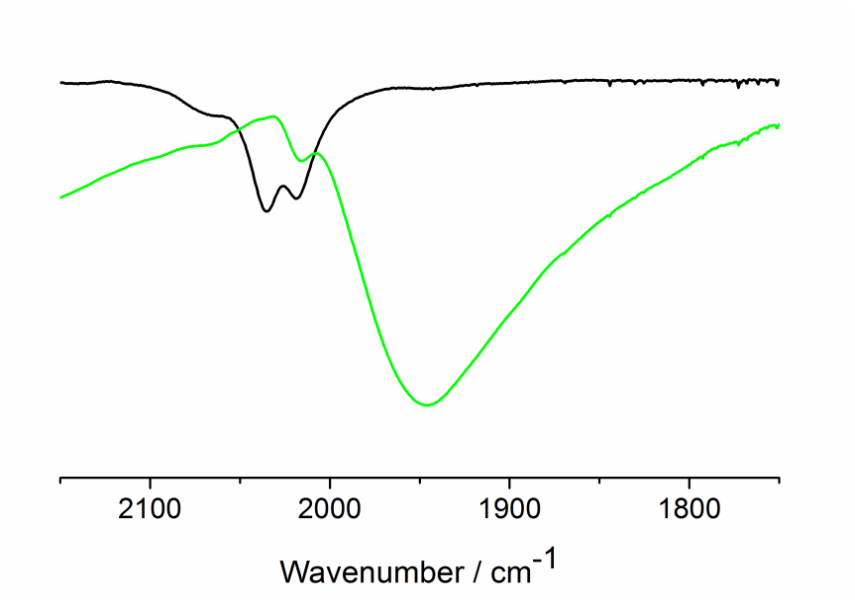

Figure 2.5. IR spectra of 6 (black) and [6]$^+$ (green) in 0.1 M NBu_4PF_6 / CH_2Cl_2.

The chemical oxidation of **6** with one equivalent of ferricinium hexafluorophosphate ([Fc]PF_6) in CH_2Cl_2 led to the development of a band in the NIR region, which was unique to [**6**]$^+$. Deconvolution of this band revealed that [**6**]$^+$ is characterised by three relatively intense Gaussian-shaped bands (ν_1 = 3750 cm^{-1}, ε = 13500 M^{-1}cm^{-1}; ν_2 = 5900 cm^{-1}, ε = 6900 M^{-1}cm^{-1}; ν_3 = 7700 cm^{-1}, ε = 900 M^{-1}cm^{-1}), Figure 2.6, though additional sub bands might also be considered. Once again, this is remarkably similar to the IVCT transitions observed for [**2**]$^+$ (ν_1 = 4000 cm^{-1}, ε = 12700 M^{-1}cm^{-1}; ν_2 = 6500 cm^{-1}, ε = 3400 M^{-1}cm^{-1}; ν_3 = 9000 cm^{-1}, ε = 600 M^{-1}cm^{-1}) and the associated Fe(III) d-d band (ν = 5400 cm^{-1}, ε = 300 M^{-1}cm^{-1}), which supports these bands as arising from Fe-Fe charge-transfer processes.[6] Further addition of an excess of [Fc]PF_6 to [**6**]$^+$ reveals a collapse of the absorption envelope which supports the assignment of this feature as an IVCT transition.[9]

A comparison of the half-height band width of the lowest energy component derived from the deconvolution with that derived from the Hush relationship for a weakly coupled Class II MV complex reveals that the two values are only in modest agreement ($\Delta\nu_{1/2}$(observed) = 2000 cm^{-1}; $\Delta\nu_{1/2}$(calculated) = 2700 cm^{-1}),[7] but is in good agreement with that derived from the strongly coupled MV complex [**2**]$^{+}$ ($\Delta\nu_{1/2}$(observed) = 2110 cm^{-1}; $\Delta\nu_{1/2}$(calculated) = 3040 cm^{-1}).[6] The close agreement of the spectroscopic parameters of [**2**]$^{+}$ and [**6**]$^{+}$ implies a strong coupling of the Fe centres across both bridges.

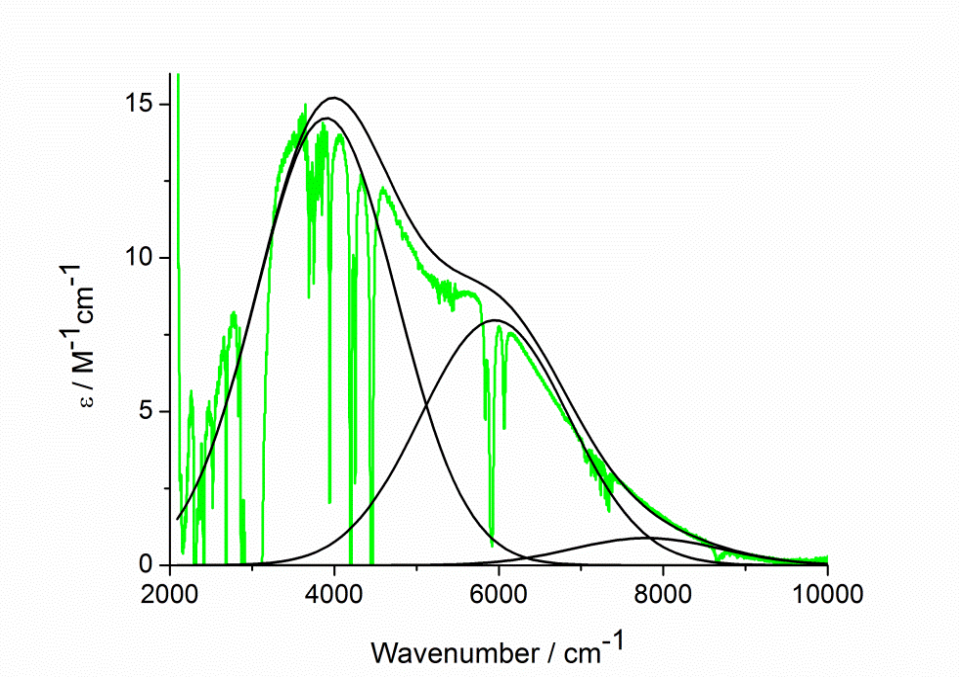

Figure 2.6. Deconvolution of the IVCT band observed in [6]$^{+}$ (green) determined from a chemical oxidation in CH_2Cl_2.

2.6 Conclusions

The team at the University of Rennes 1, France have synthesised a trimetallic molecular wire (**6**) through straight forward synthetic preparations which involve the "plugging" of redox-active metalloligands such as **4** onto Ru(II) porphyrin connectors, the "socket". Electrochemical studies show three reversible oxidation waves, the first two of which are attributed to the stepwise oxidation of the two Fe^{II} end groups, whilst the latter is attributed to the oxidation of the Ru^{II} centre of the porphyrin ring. Chemical oxidation of **6** with one and two equivalents of $[Fc]PF_6$ revealed the presence and collapse of an IVCT band in the NIR region respectively. Given previous attempts to synthesise self-assembled molecular wires with the metalloligand **4** and using Pd^{II} and Pd^{II} connectors results in the isolation of localised, very weakly coupled MV complexes,[14] the results obtained thus far are very encouraging. In particular, this study emphasises that a more electron rich central connector is crucial in obtaining an efficient molecular wire. The scope and potential of self-assembled molecular wires is therefore promising and warrants further exploration.

2.7 Experimental

All reactions were carried out under an atmosphere of nitrogen using standard Schlenk techniques. Reaction solvents were purified and dried using standard methods, and degassed before use. The compounds [Fe(C≡C-4-Py)(dppe)Cp*] (**4**),[14] and [(TMP)Ru(CH_3CN)$_2$] (**5**),[23] and were prepared by the literature methods.

Electrochemical analyses were carried out using an EcoChemie Autolab PG-STAT30 potentiostat (Rennes) or on an Autolab PG-STAT30 potentiostat (Durham), with platinum working, counter and pseudo reference electrodes, from solutions in CH_2Cl_2 containing 0.1 M NBu_4PF_6 electrolyte at ν = 100 mV s^{-1}. The working electrode was polished with alumina paste before each scan. The redox potentials in this Chapter are reported with reference to the saturated calomel electrode, SCE = 0 V.[44]

IR spectroelectrochemical measurements were performed in an air tight optically transparent thin-layer electrode (OTTLE) cell of Hartl design,[45] equipped with Pt minigrid working and counter electrodes, a Ag wire pseudo reference electrode and fitted with CaF_2 windows.[45] The cell was positioned into the sample compartment of a Nicolet Avatar 6700 FT-IR spectrometer purged with nitrogen. Bulk electrolysis was performed with a home built potentiostat. An initial potential was applied such that no electrochemical work was done. The applied potential was then increased in ca. 50 – 100 mV steps, the system allowed to equilibrate and the relative changes in the spectroscopic profile monitored, before a further increase in potential was applied until the redox process was complete. The potential was then reversed in a stepwise manner

to recover the original spectrum and to confirm the chemical reversibility of the molecule under study under the conditions of the experiment and the timescale of this technique.

2.7.1. Preparation of 6

In CH_2Cl_2 (10 ml), **4** (62 mg, 0.090 mmol) and **5** (34 mg, 0.036 mmol) were reacted for 24 h at ambient temperature. After evaporation of the solvent, the remaining solid was recrystallised from toluene-pentane mixtures (10 ml / 15 ml) before being washed several times with small fractions of *n*-pentane (3 x 15 ml) and dried *in vacuo* to give **6** as a dark orange solid (50 mg, 62 %). Crystals of **6** were obtained by slow diffusion of pentane in a toluene solution of the compound. ^{1}H NMR (500 MHz, C_6D_6): δ 8.40 (s, 8H, $H_{Pyrr.}$); 7.40 - 6.75 (m, 48H, $H_{Ar/dppe}$ + $H_{Ar/Mes.}$); 4.87(d, 4H, $^{3}J_{HH}$ = 6.6 Hz, H_{Py}); 3.22 (d, 4H, $^{3}J_{HH}$ = 6.6 Hz, H_{Py}); 2.41 (s, 12H, C$H_{3/Mes.}$), 2.17 (s, 24H, C$H_{3/Mes.}$), 2.02 (m, 4H, CH_{2dppe}); 1.44 (m, 4H, CH_{2dppe}); 1.18 (s, 30H, $C_5(CH_3)_5$). ^{31}P NMR (81 MHz, C_6D_6): δ 100.0 (s, 2P, dppe). ^{13}C{^{1}H} NMR (500 MHz, $CDCl_3$): δ 158.0 (t, $^{2}J_{CP}$ = 38 Hz, *C*≡C(C_5H_4N)); 150.7 (s, $C_{\alpha/Pyrrole}$); 144.5 (s, *C*-H_{Py}); 141.0-126.5 (m, C_{Ph}/C_{β}/Pyrrole/C_{quat}/Py), 122.2 (s, *C*-H_{Py}); 120.6 and 120.0 (s, C_{meso} and C≡*C*(4-C_5H_4N)); 88.7 (s, $C_5(CH_3)_5$); 31.2 (m, *C*H_2dppe); 22.5 (s, 2×*C*H_3); 22.2 (s, *C*H_3); 10.7 (s, $^{1}J_{CH}$ = 126 Hz, $C_5(CH_3)_5$). FT-IR (ν, KBr: Nujol/CH_2Cl_2) 2038/2039 (vs, Fe-C≡C); 1597/1596 (s, Py) $cm^{-1.}$

2.8 References

1. F. Malvolti, P. Le Maux, L. Toupet, M. E. Smith, W. Y. Man, P. J. Low, E. Galardon, G. Simonneaux and F. Paul, *Inorg. Chem.*, 2010, **49**, 9101-9103.
2. N. Le Narvor, L. Toupet and C. Lapinte, *J. Am. Chem. Soc.*, 1995, **117**, 7129-7138.
3. F. Coat, F. Paul, C. Lapinte, L. Toupet, K. Costuas and J.-F. Halet, *J. Organomet. Chem.*, 2003, **683**, 368-378.
4. F. Coat and C. Lapinte, *Organometallics*, 1996, **15**, 477-479.
5. N. Le Narvor and C. Lapinte, *Organometallics*, 1995, **14**, 634-639.
6. S. I. Ghazala, F. Paul, L. Toupet, T. Roisnel, P. Hapiot and C. Lapinte, *J. Am. Chem. Soc.*, 2006, **128**, 2463-2476.
7. N. S. Hush, *Prog. Inorg. Chem.*, 1967, **8**, 391-444.
8. M. B. Robin, P. Day, *Adv. Inorg. Chem. Radiochem.*, 1968, **10**, 247-422.
9. K. D. Demadis, C. M. Hartshorn and T. J. Meyer, *Chem. Rev.*, 2001, **101**, 2655-2686.
10. M. A. Fox, B. Le Guennic, R. L. Roberts, D. A. Brue, D. S. Yufit, J. A. K. Howard, G. Manca, J.-F. Halet, F. Hartl and P. J. Low, *J. Am. Chem. Soc.*, 2011, **133**, 18433-18446.
11. C. Engtrakul, W. J. Shoemaker, J. J. Grzybowski, I. Guzei and A. Rheingold, *Inorg. Chem.*, 2000, **39**, 5161-5163.
12. R. Packheiser, P. Ecorchard, B. Walfort and H. Lang, *J. Organomet. Chem.*, 2008, **693**, 933-946.
13. Y.-C. Lin, W.-T. Chen, J. Tai, D. Su, S.-Y. Huang, I. Lin, J.-L. Lin, M. M. Lee, M. F. Chiou, Y.-H. Liu, K.-S. Kwan, Y.-J. Chen and H.-Y. Chen, *Inorg. Chem.*, 2009, **48**, 1857-1870.
14. S. Le Stang, F. Paul and C. Lapinte, *Inorg. Chim. Acta*, 1999, **291**, 403-425.
15. M.-Y. Choi, M. C. W. Chan, S.-M. Peng, K.-K. Cheung and C.-M. Che, *Chem. Commun.*, 2000, 1259-1260.
16. F. E. Kuhn, J.-L. Zuo, F. Fabrizi de Biani, A. M. Santos, Y. Zhang, J. Zhao, A. Sandulache and E. Herdtweck, *New J. Chem.*, 2004, **28**, 43-51.
17. Q. Ge and T. S. A. Hor, *Dalton Trans.*, 2008, 2929-2936.
18. J. P. Collman, J. T. McDevitt, C. R. Leidner, G. T. Yee, J. B. Torrance and W. A. Little, *J. Am. Chem. Soc.*, 1987, **109**, 4606-4614.
19. C. Creutz and H. Taube, *J. Am. Chem. Soc.*, 1969, **91**, 3988-3989.
20. C. Creutz, *Prog. Inorg. Chem.*, 1983, **30**, 1-73.
21. A. Von Kameke, G. M. Tom and H. Taube, *Inorg. Chem.*, 1978, **17**, 1790-1796.
22. V. Marvaud and J. P. Launay, *Inorg. Chem.*, 1993, **32**, 1376-1382.
23. M. J. Camenzind, B. R. James and D. Dolphin, *J. Chem. Soc., Chem. Commun.*, 1986, 1137-1139.
24. S. L. Darling, C. Ching Mak, N. Bampos, N. Feeder, S. J. Teat and J. K. M. Sanders, *New J. Chem.*, 1999, **23**, 359-364.
25. E. Alessio, E. Ciani, E. Iengo, V. Y. Kukushkin and L. G. Marzilli, *Inorg. Chem.*, 2000, **39**, 1434-1443.
26. K. Chichak, M. C. Walsh and N. R. Branda, *Chem. Commun.*, 2000, 847-848.
27. E. Alessio, S. Geremia, S. Mestroni, I. Srnova, M. Slouf, T. Gianferrara and A. Prodi, *Inorg. Chem.*, 1999, **38**, 2527-2529.

28. F. H. Allen, O. Kennard, D. G. Watson, L. Brammer, A. G. Orpen and R. Taylor, *J. Chem. Soc, Perkin Trans., 2*, 1987, S1-S19.
29. L. D. Field, A. M. Magill, T. K. Shearer, S. B. Colbran, S. T. Lee, S. J. Dalgarno and M. M. Bhadbhade, *Organometallics*, 2010, **29**, 957-965.
30. K. M.-C. Wong, S. C.-F. Lam, C.-C. Ko, N. Zhu, S. Roué, C. Lapinte, S. Fathallah, K. Costuas, S. Kahlal and J.-F. Halet, *Inorg. Chem.*, 2003, **42**, 7086-7097.
31. M. S. Khan, M. R. A. Al-Mandhary, M. K. Al-Suti, F. R. Al-Battashi, S. Al-Saadi, B. Ahrens, J. K. Bjernemose, M. F. Mahon, P. R. Raithby, M. Younus, N. Chawdhury, A. Kohler, E. A. Marseglia, E. Tedesco, N. Feeder and S. J. Teat, *Dalton Trans.*, 2004, 2377-2385.
32. M. Ruben, A. Landa, E. Lörtscher, H. Riel, M. Mayor, H. Görls, H. B. Weber, A. Arnold and F. Evers, *Small*, 2008, **4**, 2229-2235.
33. G. M. Brown, F. R. Hopf, J. A. Ferguson, T. J. Meyer and D. G. Whitten, *J. Am. Chem. Soc.*, 1973, **95**, 5939-5942.
34. P. J. Low and N. J. Brown, *J. Cluster Sci.*, 2010, **21**, 235-278.
35. F. Barrière, N. Camire, W. E. Geiger, U. T. Mueller-Westerhoff and R. Sanders, *J. Am. Chem. Soc.*, 2002, **124**, 7262-7263.
36. F. Barriere and W. E. Geiger, *J. Am. Chem. Soc.*, 2006, **128**, 3980-3989.
37. W. E. Geiger and F. Barriere, *Acc. Chem. Res.*, 2010, **43**, 1030-1039.
38. F. Paul and C. Lapinte, *Coord. Chem. Rev.*, 1998, **178**, 431-509.
39. M. A. Fox, R. L. Roberts, W. M. Khairul, F. Hartl and P. J. Low, *J. Organomet. Chem.*, 2007, **692**, 3277-3290.
40. M. A. Fox, J. D. Farmer, R. L. Roberts, M. G. Humphrey and P. J. Low, *Organometallics*, 2009, **28**, 5266-5269.
41. N. J. Brown, D. Collison, R. Edge, E. C. Fitzgerald, M. Helliwell, J. A. K. Howard, H. N. Lancashire, P. J. Low, J. J. W. McDouall, J. Raftery, C. A. Smith, D. S. Yufit and M. W. Whiteley, *Organometallics*, 2010, **29**, 1261-1276.
42. N. J. Brown, H. N. Lancashire, M. A. Fox, D. Collison, R. Edge, D. S. Yufit, J. A. K. Howard, M. W. Whiteley and P. J. Low, *Organometallics*, 2011, **30**, 884-894.
43. F. Paul, J.-Y. Mevellec and C. Lapinte, *J. Chem. Soc., Dalton Trans.*, 2002, 1783-1790.
44. N. G. Connelly and W. E. Geiger, *Chem. Rev.*, 1996, **96**, 877-910.
45. M. Krejčik, M. Daněk and F. Hartl, *J. Electroanal. Chem.*, 1991, **317**, 179-187.

Chapter 3. Ruthenium Vinyl Complexes Bearing Tp and PMe_3 Coordinated Ligands

3.1 Introduction

The field of metal complex chemistry is defined by two extremes: (1) Werner-type transition metal coordination complexes and (2) low valence transition metal organometallic complexes which obey the 18 electron rule. The structure and physical properties of these complexes can be rationalised by an ionic and covalent bonding model respectively, though the actual bonding situation is likely to lie in between the two extremes. The failure of the first model to explain some features of Werner-type coordination complexes *via* a purely ionic model, and thus the spectrochemical series, can be qualitatively corrected by taking into account a covalent contribution to the metal-ligand bonding.[1]

In Werner-type transition metal coordination complexes, the oxidation state of a metal is easily identified due to the presence of charge defined 'innocent' ligands,[2] for example in $[Co(NH_3)_6]^{2+}$ where the ammonia ligands are charge neutral, and cobalt exists in its + 2 oxidation state. The chemistry of these complexes is thus governed by changes in the oxidation state of the metal, and the frontier orbitals are largely metal in character. However, the redox character of a system can also be more closely associated with the depopulation of the ligand orbitals; this was first recognised in a biochemical context with the non-innocent behaviour of a series of redox-active ligands

such as $O_2/O_2^{\bullet-}/O_2^{2-}$ and $NO^+/NO^{\bullet}/NO^-$ being reported.[3] For example, in oxymyglobin, dioxygen can bind innocently to Fe^{II} as O_2, or non-innocently to Fe^{III} as $O_2^{\bullet-}$. After much deliberation over the years, it is now accepted with the aid of DFT studies that the latter of these formulations is correct.[4] Similarly, it has also recently been established that NO binds non-innocently to Fe^{III} as NO^- in the brown ring ion $[Fe(NO)(H_2O)_5]^{2+}$, Scheme 3.1.[5, 6]

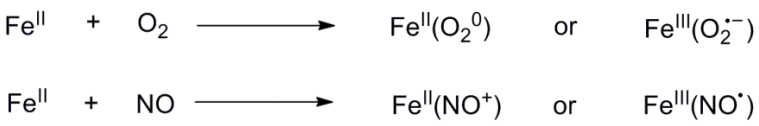

Scheme 3.1. The binding of O_2 and NO to Fe^{II}.

Similar concepts of ligand redox activity are well illustrated by related redox families of the butadiene motif for example the diothiolenes, diimines and *ortho*-quinones, Scheme 3.2a.[7-11] The high degree of electron delocalisation within these ligands, coupled with their ability to undergo a number of well defined electron transfer redox events mean that they can exist as a neutral, radical or dianionic forms, Scheme 3.2b. It is these ligand based redox changes that often account for the electrochemical behaviour of complexes that contain them.

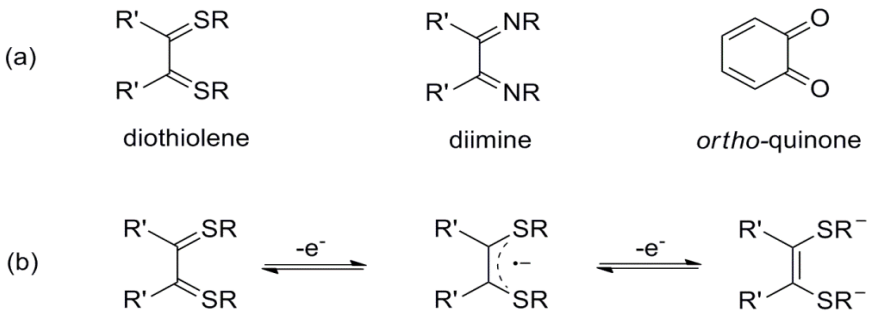

Scheme 3.2. (a) Diothiolene, dimine and *ortho*-quinone motifs and (b) canonical forms of diothiolene.

In 1966, Jorgensen defined a ligand as innocent 'when it allows the oxidation state of the central atoms to be defined', hence the unambiguous assignment of the metal oxidation state.[5] In recent times, the term "suspect" has paved the way to descriptions of 'non-innocent' behaviour, though this can be misinterpreted and inaccurately taken to mean that the ligands are redox-active.[12] On coordination of a redox-active ligand to a metal fragment, it can act in an innocent or non-innocent way. This distinction depends on the relative potentials of the ligand, supporting metal fragment, other potentially redox-active ligands and the σ- and π-bonding interactions (i.e. metal-ligand orbital mixing) within a complex.[13] When the redox activity of a complex can be well described in terms of the metal i.e. $[Co(NH_3)_6]^{2+/3+}$ or the ligand i.e. $[Cr(^tBu_2\text{-}bpy)_3]^{3+/2+/1+/0}$, then the oxidations or reductions which occur can be readily identified in terms of a metal centred oxidation,[7] or a ligand centred reduction.[14, 15] However, extensive mixing of metal and ligand orbitals of similar energy can lead to complexes of intermediate character. The relative contributions of the metal and ligands to the redox-active orbitals can therefore vary and lead to the unambiguous assignment of oxidation states.

A number of techniques can be used to establish the redox innocence or non-innocence of a ligand, for example electrochemistry, IR and UV-vis-NIR spectroelectrochemistry and EPR techniques. In addition, the recent and rapid development of quantum chemistry has led to DFT becoming a powerful tool, with it now being common to support experimental results with theoretical studies. Used alongside spectroscopic methods, DFT has become an invaluable technique, particularly in the identification of a

primary redox site and in mapping the relative contributions of individual conceptual components within metal complexes.[16]

In recent years, the design of catalytic systems with redox-active non-innocent ligands have attracted interest due to their potential to act as an alternative to cross-coupling methodologies which employ expensive noble transition metals such as Pd(0) and mediate two electron oxidative addition and reductive elimination steps. First row transition or 'base' metals have a tendency to undergo one electron redox changes.[17] Through the modification of the local environment of a base metal by a redox-active ligand, acting either as an electron reservoir or sink, it has been possible to demonstrate the shuttling of multiple electrons to a substrate *via* non-innocent ligands.[18] Soper and co-workers demonstrated this concept elegantly in Negishi-like cross-coupling reactions, which employ an alkyl halide and a paramagnetic square planar Co(III) system with two redox-active ligands (in place of a typical aryl or alkyl zinc reagent), Scheme 3.3. As a result, when this Co(III) system is oxidised, the cross-coupling reaction proceeds *via* two single, one electron oxidations of each redox-active ligand, leaving the metal in its original state.[19]

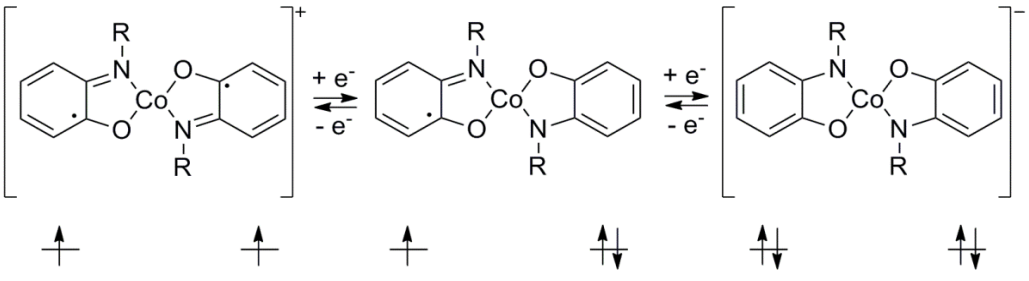

Scheme 3.3. Square planar Co(III) complex with two redox-active amidophenolate ligands.

3.1.1 Monometallic Ruthenium Alkynyl and Vinyl Complexes

In carbon rich organometallic complexes, the alkynyl ligand in aryl alkynyl ruthenium complexes is known to exhibit redox non-innocent properties. For example, Bruce, Lapinte and co-workers have investigated the redox properties of complexes of the general form $Ru(C{\equiv}CC_6H_4R)(dppe)Cp^*$ where R = NO_2, CH_3, F, H, OMe and NH_2 and found that on oxidation of these complexes, the shift in $\Delta\nu(C{\equiv}C)$ could vary from –90 to –145 cm^{-1}.[20] DFT studies have revealed a sizeable metal acetylide contribution in the HOMO of these complexes (16 – 43 %) dependent on the R group. In particular, the delocalisation of the unpaired electron on the arylacetylide ligand is observed, which is consistent with the greater involvement of the arylacetylide ligand in the HOMO. Low and co-workers have also reported similar observations in $Ru(C{\equiv}CC_6H_5)(dppe)Cp^*$, where on oxidation, the change of $\Delta\nu(C{\equiv}C)$ band shifts by 145 cm^{-1} to lower wavenumbers, indicating the depopulation of a frontier orbital with appreciable metal d admixed with ethynyl character.[21]

Unlike the analogous Fe(III) complexes, which have been isolated,[22-24] $[Ru(C{\equiv}CR)(dppe)Cp^*]^+$ complexes are highly reactive. This increased reactivity of the ruthenium systems is due to the substantial alkynyl ligand radical character. The ligand radical is evidenced also by the isolation of products from ligand dimerisation, as demonstrated by Bruce *et al* and others.[25-27] When the conjugation of the alkynyl ligand substituent, Ar, is extended in $Ru(C{\equiv}CAr)(dppe)Cp^*$ complexes, there is an increase in the contribution of the alkynyl ligand to the HOMO of these complexes.[26, 28] The series of complexes $Ru(C{\equiv}CR)(dppe)Cp^*$ where R = phenyl, 1-naphthyl and 9-anthryl, Figure 3.1 reveals a steady progression of frontier orbitals with appreciable metal character

admixed with that of an aromatic π-system. Thus in these systems, the arylalkynyl ligand is redox non-innocent.[21, 27]

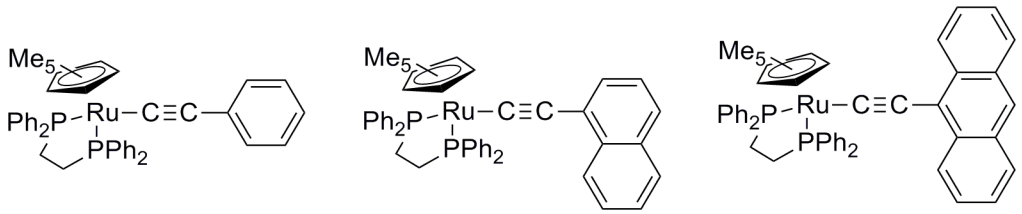

Figure 3.1. Ruthenium half sandwich acetylide complexes.

In a series of related studies, Winter and co-workers have demonstrated the redox non-innocence of the vinyl ligand in ruthenium vinyl complexes by systematically varying the phosphine ligands, the coordination number and the substituents at the ruthenium metal centre. For example, on oxidation of the complexes of the general form $Ru(CH=CHR)Cl(CO)(PR_3)_2$ where R = ^{n}Bu to a Ph and Pyr (pyrenyl) group and PR_3 = PPh_3 or $P^{i}Pr_3$, the change in ν(C≡O) ($\Delta\nu(C\equiv O) = 48 - 77$ cm^{-1}) is significantly smaller than that expected of a metal centred oxidation (ca. $\Delta\nu(C\equiv O) = 100$ cm^{-1}), and further diminishes as the vinyl CH=CH entity is incorporated into a more extended π-system.[29] Results from electron spin resonance (ESR) studies of the electrogenerated radical cations result in *g* values which deviate little from that of a free electron, thus suggesting the involvement of the organic vinyl ligand in the oxidation process. The redox non-innocence of the vinyl ligand was further supported by DFT studies, where the contribution of the vinyl ligand to the HOMO increases from 46 % to 84 % as the R group is changed from a ^{n}Bu group to a 1-pyrenyl ligand, Figure 3.2.

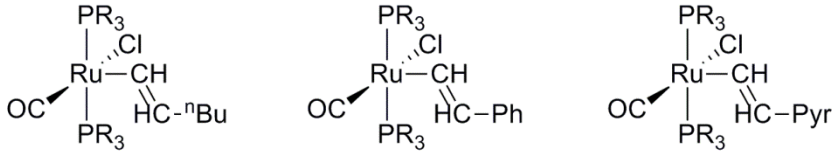

Figure 3.2. Five coordinate monometallic ruthenium vinyl complexes, where PR_3 = PPh_3 or P^iPr_3.

3.1.2 Hydroruthenation

Ruthenium vinyl complexes $Ru(CH=CHR)Cl(CO)(PR_3)_2$ can be readily prepared from the reaction of a ruthenium hydride complex and an alkyne in a solvent such as CH_2Cl_2. The reaction proceeds *via* the insertion of an alkyne into a Ru-H bond in $RuHCl(CO)(PR_3)_n$ (n = 2, 3) and leads to the formation of unsaturated five coordinate ruthenium vinyl complexes,[30] which are characteristically red in colour, in high yields. In these complexes, the strong *trans* influence of the vinyl ligand typically weakens the bond of coordinating ligands, particularly those that incorporate bulky triaryl phosphine ligands and are often isolated as the five coordinate species,[31] or exists as a mixture of the five- and six-coordinate complexes, Scheme 3.4.[32]

The reaction of an unsaturated five coordinate ruthenium complex with a wide range of neutral (carbon monoxide, pyridine) and anionic mono (acetate) and bidentate ligands such as benzo-2,1,3-selenadiazole (BSD) by binding to the vacant coordination site,[33, 34] or substitution of the supporting phosphine and chloride ligands lead to the formation of six coordinate ruthenium vinyl complexes which are characteristically yellow in colour.[35-38] Thus, unsaturated five coordinate ruthenium vinyl complexes are convenient precursors to a range of derivatives through ligand substitution reactions,

giving scope to tune the metal-ligand coordination sphere, Scheme 3.4, and thus the degree of metal *vs*. ligand redox character within an organometallic complex.[31, 39-45]

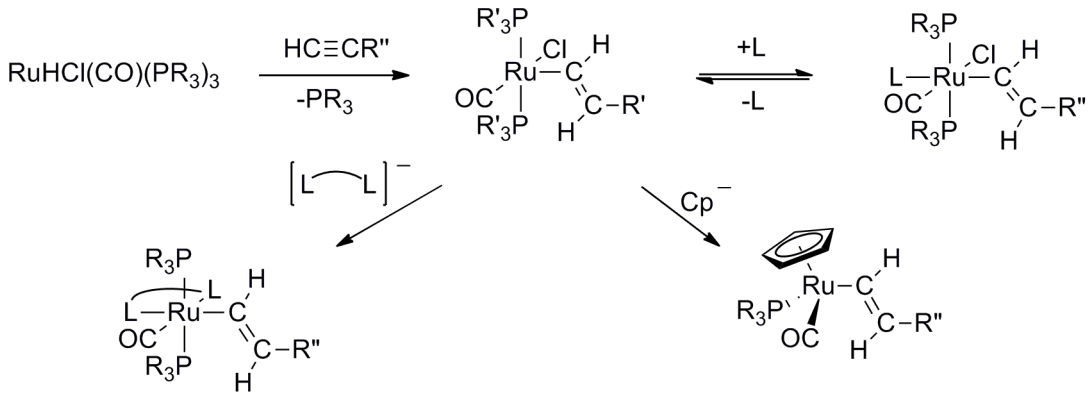

Scheme 3.4. A representative array of ligand substitution reactions associated with five-coordinate vinyl complexes Ru(CH=CHR)Cl(CO)(PR_3)$_2$.

To date the vast majority of investigations of the redox chemistry has been studied but somewhat restricted to five coordinate Ru(CH=CHR)Cl(CO)(P^iPr_3)$_2$ or six coordinate Ru(CH=CHR)Cl(CO)(PPh_3)$_2$L, Ru(CH=CHR)(CO)(O_2CR)(P^iPr_3)$_2$ systems (L = 4-ethylisonicotinate).[29, 46] Winter and co-workers have demonstrated the use of both the metal and supporting ligands in assessing the site of oxidation in some mono- and bis(vinyl) complexes (for a more in depth discussion of the latter see Chapter 3.8), with experimental and computational studies indicative of an oxidation process which typically occurs on the redox non-innocent bridging ligand.[46]

In this Chapter, further efforts to tune the electronic character of the Ru-CH=CHR fragment through the preparation and study of tris(pyrazolyl)borate (Tp^-) derivatives $Ru(CH=CHC_6H_4R\text{-}4)(CO)(PPh_3)Tp$ are described. The syntheses, structures and electrochemical properties of the complexes $Ru(CH=CHC_6H_4R\text{-}4)(CO)(PPh_3)Tp$ (R = $N(C_6H_4Me\text{-}4)_2$, OMe, Me, CO_2Me, NO_2) are reported, together with the UV-vis-NIR and IR spectroelectrochemical studies of the complexes $[Ru(CH=CHC_6H_4R\text{-}4)(CO)(PPh_3)Tp]^{n+}$ (n = 0, 1). The resulting descriptions of the redox character of the vinyl ligand will be supported by DFT studies.

3.2 Synthesis

The reaction of $RuHCl(CO)(PPh_3)_3$ with terminal aryl alkynes, $HC{\equiv}CC_6H_4R$-4 [**7**: R = $N(C_6H_4Me\text{-}4)_2$ (**a**), OMe (**b**), Me (**c**), CO_2Me (**d**), NO_2 (**e**)] in CH_2Cl_2 proceeded smoothly to give the five coordinate complexes $Ru(CH{=}CHC_6H_4R\text{-}4)Cl(CO)(PPh_3)_2$ (**8a** – **e**), as shown by the red colouration of the reaction mixture, which developed almost instantaneously.

Complex **8a** was isolated as a red solid in high purity following a series of precipitations, and characterised by way of example. In the ^1H NMR spectrum of **8a**, the vinyl protons were identified as resonances at 5.54 (d, J_{HH} = 13 Hz, Ru-CH=C*H*) and 8.22 (dt, J_{HH} = 13Hz, J_{HP} = 2 Hz, Ru-C*H*=CH) ppm, the latter splitting pattern of which is due to the coupling of RuC*H*=CH to the two ^{31}P nuclei of the phosphine ligands. In the ^{31}P NMR spectrum, a singlet at 29.5 ppm revealed the mutually *trans* disposition of the phosphine ligands. The IR spectrum of **8a** in CH_2Cl_2 solution was characterised by a strong ν(C≡O) band at 1932 cm^{-1} which compares to other five coordinate species $Ru(CH{=}CHPh)Cl(CO)(PR_3)_2$ (PR_3 = PPh_3, 1927 cm^{-1}; P^iPr_3, 1911 cm^{-1}). The relative sensitivity of the ν(C≡O) frequency to the electron-donating character of the PPh_3 and P^iPr_3 ligands is reflected in the lower wavenumbers of these features in the IR spectrum, and due to an increase in π-backbonding from the metal centre to the π* orbitals of the carbonyl ligand. The relative insensitivity of the ν(C≡O) position to the nature of the vinyl ligand substituent is also apparent from the limited shift of the ν(C≡O) frequency as the vinyl ligand substituent is varied.[29]

Reaction of **8a** with an excess of PMe_3 gave the white coloured complex $Ru\{CH=CHC_6H_4N(C_6H_4Me\text{-}4)_2\text{-}4\}Cl(CO)(PMe_3)_3$ (**9a**), Scheme 3.5, which is another example of the *mer*-$Ru(CH=CHR)Cl(CO)(PMe_3)_3$ system.[49-53] In the ^1H NMR spectra, the vinyl proton resonances at 6.53 and 7.90 ppm display additional couplings to the PMe_3 ligand, giving rise to a ddt in each case, with varying resolution. The $^{31}P\{^1H\}$ NMR was characterised by an AM_2 pattern. The IR spectrum of **9a** in CH_2Cl_2 displayed a single strong $\nu(C\equiv O)$ band at 1919 cm^{-1}, the position of which is consistent with expectations on the basis of a more electron donating PMe_3 ligand, in comparison to the PPh_3 ligands in **8a**.

Further reaction of **8a** – **e** with the potassium tris(pyrazolyl)borate (KTp) led to the synthesis of the complexes $Ru(CH=CHC_6H_4R\text{-}4)(CO)(PPh_3)Tp$ (**10a** – **e**) which bear a *facially* capping Tp^- ligand, Scheme 3.5.[45, 55] With the exception of the orange-coloured NO_2 substituted derivative **10e**, these Tp complexes were isolated as pale yellow or green solids. The choice of the Tp^- ligand was inspired by the analogy with the anionic cyclopentadienyl ligand that has been used to support so many half sandwich ruthenium acetylide complexes.[56, 57] The Cp^- and Tp^- ligand are isoelectronic, six electron donors, which usually coordinate in a tridentate manner, and lead to similar chemistry.[56-58] For example, typical reactions in complexes such as $RuCl(PPh_3)_2Cp$ include phosphine dissociation in non-polar solvents and chloride ionisation and dissociation in polar solvents[58] and likewise the chemistry of $RuCl(PPh_3)_2Tp$ is very much the same.[59] KTp is a commercially available, air-stable solid. Consequently, complexes of the general form $[Ru(CH=CHR)(CO)(PPh_3)Tp]$ are somewhat more readily available than their isoelectronic Cp analogues,[45] and were chosen for studies of the electrochemical properties and electronic structures of ruthenium vinyl complexes.

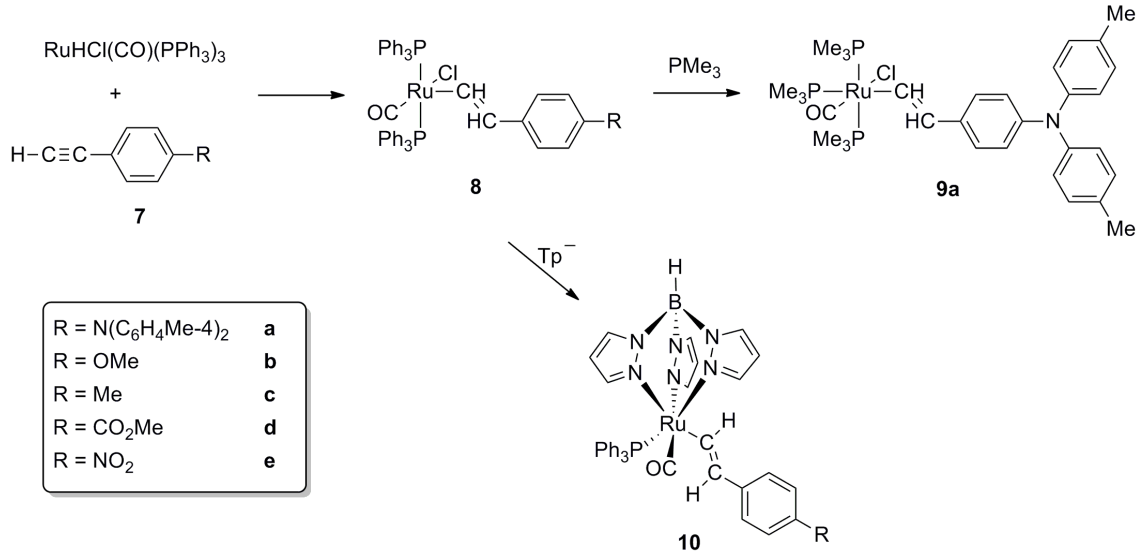

Scheme 3.5. The preparation of 8a – e, 9a and 10a – e.

The reaction of $RuHCl(CO)(PPh_3)_3$ with $HC{\equiv}CC_6H_4CN$-4 (**7f**) proceeds to give a cloudy yellow suspension almost instantly, likely to be a polymeric species $[\{Ru(CH{=}CHC_6H_4CN\text{-}4)(CO)(PPh_3)_2\}_n]$ arising from the competitive coordination of the nitrogen atom of the cyano group to the vacant site *trans* to the vinyl ligand. Whilst we were unable to conclusively characterise this species, on one occasion, addition of KTp gave small quantities of $Ru(CH{=}CHC_6H_4CN)(CO)(PPh_3)Tp$ (**10f**), which was identified crystallographically. However no further investigations were undertaken due to the capricious nature of the synthesis of **10f**.

3.2.1 Spectroscopic Investigations

The complexes **10a** – **e** were characterised by a variety of spectroscopic techniques including Atmosphere Solids Analysis Probe (ASAP) mass spectrometry, ^{1}H, ^{31}P, ^{13}C NMR spectroscopy and IR spectroscopy. The molecular structures of **10b** – **e** were confirmed by single crystal X-ray diffraction studies. In ASAP(+)-MS, the molecular ion $[M]^+$ or protonated form of the molecular ion $[M + H]^+$ was observed. In the ^{1}H NMR spectra, the vinyl protons of **10a** – **e** were identified as resonances at 6.36 – 6.54 (d, J_{HH} = 17 Hz, RuCH=C*H*) and 8.08 – 9.04 (dd, J_{HH} = 17 Hz, J_{HP} = 4 Hz, RuC*H*=CH) ppm, with coupling between H_α and the phosphorus centre of PPh_3 also apparent, whilst the $^{4}J_{HP}$ coupling of H_β was not resolved. The magnitude of the $^{3}J_{HH}$ coupling (ca. 17 Hz) is diagnostic of *trans* vinyl protons. The chemical shifts of both vinyl proton resonances are sensitive to the electronic nature of the remote *para*-substituent, with the H_α resonance the more sensitive of the two. The presence of the Tp^- ligand in the metal coordination sphere is readily apparent from a series of multiplets between 5.80 – 7.50 ppm, arising from the pyrazolyl rings. These occur in three sets of resonances, each with an integral of three, at ca. δ_H 6.0, 7.0 and 8.0 ppm. As a representative example, the B-H resonance in the $^{1}H\{^{11}B\}$ spectrum of **10e** was also observed at 4.64 ppm. The ^{31}P NMR spectra exhibited singlets between 49.4 - 51.3 ppm arising from the PPh_3 ligand. In the ^{13}C NMR spectrum, the carbonyl carbon was observed as a doublet near δ_C 207 ppm (J_{CP} = 15 – 17 Hz). The vinyl C_α also gave rise to a characteristic doublet (J_{CP} = ca. 14 Hz), the chemical shift of which was rather more sensitive to the nature of the vinyl substituent. For example, in **10a** – **c** which exhibits the more electron donating groups, C_α falls at higher field near δ_C 160 ppm and in **10d** and **10e** which bear the more electron withdrawing groups, at δ_C 171.3 and 179.2 ppm respectively, clearly

demonstrating the effectiveness of conjugation through the vinyl ligand. In contrast, the vinyl C_β resonances were observed as singlets, and located around δ_C 135 ppm in each case. The IR spectra of **10a** – **e** were characterised in each case by a ν(C≡O) band which fell in the narrow range 1940 – 1946 cm^{-1}, whilst the ν(B-H) band was observed between 2481 – 2485 cm^{-1}.

3.3 Molecular Structures

X-ray quality crystals of complex **10b** – **f** were grown from the slow diffusion of hexane (**10b**, **10c**, **10f**) or methanol (**10d**, **10e**) into CH_2Cl_2 solutions of the complexes. The molecular structures of **10b** (Figure 3.3), **10c** (Figure 3.4**)**, **10d** (Figure 3.5), **10e** (Figure 3.6) and **10f** (Figure 3.7) were determined by single crystal X-ray diffraction by Dr D.S. Yufit, at Durham University. Crystallographic data, selected bond lengths and bond angles are listed in Tables 3.1 – 3.3 respectively.

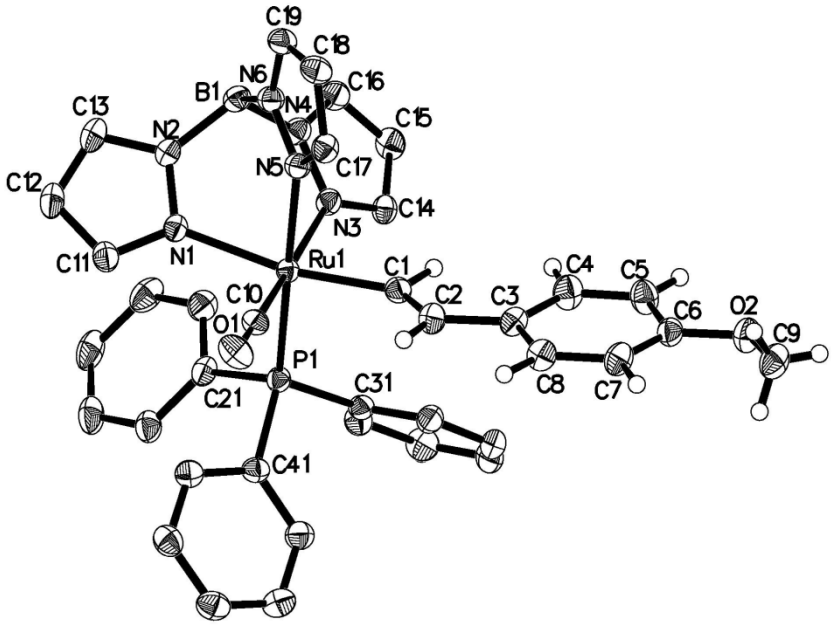

Figure 3.3. A plot of a molecule of 10b, showing the atom labeling scheme. Thermal ellipsoids in this and all subsequent figures are plotted at the 50 % probability level. Selected H atoms have been removed for clarity.

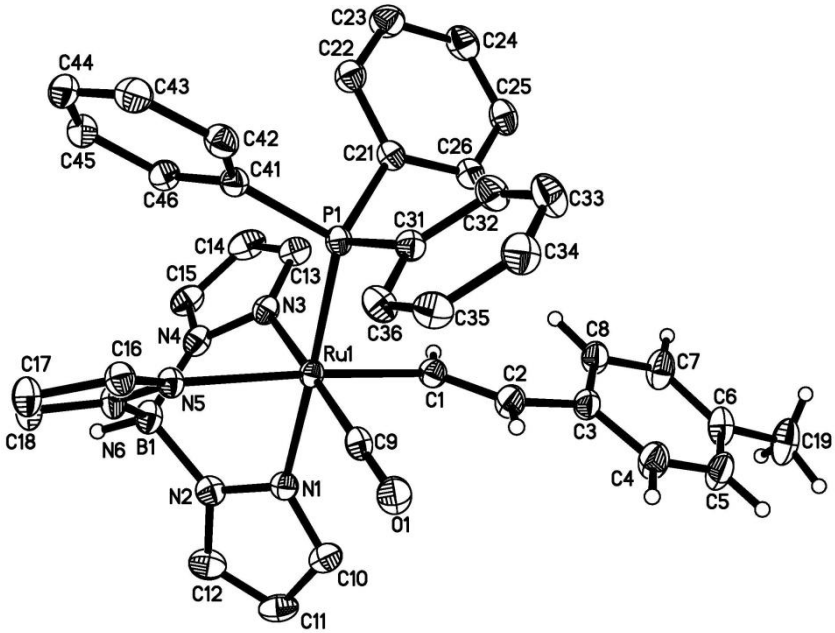

Figure 3.4. Plot of a molecule of 10c, showing the atom labeling scheme.

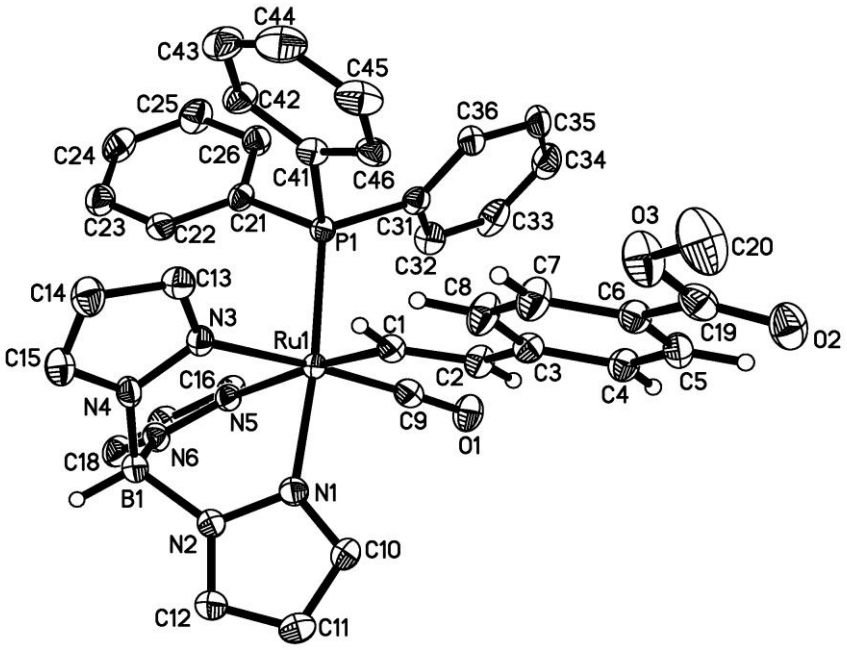

Figure 3.5. Plot of a molecule of 10d, showing the atom labeling scheme.

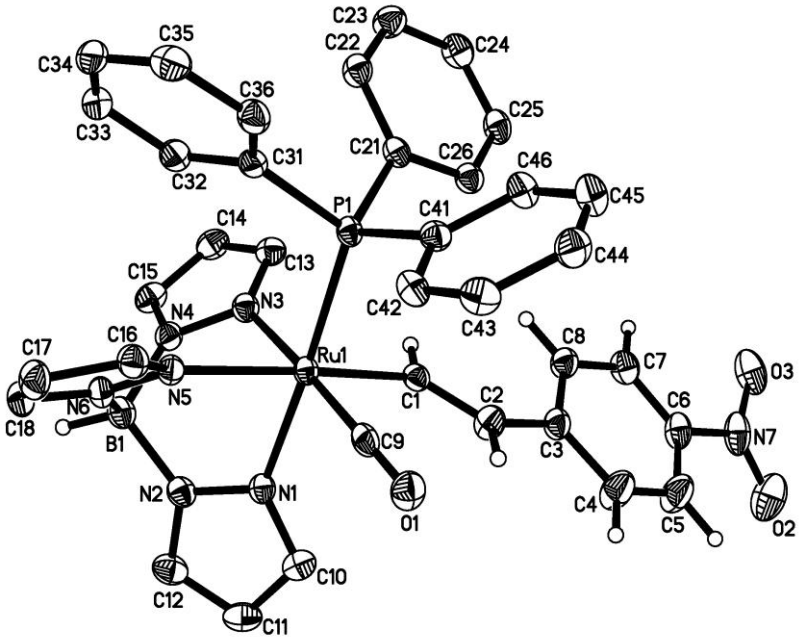

Figure 3.6. A plot of a molecule of 10e, showing the atom labeling scheme.

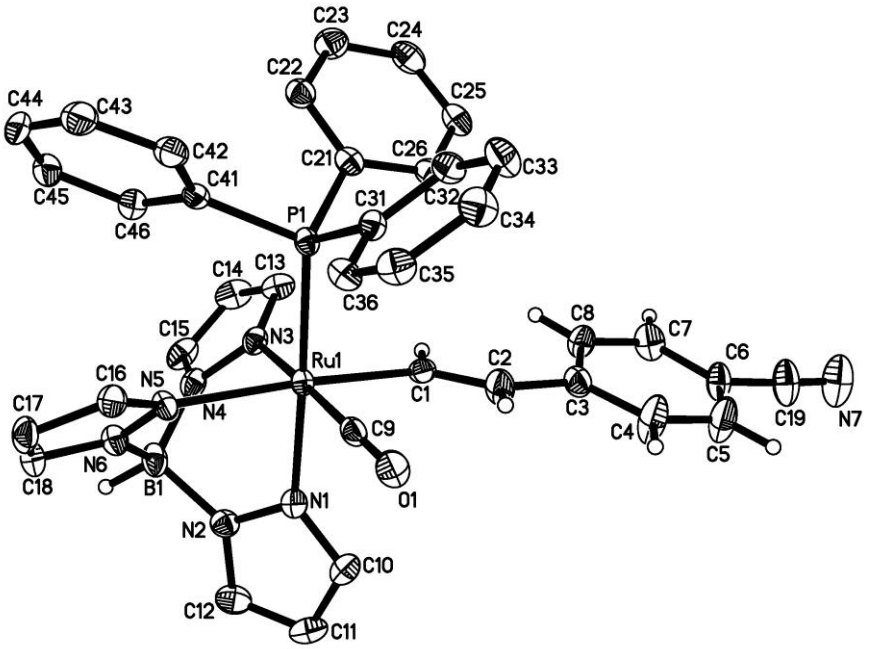

Figure 3.7. A plot of a molecule of 10f, showing the atom labeling scheme.

Table 3.1. Crystal data and structure refinement for 10b – f.

Complex	**10b**	**10c**	**10d.**CH_2Cl_2	**10e**	**10f**
Empirical formula	$C_{37}H_{34}BN_6O_2PRu$	$C_{37}H_{34}BN_6OPRu$	$C_{39}H_{36}BCl_2N_6O_3PRu$	$C_{36}H_{31}BN_7O_3PRu$	$C_{37}H_{31}BN_7OPRu$
Formula weight (g mol^{-1})	737.55	721.55	850.49	752.53	732.54
Crystal system	Orthorhombic	Monoclinic	Orthorhombic	Monoclinic	Monoclinic
Space group	Pbca	P $2_1/n$	$Pca2_1$	$P2_1/n$	$P2_1/n$
a (Å)	15.1780(3)	12.3553(4)	17.9655(9)	12.2388(2)	12.3271(4)
b (Å)	18.1705(3)	17.5258(6)	13.7346(7)	17.7482(3)	17.7540(5)
c (Å)	24.3305(5)	15.5575(5)	15.5579(9)	15.5664(3)	15.5549(4)
α (°)	90.00	90.00	90.00	90.00	90.00
β (º)	90.00	90.66(1)	90.00	90.36(10)	90.20(10)
γ (°)	90.00	90.00	90.00	90.00	90.00
Volume ($Å^3$)	6710.2(2)	3368.54(19)	3838.9(4)	3381.21(10)	3404.25(17)
Z	8	4	4	4	4
ρ_{calc} (Mg/m^3)	1.460	1.423	1.472	1.478	1.429
μ (mm^{-1})	0.559	0.553	0.635	0.559	0.549
F(000)	3024	1480	1736	1536	1496
Reflections collected	98899	44956	30441	42882	38474
Independent reflections/R_{int}	8512/0.0626	9799/0.0607	10183/0.0273	8573/0.0727	8972/0.0898
Data/restraints/parameters	8512/0/569	9799/0/560	10183/1/483	8573/0/450	8972/0/437
Goodness-of-fit on F^2	1.069	1.026	1.047	0.986	0.976
Final R_1 indices [I>2σ(I)]	0.0361	0.0324	0.0380	0.0334	0.0409
wR_2 indices (all data)	0.0990	0.0820	0.1069	0.0847	0.0904

Table 3.2. Selected bond lengths, Å.

Complex	**10b**	**10c**	**10d**	**10e**	**10f**
R	OMe	Me	CO_2Me	NO_2	CN
Ru(1)-C(1)	2.049(3)	2.0582 (19)	2.038 (3)	2.044 (2)	2.051(3)
Ru(1)-P(1)	2.3249(6)	2.3193 (5)	2.3360 (8)	2.3315 (6)	2.3326(7)
Ru(1)-N(1)	2.125(2)	2.1407 (16)	2.121 (2)	2.1368 (19)	2.142(2)
Ru(1)-N(3)	2.143(2)	2.1555 (16)	2.167 (3)	2.1504 (19)	2.155(2)
Ru(1)-N(5)	2.190(2)	2.1952 (5)	2.179 (2)	2.1879 (18)	2.195(2)
C(1)-C(2)	1.329(4)	1.342 (3)	1.352 (4)	1.338 (3)	1.334(4)
C(2)-C(3)	1.470(4)	1.474 (3)	1.472 (4)	1.466 (3)	1.473(4)
Ru(1)-C(9)	1.836(3)	1.8273 (19)	1.833 (3)	1.829 (2)	1.829(3)
C(9)-O(1)	1.149(3)	1.153(2)	1.154(4)	1.154(3)	1.161(3)

Table 3.3. Selected bond angles, °.

Complex	**10b**	**10c**	**10d**	**10e**	**10f**
R	OMe	Me	CO_2Me	NO_2	CN
C(9)-Ru(1)-C(1)	91.03(11)	86.52 (8)	88.72 (12)	87.42 (10)	86.63(11)
C(9)-Ru(1)-N(3)	174.77(9)	172.72 (7)	174.54 (12)	173.36 (9)	173.01(10)
C(1)-Ru(1)-N(5)	169.78(9)	171.96 (7)	171.04 (10)	171.91 (8)	97.55(10)
C(9)-Ru(1)-P(1)	92.61(8)	92.75 (6)	93.37 (10)	92.32 (8)	92.39(9)
C(1)-Ru(1)-P(1)	94.11(7)	91.92 (5)	92.78 (8)	92.46 (6)	91.81(7)
N(1)-Ru(1)-P(1)	175.47(6)	177.27 (4)	174.19 (7)	176.85 (5)	177.16(6)
C(2)-C(1)-Ru(1)	134.0(2)	132.10 (15)	134.3 (2)	131.89 (19)	132.4(2)
C(1)-C(2)-C(3)	127.0(3)	127.02 (19)	125.2 (3)	126.9 (2)	127.7(3)
C(9)-Ru(1)-C(1)-C(2)	-8.53	-7.83	-5.52	7.89	-3.85

Compounds **10a** – **e** exist as two enantiomers, both of which are present in the crystal; only molecular parameters from one molecule are discussed here, there being no significant differences in bond lengths between the geometric forms. The ruthenium metal centre exhibits a distorted octahedral geometry, with the Tp^- ion acting as a tridentate facially coordinating ligand and occupying three coordination sites. The Ru-C(9) [1.8273(19) – 1.836 (3) Å], Ru-P(1) [2.3193(5) – 2.3360(8) Å] and Ru(1)-C(1) [2.038(3) – 2.0582(19) Å] bond lengths are comparable with those of hydroruthenated compounds such as $Ru(CH=CHC_3H_7)Cl(CO)(PPh_3)_2(Me_2Hpz)$] [Ru-CO; 1.79(1) Å, Ru-P; 2.319(3) Å, and Ru-C_α; 2.05(1) Å][60] and [{$RuCl(CO)(PPh_3)_2(Py)CH=CH\}_3C_6H_3$-1,3,5] [Ru-CO; 1.809(10) Å, Ru-P; 2.397(2) Å, and Ru-C_α; 2.050(8) Å].[61] There is little or no evidence for significant quinoidal character within the phenylene portion of the molecule, Figure 3.8.

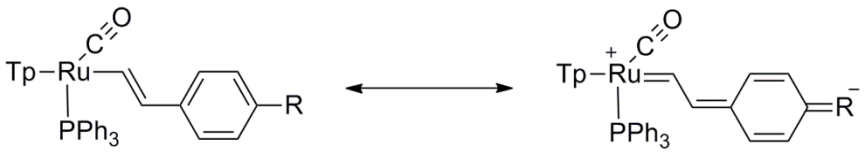

Figure 3.8. Resonance forms of complexes 10a – e, with the evolution of quinoidal character.

The strong *trans* influence of the σ-vinyl ligand causes an elongation of the Ru-N(5) [Ru(1)-N(5) 2.179(2) – 2.1952(15) Å] bond which is greater than the Ru-N(3) [Ru(1)-N(3) 2.1504(19) – 2.167(3) Å] and Ru-N(1) [Ru(1)-N(1) 2.121(2) – 2.142(2) Å] bond lengths, respectively. This difference in the three Ru-N bonds can be attributed to the structural *trans* effect[62] (STE) of each ligand *trans* to another, in this case a vinyl moiety, a carbonyl and triphenylphosphine ligand to the nitrogen atom of each pyrazolyl ring. Since the vinyl ligand is the strongest σ-donor, it exhibits the highest STE. The CO and PPh_3 ligands have both σ-donor and π-acceptor properties, with the CO being a weak σ-donor and a strong π-acceptor, whilst the inverse is true of a PPh_3 ligand. The fact that the CO ligand is a stronger π-acceptor means it exhibits a higher STE compared to the PPh_3 ligand. Whilst little difference can be seen in the Ru(1) – N(1) and Ru(1) – N(3) bond lengths, the greater STE of the vinyl ligand in the Ru(1) – N(5) bond length is evident in the crystallographic data.

In compounds **10a** – **e**, the vinyl ligand is coplanar with the CO ligand.[45] This is a feature which is common to transition metal alkenyl complexes bearing a CO ligand and a vinyl moiety, serving to maximise backbonding interactions between the metal d orbitals and the carbonyl π-systems.[63] In Figure 3.9, the two lowest energy configurations of the vinyl ligand and the *cis* carbonyl ligand are depicted, where the degree of planarity is defined by the dihedral angle (θ). In 18 electron transition metal alkenyl complexes, the metal atom has a fully occupied set of t_{2g} orbitals with π-symmetry with respect to the metal ligand bond. When the carbonyl and vinyl ligand are co-planar, π-backbonding interactions from the donation of electron density from the metal t_{2g} orbitals into the π* orbitals of both the carbonyl and vinyl ligand is favoured i.e. when θ = 0 and 180°, Figure 3.10.

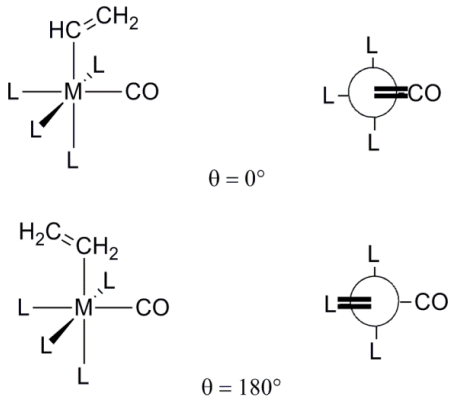

Figure 3.9. Preference of the vinyl and carbonyl ligand to be coplanar.

The coplanar orientation of the carbonyl and vinyl ligand results in a significant energy barrier to rotation about the metal alkenyl bond of up to 10 kcal.mol^{-1}. This value is significantly higher than in simple organic molecules where rotation is usually less than 2 kcal.mol^{-1}.[64, 65] Although a simple schematic MO description does not distinguish a preference for the vinyl ligand *cis* or *trans* to the CO ligand, detailed NBO (natural bond order) analysis on related model systems suggests that the *cis* geometry is marginally (< 2 kcal.mol^{-1}) more stable.[64]

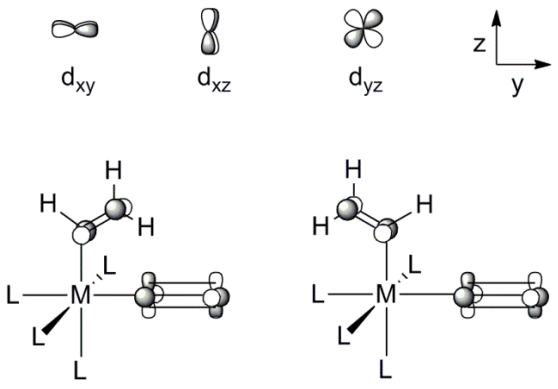

Figure 3.10. Orbital diagrams showing the t_{2g} metal d contributions and the orientation of the orbitals of the alkenyl and carbonyl ligands.

3.4 Electrochemistry

Despite the close relationships between the isoelectronic Tp^- and Cp^- ligands, and the interest of both half-sandwich complexes bearing unsaturated ligands and the five and six coordinate vinyl complexes, the redox chemistry of $Ru(CH=CHC_6H_4R\text{-}4)(CO)(PPh_3)Tp$ seems to have been little explored. The six coordinate Tp^- capped ruthenium vinyl complexes **10a – e** exhibit one or two (**10a**) oxidative waves at a platinum working electrode in 0.1 M NBu_4BF_4 / CH_2Cl_2 at potentials that reflect the electronic properties of the aryl substituent, Table 3.4.

Table 3.4. The electrochemical response of 10a – e in 0.1 M NBu_4BF_4 / CH_2Cl_2, with a Pt working electrode, ν = 100 mV s^{-1}. Values referenced to $FcH/[FcH]^+$ = 0 V.

Complex	R	$E_{1/2}$ / V	ΔE_p / mV	i_{pc}/i_{pa}
10a[a]	$N(C_6H_4Me\text{-}4)_2$	0.00	83	0.85
10b[b]	OMe	0.14	73	0.92
10c	CH_3	0.24	86	0.73
10d	CO_2Me	0.40	78	1.00
10e[c]	NO_2	0.51	112	0.88

[a] A reversible oxidation was observed at 0.39 V attributed to the oxidation of the amine moiety. [b] An irreversible oxidation was observed at E_{pa} 0.64 V attributed to the oxidation of the anisole moiety. [c] A reversible reduction was observed at – 1.72 V for the nitro moiety.

Complex **10a**, which bears a strong electron donating R group is easier to oxidise than **10b**. Complex **10d** is also easier to oxidise than **10e**, which possesses the strongest electron withdrawing R group in this series, whilst the weakly electron donating **10c** lies in between these extremes. However, there are signs of slow electron transfer, as reflected in the ΔE_p (the peak potential difference), particularly in **10e**, which is almost twice that of the 59 mV separation typically expected for an one electron diffusion controlled electrochemical reaction. Chemical decomposition of the cations was also indicated by i_{pc}/i_{pa} less than unity. Complex **10e** also has a reduction wave, reversible in CH_2Cl_2, which can be readily assigned to the reduction of the nitrophenyl moiety. The significant influence of the aryl ring substituent on the electrochemical potentials in the series of complexes **10a** – **e** indicates that the aryl group is likely closely associated with the redox-active orbitals.

3.5 IR Spectroelectrochemistry

The presence of a carbonyl ligand in a complex provides a vibrational probe through which electron density at a metal can be assessed. This is due to the synergistic interaction between the metal and the carbonyl ligand that involves the forward donation of a lone pair from the CO ligand to the d orbital of the metal, and the subsequent π-backbonding into the ligand π* orbital. Owing to the substantial decrease in metal-carbonyl backbonding, metal-based oxidations typically results in a change in the stretching frequency of the carbonyl ligand, $\Delta\nu(C{\equiv}O)$ of ~ 100 – 150 cm^{-1}.[66] The complexes **10a** – **e** are ideal candidates for IR spectroelectrochemical studies, with not only shifts in $\Delta\nu(C{\equiv}O)$, but also $\Delta\nu$(B-H) and $\Delta\nu(C{=}C)$ allowing an assessment of the structural and electronic changes accompanying each redox process.[67]

On oxidation of complexes **10a** – **e** there is a shift in $\Delta\nu$(C≡O) of ca. + 30 – 50 cm^{-1} to higher energy, Figure 3.11, Table 3.5. This relatively small shift compares to the ca. + 20 – 65 cm^{-1} that results from the oxidation of closely related systems [Ru(CH=CHAr)Cl(CO)(P^iPr_3)$_2$(L)] (Ar = Ph, pyrenyl; L = 4-ethylisonicotinate, vacant coordination site) which have been interpreted in terms of redox non-innocent vinyl ligands.[29] The small shift in $\Delta\nu$(B-H) of ~ 15 cm^{-1} also supports the concept of a redox-active (or at least non-innocent) vinyl ligand in **10a** – **e**, indicating that the Tp^- ligand is little affected by the oxidation process. In addition, on oxidation of the carbonyl ester in **10d** there was also a small shift of ca. + 11 cm^{-1} to higher energy ([**10d**] (ν(C=O) 1708, [**10d**]$^+$ (ν(C=O) 1719 cm^{-1}). This compares to the + 3 – 5 cm^{-1} shift in the 4-ethylisonicotinate ester bands upon oxidation of the five coordinate complexes [Ru(CH=CHR)Cl(CO)(P^iPr_3)$_2$(py)] (R = ^{t}Bu, Ph, 1-pyrene, py = 4-ethylisonicotinate) in which the ester reporting group is connected *via* a pyridine ligand to the metal centre.[29] Thus in Winter's systems, the non-innocent vinyl ligand is even more heavily involved in the oxidation process.

On reduction of [**10a** – **e**]$^+$, there was significant recovery of the neutral complexes, though a degree of decomposition is evident, with a persistent band at ca. 1973 cm^{-1} being formed with a concomitant decrease in the intensity of the ν(C≡O) band which was not present in the original sample. Thus, these results are consistent with electrochemical data with i_{pc}/i_{pa} values of less than unity in 0.1 M NBu_4BF_4 / CH_2Cl_2 at a platinum working electrode. An attempt to probe the dication [**10a**]$^{2+}$ was

compromised by rapid decomposition of the sample at the platinum mini-grid working electrode of the spectroelectrochemical cell and was not investigated further.

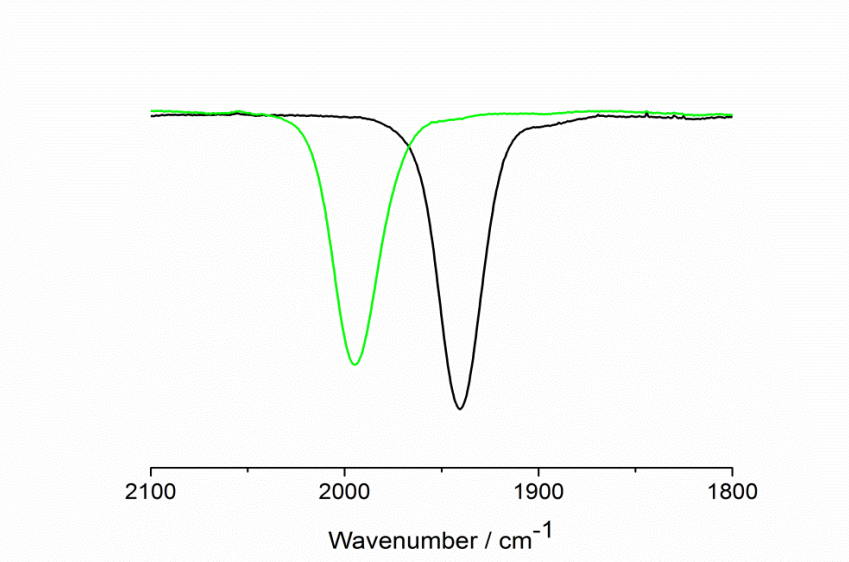

Figure 3.11. IR spectra for 10d (black) and $[10d]^+$ (green) in 0.1 M NBu_4BF_4 / CH_2Cl_2.

Table 3.5. IR spectroelectrochemical data for $[10a – e]^{n+}$ (n = 0, 1) in 0.1 M NBu_4BF_4 / CH_2Cl_2.

		Neutral		Cation			
	R	ν(C≡O) / cm^{-1}	ν(B-H) / cm^{-1}	ν(C≡O) / cm^{-1}	ν(B-H) /cm^{-1}	Δν(C≡O) / cm^{-1}	Δν(B-H) / cm^{-1}
10a	$N(C_6H_4Me\text{-}4)_2$	1940	2482	1973	2490	33	8
10b	OMe	1940	2481	1992	2497	52	16
10c	CH_3	1942	2484	1995	2496	53	12
10d[a]	CO_2Me	1944	2482	1995	2496	51	14
10e	NO_2	1946	2485	1996	2500	50	15

[a] ν(C=O, ester): **10d** 1708, **[10d]**$^+$ 1719 cm^{-1}.

3.6 UV-vis-NIR Spectroelectrochemistry

In the UV-vis-NIR spectra, complexes **10a** – **e** are characterised by an intense absorption envelope which decreases in energy, from **10a** and **10b** bearing a strongly electron donating R group (Figure 3.13) to **10d** and **10e** featuring a strongly electron withdrawing R group (Figure 3.14), Table 3.6. The decrease in energy can be attributed to a stabilisation of the frontier molecular orbitals by the electron withdrawing groups, hence a lower energy transition. Electron donating groups, for example in **10b**, have the opposite effect, resulting in a destabilisation of the frontier molecular orbitals, ultimately leading to a higher energy transition, Figure 3.13. On oxidation of **10b** – **e** there is a shift of the ML-LCT transition to lower energy by 5000 – 10000 cm^{-1}, and a new transition also develops in the NIR region near 10000 cm^{-1}, Table 3.6.

Table 3.6. UV-vis absorption bands in 0.1 M NBu_4BF_4 / CH_2Cl_2 of [10a – e]$^{n+}$ (n = 0, 1).

Complex	R	Wavenumber / cm^{-1} [ε / $M^{-1}cm^{-1}$]
10a	$N(C_6H_4Me\text{-}4)_2$	31850 [27530]
		29500 [32300]
[**10a**]$^+$		20530 [18250
		8640 [20350]
10b	OMe	33560 [20270]
[**10b**]$^+$		23420 [13200]
		12220 [6240]
10c	CH_3	32900 [18570]
[**10c**]$^+$		24390 [3270]
		13040 [1070]
10d	CO_2Me	27930 [31960]
[**10d**]$^+$		22320 [2190]
		13120 [700]
10e	NO_2	22830 [28750]
[**10e**]$^+$		16050 [4020]
		12800 [1070]

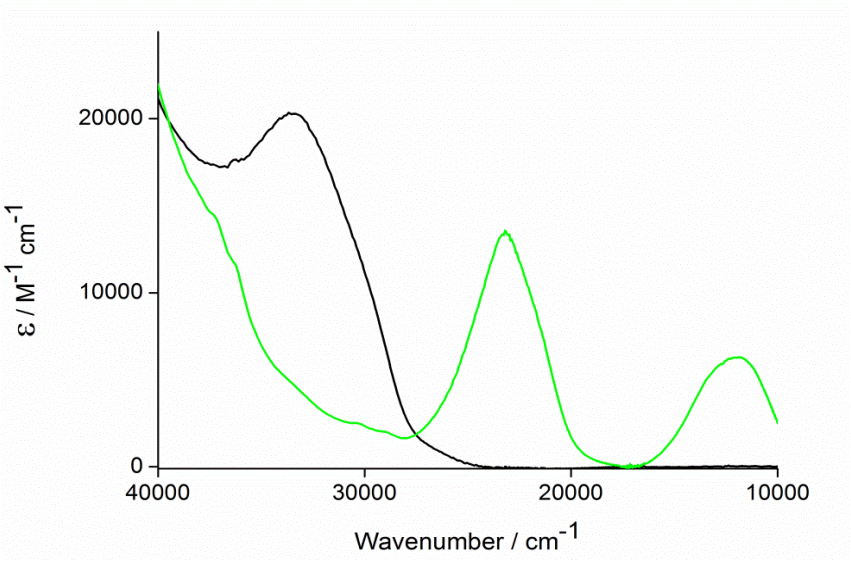

Figure 3.13. The UV-vis-NIR spectra of 10b (black) and $[10b]^+$ (green) obtained in 0.1 M NBu_4BF_4 / CH_2Cl_2.

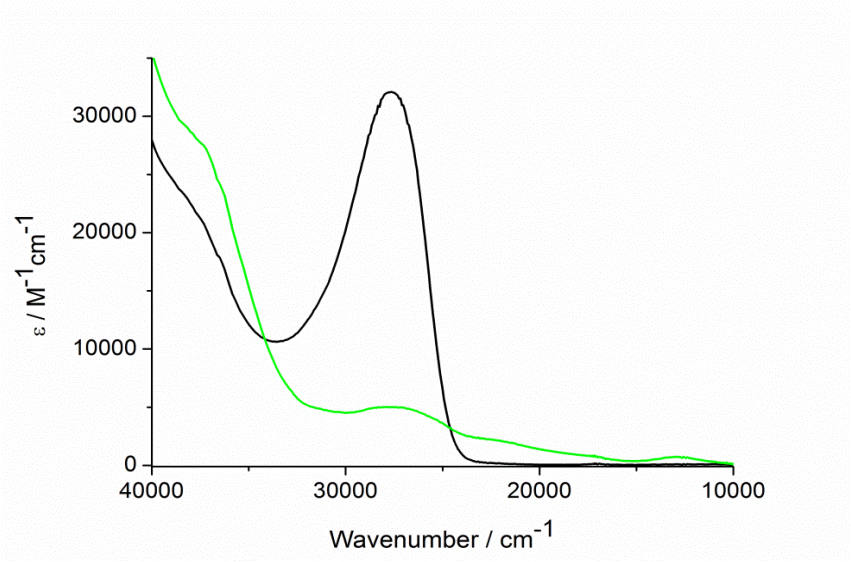

Figure 3.14. The UV-vis-NIR spectra of 10d (black) and $[10d]^+$ (green) obtained in 0.1 M NBu_4BF_4 / CH_2Cl_2.

3.7 Electronic Structure Calculations

DFT calculations were performed by Dr J.D. Farmer, Dr M.A. Fox and Prof. P.J. Low of Durham University on the model systems **10a´** – **10e´** with the same ligands as in the real complexes, using the B3LYP functional. The ruthenium atom was modelled using the LANL2DZ basis set, whilst 3-21G* was employed for all other atoms.

In complexes **10b´**– **e´** the HOMO has significant vinyl ligand character (61 – 89 %), Figure 3.12a. The β-LUSO for the oxidised species [**10b´**– **e´**]$^{+}$ is essentially the same as the HOMO in the neutral systems (44 – 78 %), with the small decrease in contributions to the HOMO attributed to the increase in metal contributions to the spin orbital, Figure 3.12b. These results are consistent with Winter's reports of the significant contribution of the vinyl ligand in the HOMO of [Ru(CH=CHR)Cl(CO)(PMe_3)$_2$] where R = Ph, Py (67 – 84 %) which exhibit a redox non-innocent vinyl ligand.[29] The HOMO in **10a´** is more heavily weighted on the triarylamine fragment (89 % on the vinyl ligand, of which 47 % is localised on the N(C_6H_4Me-4)$_2$ fragment). The ability of the triarylamine fragment to form remarkably stable one electron cationic systems is reflected in the low oxidation potential of the triarylamine,[68] with the involvement of this ligand in the oxidation process also reflected in a smaller shift of ν(C≡O) to higher wavenumber in comparison to **10b´** – **e´**.

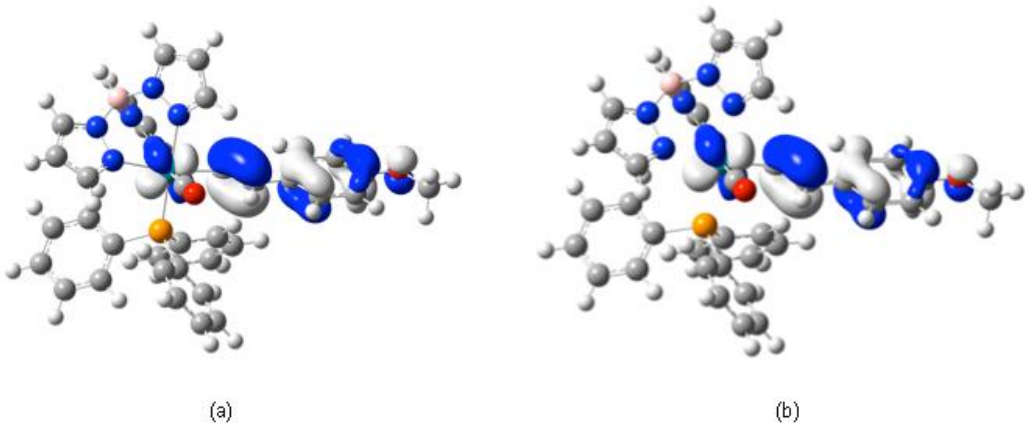

Figure 3.12. The (a) HOMO of 10b´ and (b) β-LUSO of [10b´]$^{+}$.

With the aid of time dependent-density functional theory (TD-DFT), the high energy transition in the parent complexes **10a** – **e** have been assigned as a metal ligand to ligand charge transfer (ML-LCT) i.e. from a metal orbital which is admixed with ligand character to an orbital which is ligand in character, Table 3.6. In addition, complex **10a** also features a N(p) – Ar(π*) transition (31850, 29500 cm^{-1}) which is characteristic of a triarylamine moiety, Table 3.6.[69] The ML-LCT transition in the oxidised species has essentially the same ML-LCT character as the UV band in the neutral species, whilst the new low energy bands are assigned to as excitations from the β-HOSO to the β-LUSO. In addition, in the oxidation of **10a**, both ML-LCT and N(p) – Ar(π*) transitions collapse, reflecting the mixed metal / nitrogen character of the HOMO in **10a´** and the α- and β-HOSO and LUSO in [**10a´**]$^{+}$.

3.8 Bimetallic Ruthenium Vinyl Complexes

The interest in ligand mediated electron transfer processes has prompted several studies of bimetallic complexes featuring vinyl-based bridging ligands, For example, in an IR spectroelectrochemical cell, the 4-ethylisonicotinate complexes 1,4- and 1,3-[{($EtO_2CC_6H_4N$)(PPh_3)$_2$(CO)ClRu}$_2$(μ-CH=CHC_6H_4CH=CH)], Figure 3.15, reveal small shifts in both Δν(C≡O) +13 and 33 cm^{-1} and Δν(C=O, ester) ca. +2 and 11 cm^{-1}, demonstrating the vinyl bridging ligand to be the largely redox-active site in these molecules.[46] EPR analyses of the electrochemically generated cations reveal *g* values which are similar to that of a free electron (g_e = 2.0023), deviating from a characteristic metal centred paramagnetic species and suggesting that oxidation occurs on the organic fragment. The nature of the frontier molecular orbitals as predicted by DFT studies is consistent with experimental results, suggesting a redox-active vinyl bridging ligand.

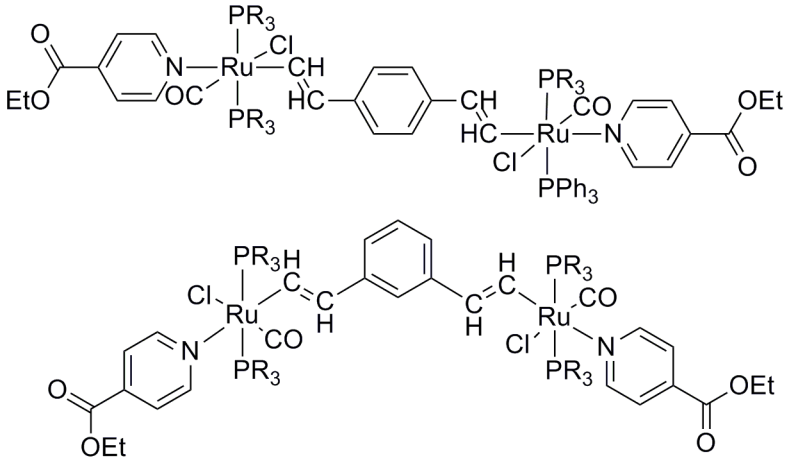

Figure 3.15. Bimetallic ruthenium complexes synthesised and studied by Winter and co-workers where PR_3 = PPh_3.

The strong mixing of the ruthenium and ligand based orbitals in a diruthenium complex spanned by a butadienediyl bridge, for example [{($EtO_2CC_6H_4N$)(PPh_3)$_2$(CO)ClRu}$_2$ (μ-C_4H_4)], also leads to substantially delocalised radicals, making the designation of redox processes as metal or ligand processes meaningless.[70] However, such strong delocalisation of charge within a molecular entity has potential materials application, for example to promote long range interactions within an assembly. As a consequence, Winter and co-workers have incorporated the RuCl(CO)(P^iPr_3)$_2$ entity into (ethynyl)(vinyl)phenylene bridged tri-ruthenium complexes, Figure 3.16, which can be oxidised by one electron to give further examples of extensively delocalised bridge centred radicals.[71-74] In addition, the incorporation of a vinyl entity allows the possibility to create even more extended systems through the coordination of a ligand to the vacant site *trans* to the vinyl ligand at the ruthenium metal centre. It is therefore imperative that a fundamental understanding of the electronic structure of a complex is developed, such that we are able to manipulate a molecular system to perform a particular electronic or spectroscopic function.

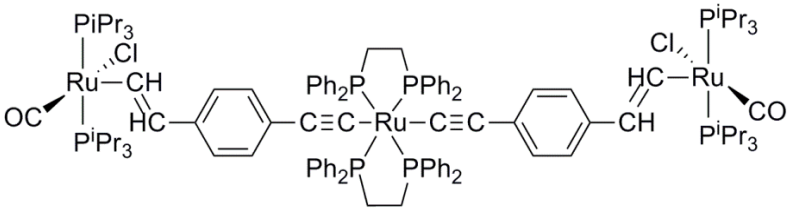

Figure 3.16. Tri-ruthenium complexes with an (ethynyl)(vinyl)phenylene bridge.

Jia and co-workers have synthesised some bimetallic five coordinate ruthenium vinyl complexes of the general form $[\{(PPh_3)_2(CO)ClRu\}_2(\mu\text{-}CH{=}CH)_n]$ where n = 3, 4, 5 and 7. The reaction of these five coordinate ruthenium vinyl complexes with monodentate ligands such as 4,4'-bipyridine, PMe_3 and ^tBuCN or tridentate pincer ligands such as $[2,6\text{-}(CH_2NR_2)_2C_5H_3N]$ and KTp give six coordinate ruthenium vinyl complexes.[51, 75-78] However, the work reported by Jia and co-workers is largely limited to synthetic studies, with electrochemical techniques used to assess the electronic interactions mediated by vinyl bridges of increasing length; as noted in Chapter 1, there are some difficulties in drawing conclusions on electronic structure from thermodynamic (electrochemical) data.

Over the last ten years, Winter and co-workers have established the redox non-innocence (or rather, redox activity) of the vinyl ligand in a variety of mono-, bi- and polymetallic ruthenium complexes using a variety of spectroscopic techniques which include IR and UV-vis-NIR spectroelectrochemistry, supported by DFT studies.[29, 46, 66, 79, 80] The ability to systematically alter the relative order of the metal- and bridge based redox sites by varying the choice of the supporting ligands at the metal centre has been noted, and discussed earlier.[81] However, in the context of these reports and the work on the Tp^{-} coordinated ruthenium vinyl complexes described above, a recent study of the bimetallic ruthenium vinyl complex $[\{(PMe_3)_3(CO)ClRu\}_2(\mu\text{-}CH{=}CHC_6H_4CH{=}CH)]$ was shown to undergo two sequential one-electron oxidation processes.[52, 54] On the assumption that these redox events were metal centred (which may be considered reasonable at first given the strongly electron donating PMe_3 ligands, but is in contrast to a considerable body of Winter's work), Liu and co-workers reported that intermetallic communication as "indicated" by $\Delta E_{1/2}$ could be tuned through the modification of donor and acceptor groups connected to the bridging ligand, Table 3.7. However, as discussed in Chapter 1, ΔE is sensitive to a number of factors such as solvation, ion-pairing energies, as well as resonance delocalisation, with only the latter of these factors giving rise to the concept of metal-metal interactions. This fundamentally raises the question of whether tuning of the 'metal-metal electronic interactions' in these bimetallic complexes can be achieved, or even if the redox chemistry is being accurately assigned.

Table 3.7. A family of bimetallic bis(vinyl)complexes, and selected electrochemical data (0.1 M NBu_4PF_6 / CH_2Cl_2; Ag/Ag^+ (0.01 M $AgNO_3$ / 0.1 M NBu_4PF_6 / NCMe) reference, separated by a salt bridge containing 0.1 M NBu_4PF_6 / CH_2Cl_2at ambient temperature.[54] $\Delta E_{1/2} = E_2 - E_1$, $K_C = \exp(\Delta EF/RT)$.

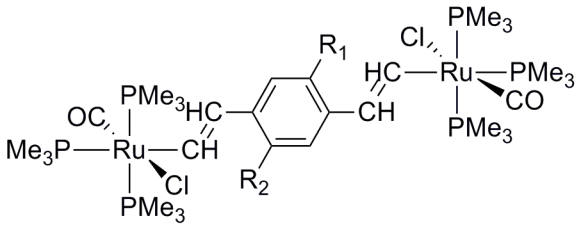

R_1	R_2	E_1	E_2	$\Delta E_{1/2}$	K_c
H	H	0.30	0.59	0.29	8.0×10^4
H	CH_3	0.24	0.54	0.30	1.2×10^5
H	OCH_3	0.19	0.50	0.31	1.7×10^5
H	F	0.33	0.59	0.26	2.5×10^4
H	Cl	0.37	0.61	0.24	1.1×10^4
H	Br	0.37	0.61	0.24	1.1×10^4
H	CN	0.46	0.66	0.20	2.4×10^3
H	NO_2	0.52	0.71	0.19	1.6×10^3
H	CF_3	0.42	0.64	0.22	5.2×10^3
CH_3	CH_3	0.20	0.50	0.30	1.2×10^5
OCH_3	OCH_3	0.10	0.46	0.36	8.2×10^5
F	F	0.41	0.64	0.23	7.7×10^3
CF_3	CF_3	0.57	0.75	0.18	1.1×10^3

3.9 Synthesis

In seeking to address the issue of ligand redox non-innocence vs. metal-metal interactions, the complexes [Ru(CH=CHC$_6$H$_4$Me-4)Cl(CO)(PMe$_3$)$_3$] (**11)** and [{(PMe$_3$)$_3$(CO)ClRu}$_2$(μ-CH=CHC$_6$H$_4$CH=CH)] (**12)** were prepared by the reported literature methods, see Scheme 3.5.[50, 52] Purification by preparative TLC techniques using an eluent system of CH_2Cl_2 and hexane (30:70) produced the desired complexes in moderate yields.

3.9.1 Spectroscopic Investigations

Complex **11** and **12** were characterised by ^{1}H and ^{31}P and infrared spectroscopies. In the ^{1}H NMR spectrum, the vinylic protons are observed as a ddt, arising from the coupling the vinylic H_α to the H_β and their subsequent coupling to the phosphorus nuclei of the coordinated PMe_3 ligands. The $^3J_{HH}$ coupling of 17 Hz is diagnostic of *trans* vinyl protons. In the ^{31}P NMR spectrum, the AM_2 pattern observed is indicative of PMe_3 ligands which are meridonally coordinated to ruthenium. In the IR spectra of **11** and **12**, a single, strong ν(C≡O) band at 1921 cm^{-1} is observed in CH_2Cl_2.

3.10 Molecular Structures

The molecular structures of **9a** (Figure 3.17), **11** (Figure 3.18) and **12** (Figure 3.19) were determined by single crystal X-ray diffraction by Dr D.S. Yufit at Durham University. Crystallographic data, selected bond lengths and bond angles are listed in Tables 3.8 and 3.9 respectively.

Table 3.8. Crystal data and structure refinement for 9a, 11 and 12.

Complex	**9a**	**11**	**12**
Empirical formula	$C_{32}H_{47}ClNOP_3Ru$	$C_{19}H_{36}ClOP_3Ru$	$C_{30}H_{62}O_2Ru_2Cl_2P_6$ x $3CH_2Cl_2$
Formula weight (g mol^{-1})	691.14	509.91	1168.43
Temperature (K)	-	120.0	120.0
Wavelength (Å)	-	0.71073	-
Crystal system	Triclinic	Monoclinic	Monoclinic
Space group	P-1	$P2_1/n$	C2/c
a (Å)	11.5356(3)	14.3554(5)	55.2276(11)
b (Å)	12.9757(4)	12.3124(4)	9.4525(2)
c (Å)	13.3499(4)	14.8419(5)	21.2707(4)
α (º)	64.04(1)	90.00	90.00
β (º)	70.43(1)	111.26	106.95(10)
γ (º)	78.61(1)	90.00	90.00
Volume ($Å^3$)	1689.77(8)	2444.7(1)	10621.8(4)
Z	2	4	8
Density (calculated) Mg/m^3	1.358	1.385	1.461
Absorption coefficient (mm^{-1})	0.710	0.953	1.179
F(000)	720	1056	4768
Crystal size (mm^3)	-	0.52 x 0.36 x 0.20	0.16 x 0.22 x 0.30
Theta range for data collection (°)	-	1.69 to 30.00	2.00 to 29.00
Index ranges	-	20<=h<=20, -17<=k<=17, -20<=l<=20	-75<=h<=75, -12<=k<=12, -29<=l<=29
Reflections collected	30109	32201	63667
Independent reflections	9862	7117 [R(int) = 0.0276]	14109 [R(int) = 0.0317]
Data/restraints/parameters	9862/0/540	7117/0/226	14109/0/485
Goodness-of-fit on F^2	1.064	1.070	1.015
Final R indices [I>2sigma(I)]	0.0286	R_1 = 0.0352 wR_2 = 0.0913	R_1 = 0.0568 wR_2 = 0.1277
R indices (all data)	0.0344	R_1 = 0.0384 wR_2 = 0.0933	R_1 = 0.0624 wR_2 = 0.1277
Largest diff. peak and hole ($e.Å^{-3}$)	-	1.780/-0.799	2.363/-1.031

Table 3.9. Selected bond lengths and bond angles for 11 and 12.

	11	**12**
Bond lengths / Å		
Ru(1)-P(1)	2.3633(6)	2.3611(11)
Ru(1)-P(2)	2.3940(6)	2.4064(11)
Ru(1)-P(3)	2.3617(6)	2.3663(11)
Ru(1)-C(1)	2.092(3)	2.112(4)
C(1)-C(2)	1.311(4)	1.333(6)
C(2)-C(3)	1.488(4)	1.483(6)
C(3)-C(4)	1.398(4)	1.399(6)
C(4)-C(5)	1.413(4)	1.388(6)
C(7)-C(8)	1.369(4)	1.387(6)
C(6)-C(9)	1.512(4)	1.481(6)
C(9)-C(11)	-	1.327(6)
C(11)-Ru(2)	-	2.115(4)
Ru(2)-P(4)	-	2.3597(12)
Ru(2)-P(5)	-	2.3969(12)
Ru(2)-P(6)	-	2.3614(13)
Bond angles / °		
P(1)-Ru(1)-P(3)	168.10(2)	161.97(4)
P(2)-Ru(1)-C(1)	177.55(7)	178.27(12)
Ru(1)-C(1)-C(2)	134.0(2)	131.3(3)
C(9)-C(11)-Ru(2)	-	130.4(3)
P(4)-Ru(2)-P(6)	-	163.44(4)
P(5)-Ru(2)-C(11)	-	178.92(13)

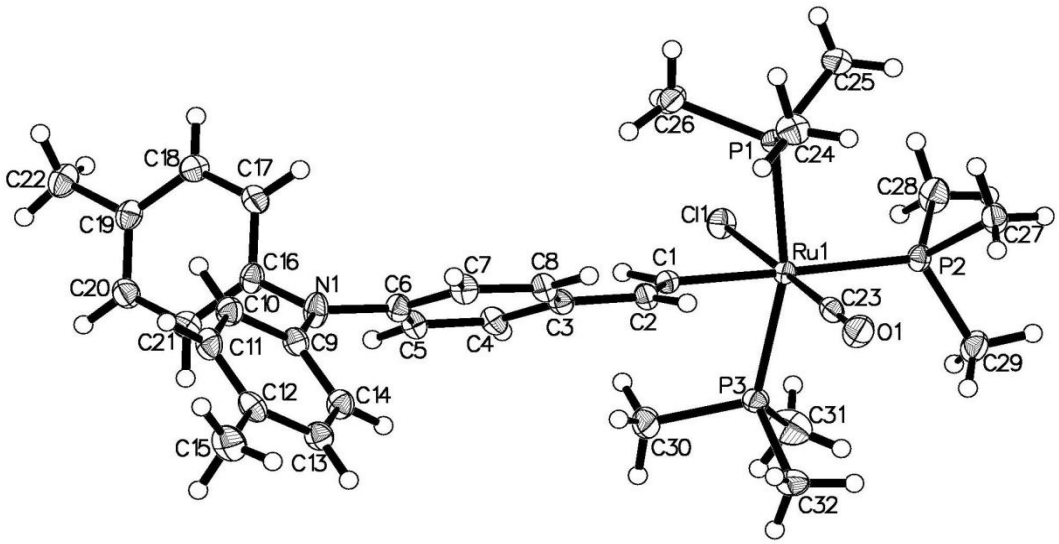

Figure 3.17. Plot of 9a, showing the atom labeling scheme. Thermal ellipsoids in this and all subsequent figures are plotted at the 50 % probability level.

Selected bond lengths (Å) : Ru(1)-P(1) 2.3539(5); Ru(1)-P(2) 2.3919(4); Ru(1)-P(3) 2.3657(5); Ru(1)-Cl(1) 2.4617(5); Ru(1)-C(23) 1.8602(19); Ru(1)-C(1) 2.1165(15); C(1)-C(2) 1.339(2); C(2)-C(3) 1.480(2); N(1)-C(6) 1.422(2); N(1)-C(9) 1.408(2); N(1)-C(16) 1.433(2). Selected bond angles (°) : P(1)-Ru(1)-P(2) 95.73(2); P(1)-Ru(1)-Cl(1) 86.11(2); P(1)-Ru(1)-C(23) 94.16(5); P(1)-Ru(1)-C(1) 82.37(4); P(1)-Ru(1)-P(3) 164.31(2).

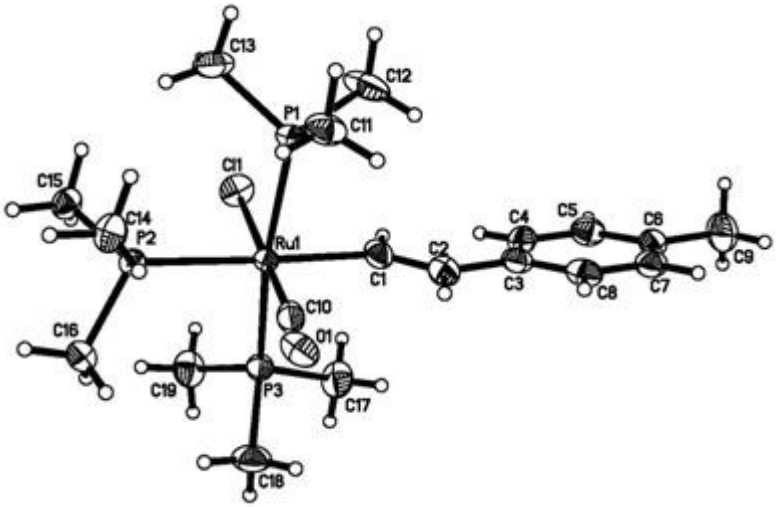

Figure 3.18. Plot of 11, showing the atom labeling scheme.

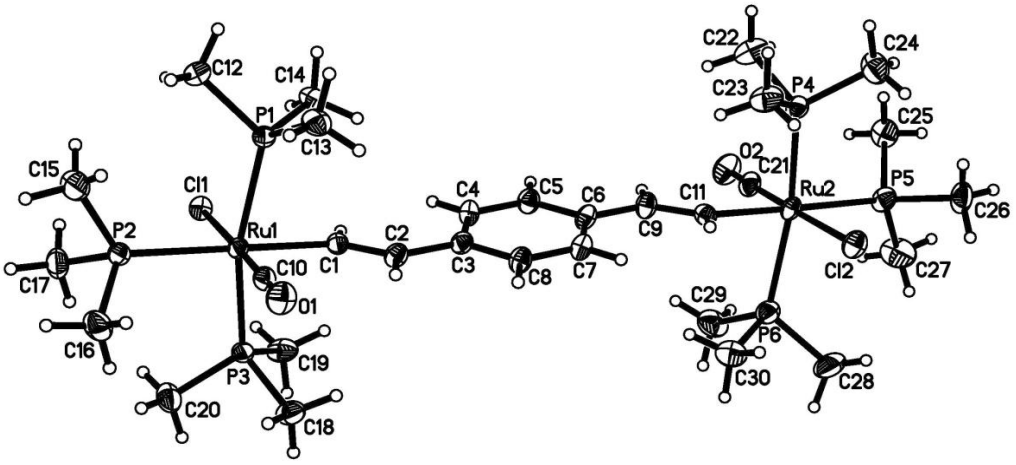

Figure 3.19. Plot of 12, showing the atom labeling scheme.

The metal centres in **9a**, **11** and **12** display a distorted octahedral geometry. The vinyl ligand is coplanar to the CO ligand as expected from orbital considerations,[63] as discussed for compounds **10b** – **f**. The aromatic rings in **9a** adopt the usual "propeller" configuration whilst the nitrogen centre is essentially planar, with the sum of angles at N(1) = 360 °, thus confirming the sp^2 nature of this atom. In all three complexes, the bond between the metal centres and the *trans* phosphines [Ru1-P(2): **9a** 2.3919(4); **11** 2.3940(6); **12** 2.4064(11)] is elongated relative to the mutually *trans* phosphines [Ru1-P(1): **9a** 2.3539(5); **11** 2.3633(6); **12** 2.3611(11); Ru(1)-P(3): **9a** 2.3657(5); **11** 2.3617(6); **12** 2.3633(11)]; this can be accounted for by the *trans* influence of the vinyl ligand. The plane of the vinyl ligand and aryl ring are not parallel (torsion angle C1-C2-C3-C4: **9a** 24.1 °; **11** –8.9 °; **12** 4.3 °). In the bimetallic complex **12**, there is no evidence for significant cumulenic contribution to the bridging ligand and thus there is no ground state delocalisation.

3.11 Electrochemisty

Liu and co-workers recently reported that monometallic ruthenium vinyl complexes of the form $[Ru(CH=CHC_6H_4R\text{-}4)Cl(CO)(PMe_3)_3]$ undergo a single, chemically irreversible, one electron oxidation process, at potentials which track linearly with the Brown σ^+ parameter of the aryl ligand substituent R.[52] The chemical reversibility of this redox event was found to be enhanced by strong donor substituents such as R = OMe, NH_2 and NMe_2. The CV of **11** exhibited a single irreversible oxidation wave, Table 3.10. At lower temperatures, the chemical reversibility of the redox wave improves with i_{pc}/i_{pa} = 0.69 at ca. –50 °C but the event is never perfectly reversible. A substantial ΔE_p is observed of 210 mV which is somewhat larger than that of the internal decamethylferrocene and therefore indicative of slow electron transfer. The CV of **12** is characterised by two oxidation waves, which become chemically but not electrochemically reversible at ca. –50 °C, Table 3.10.

Table 3.10. Cyclic voltammetry data recorded in 0.1 M NBu_4PF_6 / CH_2Cl_2 at a glassy carbon electrode, ν = 100 mV s^{-1} at – 40 °C. Values referenced to $FcH/[FcH]^+$ = 0 V.

Complex	$E_{1/2}$ (1) / V	$E_{1/2}$ (2) / V	$\Delta E_{1/2}$ / mV
11	0.59[a]	-	-
12	0.13	0.44	310

[a] Irreversible

3.12 IR Spectroelectrochemistry

To better assign the nature of the redox process, IR spectroelectrochemical studies were carried out on **11** and **12** using the ν(C≡O) band as an indicator of metal oxidation state. On oxidation of **11** in the spectroelectrochemical cell, the ν(C≡O) band shifted from 1921 cm^{-1} to 1974 cm^{-1}, Figure 3.20, Table 3.11. This shift of 53 cm^{-1} to higher wavenumbers is relatively small and compares to the ca. +100 cm^{-1} shift typically expected for a metal centred oxidation, and indicates that an appreciable fraction of the charge lost originates from the organic π system. In support of this, the phenylene ring ν(C=C) stretch at 1607 cm^{-1} also gains in intensity during the oxidation process. On reduction of $[\mathbf{11}]^+$ there is significant recovery of **11**, confirming the shift in ν(C≡O) to be associated with the electrochemical formation of $[\mathbf{11}]^+$. However, there was some decomposition, as evident in the reduced intensity of ν(C≡O) and the formation of a secondary product at 1944 cm^{-1}, which was not in the original sample.

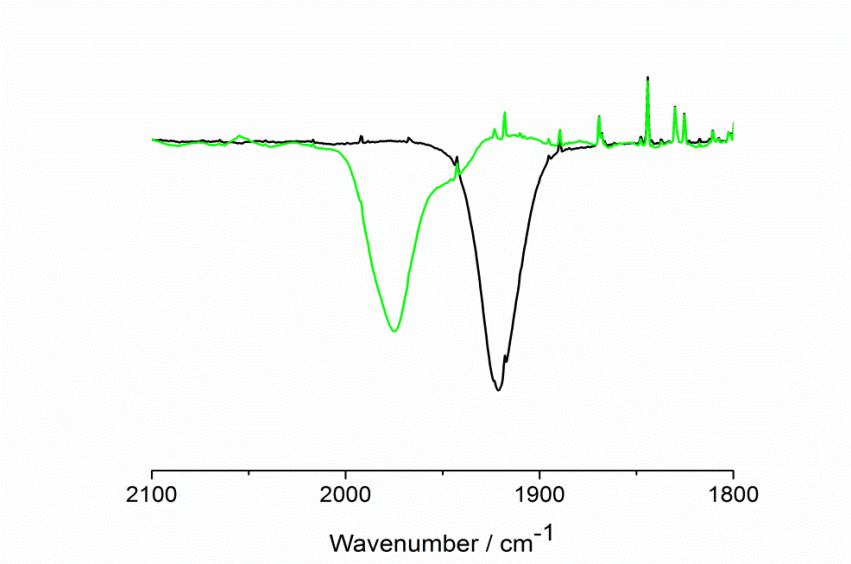

Figure 3.20. Infrared spectra for [11] (black) and $[11]^+$ (green) in 0.1 M NBu_4PF_6 / CH_2Cl_2.

Table 3.11. Spectroelectrochemically determined ν(C≡O) and ν(C=C) vibrational frequencies for $[\mathbf{11}]^{n+}$ and $[\mathbf{12}]^{n+}$ in 0.1 M NBu_4PF_6 / CH_2Cl_2.

	$[\mathbf{11}]^{n+}$		$[\mathbf{12}]^{n+}$	
n	ν(C≡O) / cm^{-1}	ν(C=C) / cm^{-1}	ν(C≡O) / cm^{-1}	ν(C=C) / cm^{-1}
0	1921	not obsd	1921	not obsd
1	1974	1607	1934	not obsd
2	-	-	1974	not obsd

On stepwise oxidation of **12** to $[\mathbf{12}]^{+}$ and $[\mathbf{12}]^{2+}$, the ν(C≡O) band shifted from 1921 to 1934 and 1974 cm^{-1} respectively, Figure 3.21, Table 3.11. Back reduction led to the recovery of **12** accompanied by the formation of a decomposition product evidenced at ν(C≡O) 1950 cm^{-1}. The shifts in ν(C≡O) are small and therefore not consistent with a metal-localised redox event. In addition, the phenylene ring stretch ν(C=C) remains silent in all oxidation states of $[\mathbf{12}]^{n+}$, consistent with a symmetric electronic structure.

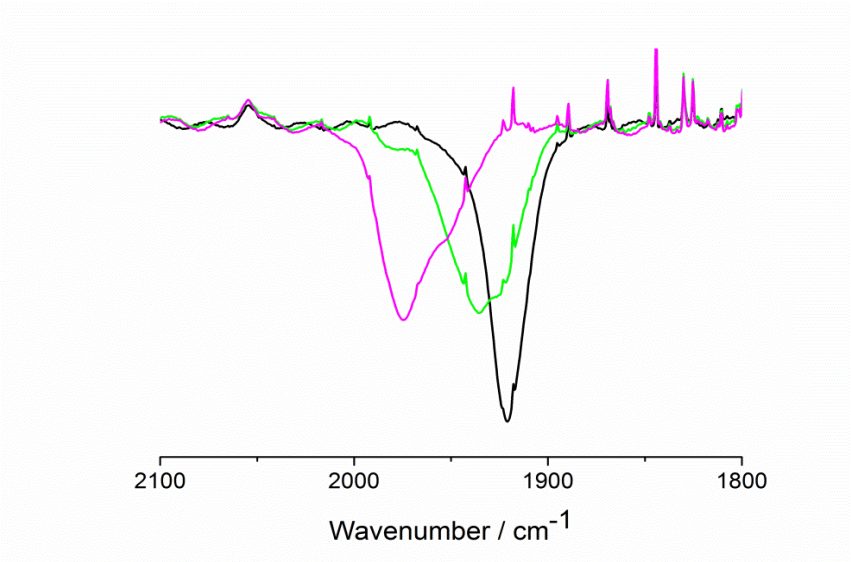

Figure 3.21. Infrared spectra for [12] (black), $[\mathbf{12}]^{+}$ (green), $[\mathbf{12}]^{2+}$ (purple) in 0.1 M NBu_4PF_6 / CH_2Cl_2.

3.13 UV-vis-NIR Spectroelectrochemistry

On oxidation of **12** to [**12**]$^{+}$, a new vibrationally structured absorption 22000 – 16000 cm^{-1} develops, characteristic of a phenylene radical, and supports the notion of considerable phenylene ligand character in supporting the unpaired electron/hole, Figure 3.22.[82] The NIR spectrum of [**12**]$^{+}$ also featured a unique absorption envelope not present in **11**, [**11**]$^{+}$, **12** or [**12**]$^{2+}$. Deconvolution of this band into a summation of Gaussian-shaped curves reveals two transitions (ν_1 = 8400 cm^{-1}, ε = 3200 M^{-1} cm^{-1}, $\Delta\nu_{1/2}$ = 2200 cm^{-1}; ν_2 = 9800 cm^{-1}, ε = 1700 M^{-1} cm^{-1}, $\Delta\nu_{1/2}$ = 2600 cm^{-1}), Figure 3.23.

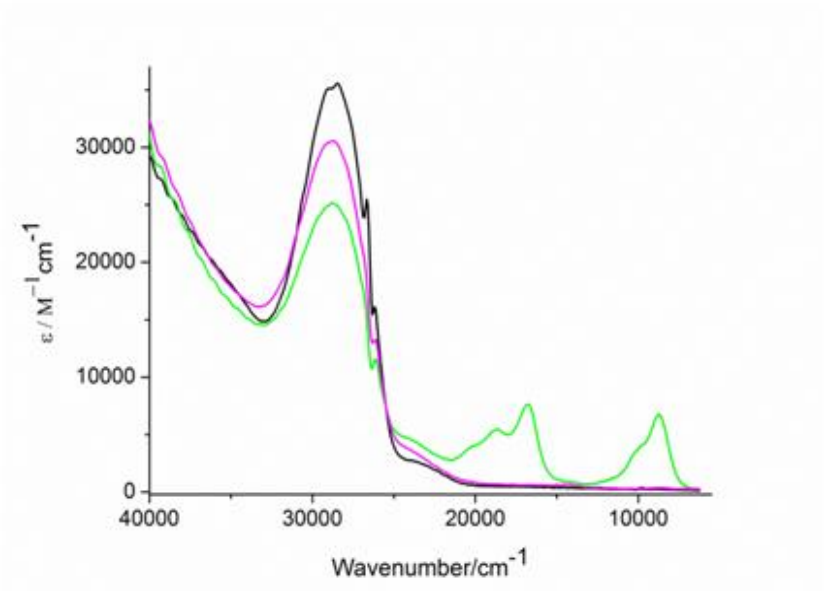

Figure 3.22. The UV-vis-NIR spectra of 12 (black), [12]$^{+}$ (green) and [12]$^{2+}$(purple) in 0.1 M NBu_4PF_6 / CH_2Cl_2.

As discussed in Chapter 1, genuine MV complexes often exhibit multiple IVCT bands in the NIR region.[83] Whilst the number of bands alone cannot distinguish between a bridge-localised or MV ground state,[84, 85] the observation of two low energy optical transitions in [**12**]$^{+}$ is consistent with a three-state model in which the bridge is appreciably involved in the stabilization of the charge. Together, the IR ν(C≡O) and the UV-vis data are compelling in the assignment of a bridge-localised ground state to [**12**]$^{+}$.

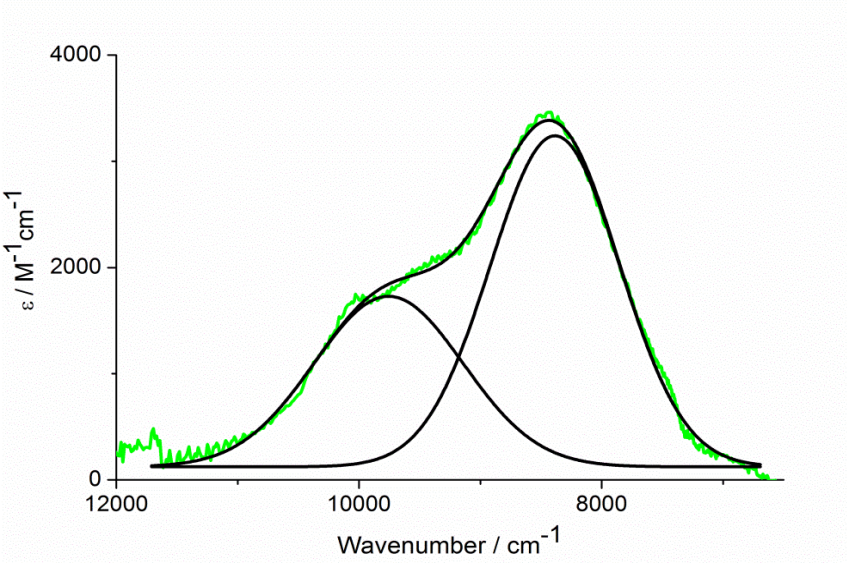

Figure 3.23. The NIR spectrum of [12]$^{+}$ (green) showing deconvolution into two Gaussian shaped sub-bands.

3.14 DFT Studies

DFT calculations were performed by Dr N.J. Brown, Dr M.A. Fox and Prof. P.J. Low of Durham University on the model systems [Ru(CH=CHC$_6$H$_5$)Cl(CO)(PH$_3$)$_3$] ([**11-H**]$^{n+}$) and [{RuCl(CO)(PH$_3$)$_3$}$_2$(μ-CH=CH-C$_6$H$_4$-CH=CH)] ([**12-H**]$^{n+}$) using B3LYP / 3-21G* level of theory.[49] The "**-H**" designation is used to highlight the use of PH$_3$ model ligands in these computational systems.

In [**11-H**], the HOMO is found to be heavily localised on the vinyl ligand (84 %), Figure 3.24a. In the oxidised [**11-H**]$^+$, the β-LUSO offers essentially the same characteristics as the HOMO. Likewise in the bimetallic model complex [**12-H**], the HOMO is largely localised on the unsaturated bridging ligand (86 %), Figure 3.24b. TD-DFT calculations of [**12-H**]$^+$ feature low energy transitions, the first of which can be described as metal to bridge (metal to ligand charge transfer, MLCT) and the second transition which has substantial chloride/metal-ligand character.

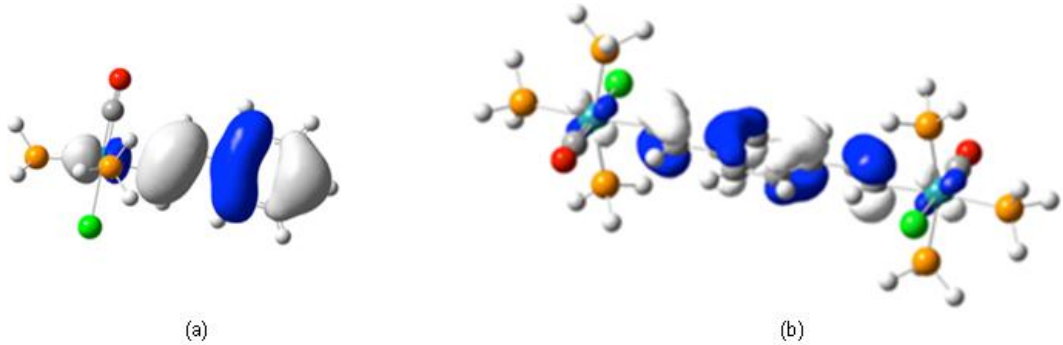

Figure 3.24. Plots of the HOMO in (a) [11-H] (b) [12-H].

3.15 Conclusions

Over recent years, through a series of studies, Winter and co-workers have demonstrated the redox non-innocence of the vinyl ligand *via* a number of techniques where the metal- and bridge based redox sites can systematically be altered by varying the choice of supporting ligands at the metal centre. In this Chapter, we have further extended Winter's work by capping the five coordinate ruthenium vinyl complexes $Ru(CH=CHC_6H_4R)(CO)(PPh_3)_2$ *in situ* with KTp or PMe_3 to produce $[Ru(CH=CHC_6H_4R\text{-}4)(CO)(PPh_3)Tp]$ where R = $N(C_6H_4Me\text{-}4)_2$ (**10a**), OMe (**10b**), CH_3 (**10c**), CO_2Me (**10d**) and NO_2 (**10e**), $Ru(CH=CHC_6H_4Me\text{-}4)Cl(CO)(PMe_3)_3$ (**11**) and $[\{(PMe_3)_3(CO)ClRu\}_2(\mu\text{-}CH=CHC_6H_4CH=CH)]$ (**12**) in moderate yields. Electrochemical studies of **10a** – **e** reveals that the oxidation is sensitive to the electronic character of the vinyl ligand substituent. On oxidation of **10a** – **e**, **11** and **12** to their monocationic states, a relatively small shift in ν(C≡O) is observed, with DFT studies also in support of the significant contribution of the vinyl ligand to the HOMO of the parent complexes and the β-LUSO of the monocations. The complex $[\mathbf{12}]^+$ is better described in terms of a radical cation with a low lying bridge state, supported by the large contribution of the bridging ligand to the β-LUSO in $[\mathbf{12\text{-}H}]^+$ rather than a genuine MV compound.

The trends in the electrochemical responses of the related complexes in Table 3.7 can therefore be rationalised in terms of the electronic effect of the substituent groups on the redox properties of the divinylbenzene moiety. The electron-donating aryl substituents (OMe, CH_3) render the oxidation of the divinyl ligand more facile whilst the electron-

withdrawing substituents have the opposite effect, according to expectations. However, whilst the difference in the first oxidation potentials spans some 0.47 V, there is less variation in the oxidation potentials. This reflects the diminished inductive effects on the oxidation of the aryl radical cation. In effect, larger K_c values reflect the greater thermodynamic stability of the aryl cation bearing these electron-donating substituent groups, however, it can by no means be regarded as a measure of the intermetallic communication between two metal centres. The combination of electrochemical, with spectroscopic (i.e. UV-vis-NIR/IR, EPR) and DFT studies provide a powerful tool in the assessment of the properties and redox behaviour or ligand bridged bimetallic complexes.

3.16 Experimental

All reactions were carried out under an atmosphere of nitrogen, using standard Schlenk techniques. Reaction solvents were purified and dried using an Inovative Technology SPS-400, and degassed before use. No special precautions were taken to exclude air during the workup. The compounds $RuHCl(CO)(PPh_3)_3$,[86] **7d**, **7e**,[87] **11** and **12** were prepared by literature methods.[50, 52] The compound **7a** was prepared by desilylation of $Me_3SiC{\equiv}CC_6H_4N(C_6H_4Me\text{-}4)_2$.[88] Other reagents were purchased (Sigma Aldrich) and used as received.

The NMR spectra were recorded on a 400 MHz Bruker Avance spectrometer from deuterated chloroform solutions and referenced against residual protio solvent resonances ($CHCl_3$: ^1H 7.26 ppm; ^{13}C 77.0 ppm) or external phosphoric acid. In ^{13}C NMR spectroscopy assignments, the carbon atoms on the aromatic ring are labelled C1 – C4 from the ethynyl substituent, and C5 – C8 for the tolyl ring carbons in **10a** from the N centre. The carbon atoms on the phosphine ligands are labelled C_i, C_o, C_m, C_p. IR spectra were recorded using a Thermo 6700 spectrometer from CH_2Cl_2 solutions in a cell fitted with CaF_2 windows. MALDI-mass spectra of organometallic complexes were recorded using Autoflex II TOF/TOF mass spectrometer (Bruker Daltonik, GmbH) equipped with a 337 nm laser. Samples in CH_2Cl_2 (1 mg / ml) were mixed with a matrix solution of *trans*-2-[3-(4-tert-butylphenyl)-2-methyl-2-propenylidene]malononitrile (DCTB) in a 1:9 ratio, with 1 μl of mixture spotted onto a metal target prior to exposure to the MALDI ionization source. Accurate mass measurements were recorded with a *Xevo QToF* mass spectrometer (Waters Ltd, UK) equipped with an Agilent 7890 GC (Agilent Technologies UK Ltd, UK). Exact mass measurements utilised a lock-mass

correction to provide < 3 mDa precision. Exact mass measurement used Elemental Composition version 4.0 embedded within MassLynx 4.1 (Waters Ltd, UK).

Electrochemical analyses were carried out using an EcoChemie Autolab PG-STAT30 potentiostat, with a Pt working, counter and pseudo reference electrodes, from solutions in CH_2Cl_2 containing 0.1 M NBu_4BF_4. Compounds **11** and **12** were analysed in 0.1 M NBu_4PF_6 / CH_2Cl_2 with a glassy carbon electrode at sub ambient temperatures. Redox potentials are reported with reference to an internal standard of the ferrocene/ferricenium couple (**10a** – **e**) ($FcH/[FcH]^+$ = 0 V) or decamethylferrocene/decamethylferricenium couple (**11**, **12**) ($[FcH^*] / [FcH^*]^+$ = –0.48 V).[89] Spectroelectrochemical measurements were made in an OTTLE cell of Hartl design,[90] from CH_2Cl_2 solutions containing 0.1 M NBu_4BF_4 (**10a** – **e**) or 0.1 M NBu_4PF_6 electrolyte (**11**, **12**). The cell was fitted into the sample compartment of the Nicolet Avatar, Thermo 6700, Thermo Array UV-Vis or Perkin-Elmer Lambda 900 spectrophotometer and electrolysis in the cell was performed with a PGSTAT30 potentiostat.

Single crystal X-ray data for all structures were collected on a Bruker SMART 6000 diffractometer equipped with a Cryostream (Oxford Cryosystems) nitrogen cooling device at 120 K using graphite monochromated MoK_α radiation (Mo-K_α, λ = 0.71073Å). The structures were solved by direct methods and refined by full-matrix least squares on F^2 for all data using SHELXTL[91] and OLEX2[92] software. *All* non-disordered non-hydrogen atoms were refined with anisotropic displacement parameters,

H-atoms were placed in the calculated positions and refined in riding mode. Disordered atoms of solvent CH_2Cl_2 molecules in structure **12** were refined isotropically.

3.16.1 Preparation of $(CH_3C_6H_4)_2N(C_6H_4CH{=}CHRu(CO)Cl(PPh_3)_2)$ (8a)

To a suspension of $RuHCl(CO)(PPh_3)_3$ (0.20 g, 0.210 mmol) in dry CH_2Cl_2 (8 ml) was added $(CH_3C_6H_4)_2N(C_6H_4C{\equiv}CH)$ (0.08 g, 0.250 mmol). The reaction was stirred for 40 minutes after which the solvent was removed. Addition of hexane (6 ml) to the red residue dissolved in CH_2Cl_2 (1 ml) led to the formation of a pink powder. A red powder was produced from CH_2Cl_2 (2 ml) and methanol (10 ml) and dried under vacuum (0.16 g, 79 %). Precipitation by CH_2Cl_2 and diethylether gave the analytically pure sample (67 mg, 22 %). ^{1}H NMR: δ 2.30 (s, 6H, CH_3), 5.54 (d, $^3J_{HH}$ = 13 Hz, RuCH=C*H*), 6.62 (d, $^3J_{HH}$ = 8 Hz, Ar), 6.80 (d, $^3J_{HH}$ = 8 Hz, Ar), 6.96 (d, $^3J_{HH}$ = 8 Hz, 4H, Ar-CH_3), 7.04 (d, $^3J_{HH}$ = 8 Hz, 4H, Ar-CH_3), 7.35 – 7.58 (m, 30H, PPh_3), 8.22 (dt, $^3J_{HH}$ = 13 and $^4J_{HP}$ = 2 Hz, 1H, RuC*H*=CH). ^{13}C NMR: δ 20.9 (s, CH_3), 123.2 ($C_{2/3}$), 124.3 ($C_{6/7}$), 125.2 ($C_{2/3}$), 128.5 (t, $^3J_{CP}$ = 5 Hz, $C_{m/m'}$), 129.9 ($C_{6/7}$), 130.3 (s, $C_{p/p'}$), 132.0 (d, $^1J_{CP}$ = 16 Hz, $C_{i/i'}$), 132.2 (s, C_8), 133.4 (s, C_4), 134.4 (t, $^2J_{CP}$ = 5 Hz, $C_{o/o'}$), 135.4 (t, $^4J_{CP}$ = 3 Hz, Ru_β), 144.2 (t, $^3J_{CP}$ = 12 Hz, Ru_α), 144.9 (s, C_1), 145.7 (s, C_5), 201.8 (unresolved, CO). ^{31}P NMR: δ 29.5. IR (CH_2Cl_2): ν(CO) 1932 cm^{-1}. MALDI(+)-MS: 987.2 [M].

3.16.2 Preparation of $(CH_3C_6H_4)_2N(C_6H_4CH=CHRu(CO)Cl(PMe_3)_3)$ (9a)

To a suspension of $RuHCl(CO)(PPh_3)_3$ (0.10 g, 0.105 mmol) in dry CH_2Cl_2 was added $(CH_3C_6H_4)_2N(C_6H_4C{\equiv}CH)$ (0.03 g, 0.105 mmol). The reaction was stirred for 30 minutes and then PMe_3 was added (0.07 ml, 0.630 mmol) and the reaction stirred for a further 12 hours. The solvent was removed *via* Schlenk techniques and the resultant oil triturated with hexane to produce a light yellow powder. Purification by preparative TLC using hexane and acetone (70:30) produced a white powder (0.05 g, 67 %). Crystallisation from CH_2Cl_2 layered with hexane by slow diffusion gave crystals suitable for X-ray diffraction. ^{1}H NMR: δ 1.40 (t, $^4J_{HH}$ = 4 Hz, 18H, PMe_3), 1.47 (d, $^4J_{HH}$ = 8 Hz, 9H, PMe_3), 2.29 (s, 6H, CH_3), 6.47 – 6.53 (unresolved ddt, 1H RuCH=C*H*), 6.93 (d, $^3J_{CP}$ = 8 Hz, 2H, Ar), 6.98 (d, $^3J_{CP}$ = 8 Hz, 4H, Ar), 7.03 (d, $^3J_{CP}$ = 8 Hz, 4H, Ar), 7.17 (d, $^3J_{CP}$ = 8 Hz, 2H, Ar), 7.87 – 7.94 (ddt, $^3J_{HH}$ = 20 Hz, $^3J_{H\text{-}P(trans)}$ = 8 Hz, $^3J_{HP}$ = 4 Hz, 1H, RuC*H*=CH). ^{13}C NMR: δ 17.0 (td, $^1J_{CP}$ = 15 and $^3J_{CP}$ = 3 Hz, PMe_3), 20.5 (dt, $^1J_{CP}$ = 20 Hz $^3J_{CP}$ =3 Hz, PMe_3), 21.1 (s, CH_3), 124.1 (s, $C_{6/7}$), 124.2 (s, $C_{2/3}$), 125.3 (s, $C_{2/3}$), 130.0 (s, $C_{6/7}$), 131.8 (s, C_8), 134.6 (t, $^3J_{CP}$ = 4 Hz, C_β), 136.8 (dt, $^4J_{CP\ (trans)}$ = 8 and $^4J_{CP}$ = 3 Hz, C_1), 144.7 (s, C_4), 146.1 (s, C_5), 163.3 (dt, $^2J_{CP\ (trans)}$ = 77 Hz, $^2J_{CP}$ = 18 Hz, C_α), 202.8 (q, J = 12 Hz, CO). ^{31}P NMR: δ -6.82 (d, J = 23 Hz, PMe_3), -18.63 (t, J = 23 Hz , PMe_3). IR (CH_2Cl_2): ν(CO) 1919 cm^{-1}. MALDI(+)-MS: 615.1 $[M\text{-}PMe_3]^+$, 587.1 $[M\text{-}PMe_3\text{-}CO]^+$.

3.16.3 Preparation of [{Ru(CO)(PPh_3)Tp}(CH=$CHC_6H_4N(C_6H_4Me\text{-}4)_2$)] (10a)

To a suspension of RuHCl(CO)(PPh_3)$_3$ (0.30 g, 0.315 mmol) in dry CH_2Cl_2 (10 ml) was added $(CH_3C_6H_4)_2N(C_6H_4C{\equiv}CH)$ (0.11 g, 0.377 mmol). The reaction was allowed to stir for 30 minutes and then KTp (0.16 g, 0.631 mmol) was added. After 18 hours, the yellow green solution was filtered through Celite, and the solvent removed. The residue was redissolved in the minimum amount of CH_2Cl_2 (1 ml) and methanol (8 ml) was added to produce a yellow precipitate. Purification by preparative TLC using CH_2Cl_2 and hexane (35:65) gave a light yellow powder (0.60 g, 21 %). ^{1}H NMR: δ 2.31 (s, 6H, CH_3), 5.92 (t, $^3J_{HH}$ = 2 Hz, Tp), 5.91 (t, $^3J_{HH}$ = 2 Hz, Tp), 6.09 (unresolved t, 1H, Tp), 6.36 (d, 1H, $^3J_{HH}$ = 16 Hz, RuCH=C*H*), 6.80 (dd, $^3J_{HH}$ = 8 and $^4J_{HP}$ = 4 Hz, 2H, 2 x Tp), 6.94 (d, $^3J_{HH}$ = 8 Hz, 2H, Ar), 6.99 (m, 10H, 2H Ar and 8H Ar'), 7.10 – 7.15 (m, 6H, PPh_3), 7.21 – 7.26 (m, 6H, PPh_3), 7.34 – 7.38 (m, 3H, PPh_3), 7.58 (unresolved triplet, 1H, Tp), 7.70 (dd, $^3J_{HH}$ = 17 and $^4J_{HP}$ = 2 Hz, 2H, 2 x Tp), 7.34 (m, 1H, Tp), 8.08 (dd, $^3J_{HH}$ = 16 and $^3J_{HP}$ = 4 Hz, 1H, RuC*H*=CH). ^{13}C NMR: δ 21.1 (s, CH_3), 105.2 (d, J = 2 Hz, Tp), 105.3 (s, Tp), 105.3 (s, Tp), 123.7 (s, $C_{6/7}$), 124.5 (s, $C_{2/3}$), 125.1 (s, $C_{2/3}$), 128.0 (d, $^3J_{CP}$ = 9 Hz, $C_{m/m'}$), 129.7 (s, $C_{6/7}$), 129.8 (d, $^4J_{CP}$ = 3 Hz, $C_{p/p'}$), 131.4 (s, C_8), 133.1 (d, $^1J_{CP}$ = 44 Hz, $C_{i/i'}$), 134.2 (d, $^2J_{CP}$ = 9 Hz, $C_{o/o'}$), 134.5 (d, J = 3 Hz, Tp), 135.0 (s, Tp), 135.3 (s, Tp), 136.2 (s, C_β), 137.0 (s, C_1), 142.8 (s, Tp), 142.9 (s, Tp), 144.0 (s, Tp), 144.1 (s, C_4), 146.1 (s, C_5), 160.5 (d, $^2J_{CP}$ = 12 Hz, C_α), 206.9 (d, $^2J_{CP}$ = 17 Hz, CO). ^{31}P NMR: δ 49.4. IR (CH_2Cl_2): ν(CO) 1940, ν(BH) 2482 cm^{-1}. MALDI(+)-MS: 903.2 [M]. HR ASAP MS (*m/z*): 897.2664 $C_{50}H_{46}BN_7OPRu$ requires 897.2707.

3.16.4 Preparation of [{Ru(CO)(PPh_3)(Tp)}(CH=CHC_6H_4OMe-4)] (10b)

To a suspension of RuHCl(CO)(PPh_3)$_3$ (0.100 g, 0.105 mmol) in CH_2Cl_2 (6 ml) was added 1-ethynyl-4-methoxybenzene (0.07 ml, 0.524 mmol). The solution turned red and was stirred for 30 min. KTp (0.080 g, 0.315 mmol) was added and the solution turned green over the course of an hour. The solution was then filtered through Celite and the solvent removed. The residual solid was re-dissolved in CH_2Cl_2 (2 ml), hexane (4 ml) was added and some solvent removed. A light green powder was collected by filtration and dried under vacuum (0.036 g, 43 %). Crystals suitable for X-ray diffraction were obtained from the slow diffusion of hexane into a solution of CH_2Cl_2. ^{1}H NMR: δ 3.78 (s, 3H, OCH_3), 5.89 (t, $^3J_{HH}$ = 2 Hz, 1H, Tp), 5.91 (t, $^3J_{HH}$ = 2 Hz, 1H, Tp), 6.05 (unresolved t, 1H, Tp), 6.31 (d, $^3J_{HH}$ = 17 Hz, 1H, Ru-CH=C*H*), 6.78 – 6.80 (m, 4H, 2H Tp and 2H C_6H_4), 7.08 – 7.14 (m, 8H, 6H PPh_3 and 2H C_6H_4), 7.20 – 7.23 (m, 6H, PPh_3), 7.33 – 7.36 (m, 3H, PPh_3), 7.56 (unresolved triplet, 1H, Tp), 7.68 – 7.71 (m, 3H, 3 x Tp), 7.97 (dd, $^3J_{HH}$ = 17 Hz and $^3J_{HP}$ = 4 Hz, 1H, RuC*H*=CH). ^{13}C NMR: δ 55.7 (s, OMe), 105.4 (d, J = 3 Hz, Tp), 105.5 (s, 2 x Tp), 113.9 (s, C_3), 125.5 (s, C_2), 128.2 (d, $^3J_{CP}$ = 9 Hz, $C_{m/m'}$), 130.0 (d, $^4J_{CP}$ = 2 Hz, $C_{p/p'}$), 133.4 (d, $^1J_{CP}$ = 42 Hz, $C_{i/i'}$), 134.4 (d, $^2J_{CP}$ =10 Hz, $C_{o/o'}$), 134.7 (d, J = 2 Hz, Tp), 135.2 (s, Tp), 135.5 (s, Tp), 135.8 (s, C_β), 136.1 (s, C_1), 143.0 (s, Tp), 143.1 (s, Tp), 144.3 (s, Tp), 156.8 (s, C_4), 158.4 (d, $^2J_{CP}$ = 14 Hz, C_α), 207.1 (d, $^2J_{CP}$ = 17 Hz, CO). ^{31}P NMR: δ 51.3. MALDI(+)-MS 738.2 $[M + H]^+$. IR (CH_2Cl_2): ν(C≡O) 1940, ν(B-H) 2479 cm^{-1}. HR ASAP MS *(m/z)* 732.1760 $[M + H]^+$ $C_{37}H_{35}BN_6O_2PRu$ requires 732.1764.

3.16.5 Preparation of [{Ru(CO)(PPh_3)Tp}(CH=CHC_6H_4Me-4)] (10c)

The synthesis and workup is similar to **10b**, with 1-ethynyl-4-methoxybenzene replaced by *p*-tolylacetylene. A pale yellow powder was collected by filtration and dried under vacuum (0.051 g, 64 %). Crystals suitable for X-ray diffraction were obtained from the slow diffusion of hexane into a CH_2Cl_2 solution. ^{1}H NMR: δ 2.30 (s, 3H, CH_3), 5.90 (t, $^3J_{HH}$ = 2 Hz, 1H, Tp), 5.92 (t, $^3J_{HH}$ = 2 Hz, 1H, Tp), 6.05 (t, $^3J_{HH}$ = 2 Hz, 1H, Tp), 6.36 (d, $^3J_{HH}$ = 17 Hz, 1H, Ru-CH=C*H*), 6.78 (dd, $^3J_{HH}$ = 12 and $^3J_{HP}$ = 2 Hz, 2H, 2 x Tp), 7.01 – 7.13 (m, 10H, 6H PPh_3, 4H C_6H_4), 7.19 - 7.24 (m, 6H, PPh_3), 7.33 - 7.37 (m, 3H, PPh_3), 7.55 (unresolved t, 1H, Tp), 7.67 – 7.70 (m, 3H, 3 x Tp), 8.14 (dd, $^3J_{HH}$ = 17 Hz and $^3J_{HP}$ = 4 Hz, 1H, RuC*H*=CH). ^{13}C NMR: δ 21.3 (s, CH_3), 105.0 (d, J = 3 Hz, Tp), 105.1 (s, 2 x Tp), 124.3 (s, C_2), 127.9 (d, $^2J_{CP}$ = 9 Hz, $C_{m/m'}$), 128.7 (s, C_3), 129.6 (d, $^4J_{CP}$ = 2 Hz, $C_{p/p'}$), 132.9 (s, C_4), 133.0 (d, $^1J_{CP}$ = 42 Hz, $C_{i/i'}$), 134.0 (d, $^3J_{CP}$ = 9 Hz, $C_{o/o'}$), 134.4 (d, J = 3 Hz, Tp), 134.8 (s, Tp), 135.1 (s, Tp), 136.5 (s, C_β), 139.1 (s, C_1), 142.6 (s, Tp), 142.7 (s, Tp), 143.9 (s, Tp), 160.0 (d, $^2J_{CP}$ = 14 Hz, C_α), 206.7 (d, $^2J_{CP}$ = 15 Hz, CO). ^{31}P NMR: δ 50.6. MALDI(+)-MS (*m/z*): 722.2 $[M + H]^+$. IR (CH_2Cl_2): ν(C≡O) 1942, ν(B-H) 2481 cm^{-1}. HR ASAP MS (m/z) 715.1735 [M] $C_{37}H_{34}BN_6OPRu$ requires 715.1737.

3.16.6 Preparation of [{Ru(CO)(PPh_3)Tp}(CH=$CHC_6H_4CO_2$Me-4)] (10d)

The synthesis and workup is similar to **10b**, with 1-ethynyl-4-methoxybenzene replaced by methyl 4-ethynylbenzoate. A light green powder was produced (0.134 g, 56 %). Crystals suitable for X-ray diffraction were obtained from the slow diffusion of methanol into a CH_2Cl_2 solution. ^{1}H NMR: δ 3.88 (s, 3H, OCH_3), 5.91 (t, $^3J_{HH}$ = 2 Hz, 1H, Tp), 5.94 (t, $^3J_{HH}$ = 2 Hz, 1H, Tp), 6.07 (unresolved t, 1H, Tp), 6.48 (d, $^3J_{HH}$ = 17 Hz, 1H, RuCH=C*H*), 6.80 (dd, $^3J_{HH}$ = 8 Hz and $^3J_{HP}$ = 2 Hz, 2H, 2 x Tp), 7.04 – 7.09 (m, 6H, PPh_3), 7.13 (d, J = 8 Hz, 2H, C_6H_4), 7.18 – 7.23 (m, 6H, PPh_3), 7.31 – 7.35 (m, 3H, PPh_3), 7.52 (unresolved t, 1H, Tp), 7.60 (d, $^3J_{HH}$ = 2Hz, 1H, Tp), 7.71 (dd, $^3J_{HH}$ = 8 Hz and $^3J_{HP}$ = 2 Hz, 2H, 2 x Tp), 7.87 (d, $^3J_{HH}$ = 8 Hz, 2H, C_6H_4), 8.68 (dd, $^3J_{HH}$ = 17 Hz and $^3J_{HP}$ = 4 Hz, 1H, RuCH=C*H*). ^{13}C NMR: δ 52.0 (s, OMe), 105.5 (d, J = 2 Hz, Tp), 105.6 (s, Tp), 105.7 (s, Tp), 124.2 (s, C_2), 125.0 (s, C_4), 128.3 (d, $^2J_{CP}$ = 10 Hz, $C_{m/m'}$), 130.1 (s, C_3), 130.2 (d, $^4J_{CP}$ = 2 Hz, $C_{p/p'}$), 133.0 (d, $^1J_{CP}$ = 43 Hz, $C_{i/i'}$), 134.3 (d, $^3J_{CP}$ = 10 Hz, $C_{o/o'}$), 134.9 (d, J = 2 Hz, Tp), 135.3 (s, Tp), 135.6 (s, Tp), 136.7 (s, C_β), 142.9 (s, Tp), 143.0 (s, Tp), 144.3 (s, Tp), 145.5 (s, C_1), 168.0 (s, CO of ligand), 171.3 (d, $^2J_{CP}$ = 13 Hz, C_α), 206.8 (d, $^2J_{CP}$ = 16 Hz, CO). ^{31}P NMR: δ 50.9. MALDI(+)-MS (*m/z*): 766.2 $[M + H]^+$. IR (CH_2Cl_2): ν(C≡O) 1940, ν(B-H) 2483 cm^{-1}. HR ASAP MS (m/z): 760.1742 $[M + H]^+$ $C_{38}H_{34}BN_6O_3PRu$ requires 760.1714.

3.16.7 Preparation of [{Ru(CO)(PPh_3)Tp}(CH=$CHC_6H_4NO_2$-4)] (10e)

The synthesis and workup is similar to **10b**, with 1-ethynyl-4-methoxybenzene replaced by 1-ethynyl-4-nitrobenzene. An orange powder was produced (0.152 g, 64 %). Crystals suitable for X-ray diffraction were obtained from the slow diffusion of methanol into a CH_2Cl_2 solution. ^{1}H NMR: δ 5.93 (t, $^3J_{HH}$ = 2 Hz, 1H, Tp), 5.96 (t, $^3J_{HH}$ = 2 Hz, 1H, Tp), 6.08 (unresolved t, 1H, Tp), 6.54 (d, $^3J_{HH}$ = 17 Hz, 1H, Ru-CH=C*H*), 6.81 (dd, $^3J_{HH}$ = 16 Hz and $^3J_{HP}$ = 2 Hz, 2H, 2 x Tp), 7.03 – 7.07 (m, 6H, PPh_3), 7.13 (d, $^3J_{HH}$ = 9 Hz, 2H, C_6H_4), 7.19 – 7.24 (m, 6H, PPh_3), 7.34 – 7.38 (m, 3H, PPh_3), 7.59 (unresolved m, 2H, Tp), 7.72 (dd, $^3J_{HH}$ = 12 Hz and $^3J_{HP}$ = 2 Hz, 2H, 2 x Tp), 8.06 (d, $^3J_{HH}$ = 12 Hz, 2H, C_6H_4), 9.04 (dd, $^3J_{HH}$ = 17 Hz and $^3J_{HP}$ = 4 Hz, 1H, RuC*H*=CH). ^{13}C NMR: δ 105.6 (d, J = 3 Hz, Tp), 105.7 (s, Tp), 105.8 (s, Tp), 124.3 (s, C_2), 124.5 (s, C_3), 128.4 (d, $^2J_{CP}$ = 10 Hz, $C_{m/m'}$), 130.0 (d, $^4J_{CP}$ = 2 Hz, $C_{p/p'}$), 132.7 (d, $^1J_{CP}$ = 44 Hz, $C_{i/i'}$), 134.2 (d, $^3J_{CP}$ = 10 Hz, $C_{o/o'}$), 135.1 (d, $^3J_{CP}$ = 2 Hz, Tp), 135.5 (s, Tp), 135.7 (s, Tp), 136.0 (s, C_β), 142.9 (d, J = 3 Hz, Tp), 144.0 (s, Tp), 144.4 (s, Tp), 146.6 (s, C_1), 179.2 (d, $^2J_{CP}$ = 12 Hz, C_α), 206.5 (d, $^2J_{CP}$ = 16 Hz, CO). *C_1 not observed. ^{31}P NMR: δ 50.7. MALDI(+)-MS 753.10 $[M + H]^+$. IR (CH_2Cl_2): ν(C≡O) 1945, ν(B-H) 2485 cm^{-1}. HR ASAP MS *(m/z)*: 747.1533 $[M + H]^+$ $C_{36}H_{32}BN_7O_3PRu$ requires 747.1510.

3.16.8 Preparation of [Ru(CH=CHC$_6$H$_4$Me-4)Cl(CO)(PMe$_3$)$_3$] (11)

To a suspension of $RuHCl(CO)(PPh_3)_3$ (0.30 g, 0.315 mmol) in dry CH_2Cl_2 was added *p*-tolylacetylene (0.06 ml, 0.472 mmol). The solution turned red and was stirred for 30 minutes. PMe_3 (0.20 ml, 1.88 mmol) was added and the solution turned green over the course of 15 minutes. After 18 hours, the solution was filtered through Celite and the solvent removed *via* Schlenk techniques. Precipitation of the residue in CH_2Cl_2 and hexane led to the formation of a crude powder. Purification by preparative TLC using a solvent system of acetone and hexane (30:70) produced a white powder (0.070 g, 42 %). Recrystallisation from CH_2Cl_2 and hexane by slow diffusion gave crystals of X-ray quality. ^{1}H NMR: δ 1.38 (t, $^2J_{HP}$ = 4 Hz, 18H, PMe_3), 1.47 (d, $^2J_{HP}$ = 6 Hz, 9H, PMe_3), 2.29 (s, 3H, CH_3), 6.53 (ddt, $^1J_{H-H}$ = 17 Hz, $^3J_{P-H\ (trans)}$ = 11 Hz, $^3J_{P-H}$ = 2 Hz, 1H, RuCH=C*H*), 7.07 (d, 2H, J = 8 Hz, Ar), 7.24 (d, J = 8 Hz, 2H, Ar), 8.01 (ddt, $^1J_{H-H}$ = 17 Hz, $^3J_{P-H\ (trans)}$ = 8 Hz, $^3J_{P-H}$ = 3 Hz, 1H, RuC*H*=CH). ^{31}P{^{1}H} NMR: - 17.7 (t, $^2J_{C-P}$ = 23 Hz, PMe_3), - 6.0 (d, $^2J_{C-P}$ = 23 Hz, PMe_3). IR (CH_2Cl_2, cm^{-1}): ν(C≡O) 1918.

3.16.9 Preparation of [{$(PMe_3)_3(CO)ClRu$}$_2$(μ-CH=CHC$_6$H$_4$CH=CH)] (12)

To a suspension of $RuHCl(CO)(PPh_3)_3$ (0.200g, 0.210 mmol) in CH_2Cl_2 (6 ml) was added 1,4-diethynylbenzene (0.013 g, 0.105 mmol). The solution turned red and was stirred for 30 minutes. Then, PMe_3 (0.07 ml, 0.63 mmol) was added and the solution turned green over the course of 15 minutes. After 18 hours, the solution was filtered through Celite and the solvent removed *via* Schlenk techniques. Precipitation of the crude residue in CH_2Cl_2 and hexane led to the formation of a crude powder. Purification by preparative TLC using a solvent system of acetone and hexane (30:70) produced a yellow powder (0.045 g, 47 %). Recrystallisation from CH_2Cl_2 and hexane by slow diffusion gave crystals of X-ray quality. ^{1}H NMR: δ 1.40 (t, $^2J_{P-H}$ = 4 Hz, 36H, PMe_3), 1.49 (d, $^2J_{P-H}$ = 7 Hz, 18H, PMe_3), 6.55 (ddt, $^1J_{HH}$ = 17 Hz, $^3J_{P-H\ (trans)}$ = 6 Hz, $^3J_{P-H}$ = 3 Hz 1H, RuCH=C*H*), 7.28 (s, 4H, Ar), 7.97 (ddt, $^1J_{HH}$ = 17 Hz, $^3J_{P-H\ (trans)}$ = 8 Hz, $^3J_{P-H}$ = 3 Hz, 1H, RuC*H*=CH). ^{31}P{^{1}H} NMR: δ - 17.6 (t, $^2J_{PC}$ = 23 Hz, PMe_3), - 6.0 (d, $^2J_{PC}$ = 23 Hz, PMe_3). IR (CH_2Cl_2, cm^{-1}): ν(C≡O) 1922.

3.17 References

1. R. Poli, *Chem. Rev.*, 1996, **96**, 2135-2204.
2. P. Day, *Coord. Chem. Rev.*, 2003, **238–239**, 3-8.
3. W. Kaim and B. Schwederski, *Coord. Chem. Rev.*, 2010, **254**, 1580-1588.
4. H. Chen, M. Ikeda-Saito and S. Shaik, *J. Am. Chem. Soc.*, 2008, **130**, 14778-14790.
5. C. K. Jørgensen, *Coord. Chem. Rev.*, 1966, **1**, 164-178.
6. A. Wanat, T. Schneppensieper, G. Stochel, R. van Eldik, E. Bill and K. Wieghardt, *Inorg. Chem.*, 2001, **41**, 4-10.
7. K. D. Karlin and E. I. S. (Eds), *Prog. Inorg. Chem.*, 2004, **52**.
8. S. J. N. Burgmayer, *Prog. Inorg. Chem.*, 2004, **52**, 491.
9. G. v. Koten and K. Vrieze, *Adv. Organomet. Chem.*, 1982, **21**, 151.
10. C. G. Pierpont and R. M. Buchanan, *Coord. Chem. Rev.*, 1981, **38**, 45-87.
11. C. G. Pierpont and C. W. Lange, *Prog. Inorg. Chem.*, 1994, **41**, 331-342.
12. M. D. Ward and J. A. McCleverty, *J. Chem. Soc., Dalton Trans.*, 2002, 275-288.
13. W. Kaim, *Inorg. Chem.*, 2011, **50**, 9752-9765.
14. F. A. Cotton and G. Wilkinson, *Advanced Inorganic Chemistry Fifth Edition*, John Wiley and Sons, 1988.
15. C. C. Scarborough, S. Sproules, T. Weyhermüller, S. DeBeer and K. Wieghardt, *Inorg. Chem.*, 2011, **50**, 12446-12462.
16. S. Zalis, R. F. Winter and W. Kaim, *Coord. Chem. Rev.*, 2010, **254**, 1383-1396.
17. C. C. Scarborough and K. Wieghardt, *Inorg. Chem.*, 2011, **50**, 9773-9793.
18. W. I. Dzik, J. I. van der Vlugt, J. N. H. Reek and B. de Bruin, *Angew. Chem. Int. Ed.*, 2011, **50**, 3356-3358.
19. A. L. Smith, K. I. Hardcastle and J. D. Soper, *J. Am. Chem. Soc.*, 2010, **132**, 14358-14360.
20. F. Paul, B. G. Ellis, M. I. Bruce, L. Toupet, T. Roisnel, K. Costuas, J.-F. Halet and C. Lapinte, *Organometallics*, 2005, **25**, 649-665.
21. M. A. Fox, R. L. Roberts, W. M. Khairul, F. Hartl and P. J. Low, *J. Organomet. Chem.*, 2007, **692**, 3277-3290.
22. N. Le Narvor and C. Lapinte, *Organometallics*, 1995, **14**, 634-639.
23. N. Le Narvor, L. Toupet and C. Lapinte, *J. Am. Chem. Soc.*, 1995, **117**, 7129-7138.
24. S. I. Ghazala, F. Paul, L. Toupet, T. Roisnel, P. Hapiot and C. Lapinte, *J. Am. Chem. Soc.*, 2006, **128**, 2463-2476.
25. M. I. Bruce, A. Burgun, F. d. r. Gendron, G. Grelaud, J.-F. o. Halet and B. W. Skelton, *Organometallics*, 2011, **30**, 2861-2868.
26. P. A. Schauer and P. J. Low, *Eur. J. Inorg. Chem.*, 2012, 390-411.
27. W. M. Khairul, M. A. Fox, P. A. Schauer, D. Albesa-Jové, D. S. Yufit, J. A. K. Howard and P. J. Low, *Inorg. Chim. Acta*, 2011, **374**, 461-471.
28. O. M. A. Salah, M. I. Bruce, M. R. Churchill and S. A. Bezman, *J. Chem. Soc., Chem. Commun.*, 1972.
29. J. Maurer, M. Linseis, B. Sarkar, B. Schwederski, M. Niemeyer, W. Kaim, S. Zalis, C. Anson, M. Zabel and R. F. Winter, *J. Am. Chem. Soc.*, 2008, **130**, 259-268.
30. A. F. Hill, D. E. Shirver and M. I. B. (Eds), *Comprehensive Organometallic Chemistry II*, Pergamon, Oxford, 1995.

31. J. Wilton-Ely, S. J. Honarkhah, M. Wang, D. A. Tocher and A. M. Z. Slawin, *Dalton Trans.*, 2005, 1930-1939.
32. S. K. Seetharaman, M.-C. Chung, U. Englich, K. Ruhlandt-Senge and M. B. Sponsler, *Inorg. Chem.*, 2006, **46**, 561-567.
33. H. Werner, M. A. Esteruelas and H. Otto, *Organometallics*, 1986, **5**, 2295-2299.
34. H. Werner, U. Meyer, K. Peters and H. G. von Schnering, *Chem. Ber.*, 1989, **122**, 2097-2107.
35. M. R. Torres, A. Vegas, A. Santos and J. Ros, *J. Organomet. Chem.*, 1986, **309**, 169-177.
36. M. Rosario Torres, A. Santos, J. Ros and X. Solans, *Organometallics*, 1987, **6**, 1091-1095.
37. M. R. Torres, A. Perales and J. Ros, *Organometallics*, 1988, **7**, 1223-1224.
38. M. R. Torres, A. Vegas, A. Santos and J. Ros, *J. Organomet. Chem.*, 1987, **326**, 413-421.
39. A. F. Hill and R. P. Melling, *J. Organomet. Chem.*, 1990, **396**, C22-C24.
40. D. S. Bohle, G. R. Clark, C. E. F. Rickard, W. R. Roper, W. E. B. Shepard and L. J. Wright, *J. Chem. Soc., Chem. Commun.*, 1987, 563-565.
41. A. Gieren, C. Ruiz-Perez, T. Hubner, M. Herberhold and A. F. Hill, *J. Chem. Soc., Dalton Trans.*, 1988, 1693-1696.
42. W. R. Roper, G. E. Taylor, J. M. Waters and L. J. Wright, *J. Organomet. Chem.*, 1979, **182**, C46-C48.
43. W. R. Roper, G. E. Taylor, J. M. Waters and L. J. Wright, *J. Organomet. Chem.*, 1978, **157**, C27-C29.
44. M. Herberhold and A. F. Hill, *J. Organomet. Chem.*, 1989, **368**, 111-117.
45. N. W. Alcock, A. F. Hill and R. P. Melling, *Organometallics*, 1991, **10**, 3898-3903.
46. J. Maurer, B. Sarkar, B. Schwederski, W. Kaim, R. F. Winter and S. Zalis, *Organometallics*, 2006, **25**, 3701-3712.
47. K. Johno, Y. Tanaka, T. Koike and M. Akita, *Dalton Trans.*, 2011, **40**, 8089-8091.
48. J. P. Collman and J. W. Kang, *J. Am. Chem. Soc.*, 1967, **89**, 844-851.
49. W. Y. Man, J. L. Xia, N. J. Brown, J. D. Farmer, D. S. Yufit, J. A. K. Howard, S. H. Liu and P. J. Low, *Organometallics*, 2011, **30**, 1852-1858.
50. X. H. Wu, T. Q. Weng, S. Jin, J. H. Liang, R. Guo, G. A. Yu and S. H. Liu, *J. Organomet. Chem.*, 2009, **694**, 1877-1883.
51. S. H. Liu, Q. Y. Hu, P. Xue, T. B. Wen, I. D. Williams and G. Jia, *Organometallics*, 2005, **24**, 769-772.
52. X. H. Wu, S. Jin, J. H. Liang, Z. Y. Li, G.-a. Yu and S. H. Liu, *Organometallics*, 2009, **28**, 2450-2459.
53. Y. Lin, J. Yuan, M. Hu, J. Cheng, J. Yin, S. Jin and S. H. Liu, *Organometallics*, 2009, **28**, 6402-6409.
54. X.-H. Wu, J. H. Liang, J.-L. Xia, S. Jin, G.-A. Yu and S. H. Liu, *Organometallics*, 2010, **29**, 1150-1156.
55. S. H. Liu, H. Xia, K. L. Wan, R. C. Y. Yeung, Q. Y. Hu and G. Jia, *J. Organomet. Chem.*, 2003, **683**, 331-336.
56. M. A. Jiménez Tenorio, M. Jiménez Tenorio, M. C. Puerta and P. Valerga, *Organometallics*, 1997, **16**, 5528-5535.
57. M. J. Tenorio, M. A. J. Tenorio, M. C. Puerta and P. Valerga, *Inorg. Chim. Acta*, 1997, **259**, 77-84.
58. A. N. McNair, D. C. Boyd and K. R. Mann, *Organometallics*, 1986, **5**, 303-310.

59. N. W. Alcock, I. D. Burns, K. S. Claire and A. F. Hill, *Inorg. Chem.*, 1992, **31**, 2906-2908.
60. M. R. Torres, A. Santos, A. Perales and J. Ros, *J. Organomet. Chem.*, 1988, **353**, 221-228.
61. H. Xia, T. B. Wen, Q. Y. Hu, X. Wang, X. Chen, L. Y. Shek, I. D. Williams, K. S. Wong, G. K. L. Wong and G. Jia, *Organometallics*, 2005, **24**, 562-569.
62. B. J. Coe and S. J. Glenwright, *Coord. Chem. Rev.*, 2000, **203**, 5-80.
63. S.-H. Choi, I. Bytheway, Z. Lin and G. Jia, *Organometallics*, 1998, **17**, 3974-3980.
64. K. B. Wiberg and E. Martin, *J. Am. Chem. Soc.*, 1985, **107**, 5035-5041.
65. A. E. Dorigo, D. W. Pratt and K. N. Houk, *J. Am. Chem. Soc.*, 1987, **109**, 6591-6600.
66. J. Maurer, R. F. Winter, B. Sarkar, J. Fiedler and S. Zalis, *Chem. Commun.*, 2004, 1900-1901.
67. S. P. Best, S. J. Borg and K. A. Vincent, in *Spectroelectrochemistry*, The Royal Society of Chemistry, Editon edn., 2008, pp. 1-30.
68. C. Lambert and G. Nöll, *J. Am. Chem. Soc.*, 1999, **121**, 8434-8442.
69. K. Onitsuka, N. Ohara, F. Takei and S. Takahashi, *Dalton Trans.*, 2006, 3693-3698.
70. J. Maurer, R. Winter, B. Sarkar and S. Záliš, *J. Solid State Electrochem.*, 2005, **9**, 738-749.
71. F. Pevny, E. Di Piazza, L. Norel, M. Drescher, R. F. Winter and S. Rigaut, *Organometallics*, 2010, **29**, 5912-5918.
72. P. Mücke, M. Linseis, S. Záliš and R. F. Winter, *Inorg. Chim. Acta*, 2011, **374**, 36-50.
73. E. Wuttke, F. Pevny, Y.-M. Hervault, L. Norel, M. Drescher, R. F. Winter and S. Rigaut, *Inorg. Chem.*, 2012, **51**, 1902-1915.
74. P. Mücke, M. Zabel, R. Edge, D. Collison, S. Clément, S. Záliš and R. F. Winter, *J. Organomet. Chem.*, 2011, **696**, 3186-3197.
75. S. H. Liu, H. P. Xia, T. B. Wen, Z. Y. Zhou and G. C. Jia, *Organometallics*, 2003, **22**, 737-743.
76. S. H. Liu, Y. Chen, K. L. Wan, T. B. Wen, Z. Zhou, M. F. Lo, I. D. Williams and G. Jia, *Organometallics*, 2002, **21**, 4984-4992.
77. P. Yuan, X.-h. Wu, G.-a. Yu, D. Du and S. H. Liu, *J. Organomet. Chem.*, 2007, **692**, 3588-3592.
78. L. Liu, W.-Y. Wong, S.-Y. Poon, J.-X. Shi, K.-W. Cheah and Z. Lin, *Chem. Mater.*, 2006, **18**, 1369-1378.
79. J. Maurer, B. Sarkar, W. Kaim, R. F. Winter and S. Zalis, *Chem. Eur. J*, 2007, **13**, 10257-10272.
80. M. Linseis, R. F. Winter, B. Sarkar, W. Kaim and S. Zalis, *Organometallics*, 2008, **27**, 3321-3324.
81. F. Pevny, R. F. Winter, B. Sarkar and S. Zalis, *Dalton Trans.*, 2010, **39**, 8000-8011.
82. D. J. Armitt, M. I. Bruce, M. Gaudio, N. N. Zaitseva, B. W. Skelton, A. H. White, B. Le Guennic, J.-F. Halet, M. A. Fox, R. L. Roberts, F. Hartl and P. J. Low, *Dalton Trans.*, 2008, 6763-6775.
83. K. D. Demadis, C. M. Hartshorn and T. J. Meyer, *Chem. Rev.*, 2001, **101**, 2655-2686.
84. C. Lambert, S. Amthor and J. Schelter, *J. Phys. Chem. A*, 2004, **108**, 6474-6486.
85. C. Lambert, G. Noll and J. Schelter, *Nat. Mat.*, 2002, **1**, 69-73.

86. N. Ahmad, J. J. Levison, S. D. Robinson and M. F. Uttley, *Inorg. Synth.*, 1974, **15**, 45.
87. A. Klein, O. Lavastre and J. Fiedler, *Organometallics*, 2005, **25**, 635-643.
88. W. Man, K. Vincent, H. Spencer, D. Yufit, J. Howard and P. Low, *J. Cluster Sci.*, 2012, **23**, 853.
89. N. G. Connelly and W. E. Geiger, *Chem. Rev.*, 1996, **96**, 877-910.
90. M. Krejčik, M. Daněk and F. Hartl, *J. Electroanal. Chem.*, 1991, **317**, 179-187.
91. G. M. Sheldrick, *Acta Crystal. A*, 2008, **64**, 112-122.
92. O. V. Dolomanov, L. J. Bourhis, R. J. Gildea, J. A. K. Howard and H. Puschmann, *J. Appl. Crystallogr.*, 2009, **42**, 339-341.

Chapter 4. Dithia[3.3]paracyclophane Bridged Ruthenium Vinyl and Alkynyl Complexes

4.1 Introduction

Bimetallic complexes where two metal centres are connected *via* a conjugated bridge are ideal models of molecular wires.[1-4] The electronic properties of these systems can be tuned by variation in the metal end group, supporting ligands, nature of the bridge, and different chemical connections between the metal centres and bridging ligands i.e. single, double and triple bonds. The frontier orbitals of these complexes generally have both metal and π-conjugated bridge properties, the relative amounts of which depend on the nature of the end groups and the bridge. There is thus great scope to tune bimetallic complexes by varying the energy and symmetry of the metal- and bridging-ligand based orbitals from precursors of genuine MV complexes,[5] and delocalised systems where the metal centres are an intrinsic component of the π-electronic system that spans the molecular backbone[6-9] to examples of organic redox systems bearing metal-based donor substituents.[10] Of course, real applications also require contacts to external electrodes and steps to incorporate metal containing molecules into device platforms are underway.[11-15]

The redox chemistry of bimetallic ruthenium complexes with carbon-rich ligands is often dominated by the non-innocent or redox active character of the bridging fragment. For example, on stepwise oxidation of the diruthenium dialkynyl bridged complexes [{Cp(PPh$_3$)$_2$Ru}$_2$(μ-C≡CC≡C)] (**13a**), [{Cp(PPh$_3$)(PMe$_3$)Ru}$_2$(μ-C≡CC≡C)] (**13b**) and [{Cp*(dppe)Ru}$_2$(μ-C≡CC≡C)] (**13c**), Chart 4.1, there is a shift in ν(C≡C) to lower wavenumbers. On generation of the monocationic species of each of these complexes, a solvent independent IVCT transition, which also exhibited a bandwidth at half height a lot narrower than Hush's prediction, hence their assignment as Class III MV complexes.[16, 17] DFT studies were consistent with electron density residing primarily on the C_4 ligand; the HOMO is 27 % metal and 59 % ligand in character, whilst the HOMO-1 comprises of an orthogonal π-system being similarly comprised of 25 % metal and 69 % C_4 in character.

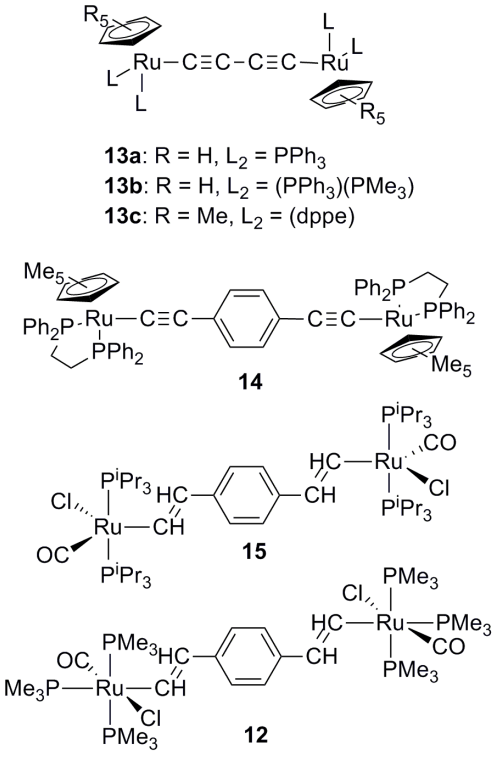

Chart 4.1. Bimetallic ruthenium alkynyl and vinyl complexes.

The introduction of a phenylene group into the C_4 spacer leads to the formation of [1,4-{Cp*(dppe)Ru}$_2$(μ-C≡CC_6H_4C≡C)] (**14**), Chart 4.1. Initial studies on **14** revealed the presence of an absorption band in the NIR region, characteristic of metal-metal charge transfer, with subsequent DFT studies revealing the redox non-innocence of the organic bridging ligand as a result of the extensive mixing of the metal and alkynyl frontier orbitals.[19] However, a more recent study has provided evidence that the radical cation of **14** exhibits both MV and organic bridging ligand characteristics.[20] For example, the redox non-innocence of the alkynyl ligand can be accounted for in UV-vis-NIR spectra by a vibrationally structured band at ca. 19000 cm^{-1} and in DFT studies, the HOMO features ethynyl aromatic moieties with considerable bridging ligand character (70 %). Deconvolution of the NIR band in [**14**]$^+$ led to a three band pattern and whilst two of these can be attributed to the bridge localised ground state, the third band is significantly broader and has a bandwidth at half height which fits well with the theoretical value predicted by the Hush analysis. IR spectroelectrochemistry reveals four distinct features in [**14**]$^+$. The strongest band at 1974 cm^{-1} is assigned to the bridge localised ground state as it gains intensity through coupling to the MLCT transitions, and is broadened or split by symmetric and asymmetric components. Two weaker additional bands are also observed, resembling a two pattern where charge is asymmetrically distributed between the metal centres across the bridge hence their assignment to the MV state. The simultaneous population of bridge localised and MV states can be attributed to a number of factors that influence the relative stability of these states, for example, solvent environment, ion-pairing interactions and the orientation of the plane of the aromatic portion of the bridging ligand with respect to the metal orbitals of appropriate symmetry and hence the metal d-bridging ligand π orbital overlap.

Further examples of the redox activity of the bridging fragment can be observed in the meta-substituted isomer [1,3-{Cp*(dppe)Ru}$_2$(μ-C≡CC_6H_4C≡C)], where the bridging moiety is shown to be heavily involved in the oxidation process. The two band pattern ν(C≡C) pattern observed in [1,3-{Cp*(dppe)Ru}$_2$(μ-C≡CC_6H_4C≡C)]$^+$ is indicative of an oxidation which is localised on one 'RuC≡CC_6H_4' arm, with the second ethynyl moiety serving as a pendant donor. This leads to a new low energy electronic transition with a degree of charge transfer character between the pendant ethynyl donor and the oxidised bridge.[21] In addition, ruthenium entities bridged by a carboranyl fragment have also been prepared lying closer to the MV limit, due to the 'decoupling' of orbital energies of the bridging moiety and the metal-ethynyl fragments.[22]

Turning to other ruthenium fragments and linking groups, recent studies by Winter and co-workers have demonstrated the redox non-innocence of the organic bridging ligand the five coordinate bis(vinyl) complex [1,4-{(P^{i}Pr$_3$)$_2$(CO)ClRu}$_2$(μ-CH=CHC_6H_4CH=CH)] (**15)**, Chart 4.1. The two sequential one electron oxidation processes were interpreted in terms of a loss of electron density from the organic π-system (38 % for the first and 28 % for the second oxidation, with smaller yet discernible contributions from the ruthenium centres (11 % and 11 %).[23] IR and UV-vis-NIR spectroelectrochemical studies are also consistent with analysis, where upon oxidation of **15** to [**15**]$^+$ a small shift in Δν(C≡O) of +22 cm^{-1} and the presence of a structured intense band at 585 nm, typical of a phenylene radical absorption is observed, respectively.

The redox processes in the related six-coordinate ruthenium vinyl analogues [{PMe_3}$_3$(CO)ClRu}$_2$(μ-CH=CHC_6H_4CH=CH)] (**12**) were also found to be vinyl ligand in character, rather than metal-based (Chapter 3).[24] Thus, IR spectroelectrochemical measurements of the ν(C≡O) frequency, UV-vis-NIR spectroscopy and DFT studies on the model system [{(PH_3)$_3$(CO)ClRu}$_2$(μ-CH=CHC_6H_4CH=CH)] using the B3LYP/3-21G* functional and basis set, indicated that the HOMO of **12-H** is largely localised on the unsaturated bridging ligand (86 %). The oxidation of this complex can therefore be thought of as the progressive depopulation of the vinyl ligand based orbital.

In seeking to fine tune the electronic character of the ruthenium based [{L_nRu}$_2$(μ-bridge)]$^{n+}$ complexes further, we have refocused attention on the bridging element. The paracyclophane moiety has been explored within novel organic materials and π-conjugated oligomers. This is due to the transannular π-π interaction between the cofacial π-electron systems and the high structural rigidity associated with the paracyclophane.[25, 26] A series of studies by Wang *et al* incorporating the dithia[3.3]paracyclophane moiety, Figure 4.1 have revealed a significant red shift was observed in the absorption spectrum in comparison to reference fluorene polymers, suggesting an extension of the π-conjugation pathway *via* through space interactions.[27-29] As such, it has now been established that the weak non-covalent π-π interactions can have a significant effect on the electron transfer processes in biological processes[30] and some chemical systems.[31-33] In addition, measurements of single-molecule electron-transfer through systems containing the paracyclophane scaffold and conductance between molecules held together by spontaneous π-π stacking has provided evidence for electron transfer across neighbouring π-systems.[34, 35] Cyclophanes therefore have promise as new wire-like constructions with potential within electronic materials,[36] or

as components in molecular electronic devices.[37, 38]

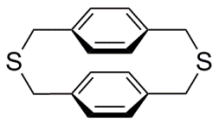

Figure 4.1. Dithia[3.3]paracyclophane.

In order to elucidate the through bond and through space pathways for electron delocalisation, Winter and co-workers have examined the diruthenium vinyl substituted cyclophane complex [{(P^iPr_3)$_2$(CO)ClRuCH=CH}$_2$(μ-[2.2]paracyclophane)] (**16a**) and [{Ru(CO)Cl(P^iPr_3)$_2$}$_2$(μ-3,7-divinyl-10,11-dihydro-5H-dibenzo[a.d]cycloheptene)] (**16b**), Figure 4.2, which is comprised of a half open [2.1]orthocyclophane, electrochemically.[39] The complexes **16a** and **16b** were characterised by two reversible consecutive one electron oxidation processes, which are separated by 210 and 107 mV respectively. Thus, it is apparent that there is a larger electronic interaction in the paracyclophane bridged moiety, where significant through space i.e. π-stacking and through bond interactions exist in comparison to **16b** where the cofacial π-electron system do not exist.

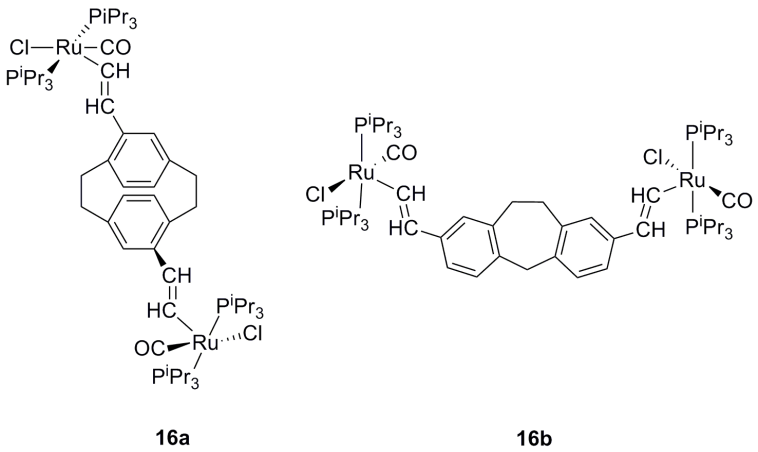

16a **16b**

Figure 4.2. Complexes 16a and 16b.

In IR spectroelectrochemical methods the stepwise oxidation of **16a** from its neutral form to its mono- and dicationic forms led to changes in Δν(C≡O) from 1909 cm^{-1} to the development of a two band pattern at 1912 and 1962 cm^{-1} and finally a single band at 1969 cm^{-1} respectively, where the modest changes in ν(C≡O) are a consequence of a strong ligand contribution to the styryl type complexes. On generation of the monocation, a broad absorption appeared in the NIR region, which was assigned as an IVCT band. Following an analysis of the carbonyl frequencies of MV complexes, the charge distribution parameter, Δρ, which estimates the relative charges at two redox active sites in a bimetallic complex can be calculated, according to

$$\Delta\rho = \frac{(\Delta\nu_{ox} + \Delta\nu_{red)})}{2[\nu'(ox) - \nu'(red)]}$$

where ν′(ox) and ν′(red) are the wavenumbers of the vibrational bands in the fully oxidised and reduced states, and $\Delta\nu_{ox} = \nu'(ox) - \nu_{meas}(ox)$, $\Delta\nu_{red} = \nu_{meas}(red) - \nu'(red)$, and the parameters $\nu_{meas}(ox)$ and $\nu_{meas}(red)$ refer to the observed vibrational bands associated with the oxidised and reduced centres in the intermediate case, i.e. the mono oxidised form. The charge distribution parameter, Δρ can range from 0 to 0.5, where 0 denotes the Class I limit of a MV system, with fully localised vacancies on two non-interacting redox sites, and when Δρ = 0.5 is indicative of the Class III limit of full charge delocalisation.[40, 41] Complex **16a** is an example of a moderately coupled Class two MV complex (Δρ = 0.08) whilst [**16b**]$^{+}$ is a very weakly coupled MV complex. Thus, the MV nature of vinyl complexes in [2.2] and [2.1]cyclophanes indicate the importance of through space interactions in these systems.

In this Chapter, we describe the synthesis and characterisation of diruthenium complexes featuring diethynyl- and divinyl-dithia[3.3]paracyclophane bridges and investigations of the electronic structure of the redox related derivatives using spectroelectrochemical and computational methods. The bridging moieties in these compounds are structural isomers to complex **16a** and **16b**, reported by Winter and co-workers.

4.2 Synthesis

The synthetic work was carried out by Dr J.L. Xia of Central China Normal University (China), and is described here briefly for completeness. The dibromo-dithia[3.3] paracyclophane **17** was prepared according to a recently reported procedure and involved the reaction of dithiol and 1,4-bis(bromomethyl)benzene in THF with K_2CO_3 in EtOH, under high dilution conditions, as illustrated in Scheme 4.1.[42] The reaction of **17** with trimethylsilylacetylene (TMSA) under standard Sonogashira reaction conditions led to the trimethylsilyl protected bis(ethynyl) proligand **18**, which following deprotection with KOH in MeOH/THF gave the diethynyl-dithia[3.3]paracyclophane **19**, Scheme 4.1.

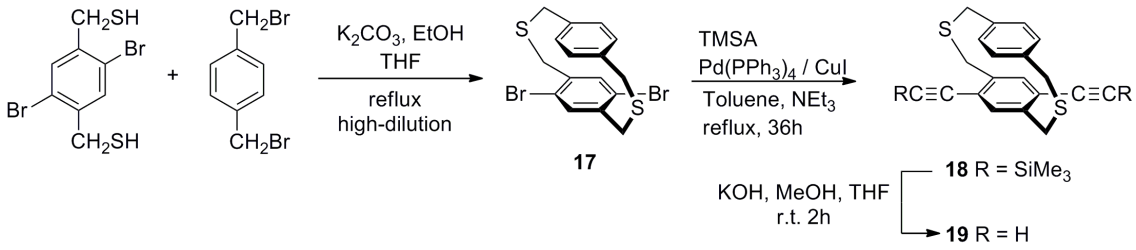

Scheme 4.1. Preparation of 19.

The cyclophane-bridged dinuclear ruthenium alkenyl compound **20** was prepared from the hydroruthenation reaction of $RuHCl(CO)(PPh_3)_3$ with **19** in CH_2Cl_2,[43] followed by phosphine exchange with PMe_3 to afford the six coordinate capped ruthenium vinyl complex **20**, Scheme 4.2.[24, 44] The cyclophane-bridged dinuclear alkynyl complex **21** was obtained from the reaction of RuCl(dppe)Cp* with **18**, and an *in situ* deprotonation of the resulting vinylidene complex, Scheme 4.2.[45]

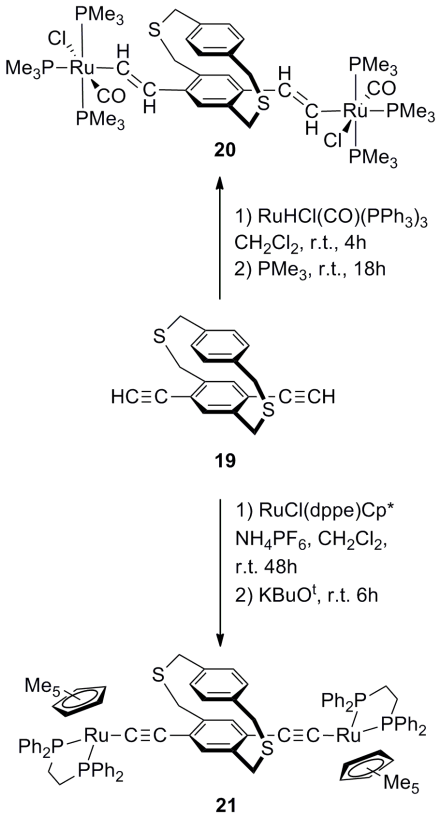

Scheme 4.2. Preparation of 20 and 21.

4.2.1 Spectroscopic Investigations

The compounds **20** and **21** were characterised by a variety of techniques including elemental analyses, IR spectroscopy, ^{31}P, ^{13}C and ^{1}H NMR spectroscopy. The identities of **20** and **21** were confirmed by elemental analyses. In **20**, a single strong ν(C≡O) band near 1920 cm^{-1} and in **21** a ν(C≡C) band near 2050 cm^{-1} was apparent in the solution and solid state IR spectra. The presence of the ruthenium vinyl and ruthenium alkynyl end groups in **20** and **21** follow from the observation of typical RuCH=CH- and RuC≡C- ^{13}C NMR resonances at 163.7 (RuCH=) and 109.3 (Ru-C≡) respectively. In the ^{1}H NMR spectrum of **20**, the characteristic vinyl proton resonances are observed at 7.78 – 7.83 ppm, though the J_{CP}, J_{HP} and J_{HH} couplings were not resolved. The thioether

methylene protons in compounds **20** and **21** can be differentiated in terms of their connection to the 'top' (C_6H_4, CH_2^a) or 'bottom' (C_6H_2, CH_2^b) aromatic moieties of the cyclophane, Figure 4.3. The CH_2^a protons were detected as an unresolved resonance at δ_H 3.74 ppm (**20**) or δ_H 3.49 ppm (**21**). The CH_2^b protons which are diastereotopic, appear as two doublets at 3.85 and 4.11 ppm in the ^{1}H NMR spectrum of **20** (J_{HH} = 15 Hz). However, in **21** one of these resonances is shifted to substantially lower field (6.02 pm) and both are substantially broadened. The low field shift is presumably due to the ring current effects of a nearby phenyl ring from the dppe protons, with similar effects also reported on the benzylic protons in non-peripherally substituted phthalocyanines.[46] In **21**, the dppe methylene protons give rise to a set of four, broad resonances between 2.21 – 2.97 ppm whilst in the ^{31}P NMR spectrum complex **21** displayed two resonances at 81.2 and 82.8 ppm. This is consistent with the two metal fragments in different magnetic environments, which may be indicative of a predominantly *transoid* arrangement of the half sandwich moieties. The ^{31}P NMR spectrum of **20** exhibited an AM_2 pattern, demonstrating the meridonal geometry of the three PMe_3 ligands about the ruthenium centre.

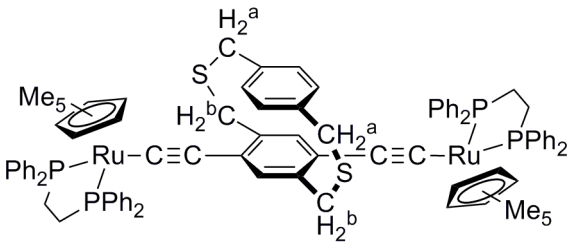

Figure 4.3. Differentiation of the protons connected to the 'top' (C_6H_4, CH_2^a) and 'bottom' (C_6H_2, CH_2^b) aromatic moieties of the cyclophane.

4.3 Molecular Structures

X-ray quality crystals of **21** were grown from the slow diffusion of hexane into a CH_2Cl_2 solution of the complex by Dr J.L. Xia, and solved at the Central China Normal University. The molecular structure of **21.CH_2Cl_2** is shown in Figure 4.4. Details of the data collection and refinement are presented in Table 4.1, and selected bond lengths and bond angles are listed in the caption of Figure 4.4.

Table 4.1. Crystal data and structure refinement for 21.

Complex	**21·CH_2Cl_2**
Empirical formula	$C_{93}H_{94}Cl_2P_4Ru_2S_2$
Formula weight (g mol^{-1})	1672.72
Temperature (K)	298(2)
Crystal system	Monoclinic
Space group	P2(1)/c
a (Å)	20.4758(12)
b (Å)	30.8470(18)
c (Å)	13.1932(7)
α (°)	90
β (°)	96.8470(10)
γ (°)	90
Volume($Å^3$)	8273.6(8)
Z	4
ρ_{calcd} (mg/mm^3)	1.343
μ (mm^{-1})	0.603
F(000)	3464
Reflections collected	55760
Independent reflections, R_{int}	16228 [$R_{(int)}$ = 0.0535]
Data/restraints/parameters	16228/15/957
Goodness-of-fit on F^2	1.167
Final R_1indexes [I>2σ(I)]	R_1 = 0.0594
Final R_1 wR_2 indexes(all data)	wR_2 = 0.1397

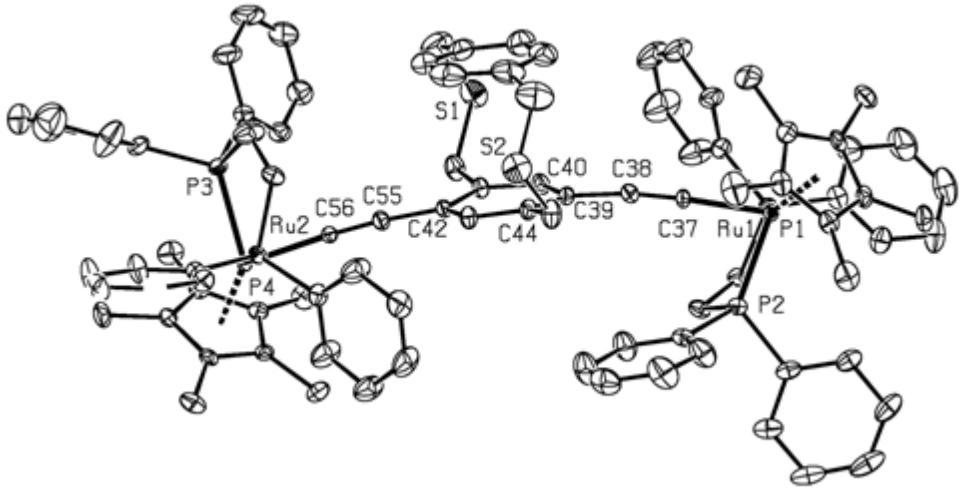

Figure 4.4. A plot of 21.CH_2Cl_2, showing the atom labeling scheme. Thermal ellipsoids are plotted at the 50 % probability level. The hydrogen atoms and solvent molecules are omitted for clarity.

Selected bond lengths (Å): C(37)-C(38) 1.208(5); C(37)-Ru(1) 2.004(4); C(38)-C(39) 1.435(5); C(55)-C(56) 1.208(5); C(56)-Ru(2) 2.016(4); C(42)-C(55) 1.448(5). Selected bond angles (°): C(38)-C(37)-Ru(1) 176.3(4); C(37)-C(38)-C(39) 171.6(4); C(56)-C(55)-C(42) 173.9(4); C(55)-C(56)-Ru(2) 175.7(3).

In complex **21**, the ruthenium atoms are separated by 11.95 Å. The ruthenium atoms reside in a pseudo octahedral geometry. The interplane distance of the two benzene rings of 3.29 Å is similar to other dithia[3.3]cyclophanes, and less than the normal packing distance of aromatic rings in organic aromatic molecules (~ 3.4 Å).[47] There is some disorder at S(2) which arises from the isomerisation of the dithia[3.3]paracyclophane bridge between the boat and chair conformations of the CH_2-S-CH_2 moiety. In **21** the C(37)-C(38) and C(55)-C(56) bond lengths of 1.208(5) Å confirm the presence of an alkynyl bond, falling within the expected range, with the Cp* ligands *trans* disposed.[48] The unsaturated carbon chain deviates from linearity at C(38) and C(55), with the bond angles at C(37)-C(38)-C(39) and C(56)-C(55)-C(42) angles being 171.6(4) and 173.9(4) ° respectively. The bending of the alkynyl core has been noted previously in dinuclear alkynyl bridged complexes.[19, 49-52]

4.4 Electrochemistry

The compounds **20** and **21** exhibited two consecutive one-electron oxidation processes in 0.1 M NBu_4PF_6 / CH_2Cl_2, Table 4.2; additional electrochemical processes were observed at higher potentials, but have not been examined further.

Table 4.2. The electrochemical response of 20 and 21 and related systems.[a]

Compound	$E_{1/2}(1)$ / V	$E_{1/2}(2)$ / V	$\Delta E_{1/2}$ (mV)	K_c
12 [44]	0.30	0.59	290	8.0×10^4
14 [19]	–0.27	0.01	280	5.4×10^4
20	0.23	0.53	300	1.0×10^5
21	–0.25	0.00	250	1.8×10^4

[a]Data was determined in CH_2Cl_2 containing 1mM compound and 0.1 M NBu_4PF_6; The Ag/Ag^+ electrode (internal solution: 0.01 M $AgNO_3$ + 0.1 M NBu_4PF_6 in MeCN; salt bridge: 0.1 M NBu_4PF_6 in CH_2Cl_2) was used as a reference, the potential of the $FcH/[FcH]^+$ couple is + 0.23 V under these conditions. Additional waves were observed at higher potentials but not examined further.

The first one-electron redox waves in the voltammograms of **20** and **21** exhibited i_{pc}/i_{pa} peak current ratios of unity at ν = 100 mV/s and room temperature. In **20** and **21**, the high chemical reversibility of the first wave is demonstrated by the unitary ratio of peak currents at ν = 100 mV/s. The Randles-Sevcik equation shows that the electrochemical reversibility of a system can be established from the linear dependence of the peak current with $\nu^{1/2}$, according to

$$i_p = (2.69 \times 10^5) n^{\frac{3}{2}} A C D^{\frac{3}{2}} \nu^{\frac{1}{2}}$$

where i_p is the anodic or cathodic peak current of the voltammetry wave, n is the

number of electrons in the process, A is the area of the working electrode, C is the analyte concentration, D is the diffusion constant of the analyte and ν is the scan rate.

However, the first wave in **20** is strictly electrochemically quasi-reversible with $\Delta E_p(1)$ varying from 80 mV (100 mV/s) to 100 mV (800 mV/s), Figure 4.5. In contrast, the peak to peak separation, $\Delta E_p(1) = |E_{pa}(1) - E_{pc}(1)| = 80$ mV for **21** is independent of scan rate, and as such, can be described as a fully reversible oxidation wave, Figure 4.6. This is further supported by a linear plot of i_{pa} vs $\nu^{1/2}$ for **20** and **21**, Figure 4.7 and 4.8.

The second oxidation process E(2) is electrochemically irreversible in each case. For the vinyl complex **20**, $\Delta E_p(2)$ is sensitive to scan rate, and is as large as 150 mV at 800 mV/s, while i_{pc}/i_{pa} ranges from ca. 0.7 to close to 1 over scan rates from $\nu = 100 - 800$ mV/s, Figure 4.9. Likewise in the acetylide complex **21**, $\Delta E_p(2)$ varies with scan rate up to 120 mV (800 mV/s) with i_{pc}/i_{pa} varying from 0.8 at 100 mV/s to closer to unity at 800 mV/s, Figure 4.10. The half wave potentials ($E_{1/2}(1)$ and $E_{1/2}(2)$) for complexes **20** and **21** are listed in Table 4.2 along with their 1,4-divinylphenylene and 1,4-diethynylphenylene counterparts **12** and **14**, Chart 4.1.[19, 20, 44]

The electrochemical data of **20** is in excellent agreement with that obtained from the analogous 1,4-divinyl-2,5-dimethylphenylene bridged complex under identical conditions (0.20, 0.50 V).[44] Compound **20** has a ΔE value (300 mV at 100 mV/s) that is indistinguishable (within experimental error) from that of **12** (ΔE = 290 mV). The first oxidation potential $E_{1/2}(1)$ of **21** is essentially identical to that of **14** while $E_{1/2}(1)$ for **20** is lower than in **12**. The potential separation of **21** is marginally smaller than the phenylene-bridged counterpart **14** (ΔE = 280 mV at 100 mV/s). However, the redox

potentials of vinyl complexes derived from **12** are more sensitive to the substituents on the phenylene ring[44] compared to the alkynyl complexes derived from **14**,[20] due to the substantial redox non-innocent nature of this moiety (Chapter 3).[23, 24, 53, 54]

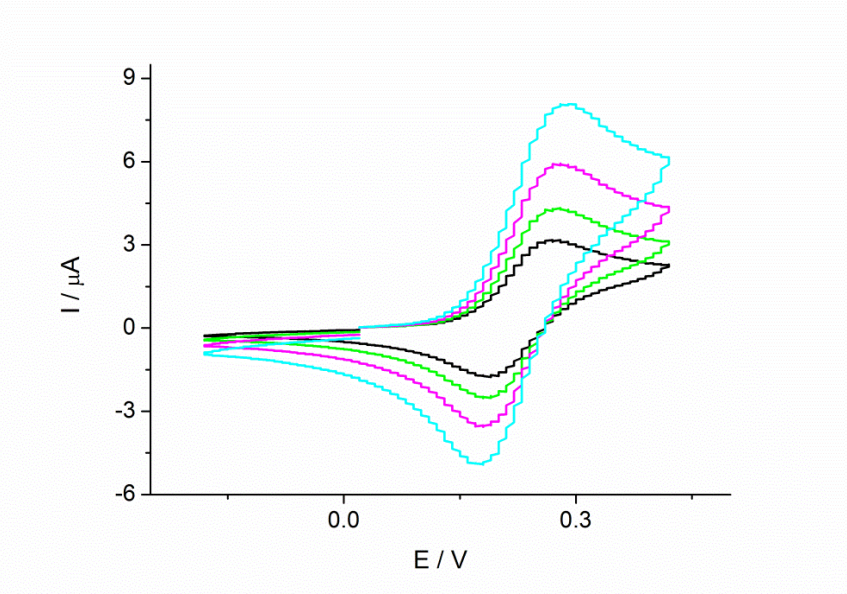

Figure 4.5. First redox wave of $[20]^+$ in 0.1 M NBu_4PF_6 / CH_2Cl_2 at ν = 100 mV/s (black), 200 mV/s (green), 400 mV/s (purple), 800 mV/s (blue).

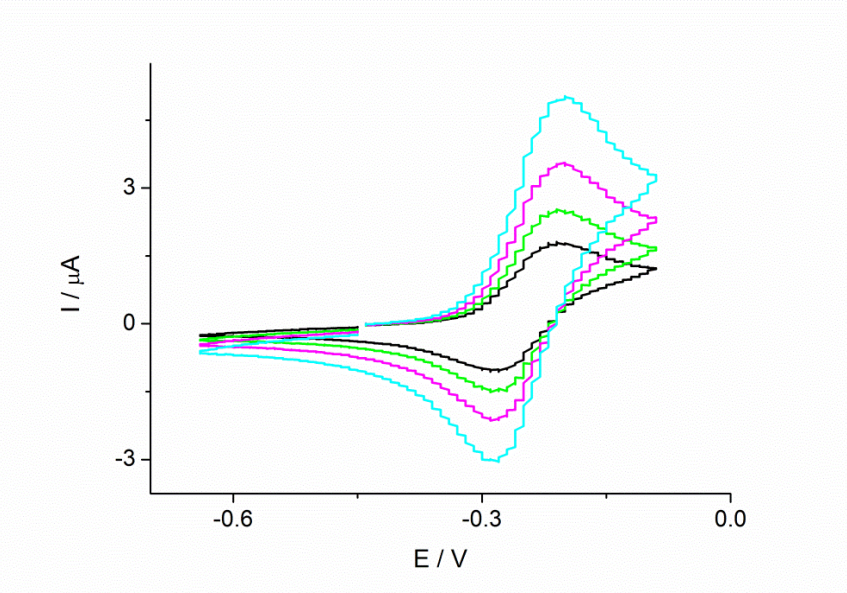

Figure 4.6. First redox wave of $[21]^+$ in 0.1 M NBu_4PF_6 / CH_2Cl_2 at ν = 100 mV/s (black), 200 mV/s (green), 400 mV/s (purple), 800 mV/s (blue).

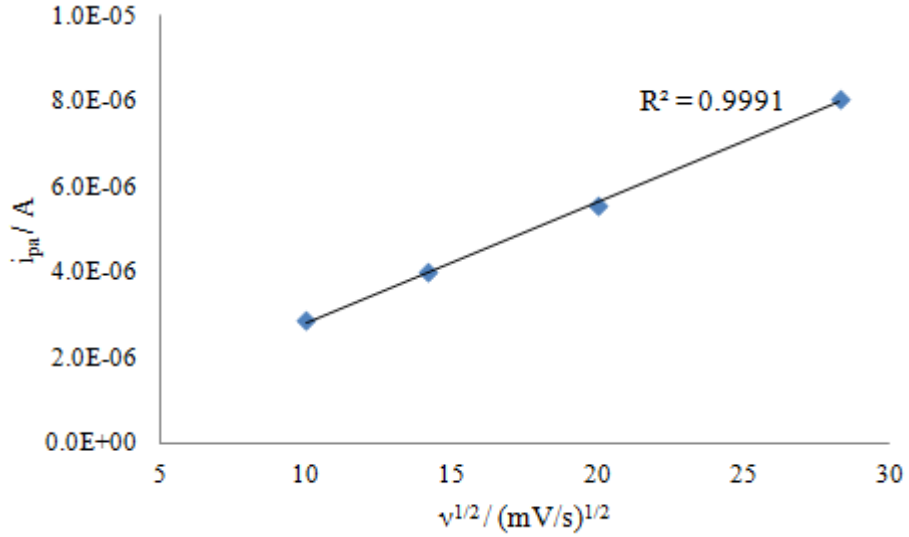

Figure 4.7. Plot of i_{pa} vs. $\nu^{1/2}$ / (mV/s)$^{1/2}$ for 20.

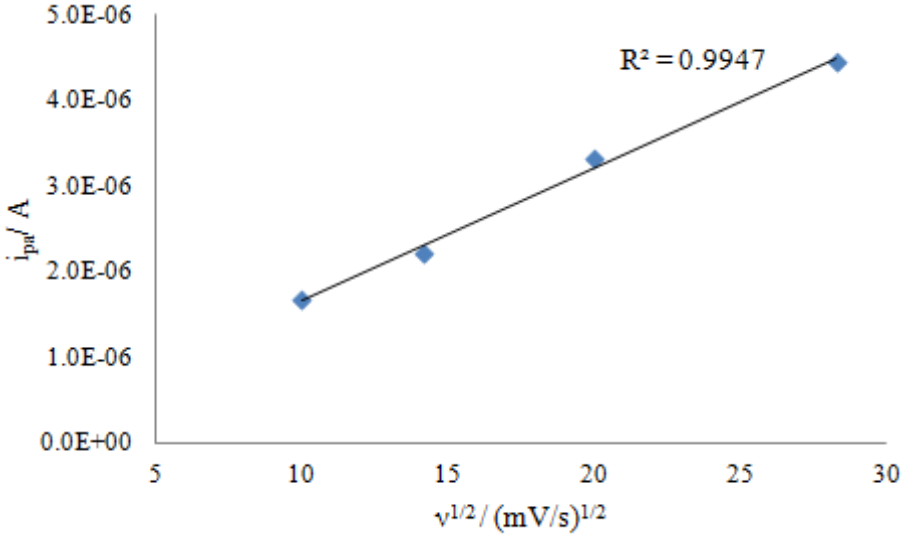

Figure 4.8. Plot of i_{pa} vs. $\nu^{1/2}$ / (mV/s)$^{1/2}$ for 21.

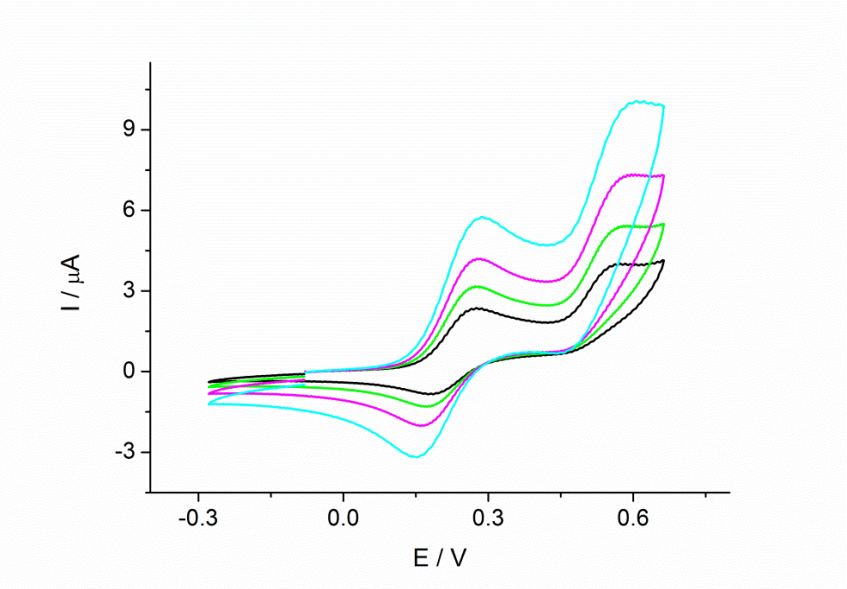

Figure 4.9. Electrochemical response of 20 in 0.1 M NBu_4PF_6/ CH_2Cl_2 at ν = 100 mV/s (black), 200 mV/s (green), 400 mV/s (purple), 800 mV/s (blue). The second redox wave is irreversible.

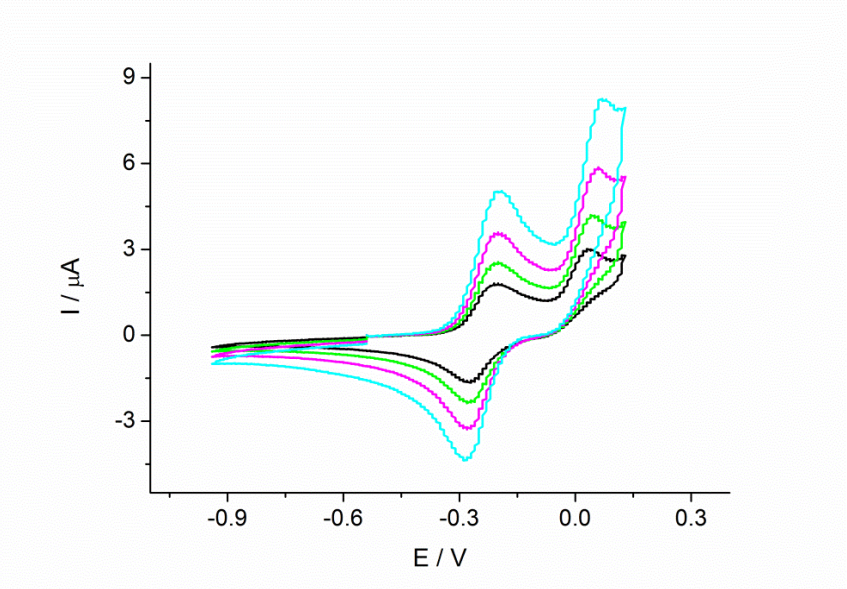

Figure 4.10. Electrochemical response of 21 in 0.1 M NBu_4PF_6 / CH_2Cl_2 at ν = 100 mV/s (black), 200 mV/s (green), 400 mV/s (purple), 800 mV/s (blue). The second redox wave is irreversible.

4.5 IR Spectroelectrochemistry

Owing to the rather substantial splitting between the redox waves in the complexes **20** ($\Delta E_{1/2}$ = 300 mV) and **21** ($\Delta E_{1/2}$ = 250 mV), the monoxidised radical intermediates [**20**]$^{+}$ and [**21**]$^{+}$ constitute thermodynamically stable species with large comproportionation constants K_c = 1.8 x 10^4 and 1.0 x 10^5 respectively. The presence of charge-sensitive infrared spectroscopic labels for the complexes **20** (ν(C≡O), 1923 cm^{-1}) and **21** (ν(C≡C), 2060 cm^{-1}) allowed the study of spectroscopic changes accompanying stepwise oxidation in an optically transparent thin-layer electrode (OTTLE) cell.

Table 4.3. Spectroelectrochemically determined ν(C≡C) and ν(C≡O) vibrational frequencies (cm^{-1}) for [20]$^{n+}$, [21]$^{n+}$ and related systems.

Compound	Frequency	n = 0	n = 1	n = 2
[12]$^{n+}$ [24]	ν(C≡O)	1921	1934 2061w 1997s	1974
[14]$^{n+}$ [20]	ν(C≡C)	2068m	1974vs 1915w,sh 1564m	1970vw, 1924w
[15]$^{n+}$ [23]	ν(C≡O)	1910	1942	1991
[20]$^{n+}$	ν(C≡O)	1923s	1924s	1922
[21]$^{n+}$	ν(C≡C)	2060s	2055vw 1970vs 1560m	not obsd
[22]$^{n+}$ [55]	ν(C≡C)	2071m	2068m 1966vs 1570s	1918s

On oxidation of **20** to $[\mathbf{20}]^{+}$ in the spectroelectrochemical cell, the ν(C≡O) band appeared at almost the same position, shifting from 1923 cm^{-1} to 1924 cm^{-1} respectively, Figure 4.11. The divinylphenylene-bridged five or six-coordinate diruthenium complexes **15** and **12** exhibited shifts in the positions of the Δν(C≡O) bands from the neutral to the monocationic forms of +32 and +13 cm^{-1} respectively. The small shifts, as reported by Winter and co-workers (discussed in Chapter 3), indicate the significant involvement of the bridging ligand in the oxidation process. Thus, the 1 cm^{-1} shift in complex **20** indicates that the oxidation occurs primarily and almost entirely on the bridge. Upon further oxidation to $[\mathbf{20}]^{2+}$, a strong ν(C≡O) band at 1922 cm^{-1} developed, with an additional band with an apparent maximum at 1949 cm^{-1}. On reduction of $[\mathbf{20}]^{2+}$ through $[\mathbf{20}]^{+}$ to **20**, the primary ν(C≡O) band was recovered, with reduced intensity. The persistence of the band at 1949 cm^{-1} was attributed to the partial decomposition of the sample. In comparison, $[\mathbf{15}]^{2+}$ and $[\mathbf{12}]^{2+}$ were reported to contain bands at 1991 and 1974 cm^{-1} respectively.

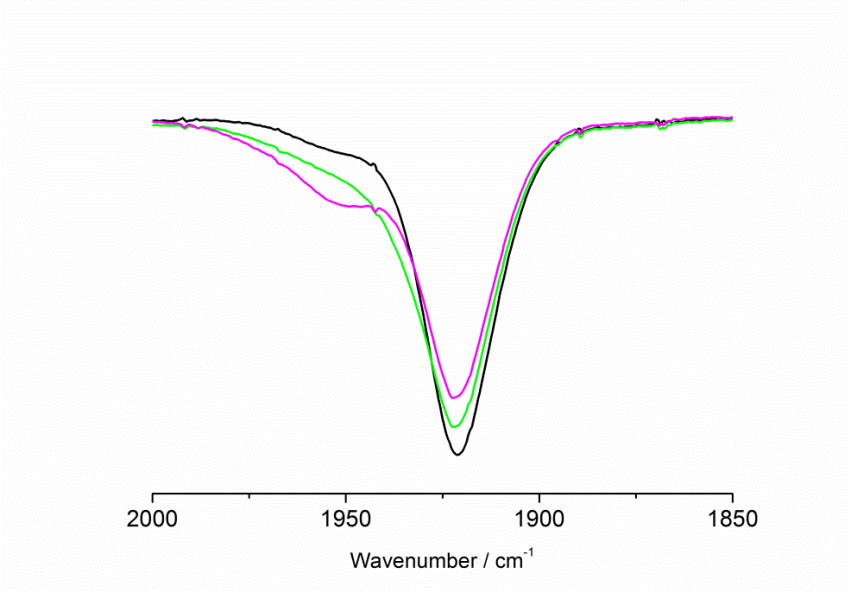

Figure 4.11. IR spectra for 20 (black), $[20]^{+}$ (green) and $[20]^{2+}$ (purple) collected during an *in situ* oxidation in an IR spectroelectrochemical cell in 0.1 M NBu_4PF_6 / CH_2Cl_2.

During the first oxidation of **21**, the ν(C≡C) band at 2060 cm^{-1} decreased, while a very strong band at 1970 cm^{-1} appeared ($\Delta\nu$(C≡C) = 90 cm^{-1}), together with a very weak band at 2055 cm^{-1}, Figure 4.12. Upon oxidation of $[\mathbf{21}]^{+}$ to $[\mathbf{21}]^{2+}$, the ν(C≡C) band at 1970 cm^{-1} disappeared and there were no other detectable absorptions in the 1500 to 2150 cm^{-1} range, which can be taken as evidence for the highly symmetric distribution of charge in the dication. On back-reduction of $[\mathbf{21}]^{2+}$ through $[\mathbf{21}]^{+}$, the chemical reversibility of the system was verified by complete recovery of the **21**, which suggests that the electrochemical irreversibility in the cyclic voltammogram is due to slow electron transfer, rather than to the inherent chemical instability of $[\mathbf{21}]^{2+}$.

In the radical cations of the symmetrical diethynyl-bridged complexes [1,4-{Cp*(dppe)Ru}$_2$(μ-C≡CC_6H_4C≡C)][19,20] (**14**) and [1,4-{Cl(dppe)$_2$Ru}$_2$(μ-C≡CC_6H_4C≡C)][56] (**22**), the significant shift of the most intense band has been interpreted in terms of the strong participation of the bridge in the first oxidation process. However, as discussed earlier, $[\mathbf{14}]^{+}$ is further complicated by the presence of conformational isomers which influence the distribution of charge between the metal centres and bridging ligands, giving rise to vibrational bands which correspond to the MV state.[20] The presence of multiple ν(C≡C) bands in $[\mathbf{21}]^{+}$ may also be accounted for by the same reasoning, with the weak band in $[\mathbf{22}]^{+}$ indicating a small contribution from similar conformation distributions though there is no further spectroscopic evidence to support this.

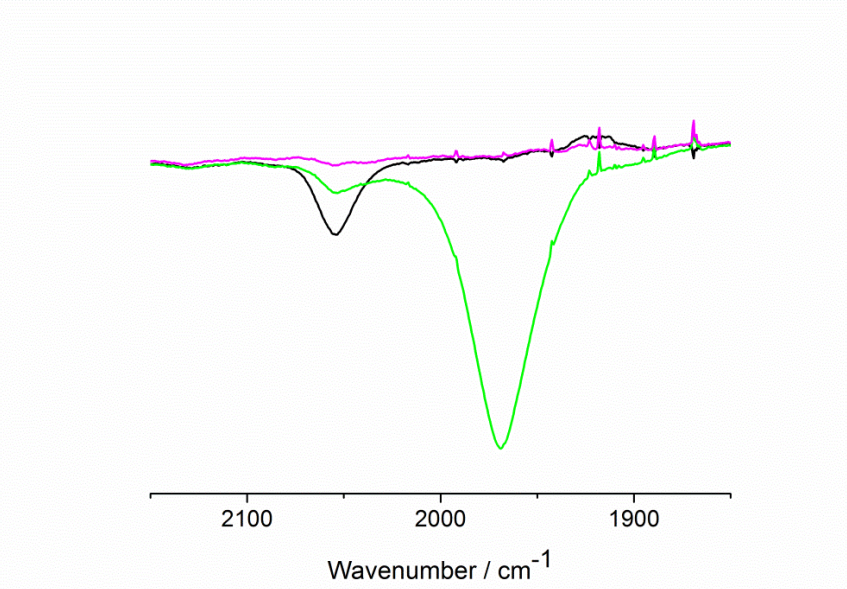

Figure 4.12. IR spectra for 21 (black), $[21]^{+}$ (green) and $[21]^{2+}$ (purple) collected during an *in situ* oxidation in an IR spectroelectrochemical cell in 0.1 M NBu_4PF_6 / CH_2Cl_2.

The IR spectrum of [**21**]$^{2+}$ is fundamentally different to other 1,4-diethynylphenylene based dications, which often exhibit a ν(C≡C) band of medium or weak intensity, despite their apparently delocalised nature, and thought to be due to intensity borrowing by coupling of the ν(C≡C) mode to an electronic MLCT transition, or a small degree of asymmetry produced by experimental factors.[16, 56, 57] For example, [**14**]$^{2+}$ exhibits two weak bands at 1970 and 1924 cm^{-1} arising from the symmetric and asymmetric ν(C≡C) modes,[20] whilst [**22**]$^{2+}$ contains a single ν(C≡C) band of medium to weak intensity at 1918 cm^{-1}.[56] The absence of similar bands in [**21**]$^{2+}$ suggests either decreased vibronic coupling, or that the combination of cyclophane, dppe and Cp* ligands serves to more effectively insulate the bridge-localised charge from the effects of the medium, for example, solvent and ion-pairing interactions. Thus, the negligible shift of the value of ν(C≡O) upon oxidation of **20**, the large shift in ν(C≡C) of 90 cm^{-1} on oxidation of **21** to [**21**]$^{+}$ and the silent nature of [**21**]$^{2+}$ indicates that the dithia[3.3]paracyclophane unit supports substantial participation of the bridge in the redox processes.

4.6 UV-vis-NIR Spectroelectrochemistry

On oxidation of **20** and **21** to $[\mathbf{20}]^+$ and $[\mathbf{21}]^+$ respectively a new absorption band developed between 22000 – 15000 cm^{-1} with some unresolved structure, Figure 4.13 and 4.14 respectively. The related radical complexes $[\mathbf{12}]^+$ and $[\mathbf{14}]^+$ also exhibit similar absorption bands, in which the bridging ligands are heavily involved in supporting the unpaired electron/hole.[19, 20, 58]

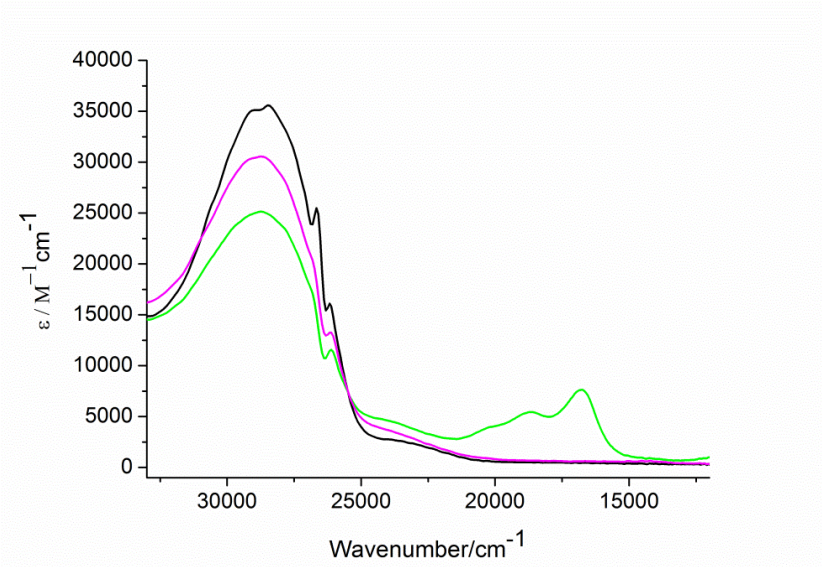

Figure 4.13. The UV-Vis spectra of 20 (black), $[20]^+$ (green) and $[20]^{2+}$ (purple) collected during an *in situ* oxidation in an IR spectroelectrochemical cell in 0.1 M NBu_4PF_6 / CH_2Cl_2.

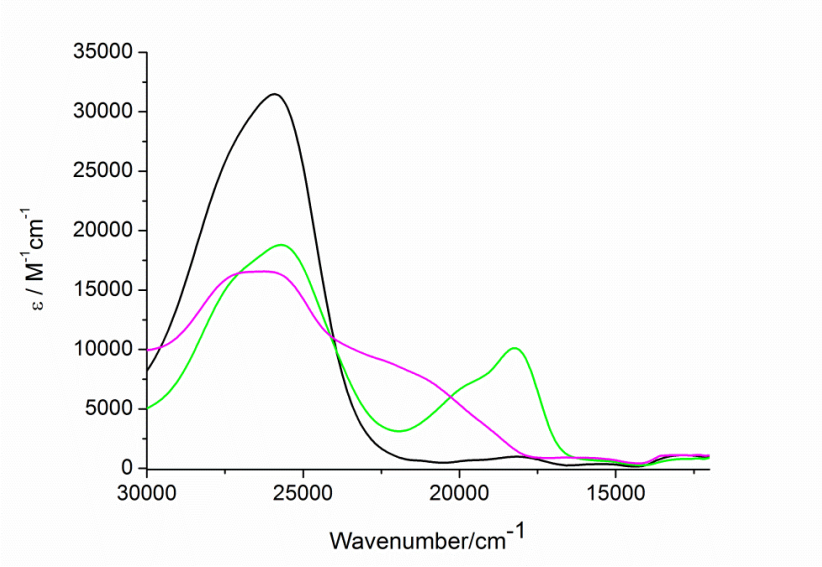

Figure 4.14. The UV-Vis spectra of 21 (black), $[21]^+$ (green) and $[21]^{2+}$(purple) collected during an *in situ* oxidation in a spectroelectrochemical cell in 0.1 M NBu_4PF_6 / CH_2Cl_2.

The NIR spectra of complexes [**20**]$^{+}$ and [**21**]$^{+}$ feature strong absorption envelopes around 10000 cm^{-1}, which were not presence in either the neutral or dicationic states. Deconvolution of the NIR band in [**20**]$^{+}$ into a summation of Gaussian-shaped curves reveal three overlapping transitions (ν_1 = 9760 cm^{-1}, ε = 3000 dm^3 mol^{-1} cm^{-1}, $\Delta\nu_{1/2}$ = 1480 cm^{-1}; ν_2 = 8700 cm^{-1}, ε = 3360 dm^3 mol^{-1} cm^{-1}, $\Delta\nu_{1/2}$ = 800 cm^{-1}; ν_3 = 8320 cm^{-1}, ε = 1100 dm^3 mol^{-1} cm^{-1}, $\Delta\nu_{1/2}$ = 2340 cm^{-1}), Figure 4.15. This three-band deconvolution is substantially different from the two-band pattern observed for the 1,4-divinylphenylene bridged diruthenium counterpart [**12**]$^{+}$, which only contains two low energy transitions in the NIR region.[24] Similarly when the NIR band in complex [**21**]$^{+}$ was deconvoluted, three overlapping transitions were revealed (ν_1 = 6875 cm^{-1}, ε = 15300 dm^3 mol^{-1} cm^{-1}, $\Delta\nu_{1/2}$ = 2800 cm^{-1}; ν_2 = 5565 cm^{-1}, ε = 9400 dm^3 mol^{-1} cm^{-1}, $\Delta\nu_{1/2}$ = 1160 cm^{-1}; ν_3 = 4420 cm^{-1}, ε = 1400 dm^3 mol^{-1} cm^{-1}, $\Delta\nu_{1/2}$ = 760 cm^{-1}), Figure 4.16. Whilst the lowest energy transition was not resolved in the NIR spectrum of the 1,4-diethynylphenylene bridged diruthenium complex [**14**]$^{+}$, the other transitions are very similar, and belong to the 'bridge localised' component.

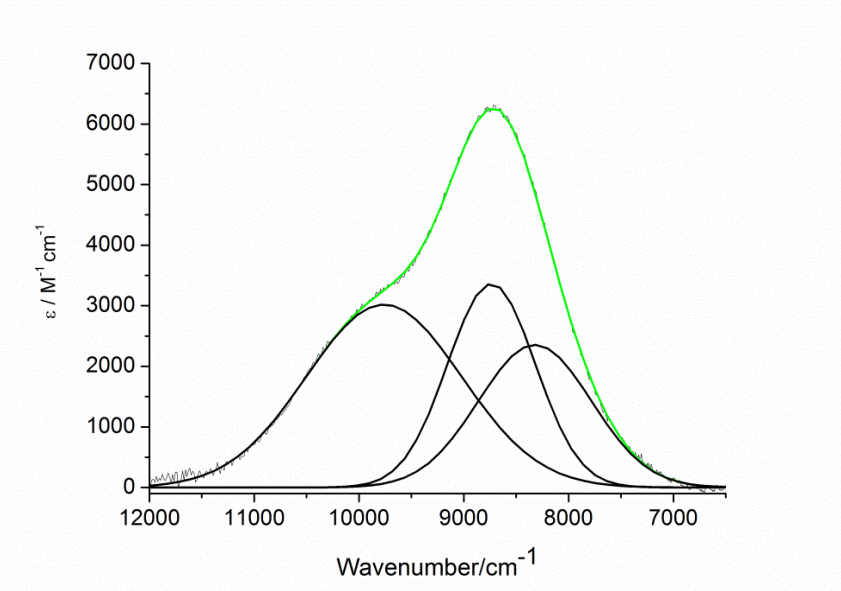

Figure 4.15. The NIR spectrum of $[20]^+$ showing deconvolution into three Gaussian shaped sub-bands.

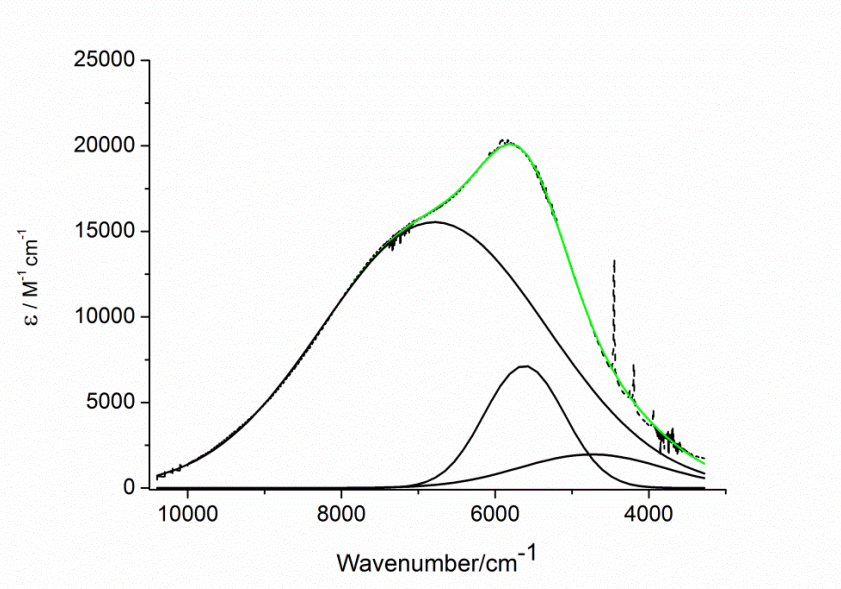

Figure 4.16. The NIR spectrum of $[21]^+$(green) showing deconvolution into three Gaussian shaped sub-bands.

4.7 DFT Calculations

DFT calculations were performed by Dr M.A. Fox and Prof. P.J. Low at Durham University (U.K) on the model systems [**20-H**]$^+$and [**21-H**]$^+$ using B3LYP/3-21G* level of theory. The PMe_3 ligands in **20** were replaced by PH_3 ligands and the η-C_5Me_5 and dppe ligands in **21** by η-C_5H_5 and two PH_3 ligands, respectively. The HOMO's in [**20-H]** and [**21-H]** are delocalised across the entire metal-organic π-system ([**20-H**]: Ru 12 %, divinylphenylene bridge 82 %; [**21-H**]: Ru 22 %, 1,4-ethynylphenylene bridge 70 %), Figure 4.17a and b. On oxidation of [**20-H]** and [**21-H]** to [**20-H]**$^+$ and [**21-H]**$^+$ respectively, the HOMO is depopulated. As a result, there is a slight increase in the ligand contribution to the β-LUSO, but it is much the same as the parent neutral complexes ([**20-H**]$^+$ Ru 14 %, divinylphenylene bridge 85%; [**21-H**]$^+$ Ru 24 %, 1,4-ethynylphenylene bridge 75 %), Figure 4.17c and d.

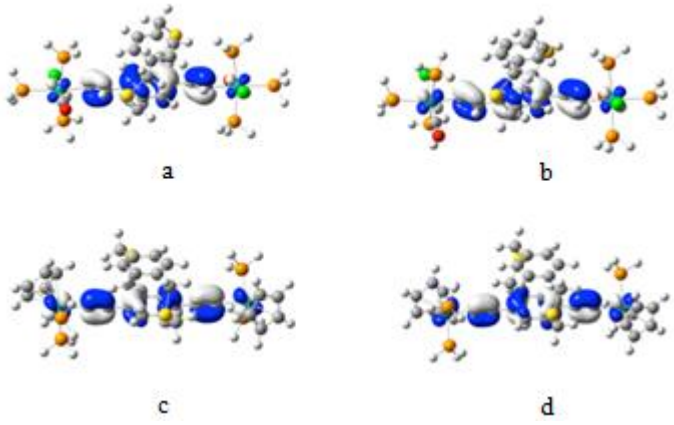

Figure 4.17. The HOMO in [20-H] (a) and [21-H] (c) and β-LUSO in [20-H]$^+$ (b) and [21-H]$^+$ (d).

TD-DFT calculations are consistent with experimental results, featuring three low energy transitions which in [**20-H**]$^{+}$ have been assigned to as Cl-LCT, MLCT and SLCT transitions (where S represents the sulfur atom on the cyclophane ring) and in [**21-H**]$^{+}$ as two MLCT transitions and a SLCT transition. In [**20-H**]$^{+}$, the low energy transition corresponds to a transition with charge transfer between the top and the bottom decks of the cyclophane ring. This weak feature aside, TD-DFT calculations are consistent with essentially a two band pattern in the near-IR region arising from charge transfer from the chloride ligands to the divinylphenylene moiety and a rather intense MLCT transition.

As discussed in Chapter 3, complex **12** also reveals two largely bridge centred oxidation processes; [**12**]$^{n+}$ and [**20**]$^{n+}$ feature similar ν(C≡O) patterns and in the near-IR spectra, similar MLCT transitions, with an additional S-LCT transition. The spectroscopic features of **12**, which has previously been interpreted in terms of both a bridged-centered and metal centered MV form are thought to be distinguishable by the relative conformation of the metal fragments with respect to the plane of the aromatic portion of the bridging ligand. However, the presence of what appears to be just the bridge-centered form in [**20**]$^{+}$ suggests that the steric bulk of the cyclophane serves to restrict the range of conformers.

4.8 Conclusions

In the growing family of bimetallic ruthenium complexes featuring branched carbon-rich ligands, the cyclophane unit in dithia[3.3]paracyclophane-bridged bimetallic ruthenium vinyl (**20**) and alkynyl (**21**) complexes is another example of a redox non-innocent ligand. As demonstrated by IR and UV-vis-NIR spectrolectrochemical experiments and supported by DFT calculations, the oxidation of these complexes is largely centered on the organic bridge. IR spectroelectrochemistry reveals a negligible shift on oxidation of **20** to its mono- and dicationic states, in support of the concept that the metal centres are not redox-active. Similarly, in **21** the ν(C≡C) shifts to lower wavenumbers by some 90 cm^{-1}, whilst $[\mathbf{21}]^{2+}$ has negligible intensity with both observations supporting the notion of redox non-innocent character in the bridging ligand. Deconvolution of the NIR bands of $[\mathbf{20}]^{+}$ and $[\mathbf{21}]^{+}$ reveals three transitions, which with the aid of TD-DFT can be attributed to a combination of Cl-LCT, MLCT and SLCT transitions. DFT studies are consistent with the involvement of the bridging ligand with the oxidation process.

4.9 Experimental

All synthetic work was carried out by Dr. J.L. Xia of Central China Normal University, China. Unless otherwise stated all reactions were carried out under a nitrogen atmosphere using standard Schlenk techniques. No special precautions were taken to exclude oxygen during work-up. Solvents were distilled under nitrogen from sodium-benzophenone-ketyl radical (toluene) or calcium hydride (CH_2Cl_2). The compounds RuCl(dppe)Cp*[17]and RuHCl(CO)$(PPh_3)_3$[59] were prepared by standard literature methods. The detailed procedures for the synthesis of compounds **17**, **18** and **19** have been described elsewhere.[42]

^1H, ^{13}C and ^{31}P NMR spectra were collected on a Varian Mercury Plus 400 spectrometer (400 MHz) or 600 spectrometer (600 MHz). ^1H and ^{13}C NMR chemical shifts are relative to TMS, and ^{31}P NMR chemical shifts are relative to 85% H_3PO_4. Mass spectra were analyzed on a Thermo-Finnigan LTQ FT instrument. Infrared spectra were obtained on a Nicolet AVATAR 360 FT-IR instrument using KBr pellets. Elemental analyses (C, H, N) were performed by the Microanalytical Services, College of Chemistry, CCNU.

Electrochemical measurements were performed on a CHI660C potentiostat (CH Instruments Company, USA). A three-electrode one-compartment cell containing a solution of the analyte and supporting electrolyte in dry CH_2Cl_2 was utilised. The solution was degassed by bubbling argon through the solution for about 10 min before measurement. Analyte and electrolyte (NBu_4PF_6) concentrations were typically 0.001 and 0.1 M, respectively. A 500 μm diameter platinum disc working electrode, a

platinum wire counter electrode, and an $Ag|Ag^+$ reference electrode were used. The Ag/Ag^+ reference electrode contained an internal solution of 0.01 M $AgNO_3$ in acetonitrile and was incorporated to the cell with a salt bridge containing 0.1 M NBu_4PF_6 in CH_2Cl_2. All electrochemical experiments were carried out at ambient temperature.

Spectroelectrochemical experiments were performed at room temperature in an airtight optically transparent thin-layer electrochemical (OTTLE) cell equipped with Pt minigrid working and counter electrodes (32 wires cm^{-1}), Ag wire pseudo-reference electrode and CaF_2 windows for a 200 μm path-length solvent compartment.[60] The cell was positioned in the sample compartment of a Nicolet Avatar 6700 FT-IR spectrometer or a Perkin-Elmer Lambda-900 spectrophotometer. The controlled-potential electrolyses were carried out utilizing a homebuilt potentiostat.

X-ray crystallography

Crystals suitable for X-ray diffraction were grown from a CH_2Cl_2 solution of **21** layered with hexane. A crystal with approximate dimensions of 0.20 x 0.15 x 0.10 mm^3 was mounted on a glass fiber for diffraction experiment. Intensity data were collected on a Nonius Kappa CCD diffractometer with Mo K_α radiation (0.71073 Å) at room temperature. The structures were solved by a combination of direct methods (SHELXS-97)[44] and Fourier difference techniques and refined by full-matrix least squares (SHELXL-97).[44] All non-H atoms were refined anisotropically. The hydrogen atoms were placed in the ideal positions and refined as riding atoms.

Computational Details

DFT calculations were performed with the Gaussian 03 and 09 programs,[45] at the B3LYP/3-21G* level of theory.[46] Geometry optimizations were performed without any symmetry constraints, and frequency calculations on the resulting optimized geometries showed no imaginary frequencies. Electronic transitions were calculated by the time-dependent DFT (TD-DFT) method. The MO contributions were generated using the GaussSum package and plotted using GaussView 5.0.[47]

4.9.2 Preparation of 20

To a stirred solution of $RuHCl(CO)(PPh_3)_3$ (0.86 g, 0.90 mmol) in CH_2Cl_2 (30 ml) was added dropwise a solution of **19** (0.16 g, 0.50 mmol) in CH_2Cl_2 (10 ml) at room temperature under N_2. After the addition was complete, the resulting mixture was stirred for 4 h before addition of PMe_3 (5 mL, 1M in THF, 5 mmol), and the reaction mixture allowed to stir at r.t. for a further 18h. The volatile materials were then removed under vacuum. The remaining solid residue was purified by column chromatography on silica gel, eluting with acetone / petroleum ether (1:2, v/v) to afford **20** as a yellow solid (210 mg, 38 %). ^{1}H NMR (600 MHz, $CDCl_3$): δ 1.33 (d, J_{HP} = 5 Hz, 18H, CH_3); 1.50 (d, J_{HP} = 7 Hz, 18H, CH_3); 1.65 (d, J_{HP} = 5 Hz, 18H, CH_3); 3.74 (m, 4H, CH_2); 3.85 (d, J = 15 Hz, 2H, 2×SCH); 4.11 (d, J = 15 Hz, 2H, 2×SCH); 6.72 (d, J_{HH} = 7 Hz, 2H, Ar); 6.81 (d, J_{HH} = 5 Hz, 2H, C=CHAr); 6.89 (s, 2H, Ar); 7.04 (d, J_{HH} = 7 Hz, 2H, Ar); 7.78-7.83 (m, 2H, C=CHRu). ^{13}C NMR (100 MHz, $CDCl_3$): δ 16.34-16.95 (m, PMe_3); 20.14 (d, J_{CP} = 21 Hz, PMe_3); 36.06, 37.59 (CH_2); 126.86, 127.92, 129.18, 129.33, 131.75, 135.06 (Ar); 135.23 (ArC=); 163.65 (Ru-C); 202.35 (CO). ^{31}P NMR (160 MHz, $CDCl_3$): δ -7.80 (s); -19.93 (s). IR (KBr/cm^{-1}): ν(CO) 1913s; ν(C=C) 1552m. Anal. Calc. for $C_{40}H_{74}Cl_2O_2P_6Ru_2S_2$: C, 43.28; H, 6.72. Found: C, 43.54; H, 6.47.

4.9.1 Preparation of 21

A solution of RuCl(dppe)Cp* (0.36 g, 0.53 mmol), **18** (0.080 g, 0.25 mmol) and NH_4PF_6 (0.41 g, 2.5 mmol) in CH_2Cl_2 (15 ml) was stirred for 48 h at room temperature under N_2. Then ^tBuOK (0.062 g, 0.55 mmol) was added, and the reaction mixture was stirred for another 6 h. The solvent was removed and the crude product was purified by chromatography on silica gel eluted with acetone / petroleum ether (b.p. 30 - 60 °C) (1:2, v/v) to give **21** as a yellow solid (0.19 g, 48 %). ^1H NMR (400 MHz, $CDCl_3$): δ 1.67 (s, 30H, C_5Me_5); 2.21, 2.85 (2×m, 2×2H, CH_2 of dppe); 2.39, 2.97 (2×m, 2×2H, CH_2 of dppe); 3.49 (s, 4H, 2×SCH_2); 3.73 (br, 2H, 2×SCH); 6.02 (br, 2H, 2×SCH); 6.62 (d, J_{HH} = 7 Hz, 2H, C_6H_4); 6.71 (d, J_{HH} = 7 Hz, 2H, C_6H_4); 6.97-6.99 (m, 4H, Ar); 7.17-7.47 (m, 30H, Ar); 7.84 (m, 8H, Ar). $^{13}C\{^1H\}$ NMR (100 MHz, $CDCl_3$): δ 10.24 (CH_3 of C_5Me_5); 28.89-30.17 (m, CH_2 of dppe); 35.31, 37.33 (SCH_2); 92.48 (C_5Me_5); 109.29 (br, Ru-C≡); 125.24, 127.31-129.21 (m, Ar); 132.14-135.01 (m, Ar); 136.63-140.81 (m, Ar). $^{31}P\{^1H\}$ NMR (160 MHz, $CDCl_3$): δ 81.2 (s); 82.8 (s). IR (KBr / cm^{-1}): ν(C≡C) 2056w. Anal.Calc. for $C_{92}H_{92}P_4Ru_2S_2$: C, 69.59; H, 5.84. Found: C, 69.75; H, 5.58.

4.10 References

1. S. J. Higgins, R. J. Nichols, S. Martin, P. Cea, H. S. J. van der Zant, M. M. Richter and P. J. Low, *Organometallics*, 2011, **30**, 7-12.
2. P. Aguirre-Etcheverry and D. O'Hare, *Chem. Rev.*, 2010, **110**, 4839-4864.
3. P. J. Low, *Dalton Trans.*, 2005, 2821-2824.
4. D. M. D'Alessandro and F. R. Keene, *Chem. Soc. Rev.*, 2006, **35**, 424-440.
5. N. J. Brown, H. N. Lancashire, M. A. Fox, D. Collison, R. Edge, D. S. Yufit, J. A. K. Howard, M. W. Whiteley and P. J. Low, *Organometallics*, 2011, **30**, 884-894.
6. K. D. John and M. D. Hopkins, *Chem. Commun.*, 1999, 589-590.
7. J. Manna, S. J. Geib and M. D. Hopkins, *J. Am. Chem. Soc.*, 1992, **114**, 9199-9200.
8. T. P. Pollagi, S. J. Geib and M. D. Hopkins, *J. Am. Chem. Soc.*, 1994, **116**, 6051-6052.
9. S. N. Semenov, S. F. Taghipourian, O. Blacque, T. Fox, K. Venkatesan and H. Berke, *J. Am. Chem. Soc.*, 2010, **132**, 7584-7585.
10. W. Kaim, *Inorg. Chem.*, 2011, **50**, 9752-9765.
11. Kim, J. M. Beebe, C. Olivier, S. Rigaut, D. Touchard, J. G. Kushmerick, X. Y. Zhu and C. D. Frisbie, *J. Phys. Chem. C*, 2007, **111**, 7521-7526.
12. E. A. Osorio, K. O'Neill, M. Wegewijs, N. Stuhr-Hansen, J. Paaske, T. Bjørnholm and H. S. J. van der Zant, *Nano Lett.*, 2007, **7**, 3336-3342.
13. E. A. Osorio, K. Moth-Poulsen, H. S. J. van der Zant, J. Paaske, P. Hedegård, K. Flensberg, J. Bendix and T. Bjørnholm, *Nano Lett.*, 2009, **10**, 105-110.
14. A. S. Blum, T. Ren, D. A. Parish, S. A. Trammell, M. H. Moore, J. G. Kushmerick, G.-L. Xu, J. R. Deschamps, S. K. Pollack and R. Shashidhar, *J. Am. Chem. Soc.*, 2005, **127**, 10010-10011.
15. L. M. Ballesteros, S. Martin, C. Momblona, S. Marques-Gonzalez, M. C. Lopez, R. J. Nichols, P. J. Low and P. Cea, *J. Phys. Chem. C*, 2012, **116**, 9142-9150.
16. M. I. Bruce, P. J. Low, K. Costuas, J. F. Halet, S. P. Best and G. A. Heath, *J. Am. Chem. Soc.*, 2000, **122**, 1949-1962.
17. M. I. Bruce, B. G. Ellis, P. J. Low, B. W. Skelton and A. H. White, *Organometallics*, 2003, **22**, 3184-3198.
18. E. A. Osorio, M. Ruben, J. S. Seldenthuis, J. M. Lehn and H. S. J. van der Zant, *Small*, 2010, **6**, 174-178.
19. D. J. Armitt, M. I. Bruce, M. Gaudio, N. N. Zaitseva, B. W. Skelton, A. H. White, B. Le Guennic, J.-F. Halet, M. A. Fox, R. L. Roberts, F. Hartl and P. J. Low, *Dalton Trans.*, 2008, 6763-6775.
20. M. A. Fox, B. Le Guennic, R. L. Roberts, D. A. Brue, D. S. Yufit, J. A. K. Howard, G. Manca, J.-F. Halet, F. Hartl and P. J. Low, *J. Am. Chem. Soc.*, 2011, **133**, 18433-18446.
21. M. A. Fox, J. D. Farmer, R. L. Roberts, M. G. Humphrey and P. J. Low, *Organometallics*, 2009, **28**, 5266-5269.
22. M. A. Fox, R. L. Roberts, T. E. Baines, B. Le Guennic, J.-F. Halet, F. Hartl, D. S. Yufit, D. Albesa-Jové, J. A. K. Howard and P. J. Low, *J. Am. Chem. Soc.*, 2008, **130**, 3566-3578.
23. J. Maurer, B. Sarkar, B. Schwederski, W. Kaim, R. F. Winter and S. Zalis,

Organometallics, 2006, **25**, 3701-3712.
24. W. Y. Man, J. L. Xia, N. J. Brown, J. D. Farmer, D. S. Yufit, J. A. K. Howard, S. H. Liu and P. J. Low, *Organometallics*, 2011, **30**, 1852-1858.
25. Y. Morisaki and Y. Chujo, *Angew. Chem. Int. Ed.*, 2006, **45**, 6430-6437.
26. Y. Morisaki and Y. Chujo, *Prog. Polym. Sci.*, 2008, **33**, 346-364.
27. W. Wang, J. Xu and Y.-H. Lai, *Org. Lett.*, 2003, **5**, 2765-2768.
28. W. Wang, J. Xu, Y.-H. Lai and F. Wang, *Macromolecules*, 2004, **37**, 3546-3553.
29. W.-L. Wang, J. Xu, Z. Sun, X. Zhang, Y. Lu and Y.-H. Lai, *Macromolecules*, 2006, **39**, 7277-7285.
30. M. Cordes and B. Giese, *Chem. Soc. Rev.*, 2009, **38**, 892-901.
31. G. P. Bartholomew, I. Ledoux, S. Mukamel, G. C. Bazan and J. Zyss, *J. Am. Chem. Soc.*, 2002, **124**, 13480-13485.
32. G. C. Bazan, *J. Org. Chem.*, 2007, **72**, 8615-8635.
33. D. R. Kattnig, B. Mladenova, G. n. Grampp, C. Kaiser, A. Heckmann and C. Lambert, *J. Phys. Chem. C*, 2009, **113**, 2983-2995.
34. S. M. Wu, M. T. Gonzalez, R. Huber, S. Grunder, M. Mayor, C. Schonenberger and M. Calame, *Nat. Nanotech.*, 2008, **3**, 569-574.
35. S. Martín, I. Grace, M. R. Bryce, C. Wang, R. Jitchati, A. S. Batsanov, S. J. Higgins, C. J. Lambert and R. J. Nichols, *J. Am. Chem. Soc.*, 2010, **132**, 9157-9164.
36. W. Wu, Y. Liu and D. Zhu, *Chem. Soc. Rev.*, 2010, **39**, 1489-1502.
37. G. C. Solomon, C. Herrmann, J. Vura-Weis, M. R. Wasielewski and M. A. Ratner, *J. Am. Chem. Soc.*, 2010, **132**, 7887-7889.
38. G. C. Solomon, J. Vura-Weis, C. Herrmann, M. R. Wasielewski and M. A. Ratner, *J. Phys. Chem. B*, 2010, **114**, 14735-14744.
39. P. Mücke, M. Zabel, R. Edge, D. Collison, S. Clément, S. Záliš and R. F. Winter, *J. Organomet. Chem.*, 2011, **696**, 3186-3197.
40. M. E. Stoll, S. R. Lovelace, W. E. Geiger, H. Schimanke, I. Hyla-Kryspin and R. Gleiter, *J. Am. Chem. Soc.*, 1999, **121**, 9343-9351.
41. C. G. Atwood and W. E. Geiger, *J. Am. Chem. Soc.*, 2000, **122**, 5477-5485.
42. J.-L. Xia, C. Zhang, X. Zhu, Y. Ou, G.-J. Jin, G.-a. Yu and S. H. Liu, *New J. Chem.*, 2011, **35**, 97-102.
43. M. R. Torres, A. Vegas, A. Santos and J. Ros, *J. Organomet. Chem.*, 1986, **309**, 169-177.
44. X. H. Wu, S. Jin, J. H. Liang, Z. Y. Li, G.-a. Yu and S. H. Liu, *Organometallics*, 2009, **28**, 2450-2459.
45. M. I. Bruce, *Chem. Rev.*, 1991, **91**, 197-257.
46. A. N. Cammidge, C.-H. Tseng, I. Chambrier, D. L. Hughes and M. J. Cook, *Tetrahedron Lett.*, 2009, **50**, 5254-5256.
47. T. L. Chan, C. D. Poon and T. C. W. Mak, *Acta Crystallogr. C*, 1986, **42**, 897-900.
48. F. H. Allen, O. Kennard, D. G. Watson, L. Brammer, A. G. Orpen and R. Taylor, *J. Chem. Soc., Perkin Trans 2*, 1987, S1-S19.
49. L. D. Field, A. M. Magill, T. K. Shearer, S. B. Colbran, S. T. Lee, S. J. Dalgarno and M. M. Bhadbhade, *Organometallics*, 2010, **29**, 957-965.
50. K. M.-C. Wong, S. C.-F. Lam, C.-C. Ko, N. Zhu, S. Roué, C. Lapinte, S. Fathallah, K. Costuas, S. Kahlal and J.-F. Halet, *Inorg. Chem.*, 2003, **42**, 7086-7097.
51. M. S. Khan, M. R. A. Al-Mandhary, M. K. Al-Suti, F. R. Al-Battashi, S. Al-

Saadi, B. Ahrens, J. K. Bjernemose, M. F. Mahon, P. R. Raithby, M. Younus, N. Chawdhury, A. Kohler, E. A. Marseglia, E. Tedesco, N. Feeder and S. J. Teat, *Dalton Trans.*, 2004, 2377-2385.
52. M. S. Khan, M. K. Al-Suti, M. R. A. Al-Mandhary, B. Ahrens, J. K. Bjernemose, M. F. Mahon, L. Male, P. R. Raithby, R. H. Friend, A. Kohler and J. S. Wilson, *Dalton Trans.*, 2003, 65-73.
53. J. Maurer, R. F. Winter, B. Sarkar, J. Fiedler and S. Zalis, *Chem. Commun.*, 2004, 1900-1901.
54. P. Mücke, M. Linseis, S. Záliš and R. F. Winter, *Inorg. Chim. Acta*, 2011, **374**, 36-50.
55. S. Szafert and J. A. Gladysz, *Chem. Rev.*, 2006, **106**, PR1-PR33.
56. A. Klein, O. Lavastre and J. Fiedler, *Organometallics*, 2005, **25**, 635-643.
57. M. I. Bruce, P. A. Humphrey, G. Melino, B. W. Skelton, A. H. White and N. N. Zaitseva, *Inorg. Chim. Acta*, 2005, **358**, 1453-1468.
58. W. Y. Man, J.-L. Xia, N. J. Brown, J. D. Farmer, D. S. Yufit, J. A. K. Howard, S. H. Liu and P. J. Low, *Organometallics*, 2011, **30**, 1852-1858.
59. N. Ahmad, J. J. Levison, S. D. Robinson and M. F. Uttley, *Inorg. Synth.*, 1974, **15**, 45.
60. M. Krejčik, M. Daněk and F. Hartl, *J. Electroanal. Chem.*, 1991, **317**, 179-187.

Chapter 5. Triarylamine Bridged Dicobaltdicarbon Tetrahedrane Clusters

5.1 Introduction

A cluster can be defined as 'a group of two or more metal atoms in which there are substantial and direct metal bonds between the metal atoms'.[1] In the nineteenth century, there were some fundamental discoveries which led to the development of cluster chemistry. Chief amongst these were the discovery of the $[Re_3Cl_{12}]^{3-}$ anion, Figure 5.1,[2] which led to the first general discussions of the existence of an entire class of metal atom cluster compounds,[3] and the structure determination of $Fe_2(CO)_9$ which led to the exploration of transition metal carbonyl cluster chemistries, Figure 5.2.

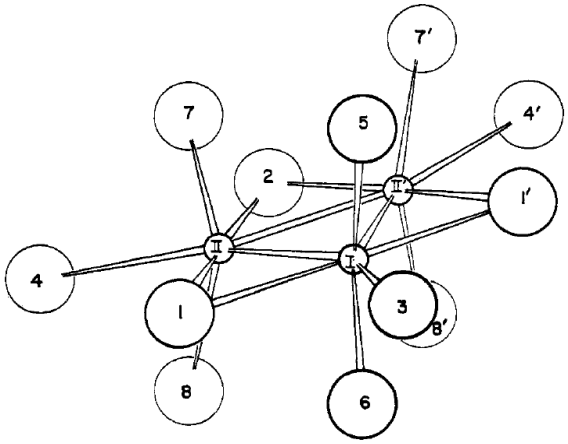

Figure 5.1. The triangular $[Re_3Cl_{12}]^{3-}$ anion.[2]

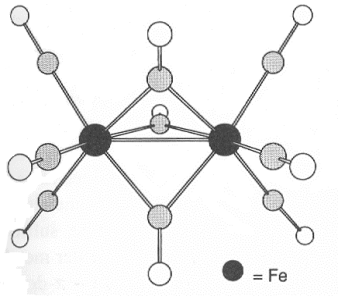

Figure 5.2. Structure of $Fe_2(CO)_9$.[4]

Nowadays, clusters are more widely recognised as 'species in which more than two atomic centres form a polyhedral shape or derivative by addition of removal of one or more vertices'. Even so, there can still be considerable ambiguity in the descriptions of some systems depending on the treatment of non-metal atoms as ligands or cluster vertices. For example, when $Co_2(CO)_8$ is reacted with an alkyne, RC≡CR', the alkyne can be considered to act as a four electron donor and coordinate to the bimetallic Co_2 complex, Figure 5.3a. Alternatively, the alkyne can be considered as having been inserted into a metal-metal bond forming a tetrahedral cluster comprised of two carbon and two cobalt atoms, Figure 5.3b. Of course, such descriptions are only aids to discussion, and both descriptions give a comparable result in terms of the arrangement of atoms.

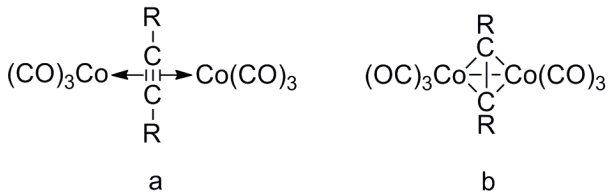

Figure 5.3. Modes of coordination of an alkyne and a metal-metal bond.

Transition metal clusters can adopt a variety of geometries, and the rationalisation of these structures has helped to drive the development and appreciation of molecular orbital descriptions of bonding. In small 'electron-precise' clusters there are a sufficient number of electrons for each atom to form a two-centre two-electron bond and each transition metal obeys the 18 electron rule. Within this localised bonding model, the structure of the cluster can be rationalised by considering the number of valence electrons available for metal-metal bonding and satisfy the 18 electron rule at each metal centre. Each cluster geometry has a characteristic number of vertices (i.e. metal centres) and edges (i.e. metal-metal bonds) and hence the cluster valence electron count associated with the cluster can be readily derived, Table 5.1.

Table 5.1. Characteristic valence counts for selected transition metal clusters.

Cluster cage geometry	Valence electron count
Triangle	48
Tetrahedron	60
Butterfly	62
Square	64
Trigonal bipyramid	72
Square based bipyramid	74
Octahedron	86

However, as the nuclearity of the cluster increases, a more delocalised bonding model may be more appropriate. The Polyhedral Skeletal Electron Pair Theory (PSEPT) and Wade's rules provide a powerful, if somewhat empirical, method for rationalising the geometries of boranes, carboranes and transition metal carbonyl cluster based on what we can now consider as isolobal analogies and simple orbital overlaps.[5] Thus by considering the number of valence electrons provided by each atom, the number of

electrons involved in bonding ligands *exo* to the cluster core and those skeletal electron pairs (SEP) available for cluster bonding, the geometry of a deltahedron can be determined which is consistent with the number of electron pairs and vertices.

For the borane clusters based on B-H vertices:

1. A *closo* cluster has n boron atoms at the corners of a (n) vertex deltahedron and requires (n+1) SEP for cluster bonding
2. A *nido* cluster has n boron atoms at the corners of a (n+1) vertex deltahedron and requires (n+2) SEP for cluster bonding
3. An *arachno* cluster has n boron atoms at the corners of a (n+2) vertex deltahedron and requires (n+3) SEP for cluster bonding
4. A *hypho* cluster has n boron atoms at the corners of a (n+3) vertex deltahedron and requires (n+4) SEP for cluster bonding

In the most common expression of PSEPT, metal clusters are considered to be composed of ML_3 'conical' fragments, derived from an octahedral ML_6 parent. The number of electrons that an ML_3 fragment provides for cluster bonding (x) can be determined according to

$$x = v + n - 12$$

where v = number of valence electrons from a metal atom, n = number of electrons donated by the supporting ligands and 12 is the number of electrons required to populate the metal-ligand *exo* orbital and metal based non-bonding orbitals.

Both models can be satisfactory applied to the problem of the $Co_2(\mu\text{-}RC_2R)(CO)_6$ clusters. Within the localised bonding mode:

2 x Co	= 2 x 9	= 18 electrons
6 x CO	= 6 x 2	= 12 electrons
RC_2R	= 2 x 2	= 4 electrons
Total valence count		= 34 electrons

Two 18 electron fragments require 36 electrons, and hence a single 2 electron metal-metal bond is required to complete the electron count, giving rise to a description consistent with Figure 5.3a.

Alternatively using PSEPT and considering each carbon atom of the alkyne as a vertex, then

2 x Co	= 2 x 9	= 18 electrons
2 x C	= 2 x 4	= 8 electrons
6 x CO	= 6 x 2	= 12 electrons
2 x R	= 2 x 1	= 2 electrons
Total valence count		= 40 electrons

Each Co vertex requires 12 *exo*- and non-bonding electrons, each carbon vertex 2 electrons for bonding to the R group. Hence

$$40 - (2 \times 12) - (2 \times 2) = 12 \text{ skeletal electrons or } 6 \text{ SEPs}$$

Since n = 4, and there are (n + 2) SEPs, then the geometry is based on a *nido* structure. The cluster geometry is based on an (n + 1) vertex deltahedron (i.e. a trigonal bipyramid) with one vertex missing, i.e. a tetrahedron.

The critical point from both models is the implication of overlap of the cobalt and alkyne based orbitals, giving rise to a cluster fragment in which the metal and carbon character is intimately mixed. This delocalisation between the alkyne and metal centres has been recognised in the design of systems in which the Co_2C_2 is conjugated to other parts of a larger molecule or multi-cluster array.[7]

5.1.1 Electronic Interactions Between $Co_2(\mu\text{-}RC_2R')(CO)_6$ Based Moieties

Bimetallic complexes where two metal centres are connected *via* a polyynediyl chain have long been known to be effective in promoting electronic interactions between two redox sites.[6] However, whilst the majority of studies have focused on bis(monometallic) systems, transition metal cluster systems have not been overlooked.[7] The potential of transition metal clusters to undergo multi-electron processes and to act as electron sinks capable of accepting and releasing electrons,[8] as well as allowing the rate of intra- and intermolecular electron transfer to be investigated through redox active handles which are sensitive to the electron density at the cluster core, makes them interesting systems with which to explore electron transfer processes.[9-12]

Dicobalt tetrahedrane clusters of the general form $Co_2(\mu\text{-}RC_2R')(CO)_6$ can be conveniently prepared from the reactions of $Co_2(CO)_8$ and alkynes, RC≡CR' in petroleum solvents at room temperature, and can be readily purified by column chromatography.[13] The 'electron sink' concept is based on the idea of being able to readily add or remove electrons to a cluster core (either by changing the population of non-bonding orbitals, or accommodated through an opening or closing of skeletal bonds) and implies a rich electrochemical response for cluster. However, the electrochemical response of $Co_2(\mu\text{-}RC_2R')(CO)_6$ systems can often be complicated by the strong adsorption on the surface of the electrode and by the short lifetimes of the redox products.[14] For instance, on generation of the radical anion $[Co_2(\mu\text{-}RC_2R')(CO)_6]^{\bullet -}$, one electron diffusion controlled reduction processes are observed, followed by a series of fast chemical reactions which lead to their rapid decomposition.[15, 16] At low temperatures, the electrochemical response is greatly improved, and the electrochemical-chemical-electrochemical (ECE) reactions of the radical anions are quenched. The chemical reversibility of the reduction processes can be enhanced by faster scan rates or with electron withdrawing groups (e.g. CF_3) and bulky substituents (e.g. *t*-Bu) on the alkyne.[17]

From the analysis of a cluster tetrahedral core, Hoffmann and co-workers[18] determined that in the HOMO, a carbon p orbital lies parallel to the Co-Co vector which allows interaction with the highest occupied π-molecular orbital of a phenyl group as illustrated in Figure 5.4.[19] The HOMO can therefore be described as a bonding molecular orbital with considerable metal and ligand character, whilst the LUMO is an anti-bonding molecular orbital of metal-metal character.[20-22] Thus, on generation of the radical anion, an electron is populated into this anti-bonding molecular orbital leading to bond rupture and the loss of fragments such as $[Co(CO)_4]^-$ and $[Co(RC_2R')(CO)_3]$, the former of which can be readily identified as a new oxidative peak in the cyclic voltammogram.[15, 23]

The complexes $Co_2(\mu\text{-}RC_2R')(CO)_6$ have also been studied by electron paramagnetic resonance (EPR). On generation of the radical anion by electrolysis, X-band EPR spectra in THF of the frozen solution (–160 °C), revealed the expected 15 hyperfine lines which are due to the interaction of an unpaired electron with two equivalent ^{59}Co nuclei of spin 7/2. An analysis of the anisotropic *g* and hyperfine couplings reveal that the unpaired electron occupies an orbital which is largely metal and anti-bonding in character, and therefore consistent with Hoffmann's MO analyses.[24] In addition, at –30 to –50 °C, an apparent 8 line spectrum was obtained, arising from the coupling of an unpaired electron to a single cobalt nucleus and further illustrating the cluster fragmentation process which leads to the formation of $[Co(RC_2R)(CO)_3]^{\bullet-}$.[25]

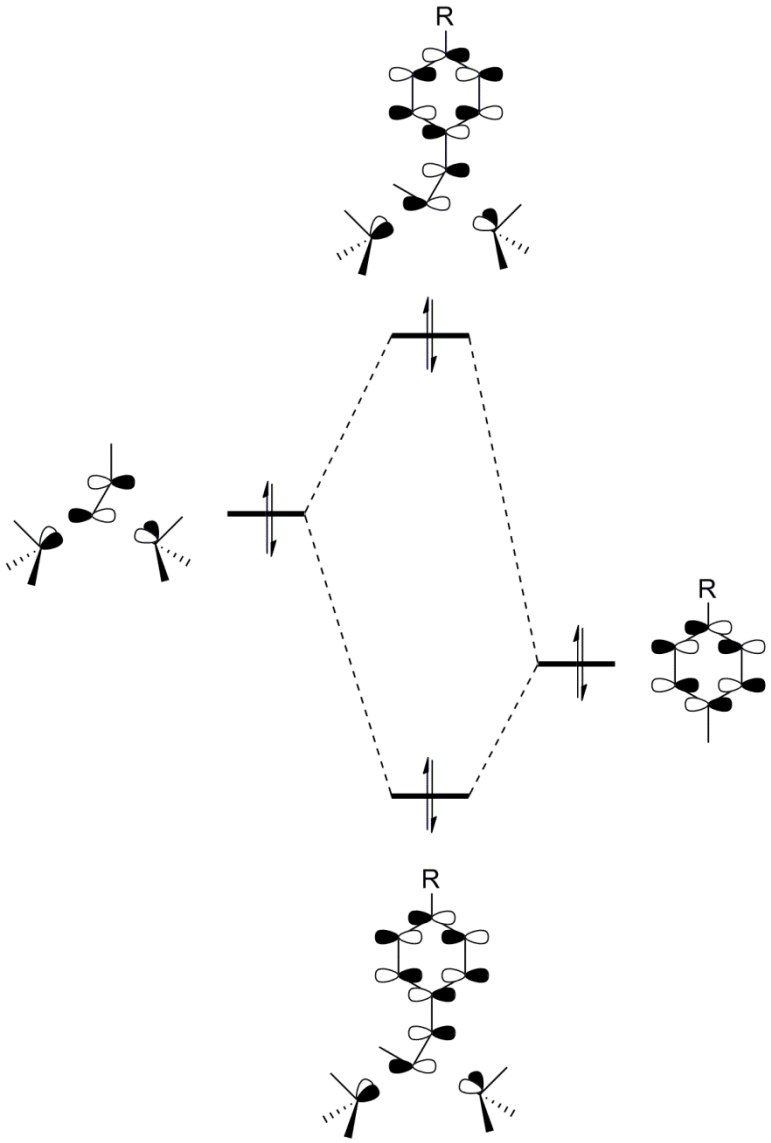

Figure 5.4. π-interactions between the $Co_2(alkyne)(CO)_6$ and aryl fragments.[19]

5.1.2 SNIFTIRS

As discussed earlier, metal carbonyl cluster complexes of the general form $Co_2(\mu\text{-}RC_2R')(CO)_6$ have a tendency to undergo an ECE type electrochemical process. However, in cases where the electrochemical reduction of $Co_2C_2(CO)_6(CF_3)_2$ leads to a stable radical anion $[Co_2C_2(CO)_6(CF_3)_2]^{\bullet-}$, the cluster can become activated towards nucleophilic substitution and becomes a substrate in electron transfer catalysed (ETC) reactions, allowing the production of useful quantities of substituted material *via* an efficient electrochemical method.[20] Using subtractively normalised interfacial Fourier transform infrared spectroscopy (SNIFTIRS), an *in situ* spectroelectrochemical method which involves the bulk electrolysis of a material in a thin layer cell on a timescale which is compatible with a chemical reaction, the short lived intermediates of metal carbonyl anions have been elucidated and identified. For example, as the potential is stepped up from –0.6 to –0.90 V, $Co_3(\mu_3\text{-}CPh)(CO)_9$ is reduced to $[Co_3(\mu_3\text{-}CPh)(CO)_9]^{\bullet-}$. The formation of $[Co_3(\mu_3\text{-}CPh)(CO)_9]^{\bullet-}$ can be correlated with the committal decrease of $Co_3(\mu_3\text{-}CPh)(CO)_9$, as shown by the positive and negative absorption peaks respectively. Importantly, SNIFTIRS can also provide evidence of cluster decomposition, since at –0.90 V a characteristic broads peak appears at 1904 cm^{-1} for $[Co(CO)_4]^-$.[14, 26]

5.1.3 Electronic Interactions in $Co_2(CO)_4(dppm)$

The reaction of $Co_2(\mu\text{-}RC_2R')(CO)_6$ with phosphite and phosphine ligands allows the tuning of the cluster centre by controlling the electron density at the cobalt metal centre, which, importantly leads to complexes of increasing stability, with simplified electronic responses.[27] For example, chemical and electrochemical reversibility can be achieved through the coordination of four phosphite ligands to the cluster centre, or through a bidentate ligand such as dppm, with the equivalent loss of four and two carbonyl ligands respectively. The increased electron density at the cluster core has the effect of stabilising the Co-Co bond, preventing cluster fragmentation and also converts a redox centre which is irreversibly reducible to a readily oxidisable centre.

Following initial studies by Osella and co-workers, who investigated the electronic communication in $[\{Co_2(CO)_6\}_2(\mu\text{-diyne})]$ and $[\{Co_2(CO)_4(dppm)\}_2(\mu\text{-diyne})]$ complexes,[28] the Otago group have demonstrated that the complex $[Ph_2C_2Co_2(CO)_4(dppm)(C_2Co_2(CO)_4(dppm)Ph]$ (**23**) exhibits two reversible oxidation waves, where $\Delta E_{1/2}$ = 448 mV was taken as being indicative of effective communication between the cluster sites.[27] The interpolation of other π-conjugated moieties for example, 2,4- (**24**) and 2,5-bis(trimethylsilyl)ethynyl)thiopene (**25**) and 2,6-pyridiyl acetylene motifs (**25**), Figure 5.5 leads to less strongly coupled ($\Delta E_{1/2}$ = 200 mV), moderately coupled ($\Delta E_{1/2}$ = 100 mV), and decoupled ($\Delta E_{1/2}$ = 80 mV), systems respectively.[29-31] However, as described in Chapter 1, $\Delta E_{1/2}$ is sensitive to a number of a factors, and whilst the addition of a spacer effect might genuinely have the effect of decreasing the electronic communication between cluster complexes of this type, it is

difficult to ascertain whether this is due to the spacer or structural effects and the role other factors might also play.[32, 33]

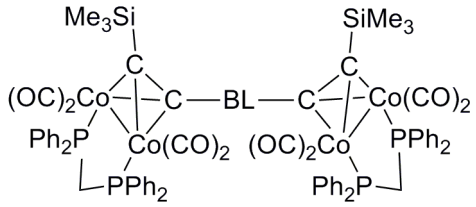

BL = 2,4-thiopene (**24**)
2,5-thiopene (**25**)
2,6-pyridine (**26**)

Figure 5.5. General structure of bis(cluster) bridged assemblies.

In other studies, the complexes [{$Co_2(CO)_4$(dppm)}$_2$(μ-$Me_3SiC_2CB_{10}H_{10}CC_2SiMe_3$)] (**27**), [{$Me_3SiC_2Co_2(CO)_4$(dppm)}$_2$(μ-$C_6H_4$)] (**28**) and [{$Me_3SiC_2Co_2(CO)_4$(dppm)}$_2$(μ-C≡CC≡C)] (**29**) were studied under identical electrochemical conditions, Figure 5.6. With likely comparable ion-pairing and solvation effects, and the large through space separation which could minimise electrostatic contributions, variations in ΔE may also reflect underlying differences in cluster-cluster interactions. Given that the cluster moieties in **27** are separated by 6 Å, the two oxidation and two reduction processes, which are separated by 100 mV and 80 mV respectively, are indicative of a moderate through bond interaction, the pathway through the occupied orbitals apparently being modestly more efficient. Likewise, the electrochemical response of **28** is similar (ΔE_{ox} = 110 mV; ΔE_{red} = 80 mV), whilst electrochemical analysis in **29** was complicated by the chemical irreversibility of the redox products which meant $\Delta E_{1/2}$ could not ambiguously resolved. DFT studies reveal the *para*-carborane cage to act like a σ-bridging entity due to the energy mismatch of the carborane and the π-orbitals of the ethynyl group, whilst the role of the bridge is more significant in **28** and even more so in **29**.[34, 35]

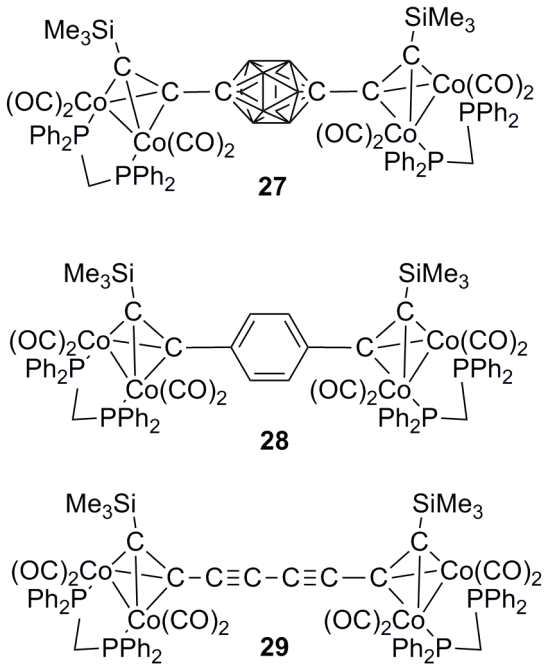

Figure 5.6. Complexes studied by Low and co-workers under identical electrochemical conditions.

In seeking to examine the nature of the electronic interactions within a complex, Carty and co-workers synthesised heterometallic complexes featuring a cobalt cluster moiety and a ruthenium fragment; $Co_2\{\mu\text{-}Me_3SiC{\equiv}CC_2C{\equiv}C[Ru(PPh_3)_2Cp]\}(CO)_4(dppm)$ (**30**) and $Co_2\{\mu\text{-}Me_3SiC_2C{\equiv}CC{\equiv}C[Ru(PPh_3)_2Cp]\}(CO)_4(dppm)$ (**31**), Figure 5.7.[36] The parent complexes $Co_2(\mu\text{-}Me_3SiC{\equiv}CC_2C{\equiv}CSiMe_3)(CO)_4(dppm)$ (**32**) and $Co_2(\mu\text{-}Me_3SiC_2C{\equiv}CC{\equiv}CSiMe_3)(CO)_4(dppm)$ (**33**), were each characterised by a single, reversible one electron oxidation and a single, reversible one electron reduction, corresponding to the formation of the radical cations $[\mathbf{32}]^{\bullet+}$ (E_{ox} = 1.49 V) and $[\mathbf{33}]^{\bullet+}$ (E_{ox} = 1.60 V) and the radical anions $[\mathbf{32}]^{\bullet-}$ (E_{red} = –1.09 V) and $[\mathbf{33}]^{\bullet-}$ (E_{red} = –1.06 V). Electrochemical analysis of **30** and **31** reveal the presence of a single reversible one electron reduction wave (**30** = –1.29 V, **31** = –1.36 V) as well as two quasi-reversible oxidation processes (**30** E_{ox} = 0.96, 1.16 V, **31** E_{red} = 0.86, 1.14 V).

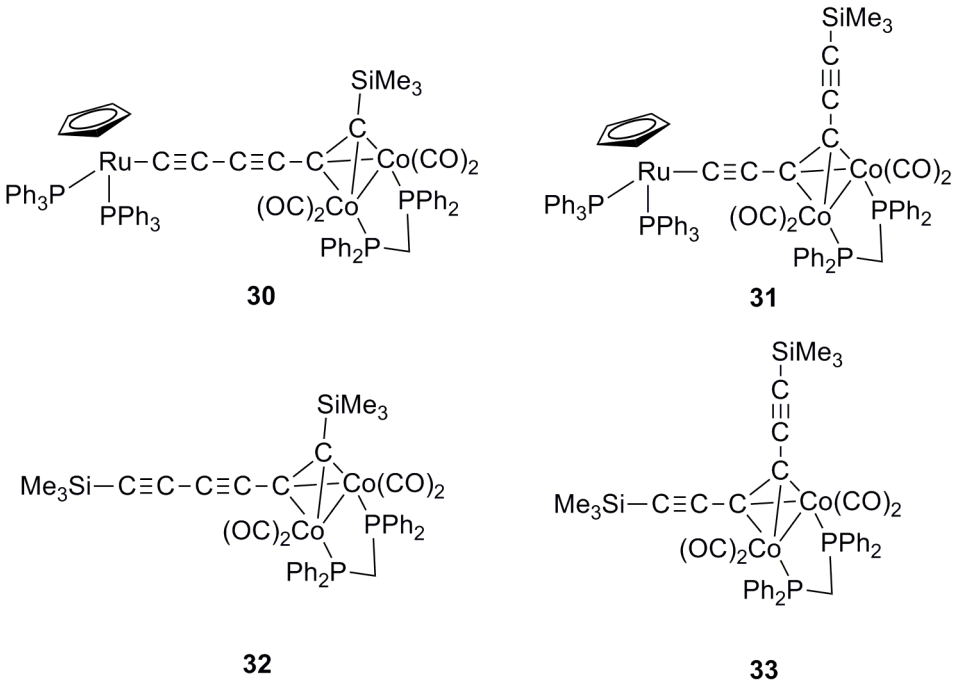

Figure 5.7. Compounds 30 – 33.

Given that there are clearly interactions between the Ru and Co_2C_2 moieties in **30** and **31** (the E values for the $Ru^{II/III}$ and $[Co_2C_2]^{0/+1}$ are not the same as the parent complexes), which are not operating through a simple through space mechanism (in which case the first oxidation would result in a second less thermodynamically favourable oxidation event when compared to the isolated parent species due to additional Coulombic repulsion), then a through bond mechanism must account for the presence of two, one electron oxidation processes. The fact that both of these oxidation processes are more favourable than the nature of the electronic interactions in the organometallic fragments indicates a mixing of the electronic character of the orbital, with DFT studies revealing that the HOMO includes a significant contribution from the ruthenium fragment, acetylenic moiety and the cobalt cluster core. Thus the nature of the electronic interactions cannot be ascribed to a simple donor-acceptor effect.

Given the sensitivity of ν(C≡O) frequencies to electron density and the fast time scale of the IR experiment, IR spectroelectrochemistry provides an extraordinarily useful tool through which to assess details of electron transfer and electronic interactions.[37-41] For example, in **23** the $\Delta E_{1/2}$ of 448 mV led to a large K_c value of 4 x 10^7 and warranted investigations to ascertain the nature of the electrochemically generated species. Thus, stepwise oxidation to its mono- and dication led to changes in ν(C≡O) of approximately 27 cm^{-1} each time, whereas on oxidation of [{$PhC_2Co_2(CO)_4$(dppm)}(μ-C≡C-Ph)] (**34**) a shift in ν(C≡O) of 52 cm^{-1} is observed. If the Co_2C_2 moieties in the bis(bimetallic) cluster were localised, then the MV state should exhibit two bands, one corresponding to the mono-oxidised state, with the other in its ground state, whereas if they were delocalised on the IR timescale then a ν(C≡O) band at an averaged frequency would be expected. Intermediate scenarios can lead to intermediate ν(C≡O) shifts in the simplest interpretation.[40, 42] Thus, in **23** the two cluster moieties give rise to a monocation in which the cluster centres are in identical environments and are therefore delocalised on the IR timescale.[27]

5.1.4 Towards Interactions Between More than Two Sites: the Triarylamine Motif as a Bridging Ligand

The triarylamine core has long been employed in optoelectronics, for example, as a hole-transport material in light emitting devices and field effect transistors, attributed to the ability of this species to undergo one electron oxidation, and to transport charge *via* the radical cation with high stability.[43] Furthermore, the chemical and thermodynamic stability of triarylamine based radical cations can be tuned through electronic and steric effects by the variation of substituents on the aryl groups, so that extensive materials chemistry applications can be envisioned.[44-46] In addition, the starburst propeller structure of the triarylamine moiety has also attracted attention for its ability to promote electronic interactions between up to three remote sites through a central nitrogen atom. For example Onitsuka and co-workers reported a trinuclear ruthenium acetylide complex attached to a triarylamine core which exhibited four well resolved oxidations. On addition of one equivalent of a chemical oxidant, an IVCT band developed in the NIR region; together, these results were interpreted in terms of evidence of electronic interactions.[47] As a result, this has led to the synthesis of some ruthenium dendrimers attached to an amine core, through a convergent method.[48] An analysis of these molecules shows that they exhibit promise for their non-linear optical behaviour;[49-51] the reversible redox processes in metals also offering the possibility of switching the molecular nonlinearity.[52-54]

In this Chapter, we shall explore Co_2C_2 clusters linked by a redox active triarylamine group. The synthesis, structures, electrochemical and spectroelectrochemical response of the complexes $[\{Co_2(CO)_4(dppm)\}\{\mu\text{-}(Me_3SiC_2\text{-}4\text{-}C_6H_4)N(C_6H_4Me\text{-}4)_2\}]$ (**39a**), $[\{Co_2(CO)_4(dppm)\}_2\{\mu\text{-}(Me_3SiC_2\text{-}4\text{-}C_6H_4)_2N(C_6H_4Me\text{-}4)\}]$ (**40b**) and $[\{Co_2(CO)_4(dppm)\}_3\{\mu\text{-}Me_3SiC_2\text{-}4\text{-}C_6H_4)_3N]$ (**41c**) are reported. The experimental results support a description of $[\mathbf{40b}]^{n+}$ and $[\mathbf{41c}]^{n+}$ in terms of a localised electronic structure, with the radical confined to a single cluster redox centre in the case of n = 1.

5.2 Synthesis

The thermal reaction of $Co_2(CO)_6$(dppm) (**35**) with an alkyne gives complexes of the general form $Co_2(\mu\text{-}RC_2R')$(dppm). Compound **35** can be synthesised from the room temperature reaction of $Co_2(CO)_8$ and one equivalent of dppm in benzene, followed by chromatographic purification and crystallisation.[55] However, when the reaction is carried out in toluene, compound **35** precipitates directly from the reaction mixture as a high purity powder, in an essentially quantitative yield. The mono- and di-substituted tertiary amines $N(C_6H_4Br\text{-}4)(C_6H_4Me\text{-}4)_2$ (**36**) and $N(C_6H_4Br\text{-}4)_2(C_6H_4Me\text{-}4)$ (**37**) were prepared from di(tolyl)amine and *para*-toluidene respectively by Hartwig-Buchwald reactions, Scheme 5.1.[56, 57] The tri-substituted tertiary amine $N(C_6H_4Br\text{-}4)_3$ (**38**) was prepared by a bromination reaction.[58] Compounds **36** and **38** were synthesised and kindly donated by Mr Kevin Vincent and Dr Phil Schauer respectively, of Durham University.

The ligand building block 4,4'-dimethyldiphenylamine $NH(C_6H_4Me\text{-}4)_2$ is available commercially, however, it can also be prepared from the arylation reactions of *para*-toluidene with 4-chloro-,[59-63] bromo-,[64] or iodotoluene.[65] Using a Hartwig-Buchwald based methodology, 4-iodotoluene was cross-coupled with *para*-toluidene using the readily available palladium source $Pd_2(dba)_3$, supporting phosphine (dppf) and base (NaO^tBu) in toluene. Under these conditions 4,4'-dimethyldiphenylamine was obtained in good yields after purification. Similarly, the iodo moiety in 1-bromo-4-iodobenzene was selectively coupled to 4,4'-dimethyldiphenylamine and *para*-toluidene to afford **36** **37** respectively. The application of the $Pd_2(dba)_3$ / dppf / NaO^tBu system is thus a simple protocol, presenting advantages to an Ullmann reaction, which require harsh

reaction conditions and can give unrelible yields. Compound **38** was synthesised *via* a bromination reaction of triphenylamine in chloroform at 0 °C. The reaction of **36**, **37** and **38** with trimethylsilyacetylene under standard Sonogashira reactions gave the alkynes **39**, **40** and **41** respectively, Scheme 5.1.[66]

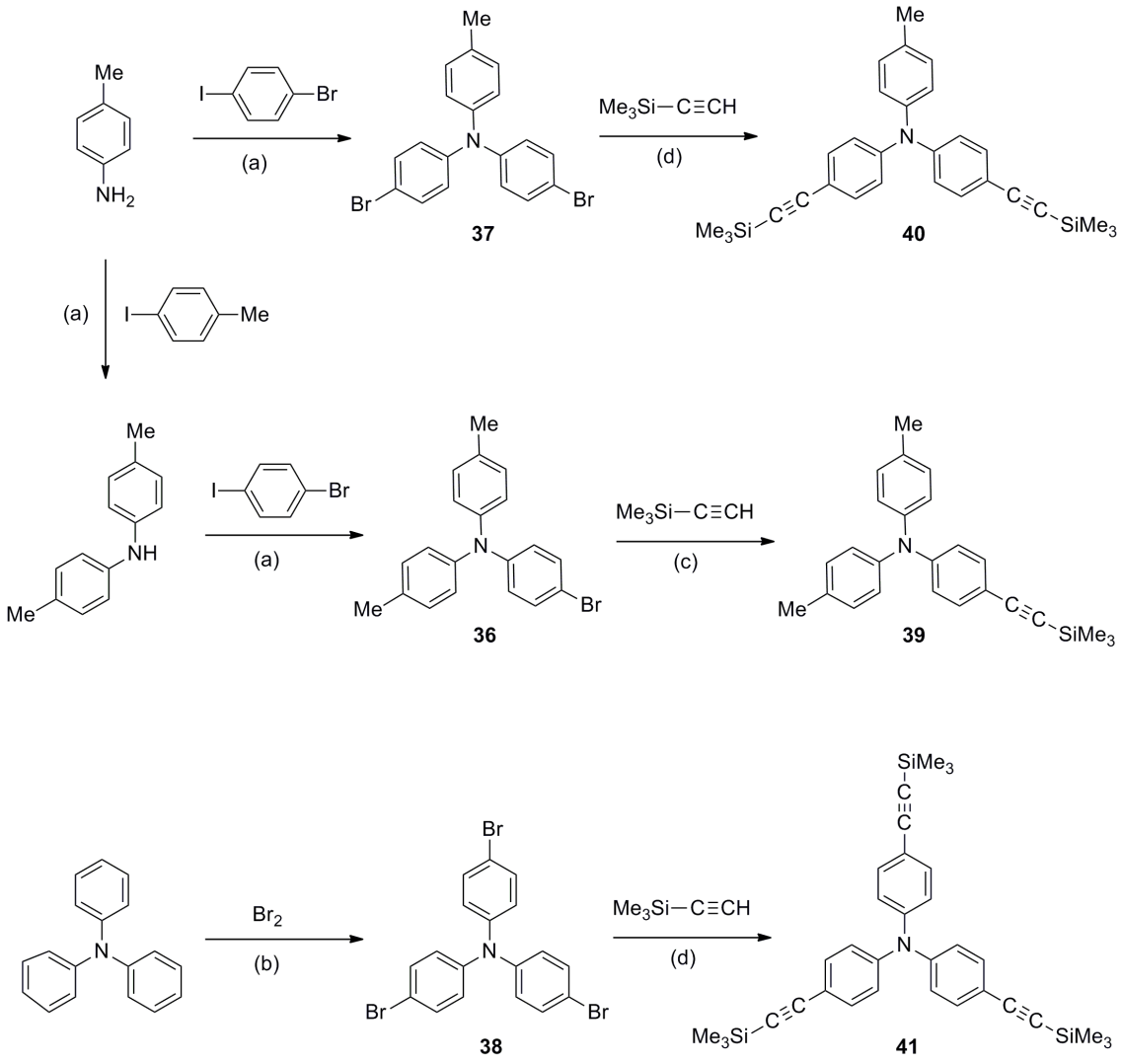

Scheme 5.1. Preparation of the ligands 39, 40 and 41. Conditions: (a) $Pd_2(dba)_3$ / dppf / NaO^tBu / toluene / reflux; (b) Br_2, $CHCl_3$, 0 °C; (c) $PdCl_2(PPh_3)_2$ / CuI / NEt_3 / reflux; (d) $Pd(PPh_3)_4$ / CuI / NEt_3 / reflux.

Subsequent reaction of compound **35** with the alkynes **39**, **40** and **41** gave the anticipated Co_2C_2 clusters with pendant (**39a**, **40a**, **41a**) or bridging (**40b**, **41b**, **41c**) triarylamine groups, Schemes 5.2 – 5.3.

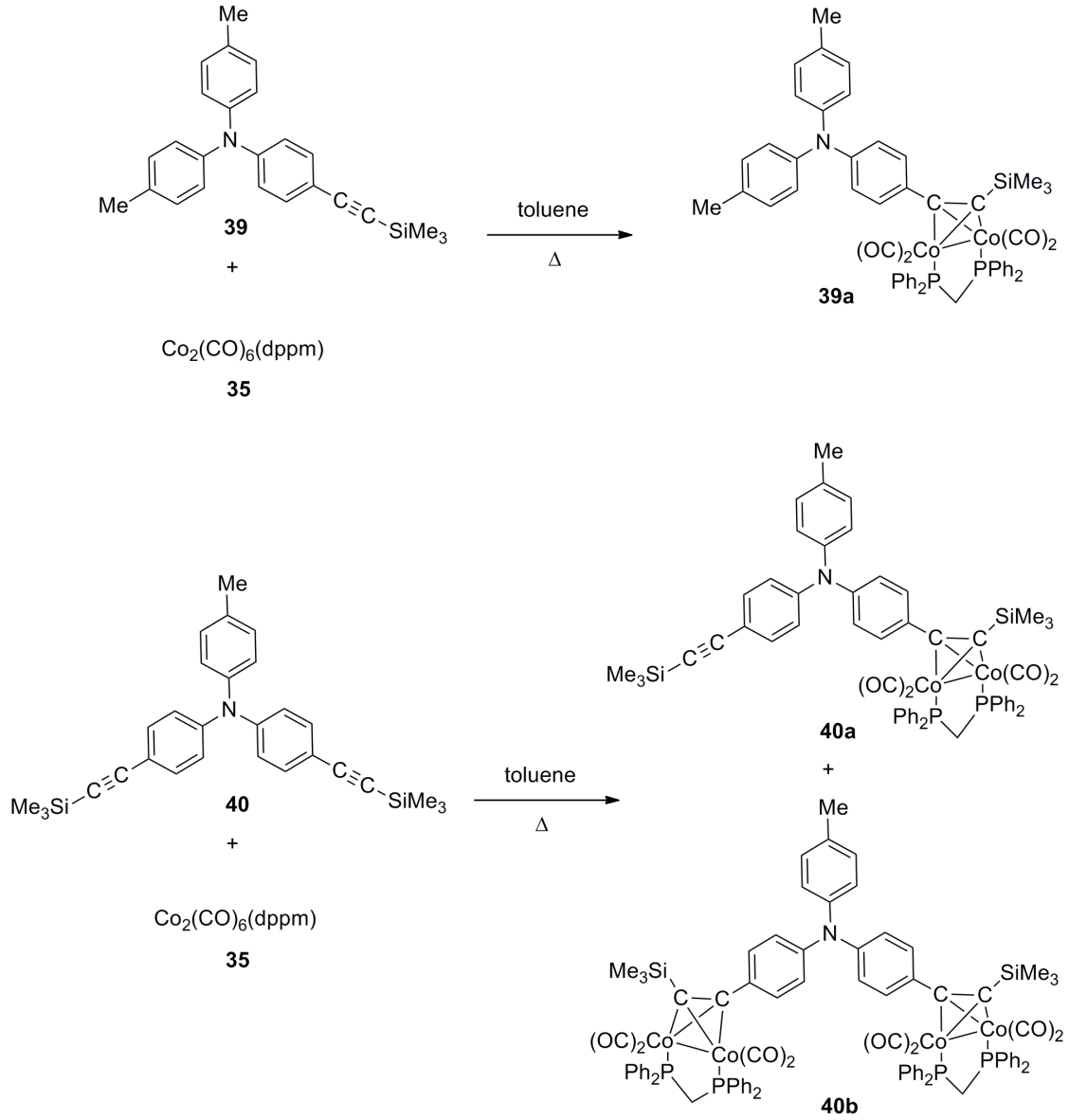

Scheme 5.2. The preparation of 39a, 40a and 40b.

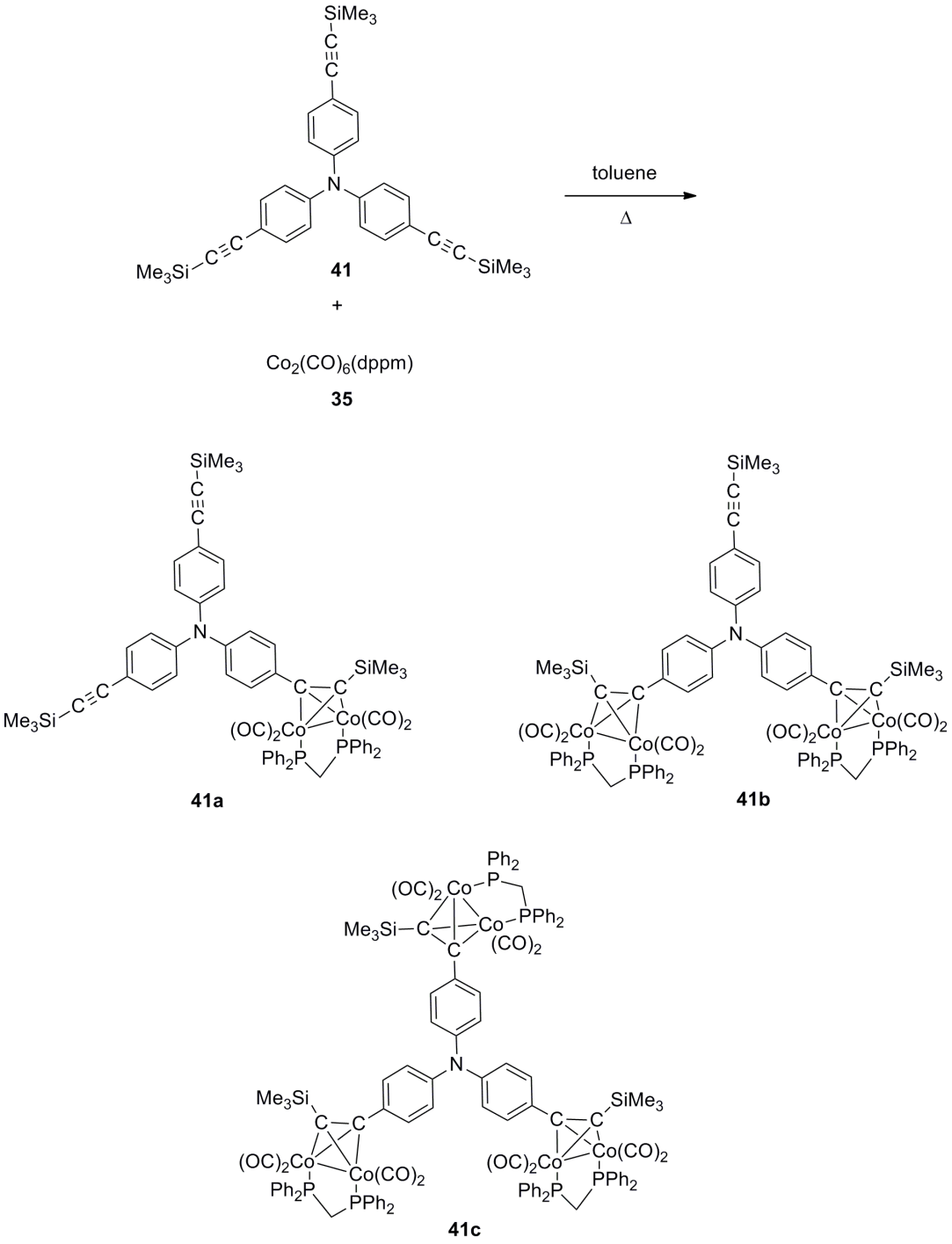

Scheme 5.3. The preparation of 41a, 41b and 41c.

5.2.1 Spectroscopic Investigations

The complexes **39a**, **40a**, **40b**, **41a**, **41b** and **41c** were characterised by a variety of techniques including elemental analyses, MALDI(+)-MS, ^{1}H, ^{31}P, ^{13}C NMR and IR spectroscopy. The identities of **39a**, **40a** – **40b**, **41a** – **41c** were confirmed by elemental analyses. Mass spectra obtained using MALDI methods display extensive fragmentation, with $[M–4CO]^+$ (**39a**, **40a**, **41a**), $[M–4CO–\{Co_2(CO)_4(dppm)\}]^+$ (**40b**, **41b**) and in the case of **41c** $[M–4CO–\{Co_2(CO)_4(dppm)\}_2]^+$ ions being predominant. The IR and NMR data indicate the electronic environment to be similar across the entire series. In ^{31}P NMR spectroscopy, the dppm ligands give rise to singlets δ_P ~ 31 ppm. In ^{13}C NMR spectroscopy, the carbon nuclei of the cluster cores in all complexes are identified as triplets (J_{CP} = ca. 9 Hz) δ_C ~ 89 and 106 ppm, in addition, the alkynyl carbons in **41a** and **41b** are represented as singlets δ_C ~ 93 and 105 ppm. The carbon nuclei of the phenyl rings on the dppm ligands are identified as pseudo triplets, with the magnitude of the J coupling dependent on the distance to the phosphorus nuclei; the carbon in the *para* position was often observed as an unresolved multiplet or a broad singlet. Each phenyl ring on a single phosphorus atom is identified, with the second set of PPh_2 identical to the first. The CO ligands give resonances δ_C ~ 203 and 207 ppm.

The IR ν(C≡O) spectra of **39a**, **40a** and **40b** are essentially identical, Figure 5.8 with an additional ν(C≡C) evident in the spectra of **40a**, Table 5.2. When compared to related systems for example $Co_2(\mu\text{-}HC_2Ph)(CO)_4(dppm)$ (ν(C≡O) 2027vs, 1999s, 1975s, 1956w cm^{-1}) and $Co_2(\mu\text{-}HC_2C_6H_4NMe_2)(CO)_4(dppm)$ (ν(C≡O) 2023vs, 1995s, 1971s, 1952w cm^{-1}),[19] there is a shift to lower wavenumbers, attributed to the influence of the relatively strong electron donating triarylamine group on the cluster core. Similarly, the IR spectra of **41a** – **41c** are essentially identical, with an additional ν(C≡C) band evident in the spectra of **41a** and **41b**, Table 5.2. On replacement of one or two tolyl groups with an electron withdrawing trimethylsilylethynyl phenylene group, a shift to higher energy is observed due to a decrease in electron density available for π-backbonding at the cobalt centre.

Table 5.2. ν(C≡O) / cm^{-1} in CH_2Cl_2.

Complex	ν(C≡O) / cm^{-1}
39a	2017m, 1989s, 1961m, 1942w
40a	2016m, 1988s, 1961m, 1941w
40b	2016m, 1989s, 1960m, 1942w
41a	2045w, 2018m, 1991s, 1962m, 1942sh
41b	2046w, 2018m, 1990s, 1962m, 1942sh
41c	2045w, 2017m, 1990s, 1962m, 1942sh

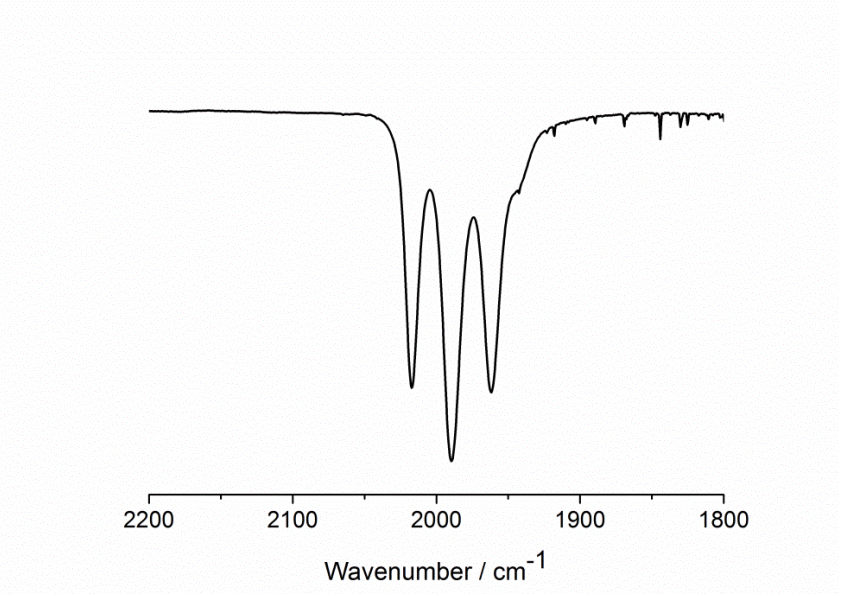

Figure 5.8. The IR ν(C≡O) of 39a in CH_2Cl_2.

5.3 Molecular Structures

X-ray quality crystals of complex **39a**, **40a**, **40b**, **41a** and **41b** were grown from the slow diffusion of methanol into CH_2Cl_2 solutions of the complexes. The molecular structures of **39a** (Figure 5.9), **40a** (Figure 5.10), **40b** (Figure 5.11), **41a** (Figure 5.12), **41b** (Figure 5.13) were determined by single crystal X-ray diffraction by Dr D.S. Yufit, at Durham University (U.K). Crystallographic data, selected bond lengths and torsion angles are listed in Tables 5.3 and 5.4 respectively.

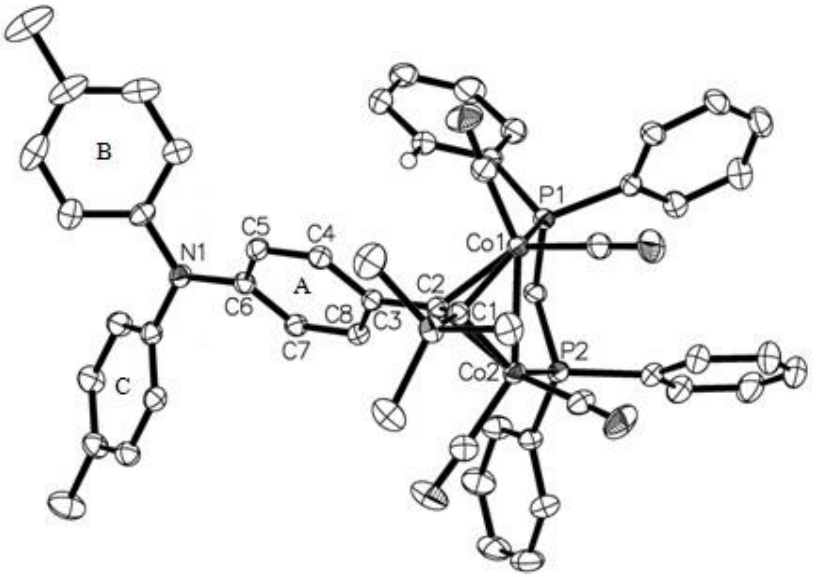

Figure 5.9. The molecular structure of 39a, showing the atom labeling scheme. Hydrogen atoms have been omitted for clarity.

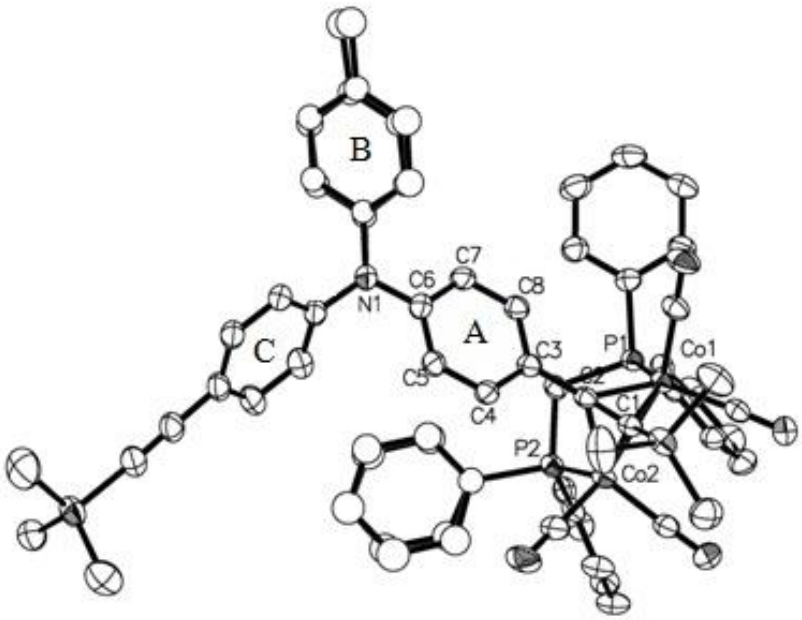

Figure 5.10. The molecular structure of 40a, showing the atom labeling scheme.

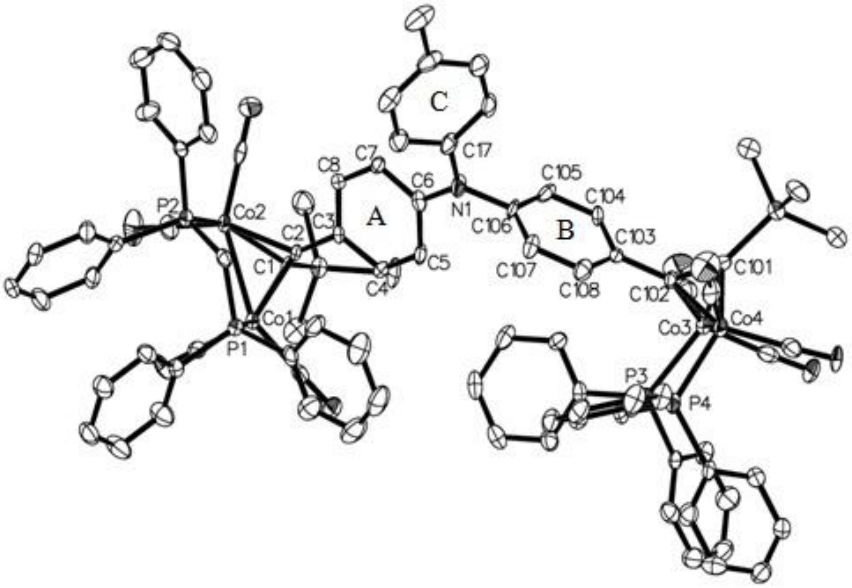

Figure 5.11. The molecular structure of 40b, showing the atom labeling scheme.

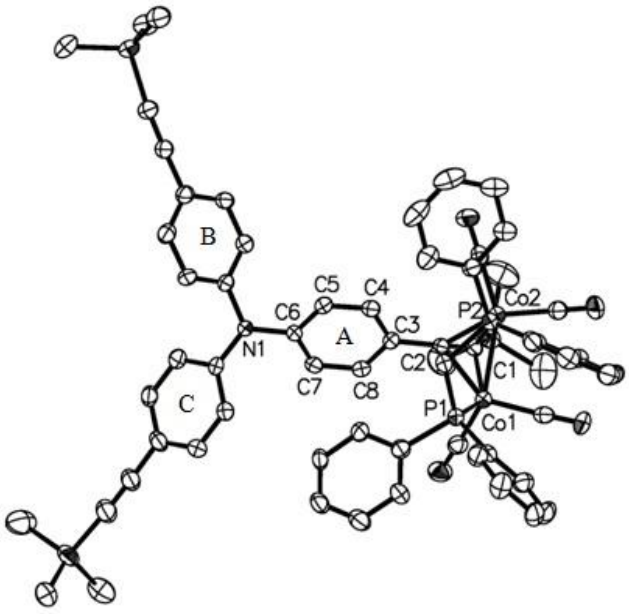

Figure 5.12. Molecular structure of 41a, showing the atom labeling scheme.

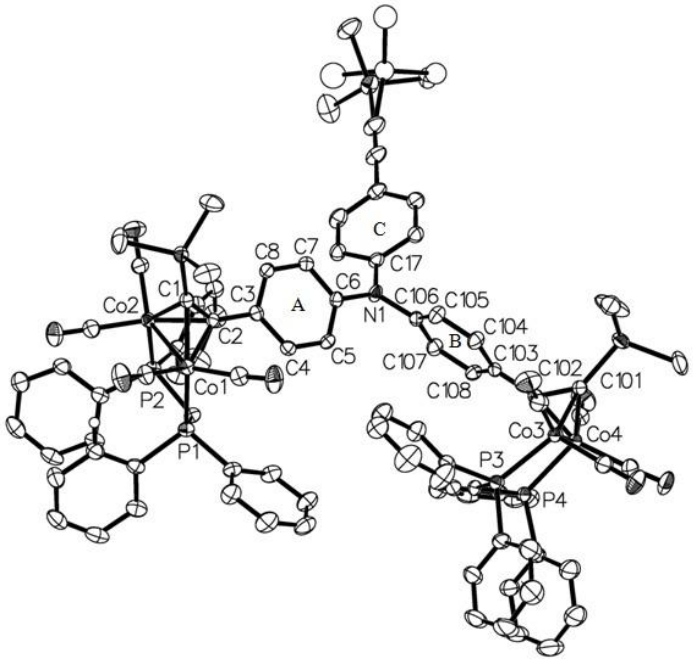

Figure 5.13. Molecular structure of 41b, showing the atom labeling scheme.

Table 5.3. Crystal data and structure refinement for complex 39a, 40a, 40b, 40a and 40b.

Complex	**39a**	**40a**	**40b**	**41a**	**41b**
Empirical formula	$C_{54}H_{49}Co_2NO_4P_2Si$ x CH_2Cl_2	$C_{58}H_{55}Co_2NO_4P_2Si_2$ x CH_2Cl_2	$C_{87}H_{77}NO_8Si_2P_4Co_4$	$C_{62}H_{61}Co_2NO_4P_2Si_3$ x $0.25CH_2Cl_2$	$C_{91}H_{83}Co_4NO_8P_4Si_3$ x $2CH_2Cl_2$
Formula weight (g mol^{-1})	1068.76	1150.94	1680.28	1169.42	1932.31
Temperature (K)	120	120	100	100.15	-153
Crystal system	triclinic	triclinic	triclinic	monoclinic	triclinic
Space group	P-1	P-1	P-1	$P2_1/n$	P-1
a (Å)	10.0519(2)	13.4179(3)	12.5714(5)	23.0894(6)	12.2872(5)
b (Å)	15.3922(3)	14.6648(3)	14.0341(6)	19.6044(5)	18.5165(7)
c (Å)	18.525247(4)	15.7740(4)	24.9132(10)	26.6193(8)	21.1086(8)
α (°)	72.071(10)	75.9950(10)	101.688(2)	90.00	105.8590(10)
β (°)	79.906(10)	72.6230(10)	100.653(2)	95.3830(10)	92.5980(10)
γ (°)	83.068(10)	83.1210(10)	102.245(2)	90.00	91.1120(10)
Volume ($Å^3$)	2677.94(9)	2870.37(11)	4085.4(3)	11996.2(6)	4612.5(3)
Z	2	2	2	8	2
ρ_{calc} (mg/mm^3)	1.325	1.332	1.366	1.295	1.391
μ (mm^{-1})	0.845	0.814	7.712	5.976	0.985
F(000)	1104	1192	1732	4868	1988
Reflections collected	50506	47964	14939	58821	71476
Independent reflections, R_{int}	14880, 0.0357	15262, 0.0374	9317, 0.0368	16973, 0.0568	22235, 0.0388
Data/restraints/ parameters	14880/0/604	15262/0/609	9317/0/866	16973/6/1377	22235/3/1094

Goodness-of-fit on F^2	1.047	1.061	1.050	1.014	1.047
Final R_1 indexes [$I \geq 2\sigma$ (I)]	0.0432	0.0585	0.0532	0.0534	0.0476
Final wR_2 indexes [all data]	0.1307	0.1707	0.148	0.1569	0.1447

Table 5.4. Selected bond lengths and bond angles.

Complex	**39a**	**40a**	**40b**	**41a**	**41b**
Bond lengths / Å					
Co(1)-Co(2)	2.4884(5)	2.4821(5)	2.4853(10)	2.4742(8)	2.4895(5)
Co(1)-P(1)	2.2211(5)	2.2036(8)	2.2244(14)	2.2211(11)	2.2072(8)
Co(2)-P(2)	2.2161(6)	2.2130(8)	2.1995(14)	2.1989(12)	2.2243(8)
Co(1)-C(1)	1.9674(19)	1.975(3)	1.976(5)	1.979(4)	1.984(3)
Co(1)-C(2)	1.9924(18)	1.944(3)	1.973(4)	1.986(3)	1.944(3)
Co(2)-C(1)	2.9835(18)	1.972(3)	1.976(4)	1.993(4)	1.968(3)
Co(2)-C(2)	1.9617(18)	1.989(3)	1.966(4)	1.958(3)	1.986(3)
C(1)-C(2)	1.350(2)	1.351(4)	1.351(6)	1.347(5)	1.353(4)
C(2)-C(3)	1.465(2)	1.475(4)	1.461(6)	1.461(5)	1.466(4)
C(3)-C(4)	1.404(2)	1.399(4)	1.405(6)	1.396(5)	1.397(4)
C(4)-C(5)	1.383(2)	1.387(4)	1.383(6)	1.378(5)	1.387(4)
C(5)-C(6)	1.401(3)	1.398(4)	1.402(6)	1.389(5)	1.397(4)
C(6)-C(7)	1.395(3)	1.391(4)	1.390(7)	1.393(5)	1.400(4)
C(7)-C(8)	1.389(2)	1.393(4)	1.387(6)	1.381(5)	1.374(4)

C(8)-C(3)	1.399(2)	1.396(4)	1.398(6)	1.399(5)	1.402(4)
N(1)-C(A)	1.419(2)	1.413(4)	1.405(6)	1.426(5)	1.408 (3)
N(1)-C(B)	1.423(2)	1.3850(5), 1.500(5)	1.439(6)	1.427(4)	1.433(3)
N(1)-C(C)	1.431(2)	1.414(4)	1.430(6)	1.410(5)	1.413(3)
Co(3)-Co(4)	-	-	2.4933(10)	-	2.4819(6)
Co(3)-P(3)	-	-	2.2182(14)	-	2.2205(8)
Co(4)-P(4)	-	-	2.2136(15)	-	2.4819(6)
Co(3)-C(101)	-	-	1.981(5)	-	2.2205(8)
Co(3)-C(102)	-	-	1.985(4)	-	2.2111(8)
Co(4)-C(101)	-	-	2.000(5)	-	1.966(3)
Co(4)-C(102)	-	-	1.964(5)	-	1.976(3)
C(101)-C(102)	-	-	1.353(6)	-	1.353(4)
C(102)-C(103)	-	-	1.468(6)	-	1.961(3)
C(103)-C(104)	-	-	1.407(7)	-	1.473(4)
C(104)-C(105)	-	-	1.376(6)	-	1.395(4)
C(105)-C(106)	-	-	1.390(7)	-	1.389(4)
C(106)-C(107)	-	-	1.392(7)	-	1.383(4)
C(107)-C(108)	-	-	1.401(7)	-	1.394(4)
C(108)-C(103)	-	-	1.376(6)	-	1.395(4)
Bond angles / °					
C(A)-N(1)-C(B)	120.51(15)	-118.7(3)	-118.9(4)	-119.2(3)	-119.7(2)
C(A)-N(1)-C(C)	119.79(15)	-119.8(3)	-122.1(4)	-119.4(3)	-121.1(2)
C(B)-N(1)-C(C)	119.55(15)	-121.3(3)	-118.7(4)	-120.1(3)	-119.0(2)

In complexes **39a**, **40a** – **40b, 41a – 41c**, the triarylamine moieties exhibit a planar environment at N(1), with the aryl rings in a propeller arrangement. The geometry of the cluster core is tetrahedral, with a pseudo octahedral environment about each cobalt metal centre. The dppm ligands are disposed so as to minimise the steric interactions with the $SiMe_3$ groups. The N(1) – C(A) bond lengths fall in the same range within this series of complexes between 1.4056(6) and 1.426(5) Å, whilst in **40b** and **41b** the N(1) – C(B) bond lengths attached to the second cluster moiety are also comparable at 1.439(6) and 1.433(3) Å respectively. Within the phenylene rings, the C(3) – C(8) bond lengths are similar within experimental error, and display no significant quionoidal distortions. In comparison to literature compounds, the bond lengths in the Co_2C_2 tetrahedrane cluster core the Co(1, 3) – Co(2, 4) span a narrow range (2.4742(8) - 2.4993(10) Å) whilst the C(1) – C(2) and C(101) – C(102) (**40b**, **41b**) distances are identical (**39a** 1.350(2) ; **40a** 1.351(6) ; **41b** 1.351(6), 1.353(6) ; **41a** 1.347(5) ; **41b** 1.353(4), 1.353(4) Å) and are similar to those found in $Co_2(\mu\text{-}HC_2Ph)(CO)_4$(dppm), (Co-Co 2.4873(3) Å; C-C 1.348(2) Å).[19] Thus from the structural data, there is no evidence for substantial ground state delocalisation between the cluster core and the pendant amine nitrogen centre in **39a**, **40a**, **41a** and the similarity of the bond parameters between the mono-cluster compounds and the analogous parameters in **40b** and **41b** is not in support of extended conjugation in the bis(cluster) systems.

5.4 Electrochemistry

The ethynyl substituted triarylamines **39** – **41** exhibited a single, electrochemically reversible oxidation wave in 0.1 M NBu_4PF_6 / CH_2Cl_2 at a platinum working electrode, Table 5.5. The half-wave potentials of these triarylamine derivatives vary modestly as a function of the peripheral groups, with the substitution of one and two weakly electron donating methyl groups by one and two more electron withdrawing trimethylsilylethynyl groups in **39** and **40** resulting in a shift of $E_{1/2}$ by ca. +70 mV (from 0.53 V (**39**) to 0.60 V (**40**)) and +90 mV (from 0.60 V to 0.69 V (**41**)) respectively.

The clusters $Co_2(\mu\text{-}HC_2C_6H_4R\text{-}4)(CO)_4(dppm)$ are well known to undergo a one electron oxidation and reduction process, at redox potentials which are sensitive to the electron donating or withdrawing properties of the phenyl substituent, R.[19] For example, the oxidation wave shifts from ca. –0.10 V (R = NMe_2) to +0.23 V (R = H) and +0.29 V (R = NO_2) (vs. ferrocene/ferricenium in 0.1 M NBu_4PF_6 / THF). Complexes **39a** and **40a** feature both Co_2C_2 and triarylamine based redox centres, and unsurprisingly exhibit two one-electron oxidative waves which are essentially chemically reversible at room temperature. By comparison with the data from the ligands **39** and **40** and the complexes $Co_2(\mu\text{-}HC_2C_6H_4R)(CO)_4(dppm)$, the first of these oxidation processes ($E_{1/2}$ = 0.04 V, **39a**; 0.08 V, **40a**) can be assigned to the oxidation of the cluster, whilst the second wave ($E_{1/2}$ = 0.56 V, **39a**; 0.60 V, **40a**) can be attributed to the triarylamine group. The relative potentials of these oxidation processes in **39a** vs. **40a** follow the same substituent effects observed for **39** vs. **40**.

Table 5.5. The electrochemical response of 39 – 42 in CH_2Cl_2 / 0.1 M electrolyte solutions, with a platinum working electrode, ν = 100 mV s^{-1}. Values referenced to $FcH/[FcH]^+$ = 0 V.

Complex	Electrolyte	$E_{1/2}$ (1) / V	$E_{1/2}$ (2) / V	$\Delta E_{1/2}$ / mV	$E_{1/2}$ (amine)/ V
39[a]	NBu_4PF_6				0.53
40[a]	NBu_4PF_6				0.60
41[a]	NBu_4PF_6				0.69
39a[b]	NBu_4PF_6	0.04	-	-	0.56
	$NBu_4[BAr^F{}_4]$	0.05	-	-	0.63
40a[a]	NBu_4PF_6	0.08	-	-	0.60
40b[b]	NBu_4PF_6	0.07	0.17	100	0.63
	$NBu_4[BAr^F{}_4]$	0.07	0.29	220	0.87
41a[b]	NBu_4PF_6	0.12	-	-	0.77[c]
41b[b]	NBu_4PF_6	0.08	0.19	110	0.79[c]
41c[b]	NBu_4PF_6	–0.03	0.13[d]	160	0.80[c]
	$NBu_4[BAr^F{}_4]$	0.07	0.23[d]	160	not detected
42-Me[a]	NBu_4PF_6	0.14	-	-	-

[a] room temperature. [b] –40 °C. [c] E_{pa} value listed, irreversible oxidation. [d] An oxidation wave representing two unresolved single electron oxidations.

At room temperature, the electrochemical analysis of **40b**, **41a** – **41c** was complicated by the rapid passivation of the platinum working electrode, leading to the formation of a film over the electrode surface, which was apparent by simple visual inspection. However, the chemical stability of the electrogenerated products does improve at lower temperatures. The bis(cluster) complex **40b** exhibited three fully resolved oxidation waves at –40 °C, the first two ($E_{1/2}$ = 0.07, 0.17 V; $\Delta E_{1/2}$ = 100 mV) which are assigned to the sequential oxidation of the cluster cores and the third ($E_{1/2}$ = 0.63 V) to the triarylamine moiety. However, whilst complex **41a** ($E_{1/2}$ = 0.12 V) and **41b** ($E_{1/2}$ = 0.08, 0.19 V; ΔE_p = 110 mV) exhibited one and two resolved cluster oxidations according to

expectations, in both cases the amine oxidation was irreversible (E_{pa} = 0.77 (**41a**), 0.79 V (**41b**)).

The cyclic voltammogram of **41c** exhibited three distinct oxidation waves. The first two oxidation waves are reversible ($E_{1/2}$ = –0.03, 0.13 V, $\Delta E_{1/2}$ = 100 mV) and the third oxidation is irreversible in nature (E_{pa} = 0.79 V). Although the peak to peak separation of the first oxidation wave (ΔE_p = 73 mV) is slighter larger than a reversible single one-electron oxidation process (ΔE_p = 59 mV), it is very similar to that of the internal decamethylferrocene reference (ΔE_p = 76 mV). In contrast, the second oxidation wave (ΔE_p = 81 mV) is representative of two unresolved one electron cluster oxidations as it is significantly larger than the peak to peak separation expected for a single two electron process (ΔE_p = 30 mV). Attempts to resolve this second oxidation wave in 0.1 M $NBu_4[BAr^F{}_4]$ / CH_2Cl_2 were not successful.

The observation of two separate oxidation events for the cluster based redox processes reflects the relative stability of the MV state [**40b**]$^+$ relative to **40b** and [**40b**]$^{2+}$ (but does not necessarily reflect the extent of charge delocalisation in the monocation). However, as discussed in Chapter 1, $\Delta E_{1/2}$ and K_c are determined by a number of factors, for example solvation, ion-pairing, electrostatic effects and resonance / delocalisation, with just the latter of these relating to the concept of stabilisation arising from 'electronic interactions' between the remote centres.[7, 67-70] Whilst many interpretations of K_c have assumed a dominant contribution from delocalisation effects, over the years Geiger and co-workers have presented a series of papers which have addressed the significance of ion-pairing interactions in the stabilisation of charged species and the consequent effects

a supporting electrolyte can have on the stabilisation of an intermediate charged species.[71-73]

In order to differentiate between through bond and through space effects, the CV measurements of **39a**, **40b** and **41c** were conducted in 0.1 M $NBu_4[BAr^F_4]$ where $[BAr^F_4]^- = [B(C_6F_5)_4]^-$, Table 5.5. In **39a** the cluster based oxidation takes place at essentially the same potential in both 0.1 M NBu_4PF_6 / CH_2Cl_2 and 0.1M $NBu_4[BAr^F_4]$ / CH_2Cl_2. However, the amine oxidation in 0.1M $NBu_4[BAr^F_4]$ / CH_2Cl_2 is some 70 mV more positive than in the NBu_4PF_6 electrolyte. On the basis of a simple electrostatic model, these results can be rationalised by the fact that the $[BAr^F_4]^-$ anion is weakly coordinating, and therefore less strongly associating with the electrochemically generated oxidation products than PF_6^- in CH_2Cl_2. Thus, the oxidation of $[\mathbf{39a}]^+$ to $[\mathbf{39a}]^{2+}$ in 0.1 M $NBu_4[BAr^F_4]$ / CH_2Cl_2 is less thermodynamically favourable, because the dication is less stabilised by ion pairing interactions. In the case of the bis(cluster) complex **40b**, whilst the first cluster oxidation occurs at the same potential in both electrolytes, changing the electrolyte from the PF_6^- to the $[BAr^F_4]^-$ anion results in an increased separation of the first two cluster based oxidative waves from $|E_{1/2}(1)-E_{1/2}(2)|$ = 100 mV (NBu_4PF_6) to 220 mV ($NBu_4[BAr^F_4]$). Once again the trication $[\mathbf{40b}]^{3+}$ is also less stabilised in the $[BAr^F_4]^-$ containing electrolyte, and consequently the difference between the second and third oxidation processes $|E_{1/2}(2)-E_{1/2}(3)|$ also increases from 460 mV in NBu_4PF_6 to 580 mV in $NBu_4[BAr^F_4]$.

In the tris(cluster) complex **41c**, the first cluster based oxidation is 100 mV more thermodynamically favourable in PF_6^- than $[BAr^F{}_4]^-$ electrolyte. The second oxidative process is also more thermodynamically favourable in PF_6^- than $[BAr^F{}_4]^-$ electrolyte, but with a difference between the first and second oxidation processes $|E_{1/2}(1)-E_{1/2}(2)|$ of 160 mV, whilst the amine oxidation was not detected by cyclic voltammetry and differential pulse techniques in a weakly associating $[BAr^F{}_4]^-$ electrolyte. The ion-pairing interactions with the electrolyte anions in **39a** and **40b**, therefore play a significant role in stabilising the charged states of these species and the use of ΔE as a measure of the ground state interactions/delocalisation between the cluster centres and between the cluster centres is not appropriate. It is however, more appropriate for **41c**, where electronic interactions are likely to occur through bond.

5.5 IR Spectroelectrochemistry

To further investigate the nature of the redox products and potential electronic interactions between the various electroactive components in **39a**, **40b** and **41c**, we turned to IR and NIR spectroscopic methods. Complex **39a** was investigated by IR spectroelectrochemistry, using the ν(C≡O) ligand as an indicator of metal oxidation state. On oxidation of **39a** to [**39a**]$^{+}$, there is a shift in the frequency of the carbonyl ligand in the ν(C≡O) frequencies of ca. +45 cm^{-1} to higher energy, Figure 5.14. This shift is large and consistent with a cluster oxidation and is in agreement with the assignment of the cluster and amine based oxidations from electrochemical studies. On reduction of [**39a**]$^{+}$ to **39a**, complete recovery of the original spectrum was obtained.

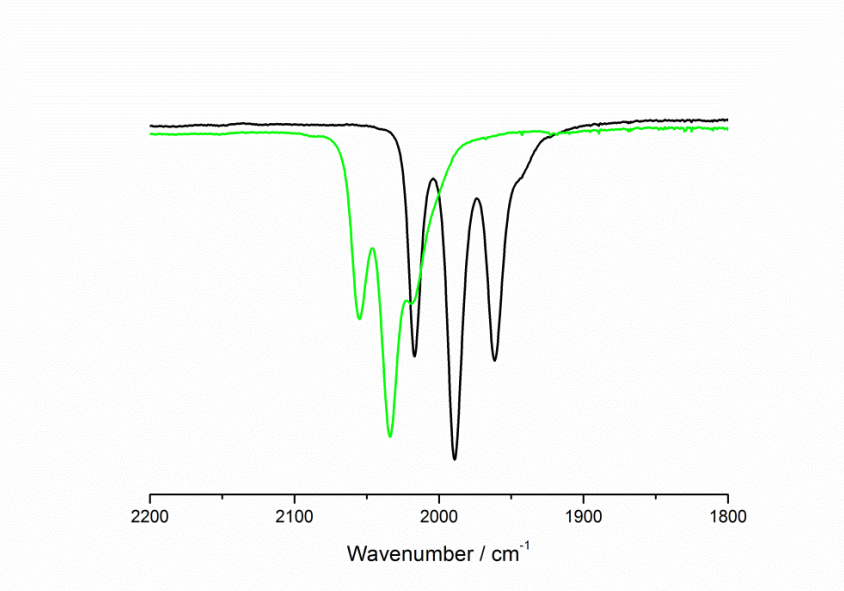

Figure 5.14. The spectroelectrochemically determined IR spectra of 39a (black) and [39a]$^{+}$ (green) in 0.1 M NBu_4PF_6 / CH_2Cl_2.

The poorer chemical stability of the redox products derived from the bis- and tris(cluster) complexes **40b** and **41c** led to the rapid passivation of the platinum electrodes in the CV experiments. Thus this precluded the further study of these compounds using our room temperature IR spectroelectrochemical cell, which is fitted with a platinum gauze working electrode. The chemical oxidation of **40b** with acetylferricenium hexafluorophosphate ([FcAc]PF_6) in CH_2Cl_2 at –40 °C (dry ice/acetonitrile) gave solutions of [**40b**]PF_6 and [**40**][PF_6]$_2$, from which spectroscopic information could be obtained. Treatment of **40b** with one equivalent of [FcAc]PF_6 gave an IR spectrum, Figure 5.15 which was characterised by a band pattern approximately a superposition of [**39a**] and [**39a**]$^+$, Table 5.6. This strongly supports a description of [**40b**]$^+$ in terms of oxidation at one of the cluster moieties, with the radical cation localised on the IR timescale. The limited shifts of the ν(C≡O) bands associated with the 'neutral' cluster in [**40b**]$^+$, Table 5.6, indicates little ground state delocalisation between the cluster moieties. On the addition of a second equivalent of [FcAc]PF_6 to [**40b**]$^+$ the dication is formed and the ν(C≡O) band pattern evolves to towards a pattern similar to that observed in [**39a**]$^+$, Figure 5.14. The IR spectrum of [**40b**][PF_6]$_2$ is therefore consistent with the presence of two oxidised, but non-interacting, cluster moieties, Figure 5.16.

Table 5.6. IR ν(C≡O) / cm^{-1} of [39a]$^{n+}$, [40b]$^{n+}$ and [41c]$^{n+}$.

Complex	ν(C≡O) / cm^{-1}
39a	2017m, 1989s, 1961m, 1942w
[39a]$^{+}$	2055m, 2034s, 2017m, 2007sh
40b	2016m, 1989s, 1960m, 1942w
[40b]$^{+}$	2054w, 2033m, 2018sh, unresolved
[40b]$^{2+}$	2058m, 2037s, 2020m, 1007sh
41c	2017m, 1990s, 1961m, 1941w
[41c]$^{+}$	2055w, 2034w, 2019m, 1991s, 1963m, 1944w
[41c]$^{2+}$	2056w, 2035w, 2020m, 1992m, 1964m, 1946w
[41c]$^{3+}$	2064w, 2040s, 2023m, 2008w

Similarly, the low temperature chemical oxidation of **41c** in CH_2Cl_2 with one, two and three equivalents of [FcAc]PF_6 yielded solutions of [**41c**]PF_6, [**41c**][PF_6]$_2$ and [**41c**][PF_6]$_3$ respectively (Figures 5.17 – 5.19) illustrating the progression of each oxidative step, as shown. The IR ν(C≡O) frequencies are listed in Table 5.6. The shift from **41c** to [**41c**][PF_6]$_3$ of ca. 45 cm^{-1} is consistent with a series of sequential cluster based oxidations.

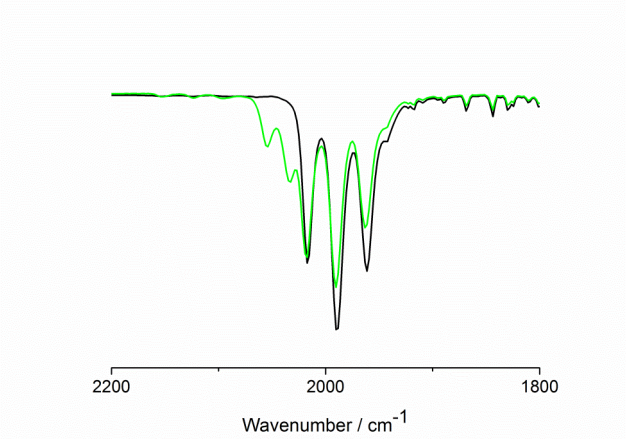

Figure 5.15. The IR ν(C≡O) of 40b (black), $[40b]^+$ (green) obtained by the stoichiometric oxidation of 40b with one equivalent of $[FcAc]PF_6$ in CH_2Cl_2 at –40 °C.

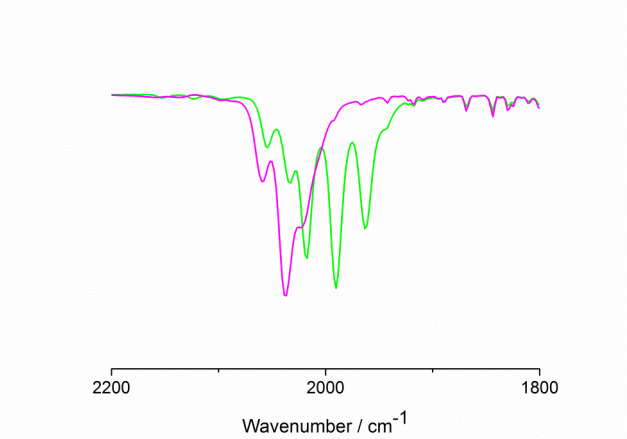

Figure 5.16. The IR ν(C≡O) of $[40b]^+$ (green) and $[40b]^{2+}$ (purple), obtained by the stoichiometric oxidation of 40b with two equivalents of $[FcAc]PF_6$ in CH_2Cl_2 at –40 °C.

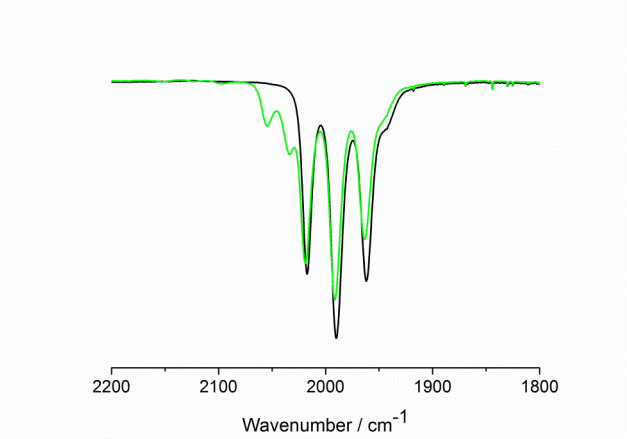

Figure 5.17. The IR ν(C≡O) spectra of 41c (black), [41c]PF_6 (green) obtained by stoichiometric oxidation of 41c with one equivalent of [FcAc]PF_6 in CH_2Cl_2 at –40 °C.

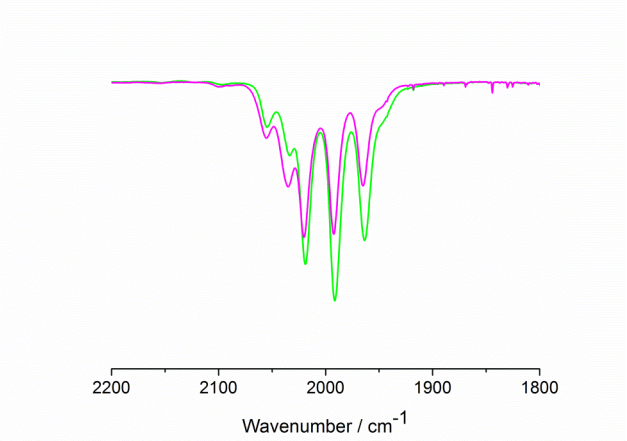

Figure 5.18. The IR ν(C≡O) spectra [41c]PF_6 (green), [41c][PF_6]$_2$ (purple) obtained by stoichiometric oxidation of 41c with two equivalent of [FcAc]PF_6 in CH_2Cl_2 at –40 °C.

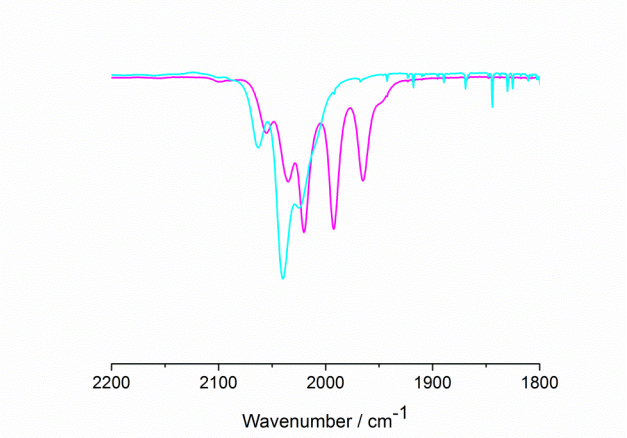

Figure 5.19. The IR ν(C≡O) spectra of [41c][PF_6]$_2$ (purple) and [41c][PF_6]$_3$ (blue) obtained by stoichiometric oxidation of 41c with three equivalents of [FcAc]PF_6 in CH_2Cl_2 at –40 °C.

5.6 NIR Spectroscopy

On oxidation of **39a** to [**39a**]$^{+}$, a new electronic transition was observed at 7920 cm^{-1} (1260 nm / ε = 1590 M^{-1} cm^{-1}). A very similar transition was also observed in the NIR spectrum of [**40b**]$^{+}$ at 8020 cm^{-1} (1250 cm^{-1} / ε = 2260 M^{-1}cm^{-1}). Further oxidation of [**40b**]$^{+}$ to [**40b**]$^{2+}$ and likewise in [**41c**]$^{+}$ to [**41c**]$^{2+}$ resulted not in a collapse of this low energy feature, characteristic of an intervalence charge transfer transiton (IVCT) in MV complexes, but rather an increase in the band intensity with a smaller shift to higher energy [**40b**]$^{2+}$ 8950 cm^{-1} (1120 nm / ε = 4320 M^{-1}cm^{-1}), Figure 5.20. Likewise, on oxidation of **41c** to [**41c**]$^{+}$ a low energy transition developed at 7270 cm^{-1} (1370 nm / ε = 2370 M^{-1} cm^{-1}) which grew in intensity in [**41c**]$^{2+}$ at 7660 cm^{-1} (1300 nm / ε = 3470 M^{-1} cm^{-1}). Subsequent generation of [**41c**]$^{3+}$ led to the observation of a more significant change in the band at 7660 cm^{-1} to higher energy 9000 cm^{-1} (1110 nm / ε = 4600 M^{-1}cm^{-1}, Figure 5.21. In order to elucidate the nature of this low energy transition in [**39a**]$^{+}$ and [**40b**]$^{+}$, the tolyl substituted cluster [{$Co_2(CO)_4$(dppm)}{μ-($Me_3SiC_2C_6H_4$-4-Me)}] (**42-Me**) was synthesised according to a literature procedure.[19] In [**42-Me**]$^{+}$, a weak band developed at 8240 cm^{-1} (1210 nm/ε = 350 M^{-1}cm^{-1}), in CH_2Cl_2 / 0.1 M NBu_4PF_6, Figure 5.20. On the basis of IR and NIR data, the cluster centres in [**40b**]$^{+}$ are electronically independent, and localised entities. Thus, the low energy electronic absorption is therefore likely to be associated with the electronic transitions within the $[Co_2C_2]^{+}$ core.

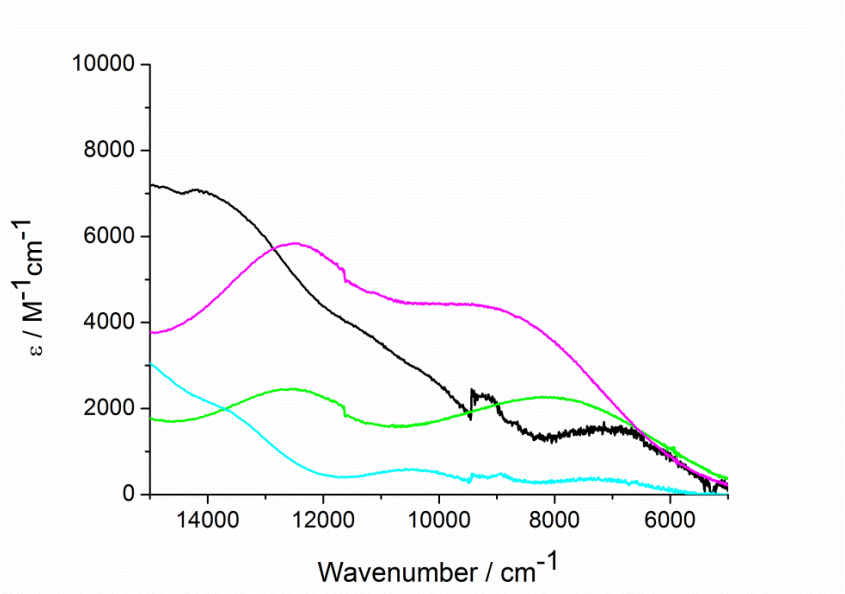

Figure 5.20. NIR transitions of the electrochemically generated $[39a]^+$ (black) and $[42\text{-}Me]^+$ (blue) in 0.1 M NBu_4PF_6 / CH_2Cl_2 and the chemically generated $[40b]^+$ (green) and $[40b]^{2+}$ (purple) in CH_2Cl_2 at –40 °C.

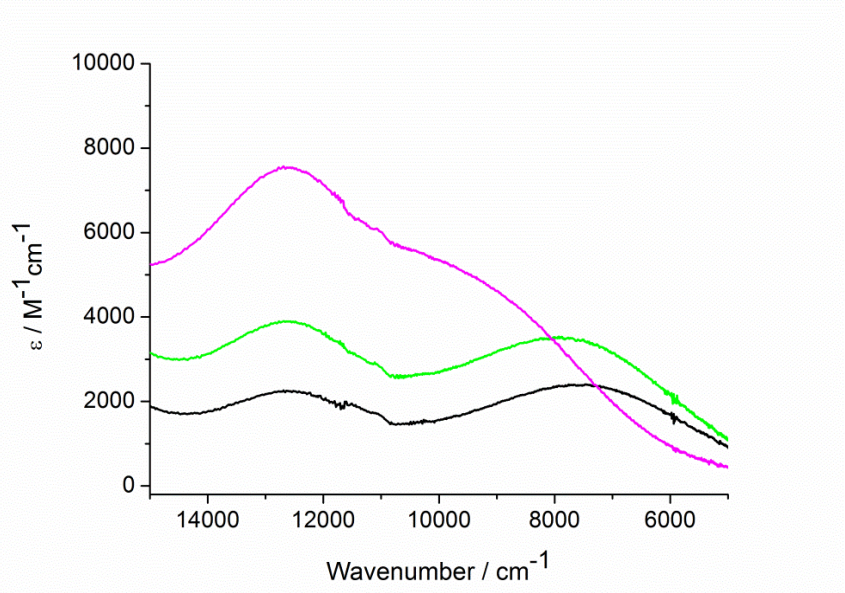

Figure 5.21. The NIR spectra of $[41c]^+$ (black), $[41c]^{2+}$ (green), $[41c]^{3+}$ (purple) obtained by stoichiometric oxidation with one, two and three equivalents of $[FcAc]PF_6$ in CH_2Cl_2 at –40 °C.

5.7 Conclusions

Simplified synthetic procedures have been developed for $Co_2(CO)_6(dppm)$ (**35**) and the mono- and di-substituted tertiary amines $N(C_6H_4Br\text{-}4)(C_6H_4Me\text{-}4)_2$ (**36**) and $N(C_6H_4Br\text{-}4)_2(C_6H_4Me\text{-}4)$ (**37**) whilst the tri-substituted tertiary amine $N(C_6H_4Br\text{-}4)_3$ (**38**) was prepared by a bromination reaction. The trimethylsilylethynyl-substituted triarylamines $N(C_6H_4\text{-}4\text{-}C{\equiv}CSiMe_3)(C_6H_4Me\text{-}4)_2$ (**39**) and $N(C_6H_4\text{-}4\text{-}C{\equiv}CSiMe_3)_2(C_6H_4Me\text{-}4)$ (**40**) and $N(C_6H_4\text{-}4\text{-}C{\equiv}CSiMe_3)_3$ (**41**) were synthesised by Sonogashira reactions. The subsequent reaction of **35** with compounds **39** – **41** gives the anticipated Co_2C_2 tetrahedrane clusters with pendant $[\{Co_2(CO)_4(dppm)\}\{\mu\text{-}(Me_3SiC_2\text{-}4\text{-}C_6H_4)N(C_6H_4Me\text{-}4)_2\}]$ (**39a**), $[Co_2\{\mu\text{-}Me_3SiC_2\text{-}4\text{-}C_6H_4N(C_6H_4\text{-}4\text{-}C{\equiv}CSiMe_3)(C_6H_4Me\text{-}4)\}(CO)_4(dppm)]$ (**40a**) $[Co_2\{\mu\text{-}Me_3SiC_2\text{-}4\text{-}C_6H_4N(C_6H_4\text{-}4\text{-}C{\equiv}CSiMe_3)_2\}(CO)_4(dppm)]$ (**41a**) and bridging triarylamines $[\{Co_2(CO)_4(dppm)\}_2\{\mu\text{-}(Me_3SiC_2\text{-}4\text{-}C_6H_4)_2N(C_6H_4Me\text{-}4)\}]$ (**40b**), $[\{Co_2(CO)_4(dppm)\}_2\{\mu\text{-}Me_3SiC_2\text{-}4\text{-}C_6H_4)_2N(C_6H_4\text{-}4\text{-}C{\equiv}CSiMe_3)\}]$ (**41b**) and $[Co_2\{\mu\text{-}Me_3SiC_2\text{-}4\text{-}C_6H_4N(C_6H_4\text{-}4\text{-}C{\equiv}CSiMe_3)_2\}(CO)_4(dppm)]$ (**41c**).

Structural parameters determined by single crystal X-ray diffraction indicate the Co_2C_2 cluster cores to be in essentially identical electronic environments with no structural evidence for ground state delocalisation in **39a**, **40a** and **41a** nor between the clusters in **40b**, **41b** or **41c**. Electrochemical and spectroelectrochemical studies reveal the first oxidation process to be cluster based. The clusters in **40b** are oxidised sequentially in two separate one-electron processes, permitting an evaluation of ion-pairing interactions in the stabilisation of the electrogenerated ions. The difference in cluster oxidation

potentials is sensitive to the nature of the supporting electrolyte anion, emphasising the importance of through space effects. This contrasts to **41c** where electronic interactions are likely to proceed *via* a through bond mechanism.

The IR ν(C≡O) spectrum of [**40b**]$^+$ indicates the localised electronic structure of the species, on the IR timescale. The cluster centres thus act independently and there is no evidence for bridge-mediated cluster-cluster interactions. The NIR spectra of the cluster radicals [**39a**]$^+$, [**40b**]$^+$ and [**41c**]$^+$ feature almost identical low energy electronic transitions, which cannot be attributed to an IVCT-type transition based on spectroscopic evidence. However, a similar ableit a weak band is also oberved in [**42-Me**]$^+$ in the same region. Thus the presence of the same transition in the aforementioned radical cation species can be readily associated with the oxidised dicobalt dicarbon tetrahedrane cluster core. On the basis of this data, it can be concluded that the cluster centres in **40b** and **41c** are electronically independent, and represent cluster based Class I Robin and Day MV systems.

5.8 Experimental

All reactions were carried out under an atmosphere of nitrogen using standard Schlenk techniques. Reaction solvents were purified and dried using an Innovative Technology SPS-400, and degassed before use. No special precautions were taken to exclude air or moisture during work-up. The compounds $Co_2(CO)_6$(dppm) (**35**),[55] $Pd_2(dba)_3$,[74] 1,1'-bis(diphenylphosphino)ferrocene (dppf),[75] $PdCl_2(PPh_3)_2$,[76] $Pd(PPh_3)_4$,[77] $N(C_6H_4Br\text{-}4)(C_6H_4Me\text{-}4)_2$ (**36**),[78] $NC_6H_4Br\text{-}4)_2(C_6H_4Me\text{-}4)$ (**37**),[58] $N(C_6H_4\text{-}4\text{-}C{\equiv}CSiMe_3)(C_6H_4Me\text{-}4)_2$ (**39**),[79] $N(C_6H_4\text{-}4\text{-}C{\equiv}CSiMe_3)_2(C_6H_4Me\text{-}4)$ (**40**),[58] $Me_3SiC{\equiv}C_6H_4\text{-}Me\text{-}4$,[80] $N(C_6H_4Br\text{-}4)_3$ (**38**),[58] and $N(C_6H_4\text{-}4\text{-}C{\equiv}CSiMe_3)_3$ (**41**)[47] were prepared by the literature routes, or minor modifications as detailed below. Other reagents were purchased and used as received.

The NMR spectra were recorded on a 400 MHz Bruker Avance spectrometer from deuterated chloroform solutions and referenced against residual protio solvent resonances ($CHCl_3$: ^1H 7.26 ppm; ^{13}C 77.0 ppm) or external phosphoric acid. IR spectra were recorded using a Thermo 6700 spectrometer from CH_2Cl_2 solutions in a cell fitted with CaF_2 windows. MALDI(+)-mass spectra of organometallic complexes were recorded using Autoflex II TOF/TOF mass spectrometer with a 337 nm laser. Samples in CH_2Cl_2 (1 mg / ml) were mixed with a matrix solution of trans-2-[3-(4-tert-butylphenyl)-2-methyl-2-propenylidene]malononitrile (DCTB) in a 1:9 ratio, with 1 μl of mixture spotted onto a metal target prior to exposure to the MALDI ionization source. Organic compounds were analysed by GC-EI(+) mass spectrometry using a Trace GCMS instrument. Elemental analyses were performed by technical staff at the Department of Chemistry, Durham University.

Electrochemical analyses were carried out using an EcoChemie Autolab PG-STAT30 potentiostat, with Pt working, counter and pseudo reference electrodes, from solutions in CH_2Cl_2 containing 0.1 M supporting electrolyte, ν = 100 mV s^{-1}. The decamethylferrocene / decamethylferricenium (FcH*/$[FcH^*]^+$) couple was used as an internal reference for potential measurements such that the FcH/$[FcH]^+$ couple falls at 0.00 V ($FcH^*/[FcH]^{*+}$ = –0.48 V).[81] Spectroelectrochemical measurements were made in an OTTLE cell of Hartl design,[82] from CH_2Cl_2 solutions containing 0.1 M NBu_4PF_6 electrolyte. The cell was fitted into the sample compartment of the Thermo 6700 or Thermo Array UV-Vis spectrophotometer, and electrolysis in the cell was performed with a PGSTAT30 potentiostat. Chemical oxidations were performed with $[FcAc]PF_6$ in CH_2Cl_2 at –40 °C (dry ice/acetone bath) and IR and UV-vis-NIR spectra were recorded in an IR cell fitted with CaF_2 windows. In ^{13}C NMR assignments, the various C_6H_4 and C_6H_5 rings are denoted Ar-cluster (for the phenylene ring pendent to the Co_2C_2 cluster core), Ar-CH_3 (for the tolyl rings pendent to the amine N centre), Ar' (for the 4-ethynyltrimethylsilyl substituted aryl ring and Ph for those rings associated with the dppm ligand. In cases where assignments were ambiguous the term 'Ar' is used.

Single crystal X-ray data were collected at 120 K on a Bruker SMART 6K with a graphite monochromator, $\lambda_{MoK\alpha}$, λ = 0.71073 Å or at 100 K on a Bruker Proteum M rotating anode (focusing mirrors, $\lambda_{CuK\alpha}$, λ = 1.54178 Å) diffractometers equipped with Cryostream and Cobra (Oxford Cryosystems) cryostats respectively. The data for all compounds were corrected for absorption by multi-scan method using SADABS program.[83] All structures were solved by direct methods and refined by full-matrix least squares on F^2 for all data using OLEX2[84] and SHELX[85] software. All non-disordered non-hydrogen atoms were refined with anisotropic displacement parameters, atoms of disordered groups were refined isotropically with fixed SOF = 0.5. All H atoms were placed in the calculated positions and refined in "riding" mode. Crystallographic data and refinement parameters are listed in Table 5.3.

5.8.1 Preparation of $Co_2(CO)_6$(dppm) (35)

A Schlenk flask was charged with degassed toluene (60 ml), to which $Co_2(CO)_8$ (5.0 g, 14.6 mmol) was added and the resulting solution stirred whilst treated with dppm (5.61 g, 14.6 mmol) in several small portions at room temperature. The CO liberated after each addition was allowed to completely evolve prior to addition of the subsequent aliquot of diphosphine. The solution gradually became burnt orange in colour, and a bright orange precipitate became evident after approximately 30 minutes of reaction. The solution was allowed to stir for several hours, during which time copious amounts of product precipitated from the reaction solution. When adjudged complete, the solution was filtered to give $Co_2(CO)_6$(dppm) as a free-flowing microcrystalline orange powder in essentially quantitative yield (ca. 9.7 g), identical with that prepared by the literature method.

5.8.2 Preparation of $NH(C_6H_4Me\text{-}4)_2$

In oven dried glassware purged with nitrogen, dry toluene (50 ml) was degassed by freeze-pump-thaw methods. To this solvent was added *para*-toluidine (2.23 g, 20.8 mmol), 4-iodotoluene (5.00 g, 22.9 mmol), $Pd_2(dba)_3$ (0.19 g, 0.21 mmol), dppf (0.35 g, 0.63 mmol) and sodium *tert*-butoxide (3.00 g, 31.2 mmol). The reaction was heated to reflux for 20 h, after which the solution was allowed to cool to room temperature, filtered and the solvent removed *in vacuo*. The residue was purified by silica column chromatography eluting with hexane increasing to a hexane and acetone (95:5) mixture. The eluent was concentrated *in vacuo* to 5 ml and the precipitated white solid collected and washed with cold hexane (2 x 5 ml) to give $NH(C_6H_4Me\text{-}4)_2$ (2.77 g, 68 %). ^{1}H NMR: δ 2.30 (s, 6H, CH_3), 5.51 (s, 1H, NH), 6.95 (d, J = 8 Hz, 4H, Ar) 7.07 (d, J = 8 Hz, 4H, Ar). ^{13}C NMR: δ 20.6 (CH_3), 117.9 (Ar_o), 129.8 (Ar_m), 130.2 (Ar_p), 141.1 (Ar_i). ES-MS(+) (*m/z*): 197.2 $[M+H]^+$.

5.8.3 Preparation of $N(C_6H_4Br\text{-}4)(C_6H_4Me\text{-}4)_2$ (36)

In oven dried glassware purged with nitrogen, dry toluene (50 ml) was degassed by freeze-pump-thaw methods. To this solvent was added $NH(C_6H_4Me\text{-}4)_2$ (2.38 g, 12.0 mmol), 1-bromo-4-iodobenzene (3.76 g, 13.2 mmol), $Pd_2(dba)_3$ (0.11 g, 0.12 mmol), dppf (0.20 g, 0.36 mmol) and sodium *tert*-butoxide (1.74 g, 18.1 mmol). The reaction was heated to reflux for 60 h, after which the solution was allowed to cool to room temperature, filtered and the solvent removed *in vacuo*. The residue was treated with petroleum ether (30 ml), the persistent solid removed by filtration, and the precipitate washed with petroleum ether (2 x 30 ml). The combined organic solutions were concentrated *in vacuo* to ca. 10 ml, which upon standing deposited a white precipitate. The precipitate was collected by filtration, and washed with cold petroleum ether (5 ml) to give $N(C_6H_4Br\text{-}4)(C_6H_4Me\text{-}4)_2$ (2.84 g, 69 %). ^{1}H NMR: δ 2.32 (s, 6H, CH_3), 6.90 (d, J = 9 Hz, 2H, Ar), 6.98 (d, J = 8 Hz, 4H, Ar), 7.08 (d, J = 8 Hz, 4H, Ar), 7.28 (d, J = 9 Hz, 2H, Ar). ^{13}C NMR: δ 20.8 (CH_3), 113.6 ($Ar_{p'}$), 123.9 (Ar_o), 125.0 ($Ar_{o'}$), 130.3 (Ar_m), 131.9 ($Ar_{m'}$), 132.9 (Ar_p), 145.0 (Ar_i), 147.4 ($Ar_{i'}$). ESI-MS(+) (*m/z*): 351.1 $[M+H]^+$.

5.8.4 Preparation of $N(C_6H_4Br\text{-}4)_2(C_6H_4Me\text{-}4)$ (37)

In oven dried glassware purged with nitrogen, dry toluene (50 ml) was degassed by freeze-pump-thaw methods. To this solvent was added *para*-toluidine (0.54 g, 5.04 mmol), 1-bromo-4-iodobenzene (2.97 g, 10.5 mmol), $Pd_2(dba)_3$ (0.05 g, 0.05 mmol), dppf (0.08 g, 0.15 mmol) and sodium *tert*-butoxide (1.35 g, 14.0 mmol). The reaction was heated to reflux for 36 hours, after which time the solution was allowed to cool to room temperature before being poured into water. The resulting suspension was extracted with dichloromethane (3 x 30 ml) and the combined organic phases washed with water (3 x 40 ml), dried over magnesium sulphate, filtered and the solvent removed to produce a black residue. The crude product was purified by column chromatography on silica (hexane) to give $N(C_6H_4Br\text{-}4)_2(C_6H_4Me\text{-}4)$ as a white crystalline solid (1.37 g, 66 %). ^{1}H NMR: δ 2.32 (s, 3H, CH_3), 6.91 (d, 4H, J = 8 Hz, Ar-Br), 6.97 (d, 2H, 8 Hz, Ar-CH_3), 7.09 (d, 2H, 8 Hz, Ar-CH_3), 7.32 (d, 4H, 8 Hz, Ar-Br). ^{13}C NMR: δ 21.2 (CH_3), 115.3 ($Ar_{p'}$), 125.2 ($Ar_{o'}$), 125.5 (Ar_o), 130.6 (Ar_m), 132.6 ($Ar_{m'}$), 134.2 (Ar_p), 144.6 (Ar_i), 147.0 ($Ar_{i'}$). GC-EI(+) MS (*m/z*): 417.0 (100 %).

5.8.5 Preparation of $N(C_6H_4\text{-}4\text{-}C{\equiv}CSiMe_3)(C_6H_4Me\text{-}4)_2$ (39)

In oven dried glassware purged with nitrogen, dry triethylamine (50 ml) was degassed by freeze-pump-thaw methods. To this solvent was added $N(C_6H_4Br\text{-}4)(C_6H_4Me\text{-}4)_2$ (1.80 g, 5.12 mmol), $HC{\equiv}CSiMe_3$ (0.85 ml, 6.15 mmol), $PdCl_2(PPh_3)_2$ (0.18 g, 0.25 mmol) and copper(I) iodide (0.02 g, 0.13 mmol). The reaction was heated to reflux for 17 h, after which the solution was allowed to cool to room temperature, filtered and the solvent removed *in vacuo*. The residue was treated with hexane (30 ml), the precipitated solid removed by filtration, and washed with hexane (2 x 20 ml). The solvent was removed from the combined filtrates *in vacuo* and the residue purified by silica column chromatography in hexane increasing polarity to a hexane and CH_2Cl_2 (80:20) mixture. The solvent was removed *in vacuo* to leave a yellow oil that solidifies on standing to give $N(C_6H_4\text{-}4\text{-}C{\equiv}CSiMe_3)(C_6H_4Me\text{-}4)_2$ (1.37 g, 73 %). ^{1}H NMR: δ 0.25 (s, 9H, $SiMe_3$), 2.33 (s, 6H, CH_3), 6.90 (d, J = 9 Hz, 2H, Ar), 6.98 (d, J = 8 Hz, 4H, Ar), 7.08 (d, J = 8 Hz, 4H, Ar), 7.28 (d, J = 9 Hz, 2H, Ar). ^{13}C NMR: δ 0.00 ($SiMe_3$), 14.0 (CH_3), 92.5 ($\underline{C}{\equiv}CSiMe_3$), 105.6 ($C{\equiv}\underline{C}SiMe_3$) 114.8 ($Ar_{p'}$), 120.8 ($Ar_{o'}$), 125.1 ($Ar_o$), 129.9 ($Ar_m$), 132.7 ($Ar_{m'}$), 133.1 ($Ar_p$), 144.6 ($Ar_i$), 148.3 ($Ar_{i'}$). ESI-MS(+) (*m/z*): 370.3 $[M+H]^+$.

5.8.6 Preparation of $N(C_6H_4\text{-}4\text{-}C{\equiv}CSiMe_3)_2(C_6H_4Me\text{-}4)$ (40)

In oven dried glassware purged with nitrogen, dry triethylamine (40 ml) was degassed by freeze pump thaw methods. The reagents $N(C_6H_4Br\text{-}4)_2(C_6H_4Me\text{-}4)$ (1.00 g, 2.41 mmol), $Me_3SiC{\equiv}CH$ (3.4 ml, 240.0 mmol), $Pd(PPh_3)_4$ (0.08 g, 0.07 mmol) and copper iodide (0.01 g, 0.07 mmol) were added to the solvent. The reaction was heated to reflux for 18 h, after which the solution was allowed to cool to room temperature, filtered and the solvent removed *in vacuo*. The crude brown oil was purified by flash column chromatography on silica in hexane increasing polarity to a hexane and CH_2Cl_2 (70:30) mixture to give a yellow oil which solidified under vacuum (0.66 g, 60 %). ^{1}H NMR: δ 0.23 (s, 18H, $SiMe_3$), 2.33 (s, 3H, CH_3), 6.94 (d, 4H, J = 8 Hz, Ar), 6.97 (d, 2H, J = 8 Hz, Ar), 7.09 (d, 2H, J = 8 Hz, Ar), 7.31 (d, 4H, J = 8 Hz, Ar). ^{13}C NMR: δ 0.4 ($SiMe_3$), 21.2 (CH_3), 93.0 ($\underline{C}{\equiv}CSiMe_3$), 106.0 ($C{\equiv}\underline{C}SiMe_3$), 115.2 ($Ar_{p'}$), 121.3 ($Ar_{o'}$), 125.5 ($Ar_o$), 130.3 ($Ar_m$), 133.2 ($Ar_{m'}$), 133.6 ($Ar_p$), 145.0 ($Ar_i$), 148.8 ($Ar_{i'}$). GC-EI(+) MS (*m/z*): 451.2. IR (CH_2Cl_2): ν(C≡C) 2105, ν(C-H) 3295, 3311 cm^{-1}.

5.8.7 Preparation of [{$Co_2(CO)_4$(dppm)}{μ-(Me_3SiC_2-4-C_6H_4)N(C_6H_4Me-4)$_2$}] (39a)

The reagents N(C_6H_4-4-C≡C$SiMe_3$)(C_6H_4Me-4)$_2$ (0.11 g, 0.30 mmol) and $Co_2(CO)_6$(dppm) (0.20 g, 0.30 mmol) were added to dry degassed toluene (12 ml) and heated to 80 °C under nitrogen for two hours. The solvent was removed and the resulting residue purified by preparative TLC using hexane and acetone (70:30). A brown band was collected, the solvent removed and X-ray quality crystals of [{$Co_2(CO)_4$(dppm)}{μ-(Me_3SiC_2-4-C_6H_4)N(C_6H_4Me-4)$_2$}] (**39a**) (0.15 g, 51 %) were obtained from the slow diffusion of methanol into a CH_2Cl_2 solution. ^{1}H NMR: δ 0.36 (s, 9H, $SiMe_3$), 2.32 (s, 6H, CH_3), 3.28 – 3.37 (m, 2H, dppm), 6.83 – 7.30 (m, 32H, 20H Ph + 12H Ar). ^{13}C NMR: δ 1.2 (s, $SiMe_3$), 21.2 (s, CH_3), 36.6 (t, $^1J_{CP}$ = 20 Hz, dppm), 88.7 (t, $^2J_{CP}$ = 9 Hz, C_2SiMe_3), 106.0 (t, $^2J_{CP}$ = 9 Hz, C_2SiMe_3), 123.4 (s, *o/m*-Ar cluster), 124.4 (s, *o/m*-Ar-CH_3), 128.2 (pseudo t, $^3J_{CP}$ = 5 Hz, *m*-PPh_2), 128.7 (pseudo t, $^3J_{CP}$ = 5 Hz, *m*-PPh_2), 129.4 (s, *p*-PPh_2), 129.9 (s, *p*-PPh_2), 130.2 (s, *o/m*-Ar-CH_3), 130.8 (s, *o/m*-Ar cluster), 131.0 (pseudo t, $^2J_{CP}$ = 6 Hz, *o*-PPh_2), 132.3 (s, *p*-Ar-CH_3), 133.0 (pseudo t, $^2J_{CP}$ = 6 Hz, *o*-PPh_2), 135.1 (pseudo t, $^1J_{CP}$ = 16 Hz, *i*-PPh_2), 136.7 (pseudo t, $^3J_{CP}$ = 3 Hz, *p*-Ar cluster), 139.4 (pseudo t, $^1J_{CP}$ = 25 Hz, *i*-PPh_3), 145.6 (s, *i*-Ar-CH_3), 146.1 (s, *i*-Ar cluster), 203.6 (s, CO), 207.7 (s, CO). ^{31}P NMR: δ 35.1. MALDI(+)-MS (*m/z*) : 871.1 $[M-4CO]^+$. IR (CH_2Cl_2): ν(CO) 2017m, 1989s, 1961m, 1942w cm^{-1}. Anal. Calcd ($C_{54}H_{49}Co_2NO_4P_2Si$): C, 65.91; H, 5.02; N, 1.42. Found: C, 66.03; H, 5.22; N, 1.36 %.

5.8.8 Reaction of $N(C_6H_4\text{-}4\text{-}C{\equiv}CSiMe_3)_2(C_6H_4Me\text{-}4)$ with $Co_2(CO)_6(dppm)$

The reagents $N(C_6H_4\text{-}4\text{-}C{\equiv}CSiMe_3)_2(C_6H_4Me\text{-}4)$ (0.06 g, 0.14 mmol) and $Co_2(CO)_6(dppm)$ (0.20 g, 0.30 mmol) were added to dry degassed toluene (12 ml) and heated to 80 °C under nitrogen overnight. The solvent was removed and the resulting residue purified by preparative TLC using hexane and acetone (70:30). Two major bands were observed and collected. The first band was identified as $[Co_2\{\mu\text{-}Me_3SiC_2\text{-}4\text{-}C_6H_4N(C_6H_4\text{-}4\text{-}C{\equiv}CSiMe_3)(C_6H_4Me\text{-}4)\}(CO)_4(dppm)]$ (**40a**) (0.044 g, 31 %) and the second band as $[\{Co_2(CO)_4(dppm)\}_2\{\mu\text{-}(Me_3SiC_2\text{-}4\text{-}C_6H_4)N(C_6H_4Me\text{-}4)\}]$ (**40b**) (0.086 g, 38 %). X-ray quality crystals of each complex were obtained from slow diffusion of methanol into a CH_2Cl_2 solution.

$[Co_2\{\mu\text{-}Me_3SiC_2\text{-}4\text{-}C_6H_4N(C_6H_4\text{-}4\text{-}C{\equiv}CSiMe_3)(C_6H_4Me\text{-}4)\}(CO)_4(dppm)]$ (**40a**): ^{1}H NMR: δ 0.25 (s, 9H, $SiMe_3$), 0.37 (s, 9H, $SiMe_3$), 2.35 (s, 3H, CH_3), 3.23 – 3.40 (m, 2H, dppm), 6.86 – 7.32 (m, 32H, 20H Ph + 12H Ar). ^{13}C NMR: δ 0.3 (s, $SiMe_3$), 1.1 (s, $SiMe_3$), 21.1 (s, CH_3), 36.4 (t, $^{1}J_{CP}$ = 20 Hz, dppm), 88.8 (t, $^{2}J_{CP}$ = 10 Hz, C_2SiMe_3), 93.1 (s, $C{\equiv}CSiMe_3$), 105.3 (t, $^{2}J_{CP}$ = 10 Hz, C_2SiMe_3), 105.7 (s, $C{\equiv}CSiMe_3$), 115.3 (s, *p*-Ar-CH_3), 121.4 (s, *o/m*-Ar), 124.6 (s, *o/m*-Ar), 125.7 (s, *o/m*-Ar), 128.0 (pseudo t, $^{3}J_{CP}$ = 5 Hz, *m*-PPh_2), 126.5 (pseudo t, $^{3}J_{CP}$ = 5 Hz, *m*-PPh_2), 129.3 (s, *p*-PPh_2), 129.6 (s, *p*-PPh_2), 130.3 (s, *o/m*-Ar), 130.7 (s, *o/m*-Ar), 130.8 (pseudo t, $^{2}J_{CP}$ = 6 Hz, *o*-PPh_2), 132.7 (pseudo t, $^{2}J_{CP}$ = 6 Hz, *o*-PPh_2), 133.0 (s, *o/m*-Ar), 133.8 (s, *p*-Ar), 134.9 (pseudo t, $^{1}J_{CP}$ = 17 Hz, *i*-PPh_2), 138.4 (unresolved pseudo triplet, *p*-Ar cluster), 139.1 (pseudo t, $^{1}J_{CP}$ = 24 Hz, *i*-PPh_2), 144.5 (s, *i*-Ar-CH_3), 144.8 (s, *i*-Ar cluster), 148.4 (s, *i*-Ar), 203.2 (s, CO), 207.3 (s, CO). ^{31}P NMR: δ 36.0. MALDI(+)-MS (*m/z*): $[M\text{-}4CO]^+$. IR (CH_2Cl_2): ν(C≡C) 2149w; ν(CO) 2016m, 1988s, 1961m, 1941w cm^{-1}. Anal. Calcd ($C_{58}H_{55}Co_2NO_4P_2Si_2$): C, 65.34; H, 5.20; N, 1.31. Found: C, 64.97; H: 5.16; N, 1.29 %.

[{$Co_2(CO)_4$(dppm)}$_2${μ-(Me_3SiC_2-4-C_6H_4)$_2$N(C_6H_4Me-4)}] (**40b**): ^{1}H NMR: δ 0.39 (s, 18H, $SiMe_3$), 2.35 (s, 3H, CH_3), 3.32 – 3.37 (t, 4H, dppm), 6.88 – 7.26 (m, 52H, 40H Ph + 12H Ar). ^{13}C NMR: δ 1.2 (s, $SiMe_3$), 21.0 (s, CH_3), 36.2 (t, $^1J_{CP}$ = 20 Hz, dppm), 88.6 (t, $^2J_{CP}$ = 9 Hz, C_2SiMe_3), 105.9 (t, $^2J_{CP}$ = 8 Hz, C_2SiMe_3), 123.6 (s, *o/m*-Ar cluster), 125.0 (s, *o/m*-Ar-CH_3), 128.0 (pseudo t, $^3J_{CP}$ = 4 Hz, *m*-PPh_2), 128.5 (t, $^3J_{CP}$ = 4 Hz, *m*-PPh_2), 129.3 (s, *p*-PPh_2), 129.7 (s, *p*-PPh_2), 130.0 (s, *o/m*-Ar-CH_3), 130.6 (s, *o/m*-Ar cluster), 130.7 (pseudo t, $^2J_{CP}$ = 8 Hz, *o*-PPh_2), 132.8 (pseudo t, $^2J_{CP}$ = 6 Hz, *o*-PPh_2), 135.0 (pseudo t, $^1J_{CP}$ = 16 Hz, *i*-PPh_2), 137.0 (s, *p*-Ar cluster), 139.1 (pseudo t, $^1J_{CP}$ = 24 Hz, *i*-PPh_2), 145.2 (s, *i*-Ar-CH_3), 145.7 (s, *i*-Ar cluster), 203.4 (s, CO), 207.4 (s,CO). **p-Ar not observed / obscured.* ^{31}P NMR: δ 35.7. MALDI(+)-MS: 953.0 [M-4CO-{$Co_2(CO)_4$(dppm)}]$^+$]. IR (CH_2Cl_2): ν(CO) 2016m, 1989s, 1960m, 1942w cm^{-1}. Anal. Calcd ($C_{87}H_{77}Co_4NO_8P_4Si_2$): C, 62.17; H, 4.62; N, 0.83. Found: C, 62.10; H, 4.58; N, 0.83 %.

5.8.9 Reaction of $N(C_6H_4\text{-}4\text{-}C{\equiv}CSiMe_3)_3$ with $Co_2(CO)_6(dppm)$

The reagents $N(C_6H_4\text{-}4\text{-}C{\equiv}CSiMe_3)_3$ (0.05 g, 0.10 mmol), and $Co_2(CO)_6(dppm)$ (0.20 g, 0.30 mmol) was added to dry degassed toluene (8 ml) and heated to 60 °C for 2 hours. The solvent was removed and the crude residue purified by preparative TLC using CH_2Cl_2 and hexane (40:60). The first band was identified as $[Co_2\{\mu\text{-}Me_3SiC_2\text{-}4\text{-}C_6H_4N(C_6H_4\text{-}4\text{-}C{\equiv}CSiMe_3)_2\}(CO)_4(dppm)]$ (**41a**) (0.032 g, 28%), the second band as $[\{Co_2(CO)_4(dppm)\}_2\{\mu\text{-}Me_3SiC_2\text{-}4\text{-}C_6H_4)_2N(C_6H_4\text{-}4\text{-}C{\equiv}CSiMe_3)\}]$ (**41b**) (0.052 g, 30 %) and the third band as $[\{Co_2(CO)_4(dppm)\}_3\{\mu\text{-}Me_3SiC_2\text{-}4\text{-}C_6H_4)_3N]$ (**41c**) (0.016 g, 7 %). X-ray quality crystals of **41a** and **41b** were obtained from slow diffusion of methanol into a solution of CH_2Cl_2.

$[Co_2\{\mu\text{-}Me_3SiC_2\text{-}4\text{-}C_6H_4N(C_6H_4\text{-}4\text{-}C{\equiv}CSiMe_3)_2\}(CO)_4(dppm)]$ (**41a**): ^1H NMR: δ 0.25 (s, 18H, $SiMe_3$), 0.37 (s, 9H, $SiMe_3$), 3.30 (m, 2H, dppm), 7.10 (m, 32H, 20H Ph + 12H Ar). ^{13}C NMR: δ 0.2 (s, $SiMe_3$), 1.2 (s, $SiMe_3$), 36.5 (t, $^1J_{CP}$ = 20 Hz, dppm), 89.1 (t, $^2J_{CP}$ = 9 Hz, C_2SiMe_3), 93.8 (s, $C{\equiv}CSiMe_3$), 104.9 (t, $^2J_{CP}$ = 8 Hz, C_2SiMe_3), 105.3 (s, $C{\equiv}CSiMe_3$), 117.1 (s, *p*-Ar'), 123.3 (s, *o/m*-Ar'), 125.3 (s, *o/m*-Ar cluster), 128.0 (pseudo t, $^3J_{CP}$ = 5 Hz, *m*-PPh_2), 128.5 (pseudo t, $^3J_{CP}$ = 5 Hz, *m*-PPh_2), 129.4 (s, *p*-PPh_2), 129.7 (s, *p*-PPh_2), 130.8 (t, $^2J_{CP}$ = 6 Hz, *o*-PPh_2), 130.9 (s, *o/m*-Ar cluster), 132.7 (pseudo t, $^2J_{CP}$ = 6 Hz, *o*-PPh_2), 133.2 (s, *o/m*-Ar'), 134.9 (pseudo t, $^1J_{CP}$ = 17 Hz, *i*-PPh_2), 139.0 (pseudo t, $^1J_{CP}$ = 24 Hz, *i*-PPh_2), 139.6 (unresolved pseudo t, *p*-Ar cluster), 144.1 (s, *i*-Ar cluster), 147.4 (s, *i*-Ar'), 203.2 (s, CO), 207.3 (s, CO). ^{31}P NMR δ: 36.0. IR (CH_2Cl_2): ν(C≡C) 2152, ν(CO) 2045w, 2018m, 1991s, 1962m, 1942sh cm^{-1}. MALDI(+)-MS: 1035.0 $[M\text{-}4CO]^+$. Anal. Calcd ($C_{62}H_{61}Co_2NO_4P_2Si_3$): C, 63.81; H, 5.44 ; N, 1.21. Found: C, 62.10; H, 4.58; N, 0.83 %.

[{$Co_2(CO)_4$(dppm)}$_2${μ-Me_3SiC_2-4-C_6H_4)$_2$N(C_6H_4-4-C≡C$SiMe_3$)}] (**41b**): ^{1}H NMR: δ 0.25 (s, 9H, $SiMe_3$), 0.39 (s, 18H, $SiMe_3$), 3.33 (m, 4H, dppm), 7.12 (m, 52H, 40H Ph + 12 H Ar). ^{13}C NMR: δ 0.3 (s, $SiMe_3$), 1.2 (s, $SiMe_3$), 36.3 (t, $^1J_{CP}$ = 21 Hz, dppm), 88.9 (t, $^2J_{CP}$ = 11 Hz, cluster C_2SiMe_3), 93.4 (s, C≡C$SiMe_3$), 105.4 (t, $^2J_{CP}$ = 7 Hz, cluster C_2SiMe_3), 105.6 (s, C≡C$SiMe_3$), 115.9 (s, *p*-Ar'), 122.1 (s, *o/m*-Ar'), 124.8 (s, *o/m*-Ar cluster), 128.0 (pseudo t, $^2J_{CP}$ = 5 Hz, *m*-PPh_2), 128.5 (pseudo t, $^2J_{CP}$ = 5 Hz, *m*-PPh_2), 129.4 (s, *p*-PPh_2), 129.7 (s, *p*-PPh_2), 130.7 (pseudo t, $^3J_{CP}$ = 5 Hz, *o*-PPh_2), 130.8 (s, *o/m*-Ar cluster), 132.7 (pseudo t, $^3J_{CP}$ = 7 Hz, *o*-PPh_2), 133.1 (s, *o/m*-Ar'), 134.9 (pseudo t, $^1J_{CP}$ = 18 Hz, *i*-PPh_2), 138.8 (pseudo t, $^3J_{CP}$ = 2 Hz, *p*-Ar cluster), 139.0 (pseudo t, $^1J_{CP}$ = 23 Hz, *i*-PPh_2), 144.6 (s, *i*-Ar cluster), 148.1 (s, *i*-Ar'), 203.4 (s, CO), 207.3 (s, CO). ^{31}P NMR: δ: 35.9. IR (CH_2Cl_2): ν(C≡C) 2150, ν(CO) 2046w, 2018m, 1990s, 1962m, 1942sh cm^{-1}. MALDI(+)-MS: 1035.4 [M-4CO-{$Co_2(CO)_4$(dppm)}]$^+$. Anal. Calcd ($C_{91}H_{83}Co_4NO_8P_4Si_3$): C, 62.00; H, 4.75; N, 0.80. Found: C, 62.10; H, 4.58; N, 0.83 %.

[{$Co_2(CO)_4$(dppm)}$_3${μ-Me_3SiC_2-4-C_6H_4)$_3$N] (**41c**): ^{1}H NMR: δ 0.41 (s, 27H, $SiMe_3$), 3.36 (pseudo t, J = 12 Hz, 6H, dppm), 6.91 – 7.21 (m, 72 H, 60H Ph + 12H Ar). ^{13}C NMR: δ 1.2 (s, $SiMe_3$), 36.1 (t, $^1J_{CP}$ = 20 Hz, dppm), 88.7 (t, $^2J_{CP}$ = 9 Hz, C_2SiMe_3), 105.9 (t, $^2J_{CP}$ = 9 Hz, C_2SiMe_3), 123.9 (s, *o/m*-Ar cluster), 128.0 (pseudo t, $^3J_{CP}$ = 5 Hz, *m*-PPh_2), 128.5 (pseudo t, $^3J_{CP}$ = 4 Hz, *m*-PPh_2), 129.3 (s, *p*-PPh_2), 129.7 (s, *p*-PPh_2), 130.6 (pseudo t, $^2J_{CP}$ = 5 Hz, *o*-PPh_2), 130.7 (s, *o/m*-Ar cluster), 132.7 (pseudo t, $^2J_{CP}$ = 6 Hz, *o*-PPh_2), 134.9 (pseudo t, $^1J_{CP}$ = 16 Hz, *i*-PPh_2), 137.5 (pseudo t, $^3J_{CP}$ = 4 Hz, *p*-Ar cluster), 139.0 (pseudo t, $^1J_{CP}$ = 24 Hz, *i*-PPh_2), 145.3 (s, *i*-Ar cluster), 203.6 (s, CO), 207.4 (s, CO). ^{31}P NMR: δ 35.0. MALDI(+)-MS: 1035.1 [M-4CO-{$Co_2(CO)_4$(dppm)}$_2$]$^+$. IR (CH_2Cl_2): ν(CO) 2045w, 2017m, 1990s, 1962m, 1942sh cm^{-1}. Anal. Calcd ($C_{120}H_{105}Co_6NO_{12}P_6Si_3$): C: 60.63; H: 4.46, N: 0.60. Found: C: 60.62; H: 4.55; N, 0.62 %.

5.8.10 Preparation of [{$Co_2(CO)_4$(dppm)}{μ-($Me_3SiC_2C_6H_4$-4-Me)}] (42-Me)

The reagents Me-4-$C_6H_4C{\equiv}CSiMe_3$ (0.06 g, 0.32 mmol) and $Co(CO)_6$(dppm) (0.20 g, 0.32 mmol) was added to dry degassed toluene (8 ml) and heated to 80 °C under nitrogen overnight. The solvent was removed and the brown residue purified by preparative TLC using an eluent system of CH_2Cl_2 and hexane (70:30). One major band was observed and collected. A red-brown powder was obtained from CH_2Cl_2 and methanol and identified as [{$Co_2(CO)_4$(dppm)}{μ-($Me_3SiC_2C_6H_4$-4-Me)}] (**42-Me**) (0.097 g, 38 %). ^{1}H NMR: δ 0.35 (s, 9H, $SiMe_3$), 2.36 (s, 3H, CH_3), 3.21 – 3.40 (m, 2H, dppm), 6.97 – 7.26 (m, 24H, 20 Ph + 4 Ar). ^{31}P NMR δ 34.2. ^{13}C NMR: δ 1.24 (s, $SiMe_3$), 21.5 (s, CH_3), 36.0 (t, $^1J_{CP}$ = 21 Hz, dppm), 88.3 (t, $^2J_{CP}$ = 9 Hz, C_2SiMe_3), 106.4 (t, $^2J_{CP}$ = 7 Hz, C_2SiMe_3), 128.1 (pseudo t, $^3J_{CP}$ = 5 Hz, m-PPh_2), 128.6 (pseudo t, $^3J_{CP}$ = 5 Hz, m-PPh_2), 129.2 (s, p-PPh_2), 129.3 (s, o/m-Ar), 129.9 (s, p-PPh_2), 130.1 (s, o/m-Ar), 130.7 (pseudo t, $^2J_{CP}$ = 7 Hz, o-PPh_2), 133.1 (pseudo t, $^2J_{CP}$ = 7 Hz, o-PPh_2), 135.1 (m, i-PPh_2), 135.5 (s, i-Ar), 139.5 (pseudo t, $^1J_{CP}$ = 23 Hz, i-PPh_2), 140.1 (pseudo t, $^4J_{CP}$ = 3 Hz, Ar_p), 203.4 (s, CO), 207.7 (s, CO). MALDI(+)-MS: 690.1 $[M-4CO]^+$. IR (CH_2Cl_2): 2017m, 1989s, 1962m, 1940w cm^{-1}. Anal. Calcd ($C_{41}H_{38}Co_2O_4P_2Si$): C, 61.34; H, 4.77. Found: C, 61.04; H, 4.80.

5.9.References

1. F. A. Cotton and G. Wilkinson, *Advanced Inorganic Chemistry Fifth Edition*, John Wiley and Sons, 1988.
2. J. A. Bertrand, F. A. Cotton and W. A. Dollase, *J. Am. Chem. Soc.*, 1963, **85**, 1349-1350.
3. F. A. Cotton, *J. Chem. Educ.*, 1983, **60**, 713.
4. C. E. Housecroft, *Metal-Metal Bonded Carbonly Dimers and Clusters*, Oxford University Press, 1996.
5. K. Wade, in *Advances in Inorganic Chemistry and Radiochemistry*, eds. H. J. Emeléus and A. G. Sharpe, A, 1976, vol. 18, pp. 1-66.
6. P. Aguirre-Etcheverry and D. O'Hare, *Chem. Rev.*, 2010, **110**, 4839-4864.
7. P. J. Low and N. J. Brown, *J. Cluster Sci.*, 2010, **21**, 235-278.
8. P. Lemoine, *Coord. Chem. Rev.*, 1982, **47**, 55-88.
9. S. D. Glover, B. J. Lear, C. Salsman, C. H. Londergan and C. P. Kubiak, *Philos. Trans Roy. Soc. A*, 2008, **366**, 177-185.
10. C. H. Londergan, J. C. Salsman, S. Ronco, L. M. Dolkas and C. P. Kubiak, *J. Am. Chem. Soc.*, 2002, **124**, 6236-6237.
11. J. C. Salsman, S. Ronco, C. H. Londergan and C. P. Kubiak, *Inorg. Chem.*, 2005, **45**, 547-554.
12. B. J. Lear, S. D. Glover, J. C. Salsman, C. H. Londergan and C. P. Kubiak, *J. Am. Chem. Soc.*, 2007, **129**, 12772-12779.
13. R. S. Dickson and P. J. Fraser, *Adv. Organomet. Chem.*, 1974, **12**, 323-377.
14. P. A. Brooksby, N. W. Duffy, A. J. McQuillan, B. H. Robinson and J. Simpson, *J. Organomet. Chem.*, 1999, **582**, 183-187.
15. M. Arewgoda, P. H. Rieger, B. H. Robinson, J. Simpson and S. J. Visco, *J. Am. Chem. Soc.*, 1982, **104**, 5633-5640.
16. D. Osella and J. Fiedler, *Organometallics*, 1992, **11**, 3875-3878.
17. N. W. Duffy, C. J. McAdam, B. H. Robinson and J. Simpson, *J. Organomet. Chem.*, 1998, **565**, 19-28.
18. D. M. Hoffman, R. Hoffmann and C. R. Fisel, *J. Am. Chem. Soc.*, 1982, **104**, 3858-3875.
19. T. J. Snaith, P. J. Low, R. Rousseau, H. Puschmann and J. A. K. Howard, *J. Chem. Soc., Dalton Trans.*, 2001, 292-299.
20. M. Arewgoda, B. H. Robinson and J. Simpson, *J. Am. Chem. Soc.*, 1983, **105**, 1893-1903.
21. D. L. Thorn and R. Hoffmann, *Inorg. Chem.*, 1978, **17**, 126-140.
22. P. T. Chesky and M. B. Hall, *Inorg. Chem.*, 1981, **20**, 4419-4425.
23. M. L. Marcos, M. J. Macazaga, R. M. Medina, C. Moreno, J. A. Castro, J. L. Gomez, S. Delgado and J. González-Velasco, *Inorg. Chim. Acta*, 2001, **312**, 249-255.
24. B. M. Peake, P. H. Rieger, B. H. Robinson and J. Simpson, *J. Am. Chem. Soc.*, 1980, **102**, 156-163.
25. L. V. Casagrande, T. Chen, P. H. Rieger, B. H. Robinson, J. Simpson and S. J. Visco, *Inorg. Chem.*, 1984, **23**, 2019-2025.
26. P. A. Brooksby, N. W. Duffy, A. J. McQuillan, B. H. Robinson and J. Simpson, *J. Chem. Soc, Dalton Trans.*, 1998, 2855-2860.

27. C. J. McAdam, N. W. Duffy, B. H. Robinson and J. Simpson, *Organometallics*, 1996, **15**, 3935-3943.
28. D. Osella, L. Milone, C. Nervi and M. Ravera, *Eur. J. Inorg. Chem.*, 1998, 1473-1477.
29. A. Arnanz, C. Moreno, M.-L. Marcos, J. González-Velasco and S. Delgado, *Eur. J. Inorg. Chem.*, 2007, 5215-5225.
30. A. Arnanz, M.-L. Marcos, C. Moreno, D. H. Farrar, A. J. Lough, J. O. Yu, S. Delgado and J. González-Velasco, *J. Organomet. Chem.*, 2004, **689**, 3218-3231.
31. B. H. Dana, B. H. Robinson and J. Simpson, *J. Organomet. Chem.*, 2002, **648**, 251-269.
32. N. Duffy, J. McAdam, C. Nervi, D. Osella, M. Ravera, B. Robinson and J. Simpson, *Inorg. Chim. Acta*, 1996, **247**, 99-104.
33. L.-A. Hore, C. J. McAdam, J. L. Kerr, N. W. Duffy, B. H. Robinson and J. Simpson, *Organometallics*, 2000, **19**, 5039-5048.
34. M. A. Fox, M. A. J. Paterson, C. Nervi, F. Galeotti, H. Puschmann, J. A. K. Howard and P. J. Low, *Chem. Commun.*, 2001, 1610-1611.
35. B. Le Guennic, K. Costuas, J. F. Halet, C. Nervi, M. A. J. Paterson, M. A. Fox, R. L. Roberts, D. Albesa-Jove, H. Puschmann, J. A. K. Howard and P. J. Low, *C.R. Chim.*, 2005, **8**, 1883-1896.
36. P. J. Low, R. Rousseau, P. Lam, K. A. Udachin, G. D. Enright, J. S. Tse, D. D. M. Wayner and A. J. Carty, *Organometallics*, 1999, **18**, 3885-3897.
37. T. Ito, T. Hamaguchi, H. Nagino, T. Yamaguchi, H. Kido, I. S. Zavarine, T. Richmond, J. Washington and C. P. Kubiak, *J. Am. Chem. Soc.*, 1999, **121**, 4625-4632.
38. S. D. Glover, J. C. Goeltz, B. J. Lear and C. P. Kubiak, *Coord. Chem. Rev.*, 2010, **254**, 331-345.
39. P. Mücke, M. Linseis, S. Záliš and R. F. Winter, *Inorg. Chim. Acta*, 2011, **374**, 36-50.
40. C. G. Atwood and W. E. Geiger, *J. Am. Chem. Soc.*, 2000, **122**, 5477-5485.
41. W. Y. Man, J. L. Xia, N. J. Brown, J. D. Farmer, D. S. Yufit, J. A. K. Howard, S. H. Liu and P. J. Low, *Organometallics*, 2011, **30**, 1852-1858.
42. M. E. Stoll, S. R. Lovelace, W. E. Geiger, H. Schimanke, I. Hyla-Kryspin and R. Gleiter, *J. Am. Chem. Soc.*, 1999, **121**, 9343-9351.
43. Z. Ning and H. Tian, *Chem. Commun.*, 2009, 5483-5495.
44. P. J. Low, M. A. J. Paterson, A. E. Goeta, D. S. Yufit, J. A. K. Howard, J. C. Cherryman, D. R. Tackley and B. Brown, *J. Mater. Chem.*, 2004, **14**, 2516-2523.
45. Y. Shirota and H. Kageyama, *Chem. Rev.*, 2007, **107**, 953-1010.
46. P. J. Low, M. A. J. Paterson, H. Puschmann, A. E. Goeta, J. A. K. Howard, C. Lambert, J. C. Cherryman, D. R. Tackley, S. Leeming and B. Brown, *Chem. Eur. J*, 2004, **10**, 83-91.
47. K. Onitsuka, N. Ohara, F. Takei and S. Takahashi, *Dalton Trans.*, 2006, 3693-3698.
48. K. Onitsuka, M. Fujimoto, N. Ohshiro and S. Takahashi, *Angew. Chem. Int. Ed.*, 1999, **38**, 689-692.
49. K. Onitsuka, N. Ohara, F. Takei and S. Takahashi, *Organometallics*, 2007, **27**, 25-27.
50. R. L. Roberts, T. Schwich, T. C. Corkery, M. P. Cifuentes, K. A. Green, J. D. Farmer, P. J. Low, T. B. Marder, M. Samoc and M. G. Humphrey, *Adv. Mater.*, 2009, **21**, 2318-2322.

51. T. Schwich, M. P. Cifuentes, P. A. Gugger, M. Samoc and M. G. Humphrey, *Adv. Mater.*, 2011, **23**, 1433-1435.
52. A. Trujillo, R. Veillard, G. Argouarch, T. Roisnel, A. Singh, I. Ledoux and F. Paul, *Dalton Trans.*, 2012, **41**, 7454-7456.
53. G. Grelaud, M. P. Cifuentes, T. Schwich, G. Argouarch, S. Petrie, R. Stranger, F. Paul and M. G. Humphrey, *Eur. J. Inorg. Chem.*, 2012, **2012**, 65-75.
54. N. Gauthier, G. Argouarch, F. Paul, L. Toupet, A. Ladjarafi, K. Costuas, J.-F. Halet, M. Samoc, M. P. Cifuentes, T. C. Corkery and M. G. Humphrey, *Chem. Eur. J.*, 2011, **17**, 5561-5577.
55. L. S. Chia and W. R. Cullen, *Inorg. Chem.*, 1975, **14**, 482-485.
56. D. Maiti, B. P. Fors, J. L. Henderson, Y. Nakamura and S. L. Buchwald, *Chem. Sci.*, 2011, **2**, 57-68.
57. J. F. Hartwig, *Acc. Chem. Res.*, 2008, **41**, 1534-1544.
58. K. Sakamaki, J. Ohshita, A. Kunai, H. Nakao, A. Adachi and K. Okita, *Appl. Organomet. Chem.*, 2001, **15**, 939-946.
59. C. Xu, J.-F. Gong and Y.-J. Wu, *Tetrahedron Lett.*, 2007, **48**, 1619-1623.
60. G. Y. Li, G. Zheng and A. F. Noonan, *J. Org. Chem.*, 2001, **66**, 8677-8681.
61. R. Rama Suresh and K. C. Kumara Swamy, *Tetrahedron Lett.*, 2009, **50**, 6004-6007.
62. U. Christmann, R. Vilar, A. J. P. White and D. J. Williams, *Chem. Commun.*, 2004, 1294-1295.
63. C. V. Reddy, J. V. Kingston and J. G. Verkade, *J. Org. Chem.*, 2008, **73**, 3047-3062.
64. X. Y. Liu and S. L. Zhang, *Synlett*, 2011, 1137-1142.
65. N. S. Nandurkar, M. J. Bhanushali, M. D. Bhor and B. M. Bhanage, *Tetrahedron Lett.*, 2007, **48**, 6573-6576.
66. R. Chinchilla and C. Najera, *Chem. Soc. Rev.*, 2011, **40**, 5084-5121.
67. D. M. D'Alessandro and F. R. Keene, *Dalton Trans.*, 2004, 3950-3954.
68. J. E. Sutton and H. Taube, *Inorg. Chem.*, 1981, **20**, 3125-3134.
69. D. E. Richardson and H. Taube, *J. Am. Chem. Soc.*, 1983, **105**, 40-51.
70. D. E. Richardson and H. Taube, *Coord. Chem. Rev.*, 1984, **60**, 107-129.
71. F. Barrière, N. Camire, W. E. Geiger, U. T. Mueller-Westerhoff and R. Sanders, *J. Am. Chem. Soc.*, 2002, **124**, 7262-7263.
72. F. Barriere and W. E. Geiger, *J. Am. Chem. Soc.*, 2006, **128**, 3980-3989.
73. W. E. Geiger and F. Barriere, *Acc. Chem. Res.*, 2010, **43**, 1030-1039.
74. I. J. S. Fairlamb, A. R. Kapdi and A. F. Lee, *Org. Lett.*, 2004, **6**, 4435-4438.
75. J. D. Woollins, *Inorganic Experiments, 2nd ed (Wiley-VCH Verlag Gmbh, Weinheim, 2003).*
76. N. Miyaura and A. Suzuki, *Org. Syth. Coll*, 1993, **8**, 532.
77. D. R. Coulson, *Inorg. Synth.*, 1990, **28**, 107.
78. Y. J. Chang and T. J. Chow, *Tetrahedron*, 2009, **65**, 9626-9632.
79. M. J. Plater and T. Jackson, *Tetrahedron*, 2003, **59**, 4687-4692.
80. N. Sakai, R. Komatsu, N. Uchida, R. Ikeda and T. Konakahara, *Org. Lett.*, 2010, **12**, 1300-1303.
81. N. G. Connelly and W. E. Geiger, *Chem. Rev.*, 1996, **96**, 877-910.
82. M. Krejčik, M. Daněk and F. Hartl, *J. Electroanal. Chem.*, 1991, **317**, 179-187.
83. G. M. Sheldrick *SADABS* (University of Goettingen, Germany, 1996).
84. O. V. Dolomanov, L. J. Bourhis, R. J. Gildea, J. A. K. Howard and H. Puschmann, *J. Appl. Crystallogr.*, 2009, **42**, 339-341.

85. G. M. Sheldrick, *Acta Crystallogr. A*, 2008, **64**, 112-122.

Chapter 6. Gold Mediated Sonogashira Cross-Coupling Reactions

6.1 Introduction

A catalyst is a substance which increases the rate of a chemical reaction, by providing an alternative pathway from the reactants to the products, through a transition state with a lower free energy of activation, G_{act}, Figure 6.1. Catalysts can accelerate the rate of a thermodynamically feasible reaction and improve the efficiency and selectivity of a reaction. As the catalyst is not consumed during the reaction, and is regenerated at a later stage at the end of the reaction, small quantities of the catalyst are generally required relative to the reagents being transformed. In principle, catalysts can be recovered unchanged at the end of a reaction, though in reality catalyst separation and recovery is rarely undertaken.

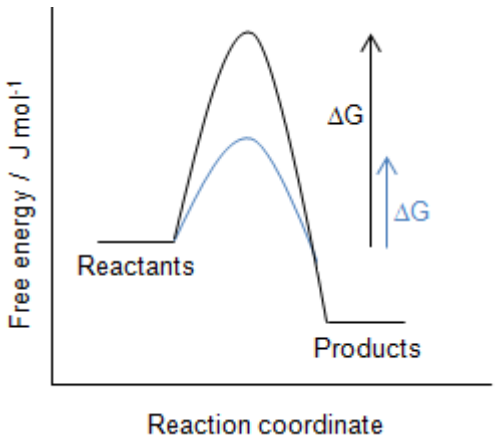

Figure 6.1. Reaction co-ordinate diagram for a catalysed and uncatalysed chemical reaction.

Transition metal based catalysts can be divided into two key reaction sequences; base metals such as iron mediate catalytic reactions which involve one-electron transfer radical chemistry;[1, 2] noble metals such as palladium, perform catalytic reactions that involve two electron transfer processes.[3] The latter class of reactions have emerged as tools of immense importance in modern synthetic chemistry, with the two-electron processes of oxidative addition and reductive elimination key to the many examples of palladium mediated cross-coupling reactions for which Suzuki, Negishi and Heck were jointly awarded the 2010 Nobel Prize in Chemistry. There is a current drive to use base metal catalysts to mimic noble metal catalysts, allowing for the development of first row transition metal catalysts for cross-coupling reactions. This typically involves the use of redox-active 'non-innocent' ligands which replace the usual change in metal oxidation state in for example oxidative addition reactions by the ligand undergoing two one electron oxidation reactions.[4-7] In addition to these electron transfer processes, metals can also play a role in mediating the transfer of substrates to other metals in a process known as 'transmetallation', and in supporting unusual formal charge and electronic states, for example in Grubb's olefin metathesis which involves intermediate carbenes and metallacyclobutadienes.[8, 9]

6.1.1 Gold Catalysis

Gold is a noble metal, it is also an inert metal with a high normal potential of +1.50 V. The high cost of gold has often led to the assumption that it would be unaffordable as a catalyst.[10] However, metals such as rhodium and palladium are significantly more expensive than gold yet the importance of these metals in catalytic processes on an industrial scale is firmly established.[11] In the 1980's, there were some fundamental breakthroughs which served to kindle the interest of gold as a catalyst in the scientific community.[12] Amongst these are the hydrochlorination of acetylene by Au^{3+} ions[13] and carbon monoxide oxidation on supported gold nanoparticles at low temperatures, Scheme 6.1.[14]

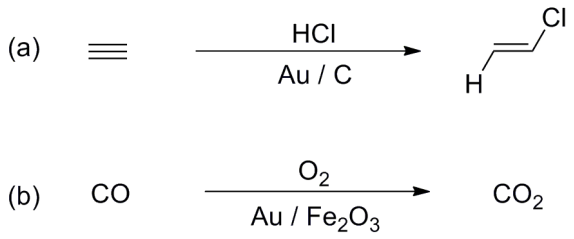

Scheme 6.1. (a) Hydrochlorination of acetylene (b) carbon monoxide oxidation.

Gold catalysis is now recognised as being applicable in a wide range of organic transformations, for example in gold catalysed hydrogenation, oxidation and nucleophilic reactions, Scheme 6.2.[10, 15] One of the most fundamental reactivity patterns in gold catalysed organic reactions is the addition of a nucleophile to a carbon-carbon multiple bond, for example in an alkyne, alkene or allene.[16] The potential of gold to act as a catalyst as a cationic Au(I) or Au(III) species lies in its ability to act as a π-Lewis acid. This has the effect of removing electron density away from a triple bond in an alkyne allowing nucleophilic attack of the substrate, Scheme 6.3.[17]

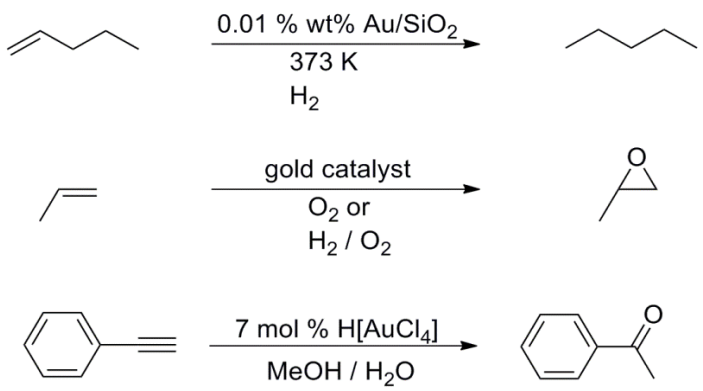

Scheme 6.2. Gold catalysed hydrogenation, oxidation reactions and nucleophilic addition reactions.

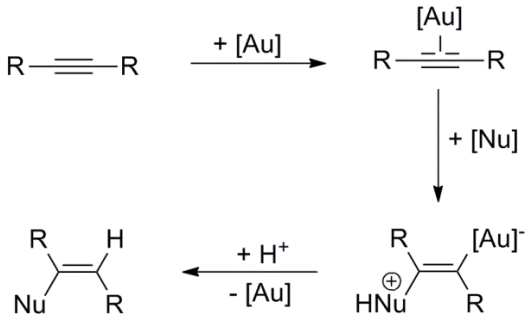

Scheme 6.3. Gold catalysed nucleophilic addition.

There are also many examples of gold catalysed oxidative coupling reactions which use the gold(III/I) redox couple and which rely on external oxidants such as $PhI(OAc)_2$,[18] Selectfluor,[19-22] AgOTf[23] and ^{t}BuOOH[24] to change the oxidation state of the gold species. For example, Wegner and co-workers reported a gold catalysed cyclisation of aryl propargyl esters, which is catalysed by an Au(III) species, but which after oxidative coupling, requires an oxidant, in this case, ^{t}BuOOH to re-oxidise an Au(I) species back into a catalytically active Au(III) species, Scheme 6.4.

The ability of gold to cross-couple unactivated substrates in organic transformations is a remarkable and achievable prospect which may be attributed to the viability of the gold(III/I) redox couple in cross-coupling reactions, albeit involving an external stoichiometric oxidant. In 2010, Nevado and co-workers reported the functionalisation of a C-H bond through a gold catalysed ethynylation of a deactivated arene ring with an electron deficient alkyne, a reaction which by more traditional cross-coupling methods would be challenging, Scheme 6.5.[25]

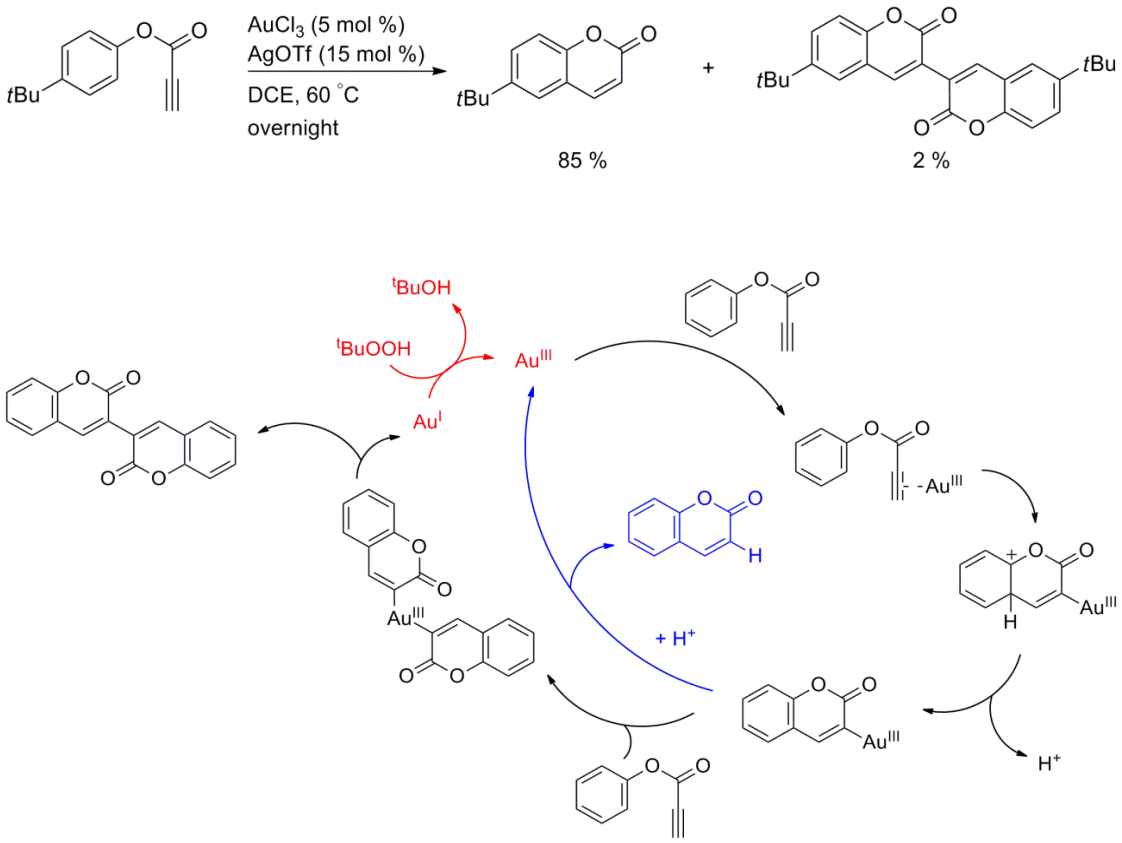

Scheme 6.4. Reaction scheme and proposed reaction mechanism.

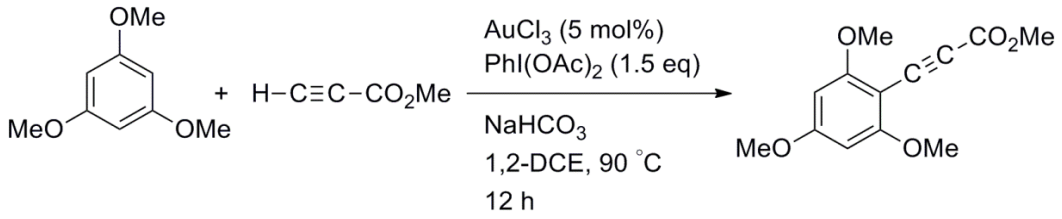

Scheme 6.5. A gold catalysed ethynylation reaction.

6.1.2 Gold Transmetallation

In addition to serving an active role in mediating the new bond forming reactions that lead from reactants to products, a metal may also play a role in the transfer of substrates to a catalytically active complex through a process known as 'transmetallation'. Transmetallation is defined as the exchange of ligands between two metal centres; it is an essential step in many catalytic cycles.[26] On a preparative scale, transmetallation reactions of tin[27-29] and mercury,[30, 31] silver[32] and copper[33-36] are well known, while those of gold have been by comparison, little explored. The transmetallation properties of gold first attracted interest a decade ago, with Yam and co-workers preparing tetranuclear copper(I) alkynyl complexes from the reaction between $[Cu(MeCN)]PF_6$ and alkynyl gold polymers of the form $[Au(C{\equiv}CAr')]_\infty$ in the presence of phosphines[37] and Ferrer and co-workers demonstrating the ready transfer of 4-pyridylethynyl from $[Au(C{\equiv}CPy)_2]^-$ salts to rhenium, following reactions with $[Re(THF)(CO)_3(bpy)]OTf$.[38]

In view of the isolobal relationship between the H^+ ion and the $[AuL]^+$ fragment, Figure 6.2, where L is a two electron donor, Van Koten and co-workers reported the transmetallation reactions between the organogold complex $[Au(NCN)(PPh_3)]$, where NCN = $[C_6H_3(CH_2\text{-}NMe_2)_2\text{-}2,6]$ and transition metal complexes such as $[NiCl_2(PPh_3)_2]$, $[PdCl_2(SEt_2)_2]$ and $[PtCl_2(SEt_2)_2]$, in quantitative yields, Scheme 6.6.[39-41] The by-product $AuCl(PPh_3)$ can be easily isolated from the reaction mixture and recycled, minimising cost.

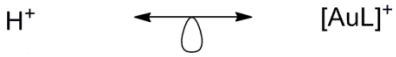

Figure 6.2. The H^+ ion and $[AuL]^+$ fragment are isolobal.

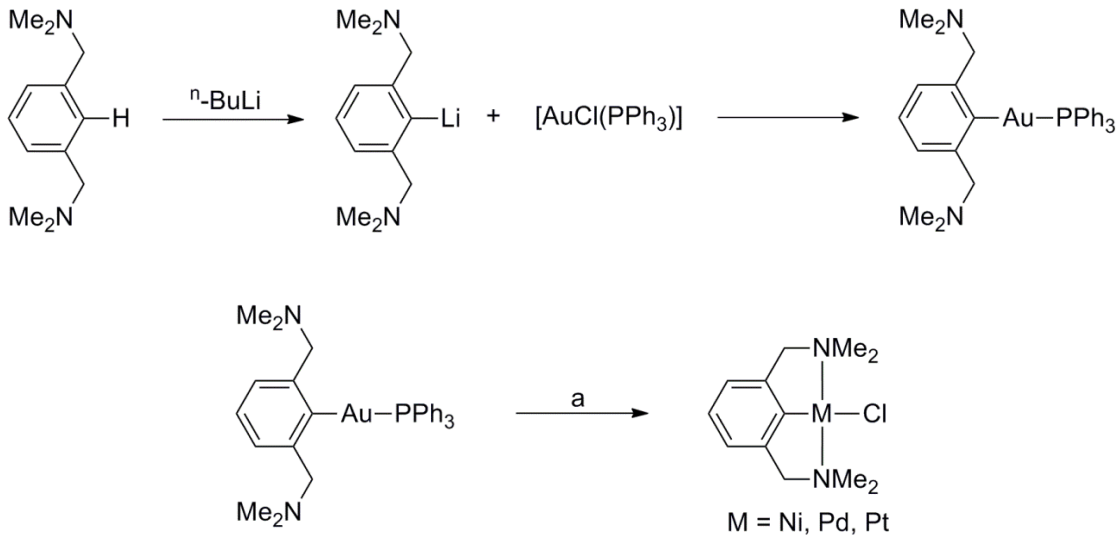

Scheme 6.6. Synthesis of $[Au(NCN)(PPh_3)]$ and transmetallation reactions of $[Au(NCN)(PPh_3)]$. (a) $[NiCl_2(PPh_3)_2]$, toluene, rt; $[PdCl_2(SEt_2)_2]$, toluene, rt; $[PtCl_2(SEt_2)_2]$, toluene, gentle reflux.[40]

Low and co-workers also reported the use of alkynyl-gold(I) complexes [Au(C≡CAr)(PPh_3)] where Ar = C_6H_5 and C_6H_4-Me-4 as reagents for the preparation of metal acetylide complexes, with transition metals such as FeCl(dppe)Cp, $RuCl(PPh_3)_2Cp$, and $NiBr(PPh_3)Cp$ to name but a few, in modest to good yields, Scheme 6.7,[42] demonstrating that gold is an effective transmetallation agent.

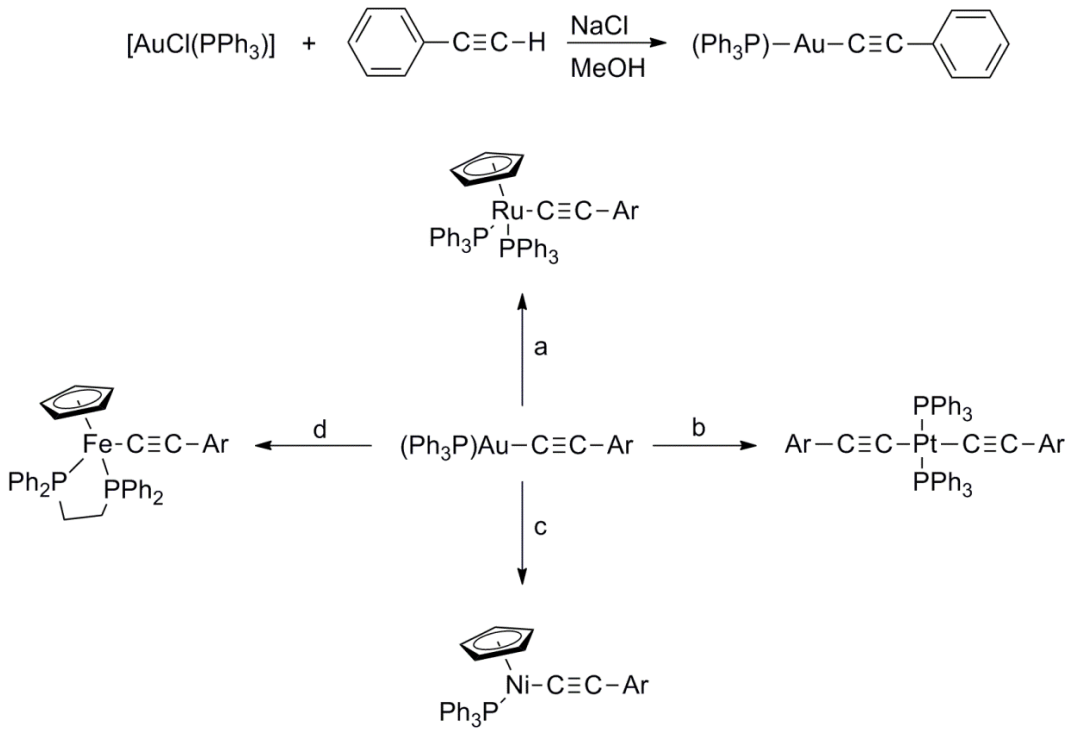

Scheme 6.7. Transmetallation reactions of [Au(C≡CAr)(PPh_3)], where Ar = C_6H_5. (a) $RuCl(PPh_3)_2Cp$, MeOH (b) *cis*-$PtCl_2(PPh_3)_2$ (c) $NiBr(PPh_3)Cp$ (d) FeCl(dppe)Cp, MeOH.[42]

6.1.3 Polyynes

Polyynes are a form of sp hybridised carbon of finite length, with alternate single and triple bonds and can be synthesised through oxidative-coupling reactions of smaller terminal (poly)ynes. These processes are typically catalysed by copper, for example in the Glaser[43] and the variant Eglinton-Galbraith[44, 45] and Hay reactions,[46] Scheme 6.8a – c. In the parent Glaser reaction, a Cu(I) acetylide complex is generated from the reaction of CuX and HC≡CR in the presence of a base. The closely related Eglinton-Galbraith reaction employs a stoichiometric amount of $Cu(OAc)_2$ while the Hay reaction uses a catalytic amount of Cu(I) and a bidentate chelating ligand, TMEDA, which improves the solubility of the copper acetylide complex, in the presence of O_2.[47] In addition, asymmetric diynes can be synthesised from the cross-coupling reaction between a terminal alkyne and an alkynyl halide using a source of Cu(I), Scheme 6.8d.

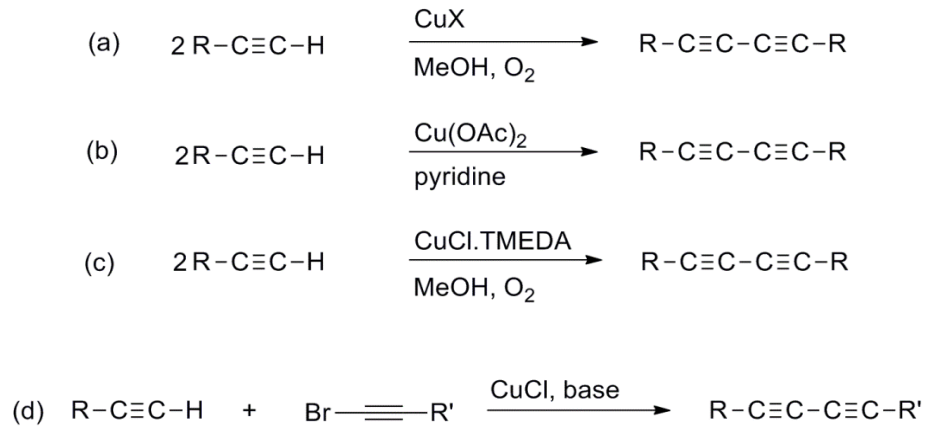

Scheme 6.8. Preparation of 1,3-diynes from terminal alkynes: (a) Glaser, (b) Eglinton-Galbraith and (c) Hay rections and asymmetric 1,3-diynes from (d) the Cadiot Chodkiewicz cross-coupling.

The Hay reaction is a particularly convenient method for preparation of 1,3-diynes in good yields, but the role of oxygen as an oxidant to recycle the copper has only recently been thoroughly addressed. Recent DFT studies of the Hay reaction between a Cu(I)-TMEDA alkyne complex with O_2 implicates a bimetallic intermediate with a [$Cu_2(\mu$-O_2)] core, and implies a formal oxidation of Cu(I) to Cu(III) with O_2 acting as a non-innocent oxidant,[48] Scheme 6.9, as opposed to a monometallic Cu(I) centre with oxygen as an innocent oxidant, as previously believed.[49] Rearrangement of **b** *via* the mononuclear complex **c**, followed by reductive elimination of the diyne gives two mononuclear Cu^{II} centres (**d**). A second cycle of alkyne acetylide addition, dimerisation and reductive elimination thus produces a second molecule of the diyne, at the same time restoring the copper catalyst to the + 2 oxidation state.[47] However, it should be noted the Hay procedure is not without potential hazards and in the preparation of 1,4-bis(trimethylsilyl)buta-1,3-diyne by a simple procedure, a serious explosion resulted, due to a source of ignition (likely a static discharge within the flask between a metal syringe needle and a digital temperature probe) in the presence of oxygen and an alkyne rich atmosphere.[50]

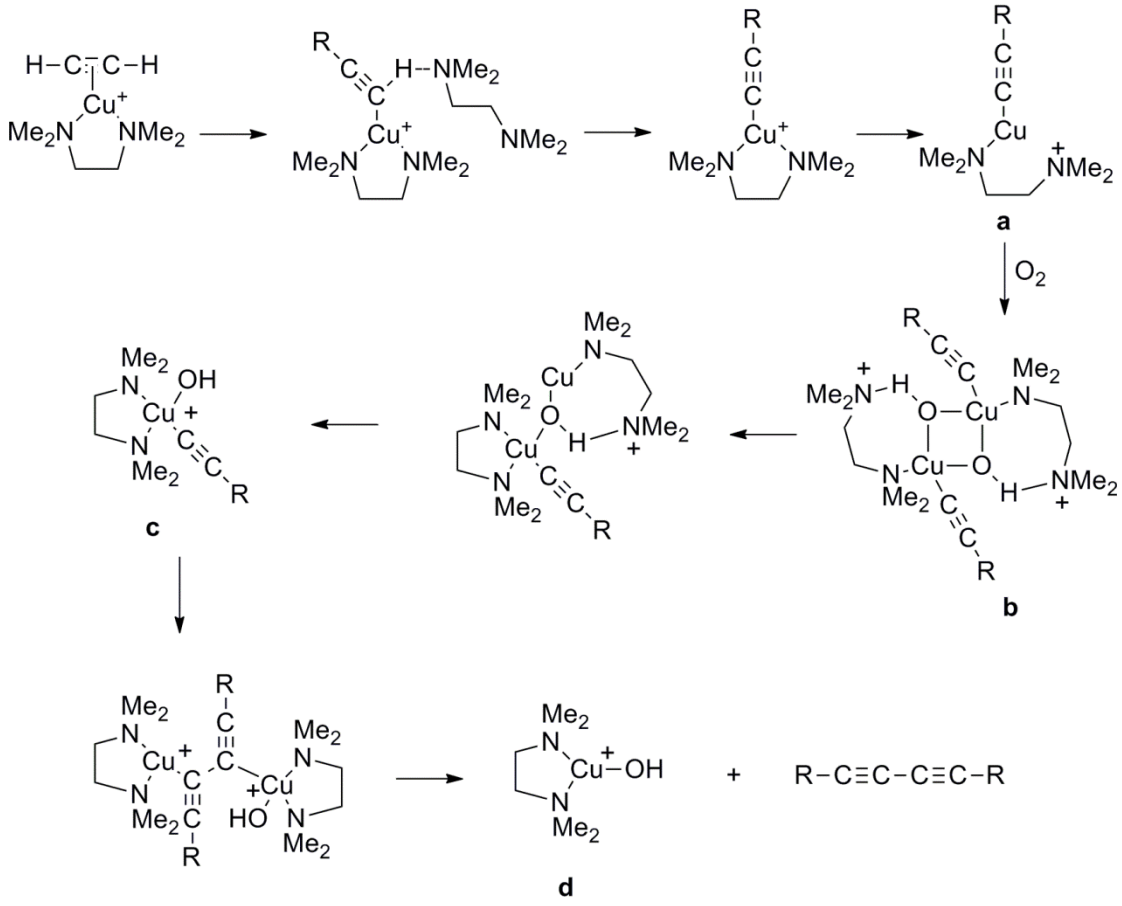

Scheme 6.9. Key mechanistic steps in the Hay reaction.[48]

Despite the number of synthetic routes to polyynes, they can still be difficult to generate, isolate and characterise.[51] This can be attributed to the length and thus stability of the terminal alkyne, the preparation of potentially explosive copper alkynes in the Glaser, oxygen in the Hay and pyridine and high temperatures in the Eglinton-Galbraith reactions. Alternate routes to polyynes include flash-vacuum pyrolysis, where linear polyynes can be synthesised from 3,4-dialkynyl-3-cyclobutene-1,2-diones from the ready loss of two carbonyl groups under pyrolytic conditions[52] and Pd/Cu mediated oxidative coupling of terminal alkynes mediated by a suitable oxidant. In the Sonogashira reaction, the reduction of Pd(II) to Pd(0) can lead to the homocoupling of terminal alkynes in the presence of oxygen.[53] The interception of a Sonogashira

reaction, *via* an *in-situ* desilylation, followed by a Glaser reaction can also lead to the formation of 1,4-disubstituted 1,3-diynes.[54]

Higher order polyynes have long been thought to be inherently unstable.[55] For example, in the initial isolation of an unsubstituted[56] and phenyl substituted hexatriyne,[57] explosions resulted on exposure to air and even at 0 °C under an inert atmosphere respectively. However in 2008, Bryce and co-workers[58, 59] reported a synthesis which led to the isolation of aryl hexatriyne and octatetrayne derivatives, [Ar-(C≡C)$_n$H] where n = 3 or 4, which were formed *via* iterative cross-coupling reactions of terminal 4-(3,6-di-*tert*-butyl-*N*-carbazolyl)phenyl alkynes with 1-iodo-4-trimethylsilyl butadiyne under Sonogashira conditions, Figure 6.3.[60] Subsequent desilylation and further cross-coupling reactions led to the synthesis of longer chain polyynes.

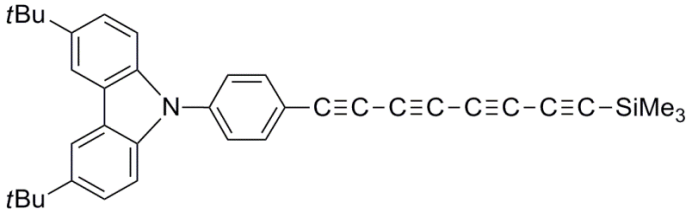

Figure 6.3. Aryl oligoyne with a carbazolyl end group.[60]

Using a similar approach, Tykwinski and co-workers[61] reported the isolation of the longest polyyne chain to date, with an impressive 44 carbon atoms stabilised by tris(3,5-di-*tert*-butylphenyl)methyl (Tr*) moieties, synthesised through a combination of modified Eglinton-Galbraith reactions, deprotection and oxidative dimerisation steps, Scheme 6.10.

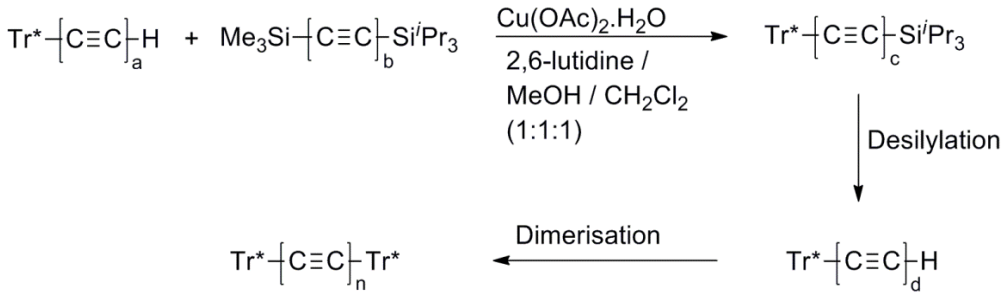

Scheme 6.10. Synthesis of a symmetric polyyne.[61]

Organometallic groups based on iron,[62] rhenium[63] and platinum derivatives,[64-67] along with cobalt,[68] ruthenium and osmium clusters[69] can also impart a substantial stabilising effect on polyynes. In 2006, Gladsyz and co-workers isolated and characterised a polyynediyl chain containing 28 carbon atoms spanned by bulky platinum end groups, Figure 6.4, which was synthesised using a combination of Hay couplings and desilylation protocols.[70]

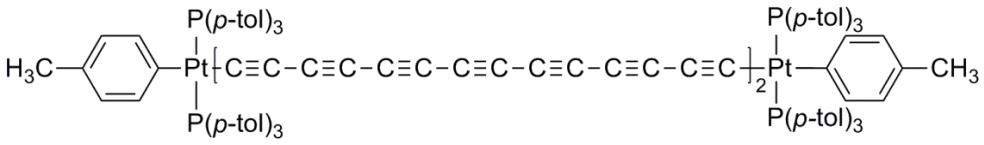

Figure 6.4. C_{28} polyynediyl chain spanned by bulky platinum end groups.

In addition to these routes to the preparation of long chain polyynes lies a curious gold-mediated variant of the Cadiot-Chodkiewicz cross-coupling that has been used to remarkable effect by the Bruce group, Scheme 6.11.[68, 69, 71-78] The use of stable gold(I) polyynes as intermediates greatly simplifies the preparation of polyynes, using air-stable and crystalline intermediates, whilst the gold can be readily recycled.

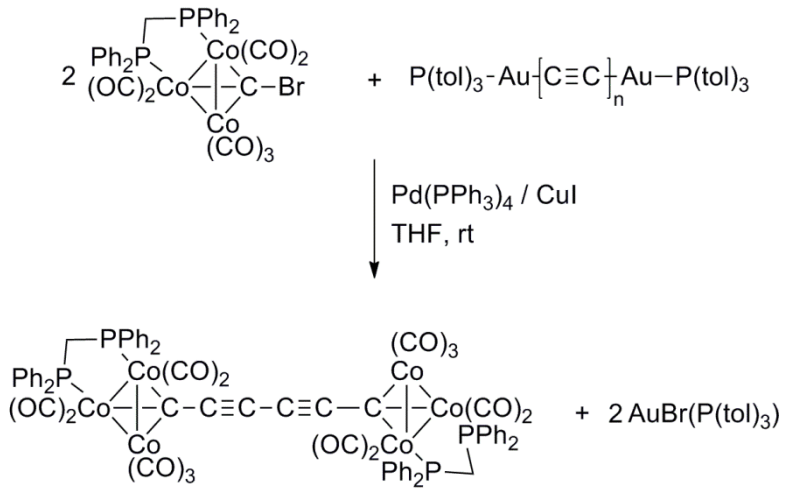

Scheme 6.11. Pd/Cu catalysed Cadiot-Chokiewicz cross-coupling with a haloalkyne.

Thus the demonstration of the facile transfer of an alkynyl ligand fragment from a relatively inert Au(I) centre to Cu(I) and then to the catalytically active Pd(II) centre prompts consideration of similar sequences of transmetallation steps to promote the transfer of stable Au(I) polyynes into other palladium catalysed cross-coupling reactions.

6.1.4 The Sonogashira Reaction

The Sonogashira cross-coupling reaction is used extensively in synthetic chemistry to create carbon-carbon bonds. It typically involves the reaction between a sp hybridised carbon of an alkyne with a sp^2 hybridised carbon of an aryl halide and requires a source of Pd(0) and CuI as a co-catalyst in an amine solvent.[79] The role of the co-catalyst copper iodide is important, as it activates the alkyne in the form of a copper acetylide and transmetallation to an organopalladium(II) species, formed by the oxidative addition of an aryl halide to a Pd(0) species, Scheme 6.12. Subsequent reductive elimination generates a cross-coupled product and at the same time regenerates the Pd(0) catalyst.[80]

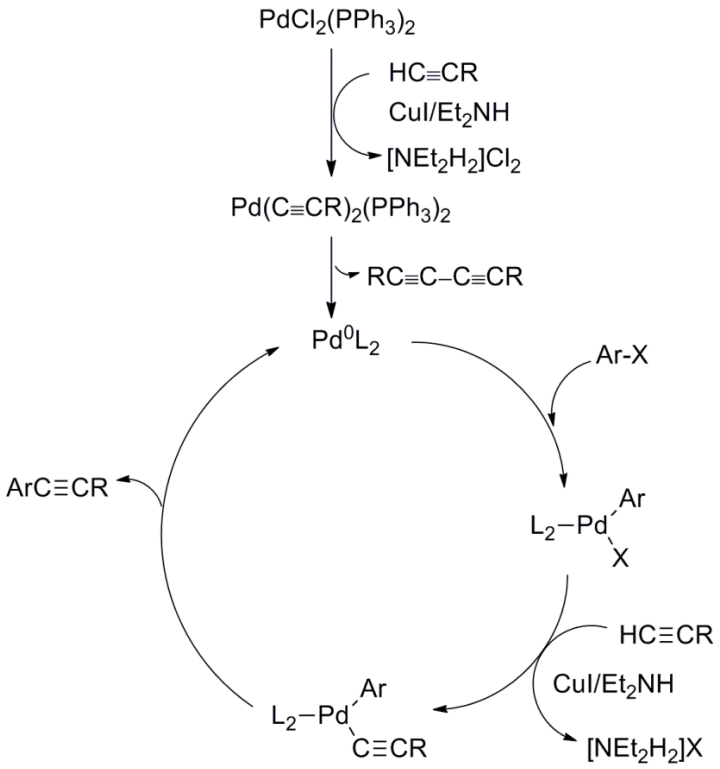

Scheme 6.12. Sonogashira cross-coupling reaction.

Recently, it has been proposed that Au(I) with the same electronic configuration as Pd(0) can catalyse reactions typically catalysed by palladium. For example, in 2007 Corma and co-workers reported that Au(I) is selective for performing a copper-free Sonogashira cross-coupling reaction.[81] Likewise in 2008, Wang and co-workers reported similar observations where a terminal alkyne reacted with aryl iodides and bromides in the presence of a AuI/dppf catalyst system in toluene to generate cross-coupled products in good yields, Scheme 6.13.[82]

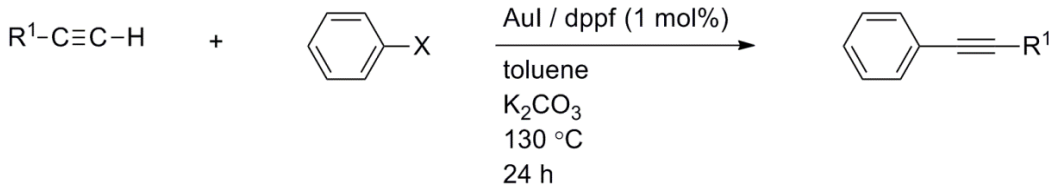

Scheme 6.13. A gold iodide catalysed Sonogashira reaction.

However, very recent re-examination of conditions suggests that this is due to adventitious palladium contamination of the gold salts used in the reaction. For example, Echavarren and co-workers found that as little as 0.1 % palladium in the form of $[Pd_2(dba)_3]$ and 2 mol% AuI/dppe with K_2CO_3 as a base leads to the cross-coupling of 4-iodoacetophenone with 1-ethynyl-4-methylbenzene in toluene under reflux conditions, Table 6.1.[83] Similar results have also been obtained from mixed Pd/Au cross-coupling reactions of aryl halides[84, 85] and arene diazonium salts[86] with terminal alkynes in amine solvents in ambient to reflux point of the solvent, where no effective coupling was observed in the absence of palladium, though kinetic and theoretical studies suggest otherwise.[87] Thus these reactions can be considered as analogues of the conventional Sonogashira reaction, with the gold reagent taking the place of the more commonly employed Cu(I) salts.

Table 6.1. The Au/Pd catalysed cross-coupling of 4-iodoacetophenone and tolylacetylene.

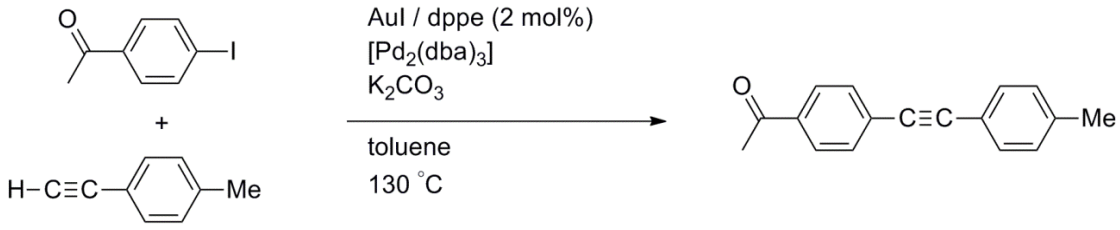

Pd/mol %	Conversion / %	Yield / %
-	< 2	< 2
1.2×10^{-4}	6	6
1.2×10^{-3}	16	16
1.2×10^{-2}	24	24
0.12	100	82
1.2	100	78
1.2	< 2	< 2[a]

[a] room temperature

In 2007, Laguna and co-workers found that Au(I) which is isoelectronic with Cu(I) acts as an efficient co-catalyst in palladium catalysed cross-couplings, Scheme 6.14. However, despite the fact that the most efficient Au(I) catalyst is still ten times slower than the most efficient Cu(I) catalyst (which is critical not only as a transmetallation agent, but also in assisting the re-oxidation of Pd(0) to Pd(II)),[88] there are still several advantages to using Au(I) over Cu(I). For example, reactions can be performed in technical grade solvents without the need for purification or air exclusion and reactions are cleaner with no evidence of homocoupling.[84] The inferior ability of gold to change oxidation states might also guarantee highly selective reactions due to the orthogonal reactivity of palladium to gold.[89]

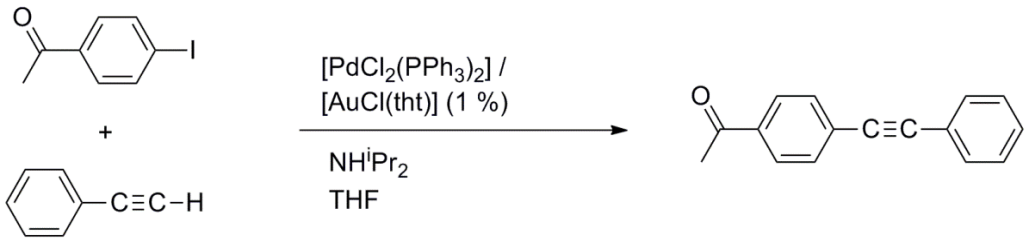

Scheme 6.14. A palladium catalysed cross-coupling, with gold as a co-catalyst.

6.2 Results and Discussion

Pre-formed gold alkynyl complexes Au(C≡CAr)(PPh_3) can be cross-coupled with aryl iodides Ar'-X under 'copper-free' palladium catalysed conditions to give cross-coupled tolans Ar-C≡C-Ar' in quantitative yields. However, these reactions require rather forcing conditions, Scheme 6.15.[83] Given that Bruce has shown that organometallic halides and gold alkynyl derivatives can be cross-coupled in the presence of both Pd(II) and Cu(I) under milder conditions in ether-based solvents at room temperature (*vide supra*), in this work a range of simple cross-coupling reactions of Au(C≡CPh)(PPh_3) (**43**) were explored, Table 6.2.

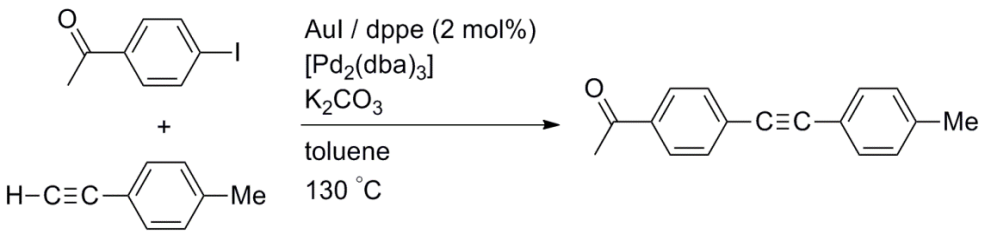

Scheme 6.15. A palladium-catalysed cross-coupling of 4-iodoacetophenone with a gold(I) alkynyl complex.[83]

The reaction **43** with iodobenzene in THF in 1 mol % of $PdCl_2(PPh_3)_2$ and CuI resulted in complete conversion to diphenylacetylene within 2 hours. However, in the absence of either of the co-catalysts, little or no conversion was detected. The reaction of **43** with bromobenzene proceeded significantly more slowly whilst chlorobenzene is an inactive coupling partner, consistent with the ease of oxidative addition of the aryl halide to the palladium co-catalyst.

Table 6.2. Effect of catalyst and halide on the Sonogashira cross-coupling of 43 with aryl halides. Reaction conditions (a) $PdCl_2(PPh_3)_2$ / CuI, THF.

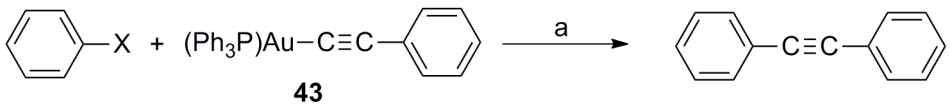

43

Ar-X	[Pd][a] / mol%	CuI / mol%	T / °C	t / h	% conversion
C_6H_5I	-	5	60	17	-
C_6H_5I	5	-	60	17	-
C_6H_5I	1	1	60	2	100
C_6H_5Br	5	5	60	22	Trace
C_6H_5Cl	5	5	60	22	-

The cross-coupling of **43** and other substituted aryl halides was also investigated, Table 6.3. The most activated aryl halides 1-iodo-4-nitrobenzene and methyl-4-benzoate cross-coupled smoothly with **43** at 25 °C in 1.5 hours, with 100 % conversion. When tested on a preparative scale, the reaction of **43** and 1-iodo-4-nitrobenzene led to the isolation of 1-phenyl-2-(4'-nitrophenyl)acetylene in 87 % yield. The protocol therefore appears to be a viable method to synthesise tolans from gold protected alkynes, though further experiments are necessary to establish the full extent to which it can be used. The more deactivated aryl halides 4-iodoaniline and 4-iodoanisole required higher temperatures (60 °C) but nevertheless showed 100 % conversion within 2 hours. The most activated aryl bromide 1-bromo-4-nitrobenzene was once again an inactive coupling partner, attributed to the formation of a weaker and therefore less thermodynamically favourable Au-Br compared to an Au-I bond.

Table 6.3. Effect of the R substituent on the Sonogashira cross-coupling of 43 with aryl halides. Reaction conditions (a) $PdCl_2(PPh_3)_2$ / CuI, THF.

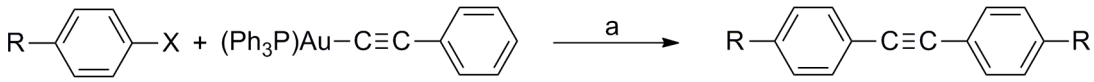

43

Ar-X	[Pd][a] / mol%	CuI / mol%	T / °C	t / h	%conversion
$IC_6H_4NO_2$	1	1	25	1.5	100
$IC_6H_4CO_2Me$	1	1	25	1.5	100
$IC_6H_4NH_2$	1	1	25	16	-
$IC_6H_4NH_2$	1	1	60	2	100
IC_6H_4OMe	1	1	60	2	100
$BrC_6H_4NO_2$	1	1	25	20	-

When compared to the conditions reported by Echavarren and co-workers, a Pd(0)/CuI catalyst system allows gold acetylide complexes to be cross-coupled with aryl iodides under significantly milder conditions in ether based solvents without the need of an additional base. It is likely that an alkynyl moiety is transmetalled from Au(I) to Cu(I), before entering a conventional Sonogashira reaction, Scheme 6.16. There are also advantages over Nishihara's sila-Sonogashira protocol[90] when trying to cross-couple aryl halides with base sensitive substituents, for example the quantity of copper salts used, and a lower boiling THF solvent. In addition, despite the cost of gold, the liberated $AuX(PPh_3)$ complexes can often be recovered as a by-product and recycled or used directly in the formation of further gold alkynes, which helps minimise cost.

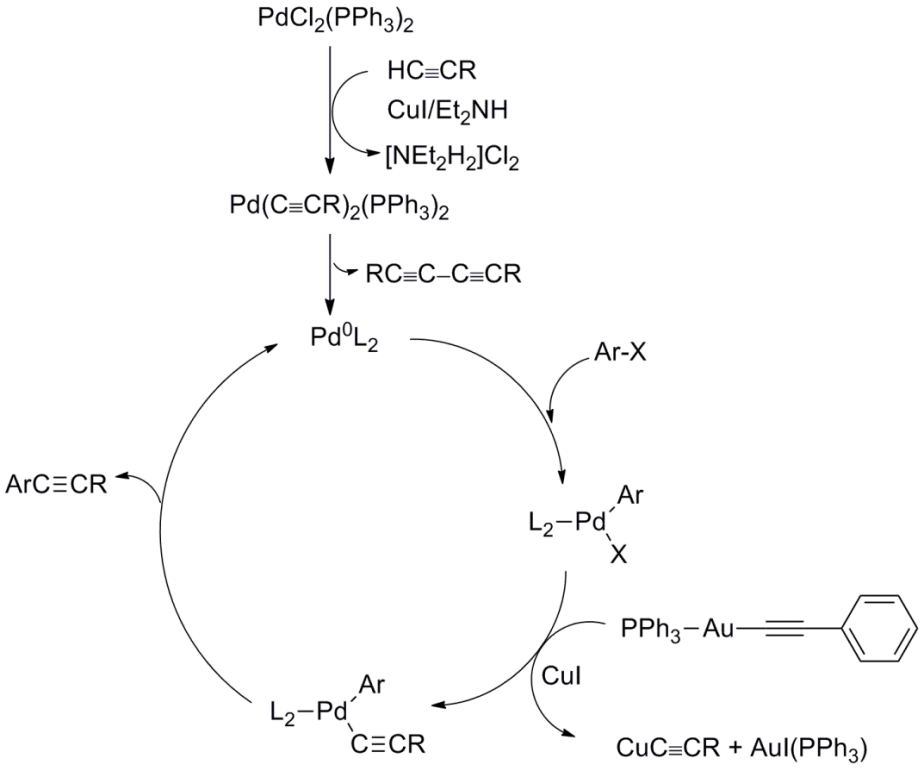

Scheme 6.16. A gold mediated Sonogashira reaction.

With these results in hand, the cross-coupling reactions of the bis(gold) complex (Ph_3P)AuC≡CC≡CAu(PPh_3) (**44**) were explored. Symmetric 1,4-substituted diynes are commonly synthesised *via* the oxidative homocoupling reactions of terminal alkynes. An alternative reaction sequence involves end group transformations of a pre-formed diyne. The bis(gold) complex (Ph_3P)AuC≡CC≡CAu(PPh_3) (**44**) was synthesised from the readily available Au(PPh_3)Cl and $Me_3SiC{\equiv}CC{\equiv}CSiMe_3$ in methanol, using sodium hydroxide as a base. However, since **44** is only sparingly soluble in THF, reactions were carried out in CH_2Cl_2 from this point onwards to ensure homogeneous reaction conditions. Complex **44** reacted smoothly with two molar equivalents of 4-iodo-nitrobenzene, 4-iodo-methylbenzoate, and 4-iodo-methylbenzene at room temperature in the presence of 0.5 mol% per gold equivalent of $PdCl_2(PPh_3)_2$ and CuI with almost complete conversion, Table 6.4.

Table 6.4. Cross-coupling reactions of 44 with aryl halides. Reaction conditions (a) $PdCl_2(PPh_3)_2$ / CuI, CH_2Cl_2.

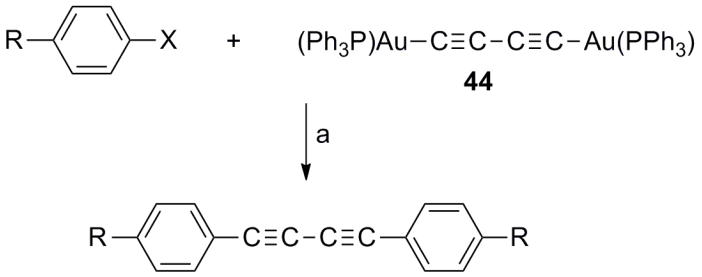

Ar-X	[Pd] / mol%	CuI / mol%	T / °C	t / h	%conversion
$IC_6H_4NO_2$	0.5	0.5	25	6	100
$IC_6H_4CO_2Me$	0.5	0.5	25	24	97
IC_6H_4Br	0.5	0.5	25	24	90
$IC_6H_4CH_3$	0.5	0.5	25	24	100
$IC_6H_4NH_2$	0.5	0.5	60	2	100
IC_6H_4OMe	0.5	0.5	60	2	100

The cross-coupling reactions of **44** with aryl halides bearing electron donating substituents were slow at room temperature but at elevated temperatures, reactions proceeded more smoothly with 100 % conversion. In addition, the reaction of **44** with 1-iodo-4-bromobenzene under the same conditions also proceeded with excellent chemoselectivity to afford 1,4-bis(4'-bromophenyl)-buta-1,3-diyne as the only detectable product. The results presented here complement those achieved for the oxidative dimerisation of 1-alkynes and whilst the process might not be deemed useful for the preparation of bulk quantities of material, it may be adventitious in the preparation of compound libraries, where a single, readily available diyne precursor is reacted with a wide range of aryl halides, Scheme 6.17a. This circumvents the sometimes laborious synthetic protocols requiring the initial pre-synthesis of the alkyne and entails a coupling and decoupling approach, Scheme 6.17b.

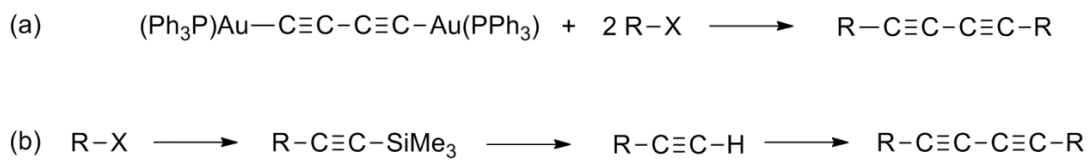

Scheme 6.17. Synthesis of substituted diynes from (a) a gold mediated cross-coupling reaction and (b) a coupling and decoupling approach.

In order to further test the applicability of these selected reaction conditions, the sequential reactions of **44** with different aryl iodides were examined. The initial reaction of **44** with one equivalent of 4-iodo nitrobenzene or 4-iodo methylbenzoate and a second aryl halide were however complicated by the facile reaction of the activated iodide with both gold groups and led to the detection of three different cross-coupled products by GC, Scheme 6.18. Cleaner reactions were obtained from the initial reaction of **44** and one equivalent of iodobenzene for three hours, followed by the treatment of another aryl iodide, Table 6.5. However, careful control of the first step of the reaction is required to avoid double coupling of **44** and iodobenzene to form 1,4-diphenyl-buta-1,3-diyne.

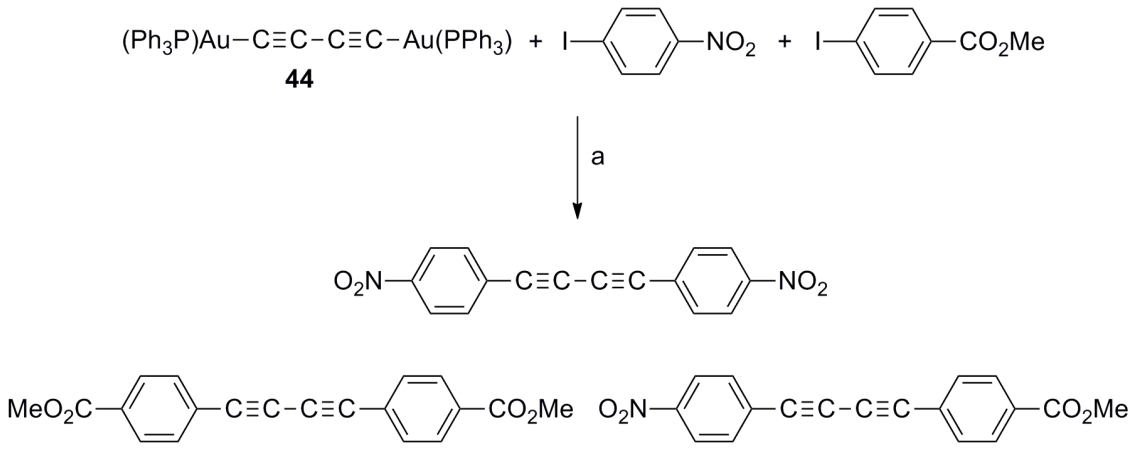

Scheme 6.18. A mixture of products obtained from the coupling of 44 and activated iodides. Reaction conditions (a) $PdCl_2(PPh_3)_2$ / CuI, CH_2Cl_2.

Table 6.5. Preparation of differentially substituted diynes. Reaction conditions (a) $PdCl_2(PPh_3)_2$ / CuI, CH_2Cl_2 (b) IC_4H_4R, $PdCl_2(PPh_3)_2$ / CuI, CH_2Cl_2.

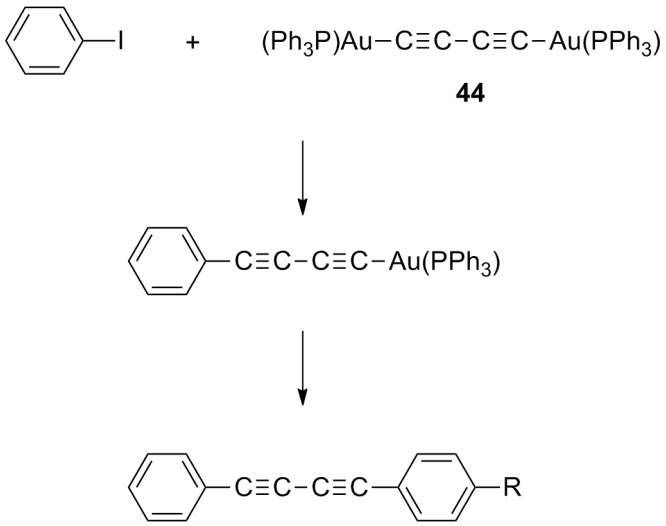

Ar-X	[Pd] / mol%	CuI / mol%	T / °C	t / h	%conversion
$IC_6H_4NO_2$	0.5	0.5	35	24	100
$IC_6H_4CO_2Me$	0.5	0.5	35	24	100
$IC_6H_4NH_2$	0.5	0.5	35	24	100
IC_6H_4OMe	0.5	0.5	35	24	100
IC_6H_4Br	0.5	0.5	35	24	100

6.3 Conclusions

Gold(I) alkynyl and diydiyl complexes can be cross-coupled with aryl iodides under mild conditions in the presence of both Pd(II) and CuI co-catalysts, in an ether based solvent and without the need for an additional base. This is likely to proceed *via* the ready transmetallation of the alkynyl fragment to Cu(I) followed by a conventional Sonogashira reaction. The masked butadiyne reagent $Me_3Si\text{-}C{\equiv}CC{\equiv}CSiMe_3$ can be converted to 1,4-diarylbuta-1,3-diynes *via* an intermediate bis(gold) diyne. Stepwise functionalisation of each Au moiety has been demonstrated to afford differentially 1,4-disubstituted 1,3-diynes, though careful control of the first step is required to avoid the double coupling of the first aryl halide. Therefore, gold mediated Sonogashira reactions are a useful method by which gold alkynyl complexes and an aryl halide under mild conditions can be coupled, without the need to expose the C-H functionality. This reaction is carried out at or near ambient temperature in common solvents, without the need for external oxidant.

6.4 Experimental

The compounds $AuCl(PPh_3)$,[91] $Au(C{\equiv}CPh)(PPh_3)$,[92] $Ph_3PAuC{\equiv}CC{\equiv}CAuPPh_3$,[93] and the catalyst $PdCl_2(PPh_3)_2$,[94] were prepared according to literature procedures, or with minor variations as described below. Other reagents were purchased and used as received. Reactions were performed under a nitrogen atmosphere in sealed air-tight test tubes, and GC vials were prepared and filled in an Innovative Technologies glove box. GC-MS analyses were performed on an Agilent Technologies 6890 N gas chromatograph equipped with a 5973 Inert Mass Selective Detector with a 10 m fused capillary column (5 % cross-linked phenylmethylsilicone) with UHP helium as the carrier gas. The percentage conversion of the starting material was monitored with reference to an internal dodecane calibrant, present in all solutions at 100 µl / 100 ml of solvent, estimated to be accurate within ±10 %.

6.4.1 General procedures

The gold reagent (25 µmol), aryl halide (25 µmol), $PdCl_2(PPh_3)_2$ (1.0 ml of a 1.24×10^{-3} M stock solution in THF, 1.24×10^{-6} mol), CuI (0.5 ml of a 2.47×10^{-3} M stock solution in NCMe, 1.24×10^{-6} mol) were added successively to a vial, topped up to 5 ml with THF and sealed with a rubber septum. The reaction was stirred, heated to 60 °C if indicated and monitored by GC-MS. For reactions described in Table 6.4, 50 µmol of aryl halide was used. For the reactions described in Table 6.5, 25 µmol of iodobenzene was used initially. After 3 hours of reaction at 35 °C, 25 µmol of the second aryl halide was added. The reaction was allowed to proceed overnight before analysis.

6.4.2 Preparations

6.4.2.1 Preparation of $AuCl(PPh_3)$

Triphenylphosphine (3.08 g, 11.7 mmol) was added to a solution of warmed ethanol (50 ml). To this solution, a filtered mixture of chloroauric acid (2.00 g, 5.87 mmol) was added. Over the course of fifteen minutes, a fine white precipitate developed and this was collected, washed with ethanol (2 x 5 ml) and dried under vacuum (1.15 g, 58 %). The compound was identified with comparisons to the literature.[91]

6.4.2.2 Preparation of $Au(C{\equiv}CPh)(PPh_3)$ (43)

In methanol (120 ml) was added $AuCl(PPh_3)$ (0.60 g, 1.21 mmol) and sodium (0.15 g, 6.50 mmol). A solution of phenylacetylene (0.12 g, 1.21 mmol) in methanol (5 ml) was then added slowly to the reaction over the course of fifteen minutes. The reaction was then allowed to stir for a further 3 hours and then the solvent removed. The grey powder was recrystallised from CH_2Cl_2 and diethyl ether to give a white powder (0.51 g, 75 %). The compound was identified with comparisons to the literature.[92]

6.4.2.3 Preparation of $(Ph_3P)AuC{\equiv}CC{\equiv}CAu(PPh_3)$ (44)

To a solution of methanol (120 ml) was added 1,4-bis(trimethylsilyl)buta-1,3-diyne (0.16 g, 0.80 mmol) and sodium hydroxide (0.64 g, 16.0 mmol). The reaction was stirred for 30 minutes, after which $AuCl(PPh_3)$ (0.75 g, 1.52 mmol) was added. The resulting white suspension was stirred for 3 hours. The white solid was collected and recrystallised from CH_2Cl_2 and diethyl ether (0.50 g, 65 %). The compound was identified with comparisons to the literature.[93]

6.4.2.4 Preparation of 1-phenyl-2-(4'-nitrophenyl) acetylene

In dry degassed THF (10 ml) was added $Au(C{\equiv}CPh)(PPh_3)$ (0.15 g, 0.27 mmol), 4-iodo nitrobenzene (0.07 g, 0.27 mmol), $PdCl_2(PPh_3)_2$ (9 mg, 0.01 mmol) and CuI (2 mg, 0.01 mmol). The reaction was stirred at room temperature for 4 hours, after which the solvent was removed. The residue was dissolved in the minimum volume of benzene and hexane added causing the precipitation of $AuI(PPh_3)$ as a white solid (0.11 g, 67 %). The resulting filtrate was purified using preparative TLC using hexane as an eluent. The first band was identified as $PhC{\equiv}CC{\equiv}CPh$ (2 mg, 6 %) and the second band as the title compound (0.05 g, 87 %). The last band contained a combination of $AuI(PPh_3)$ together with some identified material.

6.5 References

1. M. Tamura and J. K. Kochi, *J. Am. Chem. Soc.*, 1971, **93**, 1487-1489.
2. C. Bolm, J. Legros, J. Le Paih and L. Zani, *Chem. Rev.*, 2004, **104**, 6217-6254.
3. R. Chinchilla and C. Najera, *Chem. Rev.*, 2007, **107**, 874-922.
4. A. L. Smith, K. I. Hardcastle and J. D. Soper, *J. Am. Chem. Soc.*, 2010, **132**, 14358-14360.
5. W. I. Dzik, J. I. van der Vlugt, J. N. H. Reek and B. de Bruin, *Angew. Chem. Int. Ed.*, 2011, **50**, 3356-3358.
6. P. J. Chirik and K. Wieghardt, *Science*, 2010, **327**, 794-795.
7. W. Kaim, *Inorg. Chem.*, 2011, **50**, 9752-9765.
8. T. M. Trnka and R. H. Grubbs, *Acc. Chem. Res.*, 2000, **34**, 18-29.
9. G. C. Vougioukalakis and R. H. Grubbs, *Chem. Rev.*, 2010, **110**, 1746-1787.
10. A. S. K. Hashmi, *Chem. Rev.*, 2007, **107**, 3180-3211.
11. W. P. Griffith, *Platinum Met. Rev.*, 2003, **47**, 175-183.
12. M. Haruta, *Nature*, 2005, **437**, 1098-1099.
13. G. J. Hutchings, *J. Catal.*, 1985, **96**, 292-295.
14. M. Haruta, T. Kobayashi, H. Sano and N. Yamada, *Chem. Lett.*, 1987, 405-408.
15. A. S. K. Hashmi and G. J. Hutchings, *Angew. Chem. Int. Ed.*, 2006, **45**, 7896-7936.
16. R. Skouta and C.-J. Li, *Tetrahedron*, 2008, **64**, 4917-4938.
17. A. S. K. Hashmi and M. Rudolph, *Chem. Soc. Rev.*, 2008, **37**.
18. A. Iglesias and K. Muñiz, *Chem. Eur. J.*, 2009, **15**, 10563-10569.
19. M. N. Hopkinson, A. Tessier, A. Salisbury, G. T. Giuffredi, L. E. Combettes, A. D. Gee and V. Gouverneur, *Chem. Eur. J.*, 2010, **16**, 4739-4743.
20. G. Zhang, Y. Peng, L. Cui and L. Zhang, *Angew. Chem.*, 2009, **121**, 3158-3161.
21. G. Zhang, L. Cui, Y. Wang and L. Zhang, *J. Am. Chem. Soc.*, 2010, **132**, 1474-1475.
22. G. Zhang, Y. Peng, L. Cui and L. Zhang, *Angew. Chem. Int. Ed.*, 2009, **48**, 3112-3115.
23. A. K. Sahoo, Y. Nakamura, N. Aratani, K. S. Kim, S. B. Noh, H. Shinokubo, D. Kim and A. Osuka, *Org. Lett.*, 2006, **8**, 4141-4144.
24. H. A. Wegner, S. Ahles and M. Neuburger, *Chem. Eur. J.*, 2008, **14**, 11310-11313.
25. T. d. Haro and C. Nevado, *J. Am. Chem. Soc.*, 2010, **132**, 1512-1513.
26. C. Elschenbroich and A. Salzer, *Organometallics A Concise Introduction*, Wiley - VCH, Weinheim, Germany.
27. M. S. Khan, S. J. Davies, A. K. Kakkar, D. Schwartz, B. Lin, B. F. G. Johnson and J. Lewis, *J. Organomet. Chem.*, 1992, **424**, 87-97.
28. M. S. Khan, A. K. Kakkar, S. L. Ingham, P. R. Raithby, J. Lewis, B. Spencer, F. Wittmann and R. H. Friend, *J. Organomet. Chem.*, 1994, **472**, 247-255.
29. B. Cetinkaya, M. F. Lappert, J. McMeeking and D. E. Palmer, *J. Chem. Soc., Dalton Trans.*, 1973.
30. R. J. Cross and M. F. Davidson, *Inorg. Chim. Acta*, 1985, **97**, L35-L36.
31. A. F. Hill and R. P. Melling, *J. Organomet. Chem.*, 1990, **396**, C22-C24.
32. D. Miguel and V. Riera, *J. Organomet. Chem.*, 1985, **293**, 379-390.
33. O. Salah and M. Bruce, *Aust. J. Chem.*, 1976, **29**, 73-77.
34. M. Bruce, M. Humphrey, J. Matisons, S. Roy and A. Swincer, *Aust. J. Chem.*, 1984, **37**, 1955-1961.

35. K. Sonogashira, T. Yatake, Y. Tohda, S. Takahashi and N. Hagihara, *J. Chem. Soc., Chem. Commun.*, 1977, 291-292.
36. K. Sonogashira, Y. Fujikura, T. Yatake, N. Toyoshima, S. Takahashi and N. Hagihara, *J. Organomet. Chem.*, 1978, **145**, 101-108.
37. C.-L. Chan, K.-L. Cheung, W. H. Lam, E. C.-C. Cheng, N. Zhu, S. W.-K. Choi and V. W.-W. Yam, *Chem. Asian J.*, 2006, **1**, 273-286.
38. M. Ferrer, L. Rodríguez, O. Rossell, J. C. Lima, P. Gómez-Sal and A. Martín, *Organometallics*, 2004, **23**, 5096-5099.
39. M. Stol, D. J. M. Snelders, H. Kooijman, A. L. Spek, G. P. M. van Klink and G. van Koten, *Dalton Trans.*, 2007, 2589.
40. M. Contel, M. Stol, M. A. Casado, G. P. M. van Klink, D. D. Ellis, A. L. Spek and G. van Koten, *Organometallics*, 2002, **21**, 4556-4559.
41. M. Robitzer, I. Bouamaïed, C. Sirlin, P. A. Chase, G. van Koten and M. Pfeffer, *Organometallics*, 2005, **24**, 1756-1761.
42. W. M. Khairul, M. A. Fox, N. N. Zaitseva, M. Gaudio, D. S. Yufit, B. W. Skelton, A. H. White, J. A. K. Howard, M. I. Bruce and P. J. Low, *Dalton Trans.*, 2009, 610-620.
43. C. Glaser, *Ber. Dtsch. Chem. Ges.*, 1869, **2**, 422-424.
44. G. Eglinton and A. R. Galbraith, *Chem. Ind. (London)*, 1956, 737-738.
45. G. Eglinton and A. R. Galbraith, *J. Chem. Soc.*, 1959, 889-896.
46. A. S. Hay, *J. of Org. Chem.*, 1962, **27**, 3320-3321.
47. P. A. Schauer and P. J. Low, *Eur. J. Inorg. Chem.*, 2012, 390-411.
48. L. Fomina, B. Vazquez, E. Tkatchouk and S. Fomine, *Tetrahedron*, 2002, **58**, 6741-6747.
49. F. Bohlmann, H. Schönowsky, E. Inhoffen and G. Grau, *Chem. Ber.*, 1964, **97**, 794-800.
50. D. F. Perepichka and S. Jeeva, *Chem. Eng. News*, 2010, **88**, 2-2.
51. S. Szafert and J. A. Gladysz, *Chem. Rev.*, 2003, **103**, 4175-4205.
52. Y. Rubin, S. S. Lin, C. B. Knobler, J. Anthony, A. M. Boldi and F. Diederich, *J. Am. Chem. Soc.*, 1991, **113**, 6943-6949.
53. P. Nguyen, Z. Yuan, L. Agocs, G. Lesley and T. B. Marder, *Inorg. Chim. Acta*, 1994, **220**, 289-296.
54. E. Merkul, D. Urselmann and T. J. J. Müller, *Eur. J. Org. Chem.*, 2011, **2011**, 238-242.
55. F. Diederich and Y. Rubin, *Angew. Chem. Int. Ed.*, 1992, **31**, 1101-1123.
56. J. B. Armitage, C. L. Cook, E. R. H. Jones and M. C. Whiting, *J. Chem. Soc.*, 1952, 2010-2014.
57. J. B. Armitage, N. Entwistle, E. R. H. Jones and M. C. Whiting, *J. Chem. Soc. (Res)*, 1954, 147-154.
58. K. West, C. Wang, A. S. Batsanov and M. R. Bryce, *Org. Biomol. Chem.*, 2008, **6**, 1934-1937.
59. K. West, L. N. Hayward, A. S. Batsanov and M. R. Bryce, *Eur. J. Org. Chem.*, 2008, 5093-5098.
60. C. Wang, A. S. Batsanov, K. West and M. R. Bryce, *Org. Lett.*, 2008, **10**, 3069-3072.
61. W. A. Chalifoux and R. R. Tykwinski, *Nature Chem.*, 2010, **2**, 967-971.
62. J. T. Lin, J. J. Wu, C.-S. Li, Y. S. Wen and K.-J. Lin, *Organometallics*, 1996, **15**, 5028-5034.
63. R. Dembinski, T. Bartik, B. Bartik, M. Jaeger and J. A. Gladysz, *J. Am. Chem. Soc.*, 2000, **122**, 810-822.

64. W. Mohr, J. Stahl, F. Hampel and J. A. Gladysz, *Chem. Eur. J.*, 2003, **9**, 3324-3340.
65. W. Mohr, J. Stahl, F. Hampel and J. A. Gladysz, *Inorg. Chem.*, 2001, **40**, 3263-3264.
66. T. B. Peters, J. C. Bohling, A. M. Arif and J. A. Gladysz, *Organometallics*, 1999, **18**, 3261-3263.
67. J. Stahl, J. C. Bohling, E. B. Bauer, T. B. Peters, W. Mohr, J. M. Martín-Alvarez, F. Hampel and J. A. Gladysz, *Angew. Chem. Int. Ed.*, 2002, **41**, 1871-1876.
68. A. B. Antonova, M. I. Bruce, B. G. Ellis, M. Gaudio, P. A. Humphrey, M. Jevric, G. Melino, B. K. Nicholson, G. J. Perkins, B. W. Skelton, B. Stapleton, A. H. White and N. N. Zaitseva, *Chem. Commun.*, 2004, 960-961.
69. M. I. Bruce, P. A. Humphrey, G. Melino, B. W. Skelton, A. H. White and N. N. Zaitseva, *Inorg. Chim. Acta*, 2005, **358**, 1453-1468.
70. Q. Zheng, J. C. Bohling, T. B. Peters, A. C. Frisch, F. Hampel and J. A. Gladysz, *Chem. Eur. J.*, 2006, **12**, 6486-6505.
71. M. I. Bruce, M. E. Smith, N. N. Zaitseva, B. W. Skelton and A. H. White, *J. Organomet. Chem.*, 2003, **670**, 170-177.
72. M. I. Bruce, B. W. Skelton, A. H. White and N. N. Zaitseva, *J. Organomet. Chem.*, 2003, **683**, 398-405.
73. M. I. Bruce, M. L. Cole, M. Gaudio, B. W. Skelton and A. H. White, *J. Organomet. Chem.*, 2006, **691**, 4601-4614.
74. A. B. Antonova, M. I. Bruce, P. A. Humphrey, M. Gaudio, B. K. Nicholson, N. Scoleri, B. W. Skelton, A. H. White and N. N. Zaitseva, *J. Organomet. Chem.*, 2006, **691**, 4694-4707.
75. M. I. Bruce, B. W. Skelton, A. H. White and N. N. Zaitseva, *Organometallics*, 2006, **25**, 4817-4821.
76. M. I. Bruce, N. N. Zaitseva, B. K. Nicholson, B. W. Skelton and A. H. White, *J. Organomet. Chem.*, 2008, **693**, 2887-2897.
77. M. I. Bruce, M. L. Cole, C. R. Parker, B. W. Skelton and A. H. White, *Organometallics*, 2008, **27**, 3352-3367.
78. M. I. Bruce, B. K. Nicholson and N. N. Zaitseva, *C.R. Chim.*, 2009, **12**, 1280-1286.
79. E.-i. Negishi and L. Anastasia, *Chem. Rev.*, 2003, **103**, 1979-2018.
80. Z. Tan and E. Neigishi, *Handbook of Organopalladium Chemistry for Organic Synthesis*, Wiley, New York, 2002.
81. C. Gonzalez-Arellano, A. Abad, A. Corma, H. Garcia, M. Iglesias and F. Sanchez, *Angew. Chem. Int. Ed.*, 2007, **46**, 1536-1538.
82. P. Li, L. Wang, M. Wang and F. You, *Eur. J. Org. Chem.*, 2008, **2008**, 5946-5951.
83. T. Lauterbach, M. Livendahl, A. Rosellon, P. Espinet and A. M. Echavarren, *Org. Lett.*, 2010, **12**, 3006-3009.
84. L. A. Jones, S. Sanz and M. Laguna, *Catal. Today*, 2007, **122**, 403-406.
85. B. Panda and T. K. Sarkar, *Tetrahedron Lett.*, 2010, **51**, 301-305.
86. B. Panda and T. K. Sarkar, *Chem. Commun.*, 2010, **46**, 3131-3133.
87. A. Corma, R. Juarez, M. Boronat, F. Sanchez, M. Iglesias and H. Garcia, *Chem. Commun.*, 2011, **47**, 1446-1448.
88. A. S. Batsanov, J. C. Collings, I. J. S. Fairlamb, J. P. Holland, J. A. K. Howard, Z. Lin, T. B. Marder, A. C. Parsons, R. M. Ward and J. Zhu, *J. Org. Chem.*, 2004, **70**, 703-706.

89. A. S. K. Hashmi, C. Lothschuetz, R. Doepp, M. Rudolph, T. D. Ramamurthi and F. Rominger, *Angew. Chem. Int. Ed.*, 2009, **48**, 8243-8246.
90. Y. Nishihara, K. Ikegashira, A. Mori and T. Hiyama, *Chem. Lett.*, 1997, 1233-1234.
91. M. I. Bruce, B. K. Nicholson, O. Binshawkataly, J. R. Shapley and T. Henly, *Inorg. Synth.*, 1989, **26**, 324-328.
92. M. I. Bruce, E. Horn, J. G. Matisons and M. R. Snow, *Aust. J. Chem.*, 1984, **37**, 1163-1170.
93. C.-M. Che, H.-Y. Chao, V. M. Miskowski, Y. Li and K.-K. Cheung, *J. Am. Chem. Soc.*, 2001, **123**, 4985-4991.
94. H. C. Clark and K. R. Dixon, *J. Am. Chem. Soc.*, 1969, **91**, 596-599.

Chapter 7. Overall conclusions

Organometallic complexes featuring carbon rich ligands have been at the forefront of the studies of electron transfer reaction in bimetallic complexes. On the oxidation of these complexes, a number of different electronic situations can be generated. However, the language developed for MV systems is only applicable with clearly identifiable metal oxidation states. This was the case in a self assembled trimetallic molecular wire in Chapter 2, where the first and second oxidation events were unambiguously assigned to the stepwise oxidation of the redox-active organoiron moieties. Thus, on generation of the MV state, the low energy transition in the near-IR region was characteristic of a metal-metal charge transfer or IVCT transition.

Alternative situations can also arise, where the presence of a low energy transition cannot be attributed to IVCT. In such cases, it imperative to use a number of different spectroscopic techniques combined with theoretical studies to elucidate the site of oxidation within these complexes. For example, the triarylamine bridged dicobaltdicarbon tetrahedrane clusters in Chapter 5 are found to be Class I Robin and Day MV complexes, where on oxidation the electron is localised on a single metal centre, and does not interact with a second or third redox site. The low energy transition was assigned to an intracluster transition.

On the other side of the extreme, are organometallic complexes which possess a redox non-innocent ligand, as demonstrated in some mono- and bimetallic ruthenium vinyl and complexes featuring Tp or PMe_3 ligands (Chapter 3), and in bimetallic ruthenium vinyl and alkynyl complexes containing a dithia[3.3]paracyclophane bridging moiety (Chapter 4). In these complexes, electrochemistry, IR and UV-vis-NIR spectroelectrochemical techniques, together with DFT studies were consistent with the vinyl ligand being heavily involved in the oxidation process. The importance of not taking electrochemistry at face value, and the need to attribute electronic interactions to their through bond and through space contributions was addressed in Chapters 2 and 5.

Alongside this work, some gold mediated Sonogashira cross-coupling reactions have been investigated. Gold alkynyl and diyndiyl complexes can be cross-coupled with aryl halides under mild conditions in the presence of both Pd(II) and Cu(I) catalysts, without the need for an additional base, at ambient temperatures. The stepwise functionalisation of the masked butadiyndiyl gold complex $(Ph_3P)AuC{\equiv}CC{\equiv}CAu(PPh_3)$ was shown to be effective (without the need of exposing the C-H functionality), provided careful control of each step was undertaken, to avoid double coupling of the aryl halide.